Energy, Mines and Resources • *Yukon Geological Survey*

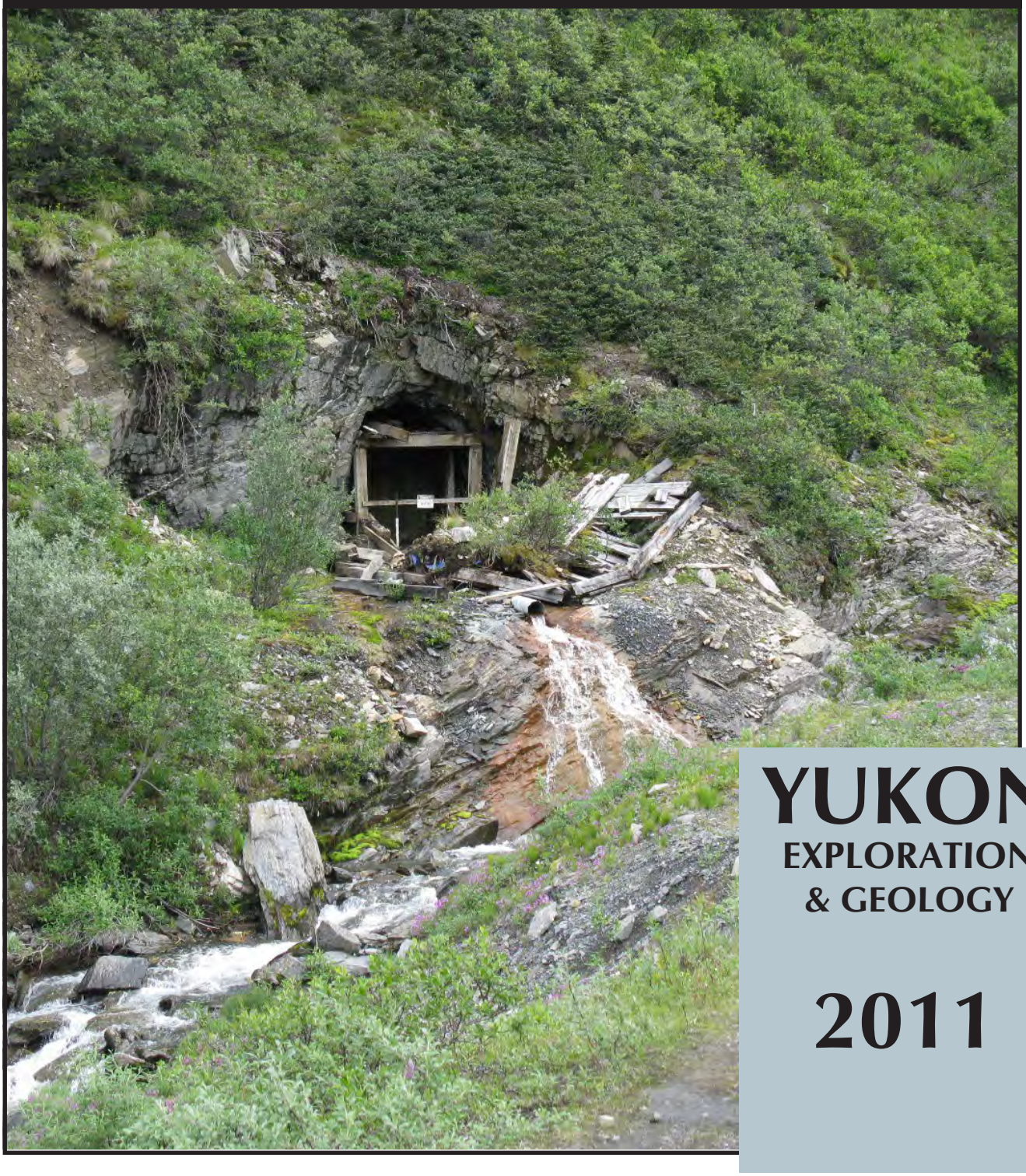

YUKON
EXPLORATION & GEOLOGY

2011

YUKON GEOLOGICAL SURVEY

Yukon
Energy, Mines and Resources

YUKON
EXPLORATION & GEOLOGY

2011

Edited by
K.E. MacFarlane and P.J. Sack

Yukon Geological Survey
Energy, Mines and Resources
Government of Yukon

Published under the authority of the Minister of Energy, Mines and Resources, Government of Yukon ***http://www.emr.gov.yk.ca.***

Printed in Whitehorse, Yukon, 2012.

Publié avec l'autorisation du ministre de l'Énergie, des Mines et des Ressources du gouvernement du Yukon, ***http://www.emr.gov.yk.ca.***

Imprimé à Whitehorse (Yukon) en 2012.

ISSN 1718-8326 (on-line version)

This, and other Yukon Geological Survey publications, may be obtained from:
Geoscience Information and Sales
Yukon Geological Survey
102-300 Main Street
Box 2703 (K-102)
Whitehorse, Yukon, Canada Y1A 2C6

phone (867) 667-3201, fax (867) 667-3198, e-mail ***geosales@gov.yk.ca***

Visit the Yukon Geological Survey website at ***www.geology.gov.yk.ca.***

In referring to this publication, please use the following citation:
Yukon Exploration and Geology 2011. K.E. MacFarlane and P.J. Sack (eds.), 2012. Yukon Geological Survey, 164 p.

Papers from this document are available in colour on the Yukon Geological Survey website.

Front cover photograph: Canex Placer, 1980 underground portal into the XY deposit, a Zn-Pb SEDEX deposit in east Yukon. The property is currently being explored by the Selwyn-Chihong joint venture. Photo by Lee Pigage.

PREFACE

Yukon Exploration and Geology (YEG) and the Yukon Exploration and Geology Overview continue to be the main publications of the Yukon Geological Survey (Energy, Mines and Resources, Government of Yukon). Individual YEG papers, with colour images, are available in digital format only and can be downloaded from our website. The YEG Overview is available in print and digital formats.

YEG 2011 contains up-to-date information on mining and mineral exploration activity, studies by industry, and results of recent geological field studies. Information in this volume comes from prospectors, exploration and government geologists, mining companies and students who are willing to contribute to public geoscience for the benefit of the scientific community, general public, and mineral and petroleum industries of Yukon. Their efforts are appreciated.

While I didn't have a co-editor for the overview this year, I do thank Patrick Sack for acting as my YEG co-editor. As always, appreciation is extended to Yukon Geological Survey staff who take the time to edit earlier versions of manuscripts; this year I thank Carolyn Relf, Jeff Bond, Maurice Colpron, Lee Pigage and Steve Israel. Finally, thanks to Bailey Staffen for lending 'another set of eyes'.

Sherry Tyrner of the Queen's Printer ensured that the printing process went smoothly.

We welcome any input or suggestions that you may have to improve future YEG publications. Please contact me at (867) 667-8519, or by e-mail at karen.macfarlane@gov.yk.ca.

Karen MacFarlane

PETER RISBY
IN MEMORIUM

Pete Risby was a long time prospector in Yukon with a lust for life and a heart for adventure. Born in Kansas in 1931, his family moved to Alberta when he was four years old. After serving in the military in the early 1950s, his first mining related job was as a heavy equipment operator with Cassiar Asbestos Corp. in northern British Columbia. His interest in minerals and prospecting blossomed while working at the Cassiar asbestos mine and set the course for the rest of his days.

Pete staked his first of many claims in 1964, in Yukon. His years of exploration garnered plenty of wild stories. In the early days, Pete had the wherewithal to jump out of a helicopter seconds before it crashed into a mountain; he was declared dead before the medevac flight arrived to collect him. During one summer on the Indian River, he unknowingly sluiced an unmarked grave and was later shocked to find a body in his sluice box.

Pete was the first person to seriously evaluate the placer gold potential of the Indian River area. He started placer mining the Indian River area in 1981. Indian River had minimal historic workings and has since become one of the highest gold-producing drainages in Yukon. Pete was voted the Yukon's placer miner of the year in 1996 and inducted into the Yukon Prospector's Hall of Fame in 1996. The same year that he and his wife Ruth Ann were awarded Mr. and Mrs. Miner by the Klondike Placer Mining Association. They were also instrumental in establishing the Yukon-Indian River Scholarship to promote Yukon placer mining.

One of a dying breed of bush savvy, hard-working, energetic prospectors, Pete was at the Mining Recorders office in Whitehorse poring over maps and planning his next exploration season mere months before he died.

Sadly, Pete succumbed to cancer on February 27, 2011.

Lara Lewis

Yukon Geological Survey staff: (front row, left to right) Tiffani Fraser, Sarah Laxton, Lara Lewis,Patrick Sack, Panya Lipovsky and Charlie Roots; (back row, left to right) Don Murphy, Nikolett Kovacs, Aubrey Sicotte, Maurice Colpron, Steve Israel, Carolyn Relf, Lee Pigage, Jeff Bond, Debbie Throssell and Robert Deklerk.
Missing from photo: Sue Roy, Bailey Staffen, Karen MacFarlane, Derek Torgerson, Johann Slam, Olwyn Bruce and Kristen Kennedy.

YUKON GEOLOGICAL SURVEY

TABLE OF CONTENTS

Lithofacies and lithostratigraphic correlation potential of the Rapitan iron formation, Snake River area (NTS 106F), Yukon

Geoffrey J. Baldwin[1] and Elizabeth C. Turner
Dept. of Earth Sciences, Laurentian University, Sudbury, ON

Baldwin, G.J. and Turner, E.C., 2012. Lithofacies and lithostratigraphic correlation potential of the Rapitan iron formation, Snake River area (NTS 106F), Yukon. *In:* Yukon Exploration and Geology 2011, K.E. MacFarlane and P.J. Sack (eds.), Yukon Geological Survey, p. 1-15.

ABSTRACT

The Neoproterozoic Rapitan iron formation in the Mackenzie Mountains of Yukon and Northwest Territories is one of the largest iron deposits in North America. The Rapitan Group can be traced along strike for several hundred kilometres, but the thickest and most extensive part of this unit is located on the border between Northwest Territories and Yukon in NTS 106F. Several stratigraphic sections in the areas of Discovery and Iron creeks were measured as part of a larger effort to understand basin architecture and marine redox history during deposition of the Rapitan Group, with special emphasis on attributes of the thick interval of iron formation. The iron formation contains diverse textures including a wide variety of jasper nodules and beds. Due to the variable presence of these diverse textures, long-distance correlation of iron formation correlation is challenging. Minor copper mineralization of probable post-depositional origin was found in local float at Discovery Creek and *in situ* at Iron Creek.

[1] *tgj_baldwin@laurentian.ca*

INTRODUCTION

The Rapitan iron formation of the Mackenzie and Wernecke Mountains (Northwest Territories (NWT) and Yukon) is the archetype of Neoproterozoic 'Rapitan-type' iron formations, and was deposited in a dynamic early rift setting. Although this iron formation has been a major component in models for the surficial and oceanic evolution of the Precambrian Earth, and despite several excellent studies in the 1980s and early 1990s, it remains relatively poorly understood. This paper reports on one component of a larger study attempt to resolve the stratigraphy, geochemistry, and basin architecture of the Rapitan iron formation in NWT and Yukon, in an effort to explain its role in the geochemical evolution of Earth's surface environments and the tectonic history of the northern Canadian Cordillera.

One of the more controversial questions about the Rapitan Group relates to the disputed temporal relationships among the major lithostratigraphic units exposed in different areas along its more than 200 hundred kilometres of strike length. Although several regional correlation schemes have been proposed, no true consensus has emerged regarding the temporal relationships among the depositional units in the two main Rapitan basins (Snake River and Redstone-Keele-Mountain Rivers). The ability to correlate at a broad regional scale (hundreds of kilometres), as well as at a comparatively local scale (kilometres to tens of kilometres) is highly desirable, because it would enable predictions about the possible presence and composition of Rapitan strata in the subsurface, permit the tracing of mineralized units (iron, and to a lesser extent, copper-rich layers), and identify marker beds that can provide the basis for interpretations regarding basin evolution. This paper provides detailed descriptions of stratigraphic sections of this iron formation in Yukon, assesses the potential for local-scale correlation within the Snake River basin, offers a preliminary solution to long-standing problems in regional stratigraphic correlation of the Rapitan Group, and discusses the implications of minor copper occurrences in the area.

PREVIOUS WORK

The Neoproterozoic Rapitan iron formation in the Snake River area, Yukon, was the subject of extensive work in past decades. Iron formation was first identified in the Snake River area during the Klondike gold rush (Keele, 1906). Associated diamictite was first interpreted as glaciogenic by Ziegler (1959). Extensive exploration for iron ore at the Crest deposit was undertaken in the 1960s, and up to 18.6 billion tonnes of iron reserves were estimated, including 5.6 billion tonnes at 47.2% iron along Iron Creek in Yukon (Stuart, 1963). Extensive research into the stratigraphy and sedimentology of the Rapitan Group was conducted through the 1970s, and focused on assessing basin architecture and glacial sedimentology (*e.g.*, Eisbacher, 1976, 1978, 1981a,b; Young, 1976); this research resulted in designation of the Mount Berg, Sayunei, and Shezal formations (Green and Godwin, 1963; Upitis, 1966; Eisbacher, 1981a). Further study of the stratigraphy, geochemistry, and depositional setting followed, leading to the suggestion that hydrothermal and glacial processes combined to form the iron deposit (Yeo, 1981, 1984, 1986). This was complemented by an intensive geochemical study of drill core archived from earlier exploration (Klein and Beukes, 1993). The latter authors produced an elegant depositional model for the iron formation, in which a low-oxygen, subglacial water mass became enriched in ferrous iron (Fe^{2+}) and was subsequently oxidized upon glacial retreat and reventilation of the ocean. At the time, this was a plausible depositional model in the context of the early iterations of the "snowball" Earth model (*e.g.*, Kirschvink, 1992), but since then new developments in the understanding of basin analysis, redox geochemistry (*e.g.*, Tribovillard *et al.*, 2006), and Proterozoic oceanic chemistry (*e.g.*, Lyons *et al.*, 2009) have necessitated a renewed stratigraphic and geochemical examination of the Rapitan iron formation.

The Crest deposit of the Rapitan iron formation straddles the border between Yukon and NWT in NTS map sheet 106F, with the bulk of the thick iron formation in the vicinity of Iron Creek, a tributary of the Snake River. Another thick exposure of the iron formation is present along the Cranswick River, and thinner exposures are present between these main localities, such as along Discovery Creek. This paper presents selected stratigraphic sections measured along Discovery Creek and Iron Creek (Fig. 1).

RAPITAN IRON FORMATION STRATIGRAPHY

DISCOVERY CREEK

Stratigraphic section Discovery Creek 2 (DC-2 on Fig. 1) was measured near the headwaters of Discovery Creek, Yukon. This section includes the entire exposure of the Rapitan Group at this location, with a measured thickness of ~430 m. Here, the Rapitan Group overlies carbonate

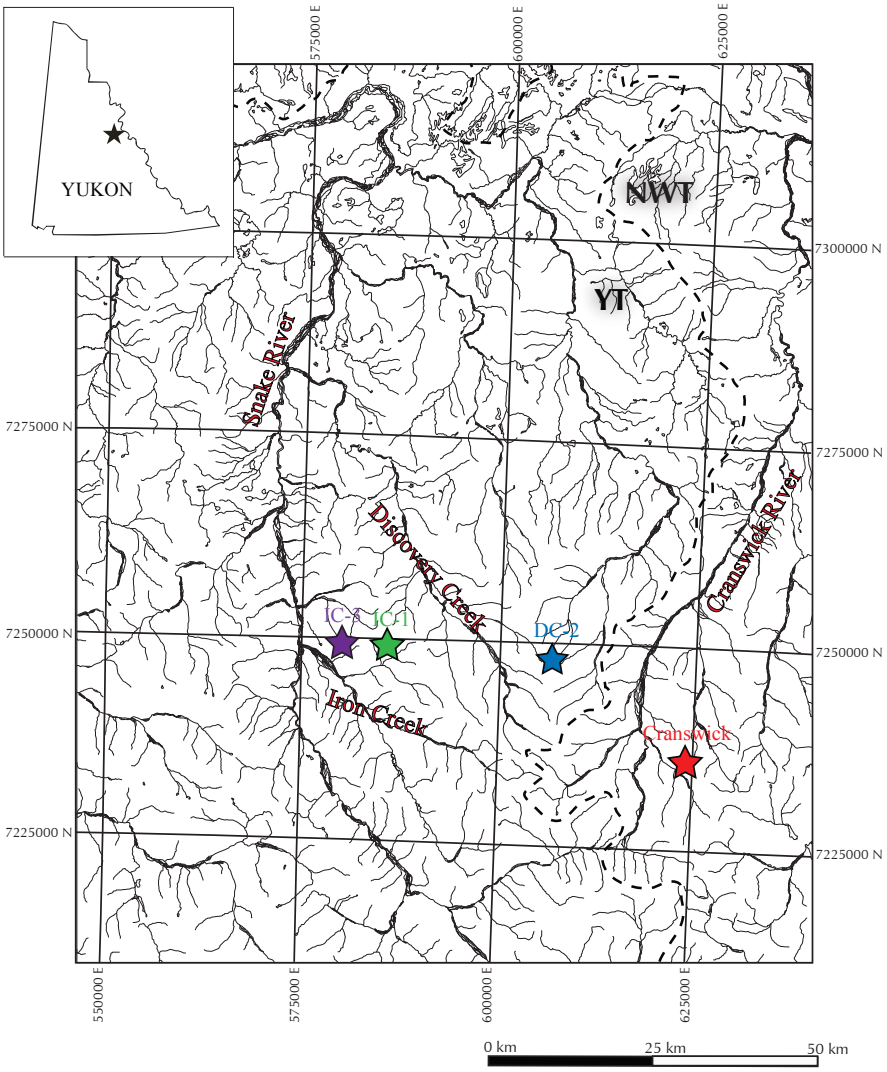

Figure 1. *Locations of measured sections in NTS 106F (NAD 83, Zone 8). Section DC-2 is marked in blue, IC-1 in green, and IC-3 in purple. A location on the Cranswick River, NWT (mentioned in text) is marked in red. Major rivers and creeks in the area are also labeled.*

rocks of the Little Dal Group and is unconformably overlain by the Cambro-Ordovician Franklin Mountain Formation. This is the thickest exposure of the Rapitan Group in the Discovery Creek area; other sections to the northwest record pronounced thinning down to zero thickness over about 10 km.

The lowermost 340 m of the section are siliciclastic rocks that have been interpreted to be glaciogenic in origin (Fig.2; Eisbacher, 1978; Yeo 1981). The dominant rock types in this section are dark red to purple, clast-poor to clast-rich intermediate diamictites (classification scheme of Moncrieff, 1989) (Fig. 3a), with a broad spectrum of clast sizes (pebble to boulder) and weathering characteristics. Previous authors (*e.g.*, Yeo, 1981) have interpreted the entirety of the Rapitan Group in the Snake River to belong to the Shezal Formation, based on the sedimentological character and weathering patterns of the diamictites in the region. Diamictites of the Shezal Formation are typically massive, clast-poor to clast-rich, intermediate pebble to boulder diamictites with characteristic fissile to platy weathering that has been referred to by the informal descriptive term "scaly" weathering, and is common in diamictites of the Discovery Creek area. The diamictites of this section are locally interbedded with matrix-supported and rare framework-supported conglomerate (Fig. 3b) and siltstone units, although in terms of overall character, each of these may be extremely clast-rich and clast-poor end-members of the diamictite spectrum, in that the clasts and/or matrix are nearly identical in all reported lithologies. The presence of dropstones in some of the siltstone units indicates that such rocks may be a variety of clast-poor diamictite, but at a minimum demonstrates their glacial association.

Iron formation is present at three distinct levels in the uppermost 67 m of the Discovery Creek section, representing about 16.5 m of this interval. The two lower iron formation units are thin (0.1 to 1 m thick). They are characterized by dark grey to blue, massive hematite bands with bright red-orange to wine-red jasper (Fig. 3c). Jasper layers are both bedded and nodular; adjacent jasper layers are commonly distinguished only by colour. The nodular jasper is typically lenticular and predominantly bright red, and often are transitional between nodular and bedded facies (Fig. 3d). The lenticular shape, coupled with the deformation of hematite beds around the nodules, suggests that the nodules are early diagenetic, pre-compactional features that developed in the upper metre or so of the sedimentary column. The two lower iron formation units form resistantly weathering prominences.

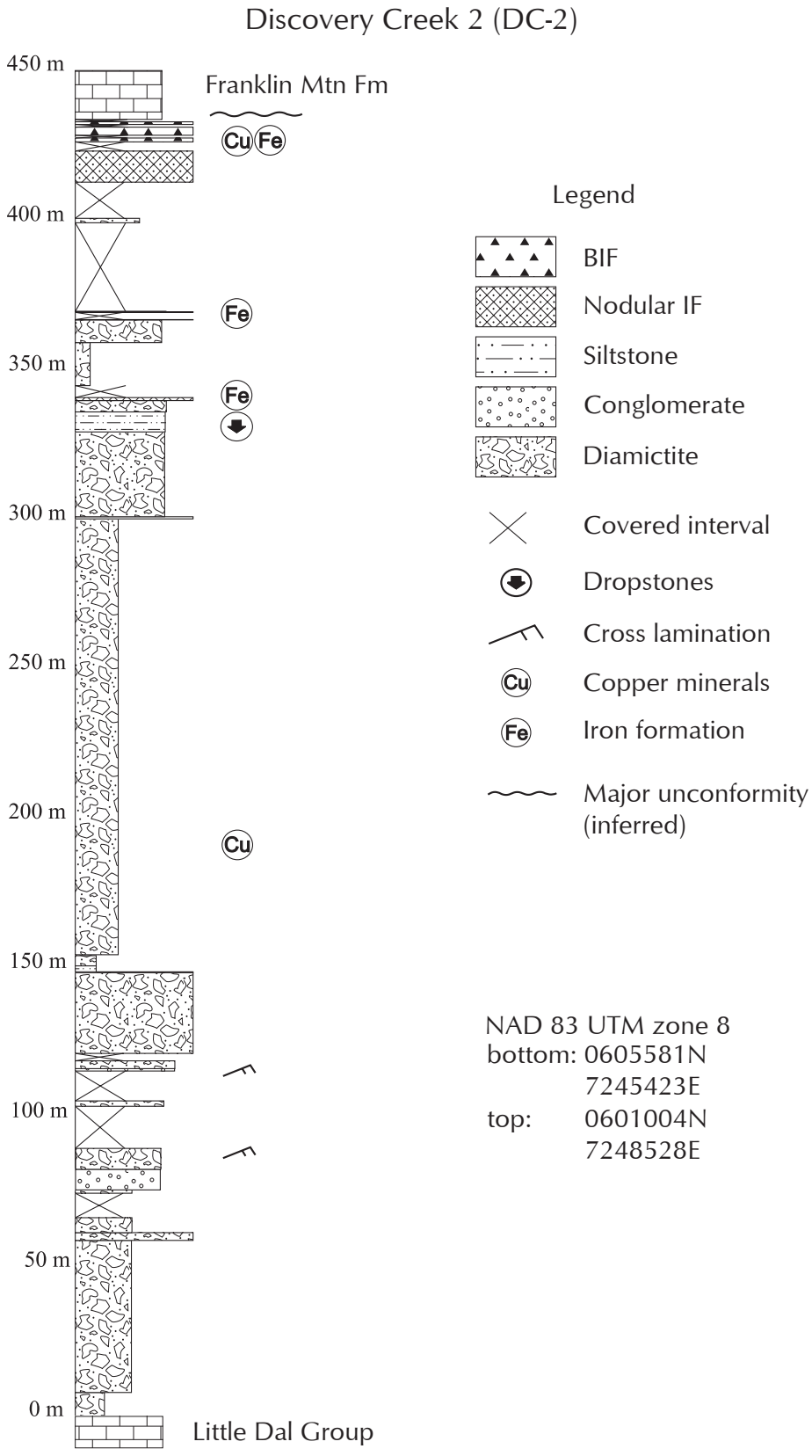

Figure 2. *Stratigraphic column of Discovery Creek 2 section (DC-2). Box widths depict the relative weathering profile of natural exposures. Iron formation units are marked by circled Fe due to the very thin exposure of this lithofacies relative to the thickness of the measured section. Copper showings are marked with a circled Cu. Base of measured section is at the contact between the underlying Little Dal Group A and the base of the Rapitan Group. Above the top of the section are unmeasured carbonate rocks of the Franklin Mountain Formation.*

As much as 15.3 m of the upper iron formation is exposed in a 20.2 m-thick unit. Unlike the lower (thinner) iron formation units, the upper unit has a greater range of textures and colours. Jasper beds are bright red-orange to wine-red, with shades of orange that are not present in lower units. Nodule shape in this unit is also more varied: subspherical nodules indicate minimal compaction, whereas lenticular and ellipsoidal nodules indicate considerable bedding-parallel flattening. The more spherical nodules do not crosscut bedding in the hematite, and so are probably of very early diagenetic origin and formed pre-compaction, much like the more flattened (lensoidal) nodules. There is no apparent relationship between stratigraphic position and the degree of nodule compaction, and so the cause for variation in nodule shape remains unknown. Contacts between jasper and hematite beds are commonly planar, although irregular contacts are also present. This iron-formation-bearing interval forms the uppermost exposure of the Rapitan Group in the Discovery Creek area and is overlain by a 1 m thick covered interval below the first exposure of the overlying Franklin Mountain Formation.

The most unusual finding in this field study was the discovery of two occurrences of copper mineralization in the Rapitan Group section at Discovery Creek. Copper has not been previously reported in the Rapitan Group in

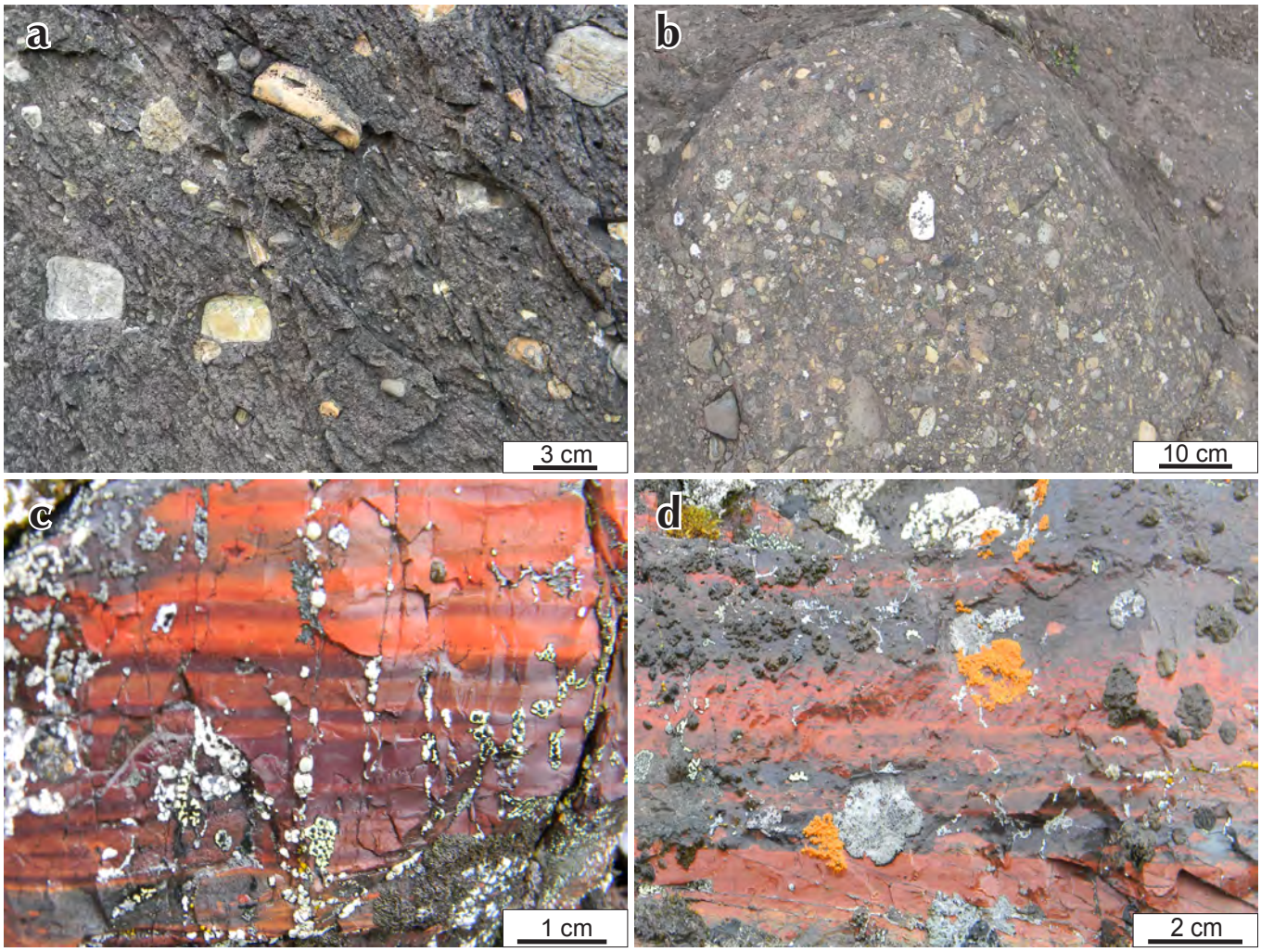

Figure 3. *Photographs of typical lithofacies from section DC-2.* ***(a)*** *Pebble-bearing clast-poor intermediate diamictite dominates the lower part of the section (located at 89.7 m).* ***(b)*** *Pebble conglomerate, the framework-supported end-member of the range of siliciclastic material (siltstone to conglomerate) present in this section (located at 145 m).* ***(c)*** *Bedded iron formation exhibiting interbedded jasper of different colours (located at 350 m). This style of bedding was suggested to be of diagenetic origin by Klein and Beukes (1993).* ***(d)*** *Iron formation with both bedded and nodular types. Some jasper bands appear to be transitional between nodules and beds, a common texture throughout the region (located at 349 m).*

this area, but it is associated with the underlying Coates Lake Group in NWT (*e.g.*, Jefferson and Ruelle, 1987). Both copper occurrences at DC-2 are in float, but are interpreted to be approximately *in situ* due to the knife-edge geometry of the ridge on which they were found, which would prevent samples that had been transported more than a few metres from remaining on the ridge crest. The lower copper occurrence is in a diamictite unit at 209.3 m, although its exact original stratigraphic position is uncertain. The occurrence consists of malachite-stained pebbles that have weathered out completely from the host rock. The upper occurrence is in a boulder of iron formation associated with the upper iron formation interval and consists of an ~2 cm diameter piece of malachite-coated chalcopyrite within an ~5 cm diameter vug in the iron formation.

IRON CREEK

The entire thickness of the Rapitan iron formation is not exposed in any one location in the Iron Creek area owing to abundant vegetation, colluvial cover, and the pervasive coating of the rocks by a modern calcite and gypsum leachate. Four stratigraphic sections were measured in order to generate a composite section covering the entire thickness of the unit. Two of these sections, covering the majority of the thickness of the iron formation, are described below.

Iron Creek 1 (IC-1)

Iron Creek section 1 (IC-1) covers the greatest thickness of the Rapitan iron formation in the area (Fig. 1). Although several intervals are covered, including the base of the iron formation, this is the only section that spans the entire thickness of the Rapitan iron formation and includes both underlying and overlying strata (Fig. 4). The lowest part of section IC-1 is in a thick package of massive, matrix-supported cobble to boulder diamictite, which is underlain by a covered interval of unknown thickness. This diamictite is dark red to purple, with clasts consisting predominantly of limestone and dolostone (Fig. 5a). The lower part of the unit is well indurated and cliff-forming, but higher units are increasingly recessive. The exposed thickness of the unit is 36.5 m, although it may be thicker because it is overlain by a 29 m-thick covered interval, above which is the lowermost exposure of iron formation.

Unlike the section at Discovery Creek, the majority of the rest of the section consists of iron formation, capped by interbedded diamictite and siltstone, whereas Discovery Creek was predominantly diamictite. Iron formation at this location includes a wide variety of colours and textures. Bedded jasper-hematite units are thinly to thickly laminated (Fig. 5b). Colours are similar to those at Discovery Creek, with the addition of thin bands of pink jasper. Jasper is predominantly nodular (2 mm to 5 cm in diameter). The nodules are common in both hematite, and to a lesser degree, jasper bands, and locally form the bulk of the host jasper band. The largest nodules commonly are cored by a variety of materials including carbonate clasts and hematite particles (Fig. 5c,d), which results in more complicated nodule shapes that range from tabular to spheroidal to irregular. Some irregular nodules contain multiple nuclei and are interpreted to have resulted from intergrowth of two or more nodules. Some irregular nodules exhibit continuous growth zones around a single nucleus, suggesting irregular, uneven growth patterns. In a layer at 158 m, nodules consist of white chert in a jasper band; this is the only known example of white nodules in the Rapitan Group (Fig. 5e), although tan chert nodules have been reported from the vicinity of Cranswick River, NWT (Baldwin *et al.* 2012 *in press*; their Figure 4f). Bedded jasper exhibits a wide range of characteristics. Layer thicknesses vary from 1 mm to several centimetres (thick laminated to thin bedded). Faint micro-laminae are locally evident in some of the thicker jasper beds. Contorted bedding, load structures, and wavy bedding are all common. In rare cases, hematite nodules are present in the thickest jasper bands, mimicking the relationship of the jasper nodules that are so common in the hematite beds.

The iron formation at section IC-1 is interbedded with intervals of siltstone and diamictite. Siltstone intervals are typically less than 1 m thick, whereas diamictite units are up to 5 m thick. These siliciclastic units are most common between 75 and ~100 m, but they may make up a significant proportion of the recessively weathering, covered intervals of the section (diamictite exposures are commonly immediately overlain by covered or vegetated intervals). At the top of the iron formation, two thin units of granular iron formation (GIF) are present (Fig. 5f). Previously referred to as 'iron formation arenite' by Klein and Beukes (1993), granular iron formation consists of sand-sized particles of chert and hematite that are typically pelloidal or oolitic (Clout and Simonson, 2005). This type of iron formation is common in late Palaeoproterozoic 'Superior-type' iron formations, such as the Gunflint (Lake Superior region) or Sokomon (Labrador Trough) iron formations. Granular iron formation is considered to indicate iron formation deposition above storm wave-base, where shoaling can occur, allowing the

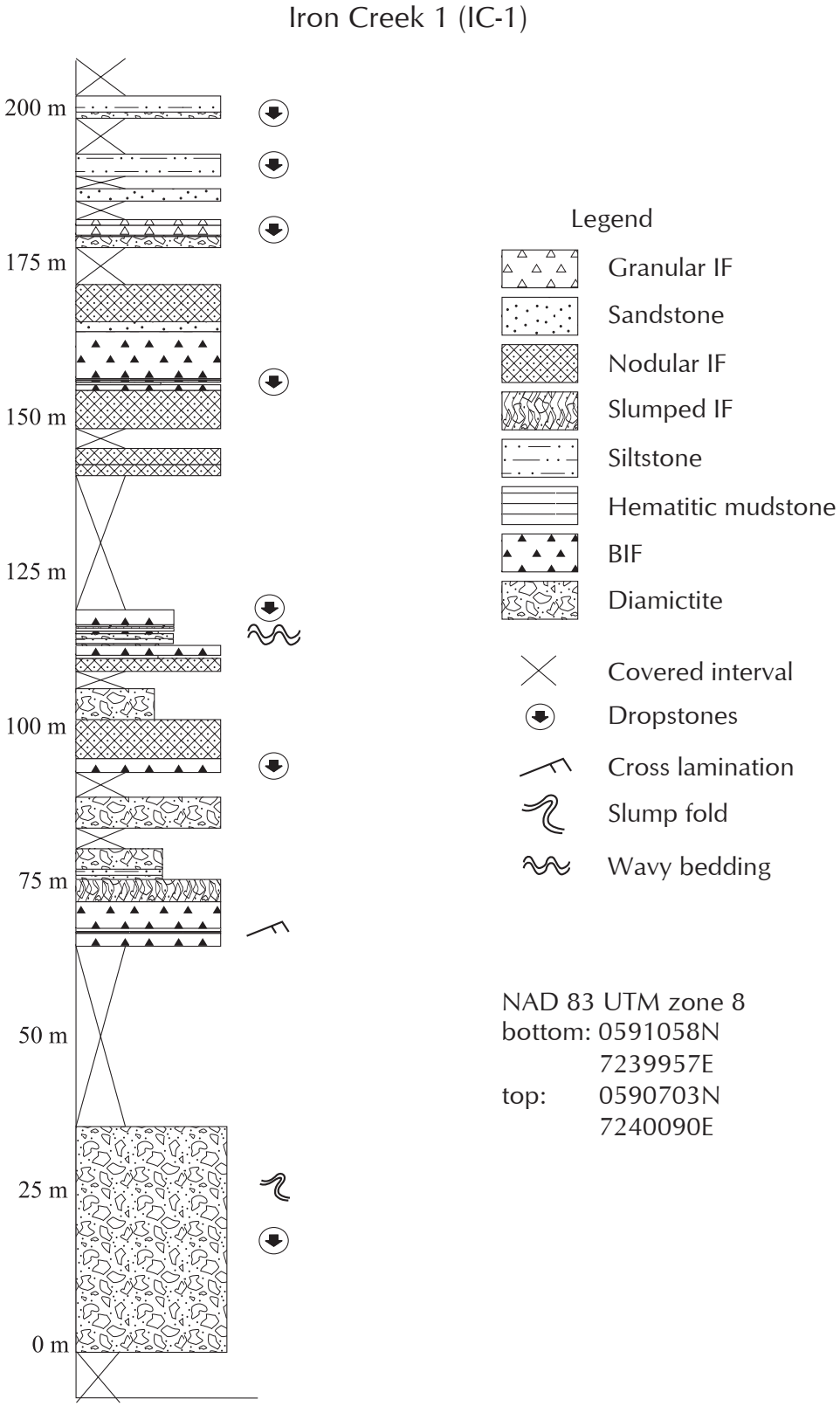

Figure 4. *Stratigraphic column of Iron Creek 1 section (IC-1). Box widths depict the relative weathering profile of natural exposures, but variations in weathering profile within a given unit are not illustrated. The section base is the lowest exposed stratigraphic level of Rapitan group at this location, and the top of the section is not the top of the Rapitan Group, exposure is very poor above the top of the measured section.*

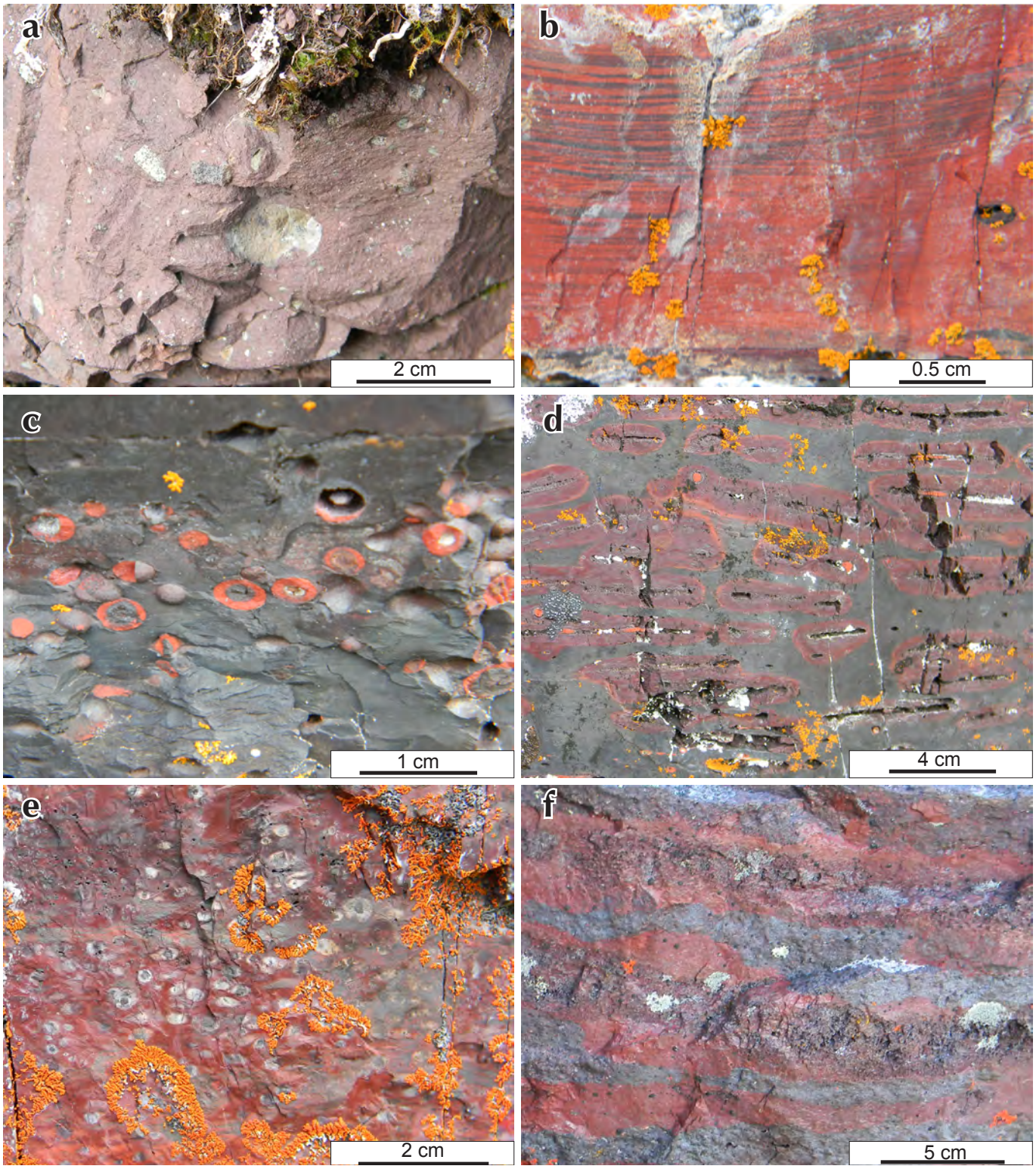

Figure 5. *Photographs of typical and unusual lithofacies from section IC-1.* ***(a)*** *Non-stratified clast-poor intermediate diamictite from below the iron formation, at ~0 m.* ***(b)*** *Thinly bedded jasper and hematite iron formation (located at 68 m).* ***(c)*** *Compound hematite-jasper nodules (located at 96 m).* ***(d)*** *Oblate jasper nodules, with tabular hematite-jasper cores that may represent rip-up clasts of bedded iron formation (located at 105 m).* ***(e)*** *White chert nodules are present only in this thin unit at ~158 m (located at 158 m).* ***(f)*** *Granular iron formation (GIF), consisting of coarse sand-sized grains of jasper and hematite (located at 184 m).*

chemogenic material to form granules. The granular iron formation in section IC-1 is overlain by a thick succession of interbedded pebble to cobble-bearing diamictite and maroon siltstone, the lower 17.4 m of which was measured. The presence of the GIF in direct contact with the transition to clastic sediment suggests that in this area, iron formation deposition was terminated by a loss of accommodation space, which initially caused shoaling of the iron formation in shallow water, but soon led to an influx of clastic sediment.

The GIF lithofacies at the top of IC-1 is also present near the tops of several other measured stratigraphic sections in the Iron Creek area, specifically IC-2 and IC-4, but is not exposed in section IC-3 (described below), probably due to colluvial and vegetation cover. The GIF is overlain by an unmeasured thickness of interbedded purple siltstone and diamictite, with a minimum thickness of 40 m, based on other sections measured in the area (IC-2).

Iron Creek 3 (IC-3)

Iron Creek section 3 (IC-3) was selected because the contact of the iron formation with underlying diamictite is exposed, even though exposure of the iron formation itself is limited (Figs. 1 and 6). The base of the lowermost iron formation lies conformably on the underlying red pebble and cobble-bearing diamictite that is common in the area, which has been attributed to the Shezal Formation despite its sharp differences in both colour and texture from classic Shezal Formation to the southeast in NWT (Eisbacher, 1981a). The diamictite here is roughly 100 m thick but was not measured. The lowermost iron formation unit is 5.4 m thick, and includes alternating layers of bedded iron formation (Fig. 7a), nodular iron formation, and a thin interval of what is referred to here as 'hematitic mudstone'. The latter lithofacies is a thinly bedded, very fine grained hematitic mudstone lacking jasper and was referred to as 'massive hematite' in other publications (*e.g.*, Klein and Beukes, 1993). The top unit of this basal iron formation contains minor copper mineralization: a vug containing copper minerals oxidized to malachite (Fig. 7b). This mineralization is significant because unlike other copper occurrences in the area (*e.g.*, the upper mineralization at DC-2), it was documented in outcrop.

The basal iron formation at IC-3 is overlain by ~7 m of recessively weathering diamictite that is texturally identical to the underlying siliciclastic rocks except for its weathering profile. This is succeeded by a 14 m covered interval. This covered interval is overlain by 83 m of iron formation with less than 50% exposure in the upper 50 m. The iron formation is in places interbedded with siliciclastic rocks, including sandstone, siltstone, conglomerate and diamictite. Iron formation that is under or overlain by these clastic intervals, particularly diamictite, commonly shows evidence of slumping and reworking marked by intense folding and convolution of jasper beds. In section IC-3, the unit is dominated by nodular iron formation, with a smaller proportion of bedded iron formation. Nodule and jasper bands exhibit a similar range of colour and morphology to beds in section IC-1. Jasper nodules are lenticular to highly spheroidal (Fig. 7c). Rare hematite nodules in jasper bands are a textural reversal from the norm but have been documented at Cranswick River, NWT (Figs. 1 and 7d). The section was terminated at this point due to very poor exposure above the top of the measured iron formation, as well as an apparent shift towards siltstone and diamictite based on the scattered boulders present.

Despite their similarity and relatively close proximity (~6 km apart), correlation of individual iron formation units between sections IC-1 and IC-3 using jasper textures does not appear to be possible. This problem is compounded by the absence from section IC-3 of any obvious marker units documented in other sections, such as the GIF unit; the absence of the GIF unit is interpreted to be a function of incomplete exposure at the top of the section. This limitation notwithstanding, it appears that a high degree of lateral variability existed at the time of deposition, a feature that has also been documented by the author in sections measured in the NWT.

DISCUSSION

CORRELATION

Long-distance correlation between different regions where the Rapitan iron formation is exposed in NTS sheet 106F appears to be impossible. Although ostensibly coeval iron formation in other regions of the world commonly include laterally persistent marker beds, no such layers have been documented in the Rapitan iron formation. Although the iron formation overall is a geographically extensive unit deposited during a single, limited time interval in the Snake River area, its internal stratigraphy and relationships with subjacent and suprajacent strata demonstrate considerable local variability, making more detailed correlation difficult. The absence of the upper diamictite at Discovery Creek may simply be a result of erosion, as indicated by the rapid pinch-out of the Rapitan Group to the northwest. This erosion makes it impossible to determine whether or how

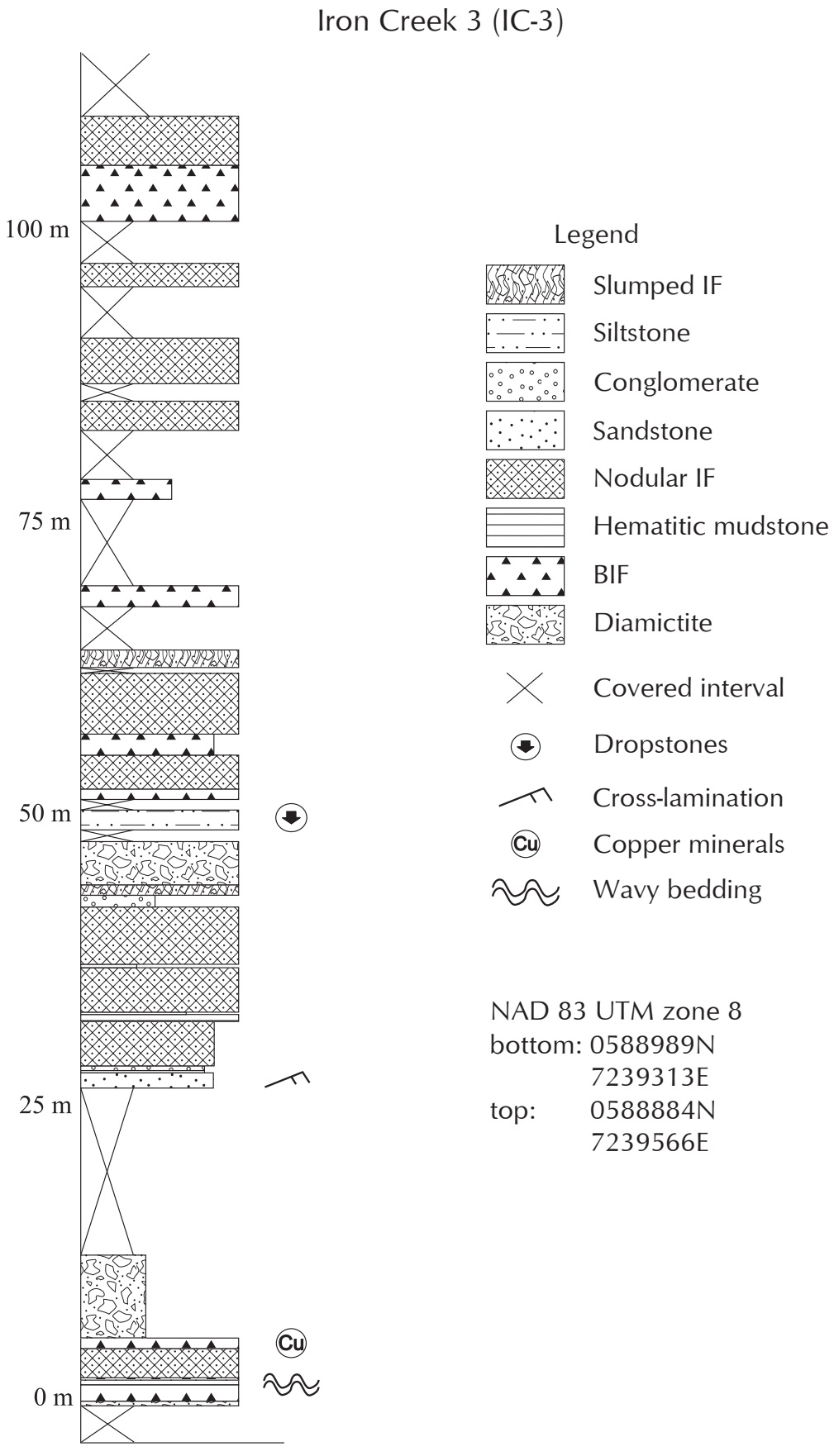

Figure 6. *Stratigraphic column of Iron Creek section 3 (IC-3). Box widths depict the relative weathering profile of natural exposures.*

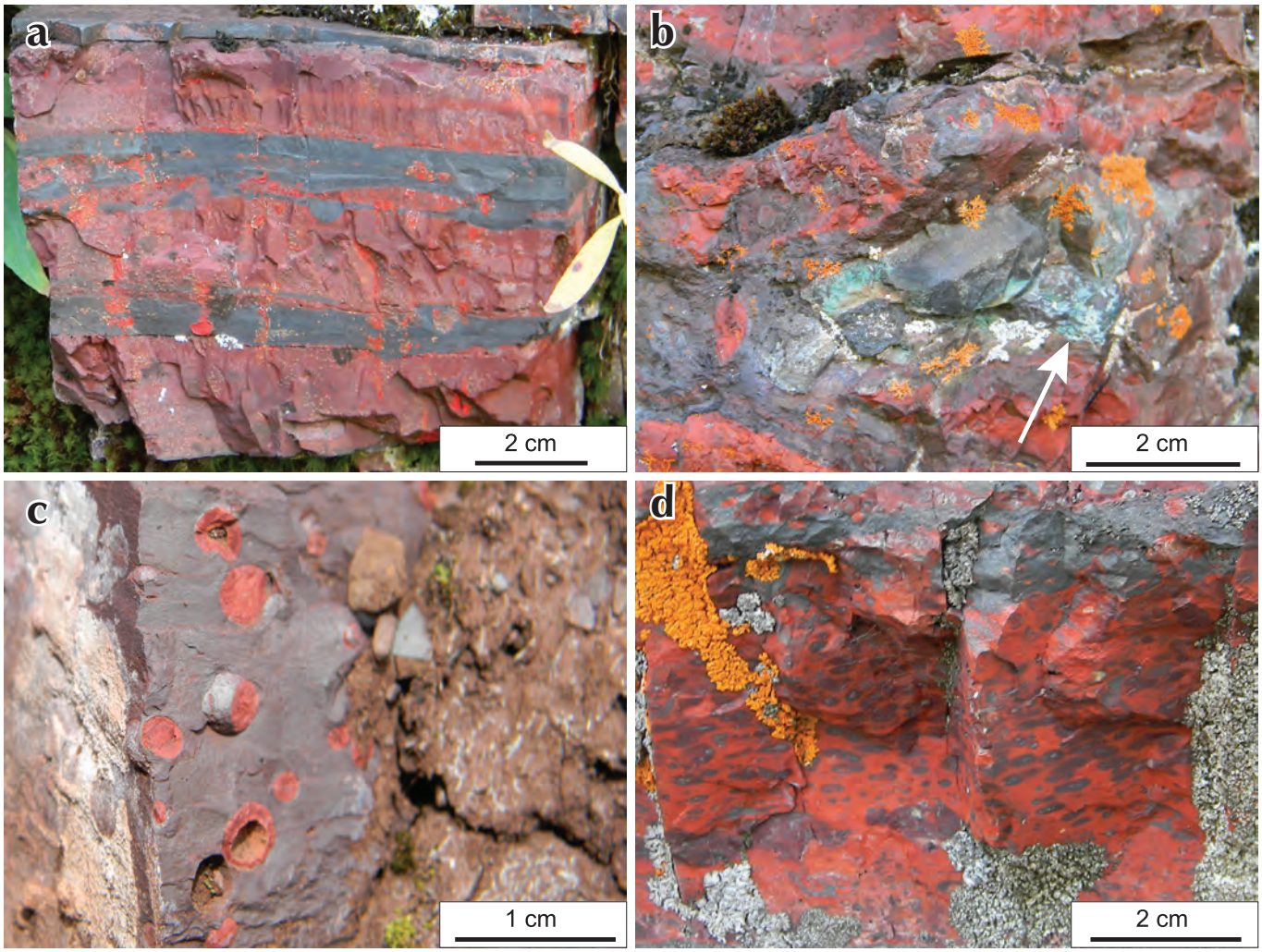

Figure 7. *Photographs of typical lithofacies from section IC-3.* ***(a)*** *Interbedded jasper and hematite from just above the basal iron formation at ~5 m.* ***(b)*** *Copper mineralization within the iron formation at 7 m characterized by malachite (arrow).* ***(c)*** *Highly spheroidal nodules at 35 m.* ***(d)*** *Hematite nodules in jasper (the reverse of the normal nodule-host rock compositional relationship) at 72 m.*

much of the upper Windermere Supergroup (e.g., Hay Creek Group and the informal 'upper group'; Yeo *et al.*, 1978; Aitken, 1989) was originally deposited in this area prior to erosion.

It is possible that different thicknesses of exposed iron formation at Discovery Creek and Iron Creek are in part a primary feature. Based on the sections measured at Iron Creek and data reported at Cranswick River, NWT (Baldwin *et al.*, *in press*) lateral facies variation is common in the Rapitan Group. For example, 30 m of iron formation pinches out to no more than 3 m over a strike-length of less than one kilometre along the Cranswick River. This suggests that small-scale facies variations or differences in paleobathymetry may have existed in the Snake River basin, complicating stratigraphic correlation across large distances. At a very local scale, this phenomenon is expressed most obviously as lateral discontinuity of distinctive individual units in the iron formation. At a larger scale, the phenomenon is expressed as localized to regional variations in the sedimentological character of associated clastic rocks, which show considerable variability in the relative proportions of sand, mud, and coarse clasts (pebbles, cobbles, and boulders) at apparently similar stratigraphic levels over very short distances (<1 km). Apparent variations in the iron content (and therefore colour) of the same clastic rocks are also visible over relatively short distances. Such variability in glacioclastic rocks is not uncommon, because local topography, glaciology, hydrodynamics, and sediment sources can profoundly influence their sedimentological character. This does not, however, imply that deposition

of the iron formation at Discovery Creek, Iron Creek, and Cranswick River was asynchronous, but merely that the textural details of each area's strata may be too different to permit definitive correlations. As discussed in the previous section, this difficulty in correlation is exacerbated by the lack of any truly distinctive marker horizons across all measured sections in the region (*e.g.*, GIF, a distinctive conglomerate bed, or an easily identifiable, texturally distinct nodule layer). Each of these features has enabled correlation within geographically limited areas, but none has extended across all three localities (Discovery Creek, Iron Creek, Cranswick River) nor conclusively across any two.

The difficulty in local to regional correlation is best interpreted as a symptom of the dynamic tectonic environment in which the Rapitan Group was deposited. The preponderance of evidence suggests that the Rapitan Group was deposited in a relatively young rift basin (Yeo, 1981), probably related to the rifting of Rodinia (Young, 1992), with ample evidence for active tectonic subsidence during deposition (Helmstaedt *et al.*, 1979). An active rift graben system would have provided considerable paleobathymetric variability, featuring bathymetric highs or 'sills', as well as highly compartmentalized sub-basins. Consequently, in addition to the larger regional Rapitan sub-basins (Snake River basin and Redstone-Keele-Mountain River basin), each of these sub-basins would have been internally subdivided and would therefore have possessed extensive sedimentological and stratigraphic variation over short distances, as is recorded in both the clastic and hydrogenous (iron formation) records. This has already been shown to be a major control on the overall distribution and thickness of iron formation across the Mackenzie Mountains (Baldwin *et al.*, 2011), and may have provided considerable local control on the stratigraphy of iron formation in any given locality. Consequently, only the top and base of the iron formation are liable to have consistent correlation of stratigraphic horizons, both sedimentologically and temporally, and even these probably varied geographically.

COPPER MINERALIZATION

Although copper mineralization has been described in the Rapitan Group southeast of the present study area (*e.g.*, Nite and June showings; Helmstaedt *et al.*, 1979, 1981; Aitken *et al.*, 1981), it has not previously been reported in the Snake River area. Copper occurrences in the present study area consist of copper-rich minerals (malachite, chalcopyrite) lining vugs in iron formation at Discovery and Iron creeks, and malachite-stained pebbles weathered out of a diamictite at Discovery Creek. Both types of occurrence could have origins as copper-rich carbonate dropstones which eroded from the diamictite (leaving behind copper-rich pebbles) and weathered out of the iron formation (leaving behind vugs with a copper-rich "crust"). The source the dropstones is uncertain, as not enough is presently known about ice movement to link them to the Redstone River Formation. Several mechanisms for copper paragenesis have been previously presented, including the remobilization of copper from the Coates Lake Group, which underlies the Rapitan Group in the Redstone-Keele-Mountain River area or through the resedimentation of carbonate and siltstone clasts of similar origin (Helmstaedt *et al.*, 1979). Neither of these explanations is especially plausible for the minor copper mineralization reported here from the Snake River area, because the Coates Lake Group is not present in this area.. The minor copper mineralization of the Snake River area probably had an authigenic, post-depositional origin similar to that found to the southeast, but the copper source and fluid conduits were undoubtedly distinct. This relates back to the overall basin architecture, in which the Snake River area formed as a separate sub-basin from areas to the southeast. Consequently, it is probable that the fluids responsible for precipitating copper minerals did not pass through the same source rocks as those responsible for the Coates Lake deposit, nor its related deposits (*e.g.*, Nite, June) hosted in the adjacent Rapitan Group.

COMPARISON WITH PREVIOUS WORK

Several previous authors have made significant efforts to resolve the controversial stratigraphy of the Rapitan Group in the Snake River area. Yeo (1981, 1984), measured numerous stratigraphic sections in the region in an effort to resolve both the map distribution and stratigraphy of the entire Rapitan Group, whereas Klein and Beukes (1993) reported details of diamond drill core logs for drillholes from both the Iron Creek and Cranswick River (NWT) areas. Comparing the stratigraphy and sedimentology of the sections documented in this paper measured with those provided in earlier publications is difficult. The details of original stratigraphic sections from some studies that favoured generalized stratigraphic composites remain unavailable (*e.g.*, Yeo, 1981), which inhibits the direct comparison of the originally observed stratigraphy and sedimentology to other work, such as the detailed work on core by Klein and Beukes (1993). The present paper describes many of the iron formation units as hybrids of bedded iron formation and nodular iron formation, which

is distinct from the practice in both previous studies, which leaned toward identification of lithofacies as either one end-member or the other, resulting in fewer and less-variable units in the iron formation, and complicated efforts to compare the stratigraphy. The best study available for direct comparison was conducted using archived drill core, with a minimal field component (Klein and Beukes, 1993). Although this core-based study had the advantage of fresh, unweathered surfaces, it lacked the small-scale lateral spatial data available in detailed field studies that is necessary to characterize the well-developed lateral variability that is expressed on a scale of metres to hundreds of metres throughout the region, despite well-reported core thicknesses and approximate drill collar locations. As a consequence of stratigraphic simplification, the core-based study inferred direct correlations between the Iron Creek area and the Cranswick River area in NWT (Klein and Beukes, 1993). The proposed correlations were based exclusively on the composition and vertical distribution of siliciclastic intervals in the iron formation, which were used as regional marker units. The present study shows that such units are probably not meaningful markers, based on major differences in sediment colour and matrix composition, among other features. Based on the observations reported here and by Baldwin *et al.* (*in press*), most sedimentary units within and associated with the iron formation are not laterally traceable due to dramatic lateral facies changes related to the tectonically influenced paleobathymetric variability of the rift basin at the time of deposition. Previous authors may have been in error in attempting to correlate across the basin based on anything more detailed than the (probable) time-marker horizons of the top and bottom of the iron formation.

FUTURE WORK

Future work on the Rapitan iron formation will focus on the geochemistry of the measured sections and the possible use of chemostratigraphy for regional correlation. A pilot study on samples from Cranswick River (NWT) is currently in press (Baldwin *et al.*, *in press*). Work to date has focused on developing a working model for basin configuration and characterizing the redox stratification of the Snake River basin, using rare earth elements and redox-sensitive metals such as molybdenum and uranium, and on implications for the depositional processes and iron source for the Rapitan iron formation. The principles established in the pilot study will be applied to samples collected elsewhere in the Rapitan iron formation, including the exposures in Yukon. It is possible that the chemostratigraphy of Mo and U may help resolve the sedimentological limitations on long-distance correlation, because water-mass chemistry may have been significantly less susceptible to lateral variability than physical sedimentology. Alternatively, each sub-basin may have been influenced by a chemically distinct water mass. If this approach fails to permit high-quality chemostratigraphic correlation, it will probably demonstrate instead that basin morphology was characterized by chemically and sedimentologically distinct sub-basins. Ongoing detrital U-Pb zircon studies on samples from across the belt may help provide further insight into time correlations and basin architecture.

ACKNOWLEDGEMENTS

The subject matter of this paper is part of GJB's PhD research. Yukon Geological Survey and Northwest Territories Geoscience Office are gratefully acknowledged for their support of the field work. Further funding for this project was provided by a SEG student grant to GJB, and an NSERC Discovery Grant to ECT. Minor additional field support was provided by Aurora Geosciences. Joyia Chakungal and Venessa Bennett are thanked for their helpful comments in the field. Tiffany Chevrier and Kirsti Medig are also thanked for their assistance in the field. Special thanks go out to Darrel G.F. Long and Carolyn Relf for their helpful comments and critical review of the text.

REFERENCES

Aitkin, J.D. 1989. Uppermost Proterozoic formations in central Mackenzie Mountains, Northwest Territories. Geological Survey of Canada, Bulletin 368, p. 1-26.

Aitken, J.D., Ruelle, J.C. and Cook, D.G. 1981. Copper mineralization near an intra-Rapitan unconformity, Nite copper prospect, Mackenzie Mountains, Northwest Territories, Canada: Discussion. Canadian Journal of Earth Sciences, 18, p. 410-413.

Baldwin, G.J., Turner, E.C. and Kamber, B.S. 2011. Reevaluating the depositional model and iron source of the Rapitan iron formation. *In:* 39th Annual Yellowknife Geoscience Forum Abstracts. Compiled by B.J. Fischer and D.M. Watson. Northwest Territories Geoscience Office, Yellowknife, p. 20.

Baldwin, G.J., Turner, E.C. and Kamber B.S., in press. A new depositional model for Neoproterozoic iron formation: Insights from the chemostratigraphy and basin configuration of the Rapitan iron formation. Canadian Journal of Earth Sciences, 2011.

Clout, J.M.F. and Simonson, B.M., 2005. Precambrian Iron Formations and Iron Formation-Hosted Iron Ore Deposits. Economic Geology 100th Anniversary Volume, p. 643-680.

Eisbacher, G.H., 1976. Proterozoic Rapitan Group and Related Rocks, Redstone River Area, District of Mackenzie. Geological Survey of Canada Paper 76, p. 117-125.

Eisbacher, G.H., 1978. Re-definition and subdivision of the Rapitan Group, Mackenzie Mountains. Geological Survey of Canada Paper 77, p. 1-21.

Eisbacher, G.H., 1981a. Sedimentary tectonics and glacial record in the Windermere Supergroup, Mackenzie Mountains, Northwestern Canada. Geological Survey of Canada Paper 80, p. 1-41.

Eisbacher, G.H., 1981b. Late Precambrian tillites of the northern Yukon-Northwest Territories region, Canada. *In:* Earth's pre-Pleistocene glacial record, M.J. Hambrey and W.B. Harland (eds.), Cambridge University Press, Cambridge, p. 724-727.

Green, L.H. and Godwin, C.I., 1963. Mineral Industry of Yukon Territory and southwestern District of Mackenzie, 1962. Geological Survey of Canada Paper, vol. 63, p. 15-18.

Helmstaedt, H., Eisbacher, G.H., and McGregor, J.A., 1979. Copper mineralization near an intra-Rapitan unconformity, Nite copper prospect, Mackenzie Mountains, Northwest Territories, Canada. Canadian Journal of Earth Sciences, vol. 16, p. 50-59.

Helmstaedt, H., Eisbacher, G.H., and McGregor, J.A., 1981. Copper mineralization near an intra-Rapitan unconformity, Nite copper prospect, Mackenzie Mountains, Northwest Territories, Canada: Reply. Canadian Journal of Earth Sciences, vol. 18, p. 414-418.

Jefferson, C.W. and Ruelle, J.C.L., 1987. The late Proterozoic Redstone copper belt. *In:* Mineral Deposits of the northern Cordillera, J.A. Morin (ed.), Canadian Institute of Mining and Metallurgy Special Vol. 37, p. 154-168

Keele, J., 1906. Report on the upper Stewart River region, Yukon. *In:* Annual Report 1904, R. Bell (ed.), Geological Survey of Canada, Annual Report vol. 16, part C, p. 5-23.

Kirschvink, J.L., 1992. Late Proterozoic low-latitude global glaciation: the Snowball Earth. *In:* The Proterozoic biosphere: A multidisciplinary study, J.W. Schopf and C. Klein (eds). Cambridge University Press, Cambridge, p. 51-52.

Klein, C. and Beukes, N.J., 1993. Sedimentology and Geochemistry of the Glaciogenic Late Proterozoic Rapitan Iron-Formation in Canada. Economic Geology, vol. 88, p. 542-565.

Lyons, T.W., Anbar, A.D., Severmann, S., Scott, C., and Gill, B.C., 2009. Tracking euxinia in the ancient ocean: A multiproxy perspective and Proterozoic case study. Annual Reviews in Earth and Planetary Science, vol. 37, p. 507-534.

Moncrieff, A.C.M., 1989. Classification of poorly sorted sedimentary rocks. Sedimentary Geology, vol. 65, p. 191-194.

Stuart, R.A., 1963. Geology of the Snake River Iron deposit. DIAND Assessment Files, Yellowknife, NWT, p. 18.

Tribovillard, N., Algeo, T.J., Lyons, T., and Riboulleau, A., 2006. Trace metals as paleoredox and paleoproductivity proxies: An update. Chemical Geology, vol. 232, p. 12-32.

Upitis, U., 1966. The Rapitan Group, southeastern Mackenzie Mountains, Northwest Territories. MSc thesis, Department of Geological Sciences, McGill University, Montreal, 70 p.

Yeo, G.M., 1978. Iron-formation in the Rapitan Group, Mackenzie Mountains, Yukon and Northwest Territories. DIAND Mineral Industry Report 1975, NWT Economic Geology Series 1978-5, p. 170-175.

Yeo, G.M., 1981. The late Proterozoic Rapitan glaciation in the northern Cordillera. *In:* Proterozoic Basins of Canada, F.H.A. Campbell (ed.). Geological Survey of Canada Paper 81-10, p. 25-46.

Yeo, G.M., 1984. The Rapitan Group: Relevance to the global association of late Proterozoic glaciation and iron formation. PhD thesis, Department of Geology, University of Western Ontario, London, 603 p.

Yeo, G.M., 1986. Iron-formation in the late Proterozoic Rapitan Group, Yukon and Northwest Territories. *In:* Mineral Deposits of the Northern Cordillera, J.A. Morin (ed.), Canadian Institute of Mining and Metallurgy Special Vol. 37, p. 142-153.

Young, G.M., 1976. Iron-formation and glaciogenic rocks of the Rapitan Group, Northwest Territories, Canada. Precambrian Research, vol. 3, p. 137-158.

Young, G.M., 1992. Late Proterozoic stratigraphy and the Canada-Australia connection. Geology, vol. 20, p. 215-218.

Ziegler, P.A., 1959. Frühpaläozoiche Tillite im östlichen Yukon-Territorium (Kanada). Ecologae Geologicae Helveticae, vol. 52, p. 735-741.

Ongoing displacement monitoring at the Dawson City landslide (Dawson map area NTS 116B/3)

Marc-André Brideau[1]
School of Environment, University of Auckland, Auckland, New Zealand

Doug Stead
Department of Earth Sciences, Simon Fraser University, Burnaby, BC

Charlie Roots
Geological Survey of Canada, Whitehorse, YT

Panya Lipovsky
Yukon Geological Survey, Whitehorse, YT

Brideau, M.-A., Stead, D., Roots, C., and Lipovsky, 2012. Ongoing displacement monitoring at the Dawson City landslide (Dawson map area NTS 116B/3). *In:* Yukon Exploration and Geology 2011, K.E. MacFarlane and P.J. Sack (eds.), Yukon Geological Survey, p. 17-26.

ABSTRACT

The Dawson City landslide is a prehistoric slope failure at the northern end of the town. It occurred along the faulted contact between an ultramafic unit from the Slide Mountain terrane and a metasedimentary unit from the Yukon-Tanana terrane. The very blocky nature (seven discontinuity sets) of the failed rock mass led to a pseudo-circular failure mechanism. Based on geomorphic observations suggesting moving masses in the headscarp and deposit, various monitoring techniques were begun in 2006 to confirm and quantify the rate of displacement. Data collected from five years of monitoring suggest that an unstable section in the headscarp is moving downslope at a rate of 4.3 to 11.9 cm/yr, whereas the lower part of the landslide deposit is moving between 8.5 and 20 cm/yr. XRD analysis of the silt and clay-size particles in the deposit revealed the presence of talc, chrysotile, and lizardite.

[1] *m.brideau@aucklan.ac.nz*

INTRODUCTION

The Dawson City landslide (also known as the Moosehide Slide) is a prehistoric slope failure that defines the northern limit of the town (Fig. 1). Based on an unpublished radiocarbon date from O.L. Hughes of the Geological Survey of Canada (see Brideau *et al.*, 2007a) the landslide occurred more than 1740 years before present (pre 200 A.D.). This part of western Yukon is located within the Beringia refugium (unglaciated for approximately 2.6 Ma; Duk-Rodkin, 1996; 1999; Froese *et al.*, 2000). The present continental climate consists of warm summers and cold winters. The climate normal record for Dawson City (1971-2000) gives an average annual air temperature of -4.4°C and an average total precipitation of 324 mm (Environment Canada, 2011). Dawson City lies within the zone of widespread but discontinuous permafrost (Natural Resources Canada, 1993).

The engineering geology and geomorphology of the landslide has been described by Brideau *et al.* (2007a,b). The slope failure is interpreted as having occurred at, or near the geological contact between serpentinite and underlying metasedimentary rocks. The contact regionally represents the overthrust of a sliver of oceanic crust (Slide Mountain terrane) onto a volcanic-arc assemblage (Yukon-Tanana terrane; Mortensen, 1988; Colpron, 2006) but has not been located in outcrop in the slide area. Cliffs in the headscarp and rock exposures of the unstable block above it reveal the presence of seven discontinuity sets which facilitated a pseudo-circular slope failure (Brideau *et al.*, 2007a).

During their initial investigation Brideau *et al.* (2007a,b) identified zones of potential ongoing slope instability in the headscarp and movement in the landslide deposit (Fig. 1). Tension cracks and split trees were observed upslope from the current headscarp and atop the landslide deposit. Monitoring stakes were installed and precisely

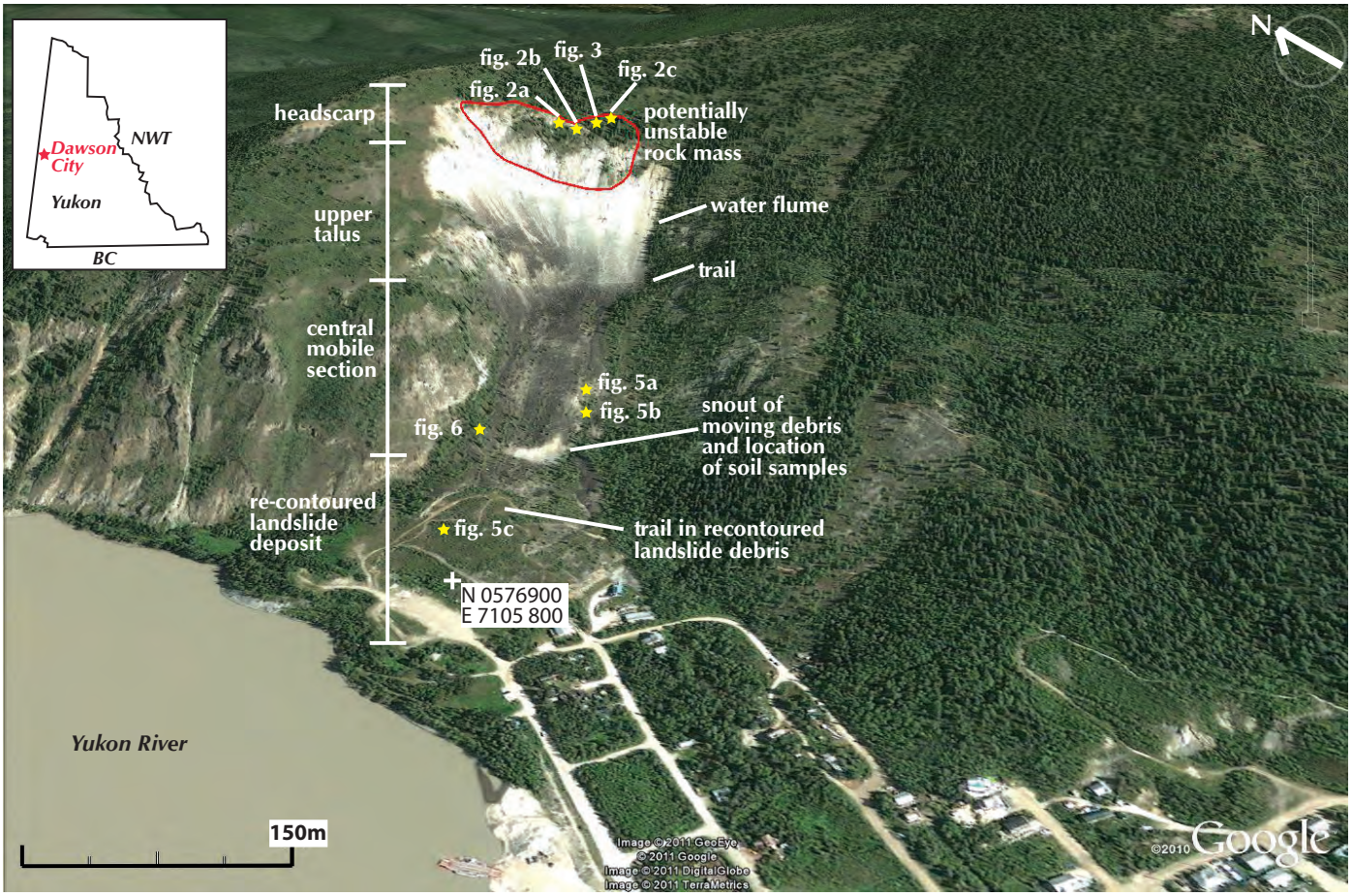

Figure 1. *Annotated oblique aerial view of the Dawson City landslide (Google Earth imagery; July 2010). Tension crack above the headscarp referred to in the text is outlined by the yellow stars denoting the location of figures 2, 3, 5 and 6.*

surveyed in 2006 (Brideau *et al.*, 2007b) to confirm and quantify subsequent displacements. The main focus of this paper is to present the displacement monitoring data collected during repeat surveys in 2009 and 2011. Also presented are additional soil property data and results of X-ray diffraction analysis on the silt and clay-sized particles from the snout of the slow-moving debris.

DISPLACEMENT MONITORING

HEADSCARP

Geomorphic evidence of ongoing movement (disturbed soil and vegetation) was identified by Brideau *et al.*, (2007a,b) along a tension crack approximately 200 m in length and upslope from the current headscarp (Fig. 1). Between this crack and the headscarp is an unstable rock mass. Assuming a length of 200 m, a width of 50 m, and a depth between 1 and 5 m, the volume of the unstable mass is between 10 000 and 50 000 m^3. It should be emphasized that the range in volume represents a first order approximation and further work is needed to refine the estimate. A number of trees located along this feature have had their trunks split (Fig. 2). One tree was photographed on four occasions between 2005 and 2011 and provides a time-series illustration of the movement along the tension crack over that period (Fig. 3). Several wooden and metal stakes were installed in 2006 to quantify the deformation rate. The displacement data presented in Figure 4 demonstrate that downslope movements of 4.3 to 11.9 cm/yr have occurred along a 40 m section of the tension crack.

LANDSLIDE DEPOSIT

The landslide deposit can be divided in three sections: the upper talus, the central moving section, and the lower re-contoured debris (Fig. 1). The upper talus represents the deposit of rockfall activity since the large prehistoric slope failure. The upper talus zone contains remnants of supports (carefully stacked, unmortared rock) for a flume that transported water (described in Tyrrell, 1910). Repeat aerial photographs document small debris avalanches between 1979 (National Air Photo Library A25131-76) and 1984 (National Air Photo Library A26718-97) that initiated from the headscarp and impacted the flume rock structure.

The central section of the deposit is currently moving. Evidence supporting this includes multiple geomorphic features such as shear zones (Figs. 5a. and 6), tension cracks oriented perpendicular to the direction of

Figure 2. *Split trees along the main tension crack located upslope from the current headscarp. See Figure 1 for the location.*

Figure 3. *Expanding split tree located along tension crack upslope from current headscarp. See Figure 1 for location. UTM 7 NAD 83 coordinates 0577496E, 7106020N.*

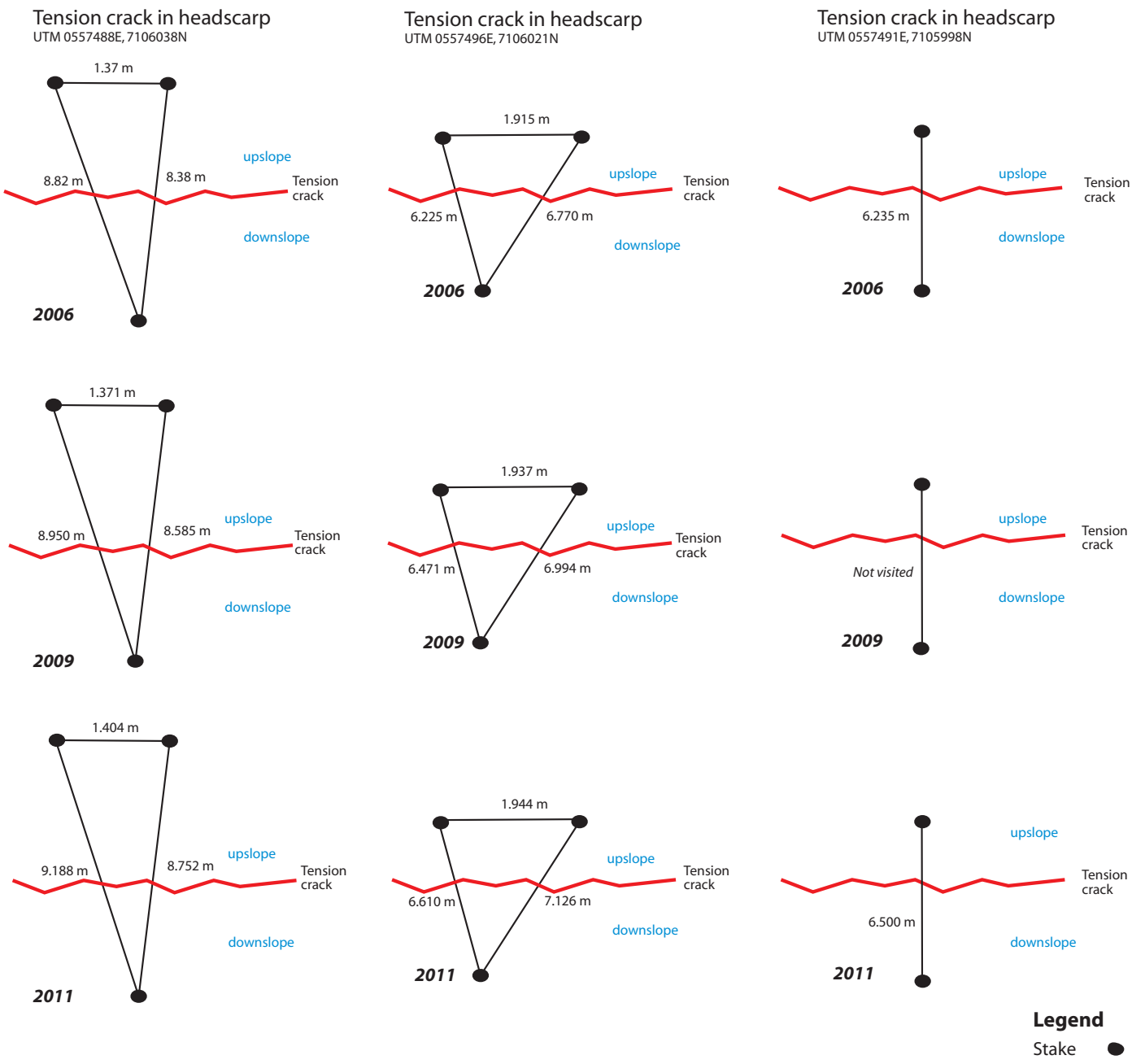

Figure 4. *Periodic measurement of displacement in arrays across tension cracks at the upslope edge of the unstable block (measurement at 3 sites). Jagged red line is approximate locus of tension crack.*

movement (Fig. 5b), and split trees (Fig. 6). In the western shear zone (Fig. 1), part of the trunk of a birch sapling was pulled from the main trunk by sliding downslope. The distance between the two parts of the tree was recorded in 2006, 2009 and 2011 (Fig. 6). Based upon the measurements the tension crack is opening at 8.5 to 20 cm/yr.

Field observations suggest that multiple sets of shear localization might be present in a shear zone at the western edge of the central portion of the debris. Geomorphic features observed in the field include several long (~100 m) linear zones with disturbed soil and vegetation. This means that the displacement values reported above might only account for part of the total movement. Brideau *et al.*, (2007a,b) discussed the

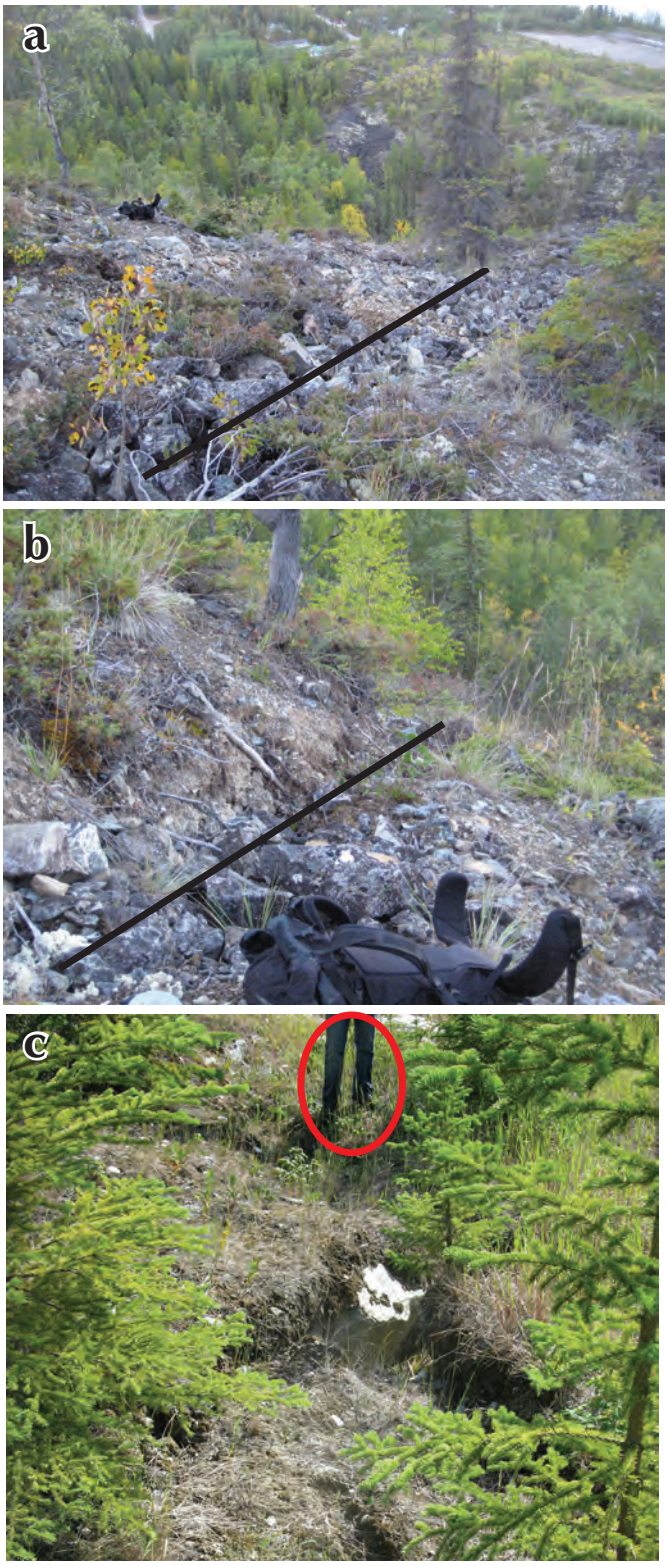

Figure 5. *Tension cracks observed in the* ***(a)*** *eastern shear zone,* ***(b)*** *upper landslide debris, and* ***(c)*** *re-contoured landslide debris. See Figure 1 for locations.*

possibility that this central moving section of the debris represents an earth flow or rock glacier.

The lower section of the deposit was re-contoured in the early 1980's after coarse aggregate had been quarried out. Observation of cracks in this area (Fig. 5c) during visits in 2009 and 2011 suggest that tensile deformation continues. A newly created walking trail is similarly affected. Although re-contouring decreased the average angle of slope, the base of the landslide deposit is creeping, or there is persistent instability within the deposit.

SOIL PROPERTIES AND XRD ANALYSIS

A soil sample was collected in 2011 from the steep scarp near the toe of the actively moving central section of the debris. The purpose was to supplement the geotechnical testing results presented in Brideau *et al.*, (2007b). A summary of the test results are presented in Table 1. The liquid and plastic limits represent the water content at which the sampled soil starts behaving as a liquid and plastic material respectively (Craig, 2004); the plasticity index represents the range of water content over which the soil behaves plastically, while the linear shrinkage represents the percent difference between the length of a sample at its liquid limit and when it is completely dry. The liquid and plastic limits testing was conducted according to the guidelines presented in ASTM (2010) while the linear shrinkage test followed NZS (1986). The plasticity index and liquid limit results indicate that the fine fraction of the deposit (<425 μm) has a high plasticity. By weight, the fine fraction represents approximately 2% of the samples. Brideau *et al.* (2007b) noted that the plasticity of their samples compared favourably to values reported by Bovis (1985) for earthflows in British Columbia. The 4% linear shrinkage value obtained in this study corresponds to a low shrink-swell potential (Holland and Richard, 1982).

An x-ray diffraction (XRD) analysis was conducted on the silt and clay-sized particles (<63 μm) of a sample collected from the snout of the slow moving part of the landslide deposit. The XRD analysis was undertaken to identify the types of clay present. The sample was brought into suspension using a sodium hexametaphosphate solution (4 g/L) to prevent the clay-size particles from flocculating. The clay mounts were then air dried on a thin glass slide, and scanned through the x-ray diffractometer. A peak analysis of the diffractogram was conducted against the ICDF powder database using the software Traces (GBC Scientific Equipment) and UPDSM (PSI international Inc.). Results of the analysis suggest the presence of talc, chrysotile, and lizardite.

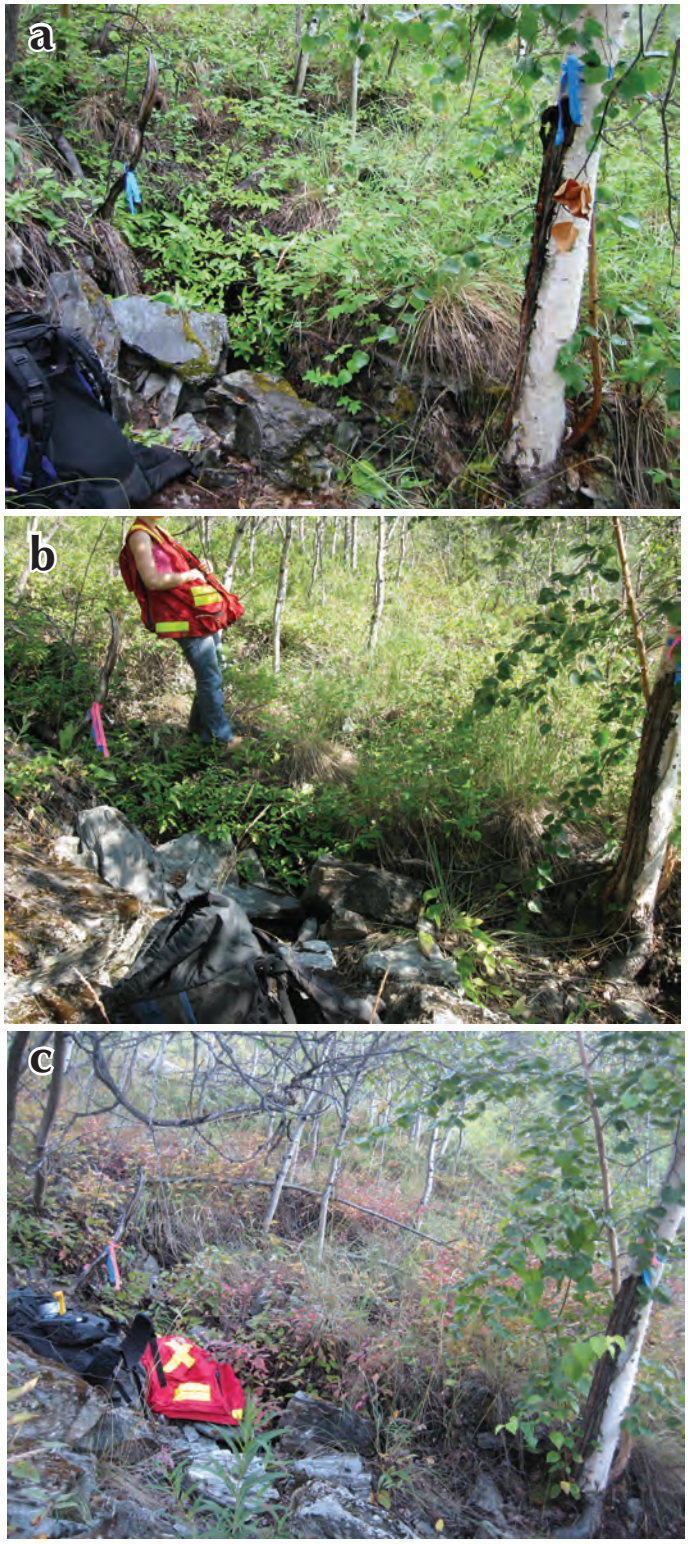

Figure 6. *Progressive separation of a split tree in the western shear zone of the moving landslide debris. See Figure 1 for location. UTM7 NAD83 coordinates 0577062E, 7105934N. The split of piece of trunk is on the left side of the photos, marked by a strip of blue (2006) or pink (2009, 2011) ribbon. The tree from which piece was split is at right.*

Table 1. *Summary of geotechnical properties for the soil fraction passing through a 425 µm sieve. Samples taken from the snout of the central actively moving section of the debris. See Figure 1 for location.*

	Sample A-2006	Sample B-2006	Sample 2011
Plastic limit (% water content)	35.7	37.2	44.5
Liquid limit (% water content)	79.1	65.7	64.9
Plasticity index (% water content)	43.4	28.5	20.4
Linear shrinkage (%)	NA	NA	4.0

DISCUSSION

Assuming a conservative measurement error of 1 cm, the data presented in this paper indicate displacements large enough to be outside the range of uncertainty and thus represent a true phenomenon. The duration of the displacement monitoring is, however, too limited to discuss trends, so we cannot currently quantify the risk associated with the unstable block in the headscarp area. Further monitoring should be used in conjunction with the progressive slope failure concept developed by Voight (1988; 1989) and Fukuzono (1990). This approach suggests that a log-normal plot of the inverse velocity *vs.* time since the monitoring was initiated can be used to estimate the time to failure which is represented by the x-axis intercept. This technique has been applied to open-pit and natural slope stability monitoring (Petley *et al.*, 2002; 2005; Crosta and Agliardi, 2003; Petley, 2004; Rose and Hungr, 2007).

Brideau *et al.*, (2007a,b) mapped a series of lineaments (tension cracks, trenches, ridges) over 200 m in length upslope from the present day headscarp. These features do not currently show evidence of movement, however all features observed and measured in this paper appear recent. It is unlikely that the displacement rates reported in this paper could be sustained for several decades without resulting in mass failure.

The average annual mean temperature between 1978 and 2007 appears to have increased >1°C for Dawson City (Fig. 7). This increase in mean annual temperature could have contributed to the renewed activity on the Dawson City landslide. It should be noted that the total annual precipitation does not appear to have changed significantly over that same period of time (Fig. 7).

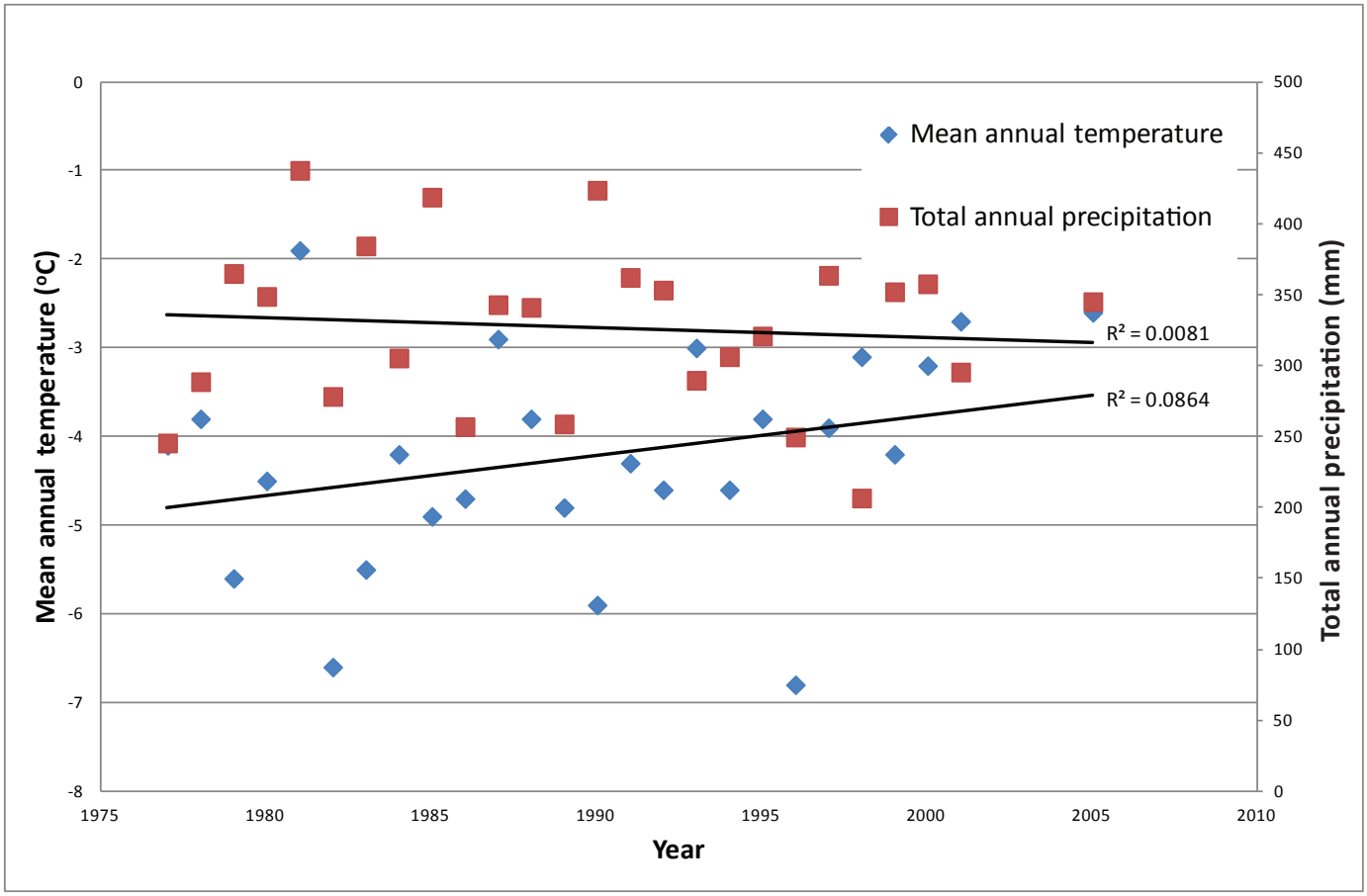

Figure 7. *Mean annual temperature and total annual precipitation at the Dawson City weather station (data from Environment Canada, 2011).*

Alternative mechanisms to explain the recent activity include progressive rock mass strength degradation (Guglielmi and Cappa, 2010), evolution stages of a large landslide (Zerathe and Lebourg, 2011) and stick-slip movement of the hillslope.

The new displacement values reported in this paper for the central section of the deposits (8.5-20 cm/yr) are greater than the initial value of 4.5 cm/yr estimated by Brideau *et al.* (2007b). This discrepancy is due to the assumption made by Brideau *et al.*, (2007b) that the tree had grown to its current size before being sheared off and as such the 4.5 cm/yr value represented a minimum displacement rate.

The DGPS station installed in 2006 in the deposit and listed in Brideau *et al.* (2007b) was intended to be resurveyed in 2011. Unfortunately only one metal rod could be located and it was out of the ground; this was attributed to the installed metal stakes being too short, smooth and thin for the coarse nature of the debris.

The survey markers are assumed to have subsided into the ground or to have been frost-jacked out of it. It is recommended that if the DGPS approach is attempted again longer and larger survey stakes be used.

CONCLUSIONS

The results presented in the paper confirm that sections upslope from the headscarp and in the landslide debris are actively moving. Based upon five years (2006-2011) of displacement monitoring data, the unstable section in the headscarp is moving downslope at a rate of 4.3 to 11.9 cm/yr whereas the lower part of the landslide deposit is moving at a rate of 8.5 to 20 cm/yr. At this point the displacement time-series is too short to identify trends and continuing displacement monitoring is recommended.

Soil laboratory testing has determined that the fine soil fraction from samples of the snout in the central mobile section of the debris has high plasticity and low linear

shrinkage values. XRD analysis of the mineralogy of the silt and clay-size particles of the component of the debris suggests the presence of talc, chrysotile, and lizardite.

ACKNOWLEDGMENTS

Over the years many people contributed in various capacities to this project. The authors would like to acknowledge the input from J. Orwin, P. VonGaza, K. Fecova, V. Stevens, E. Trochim, E. Fea, G. Patton, A. Wolter and T. Linnell. The first author would also like to thank J. Wilmshurst and P. Black for their help with the XRD analysis. This research was supported by the Northern Scientific Training Program, Natural Science and Engineering Research Council of Canada, and Yukon Geological Survey.

REFERENCES

ASTM, 2010. Standard Test Methods for Liquid Limit, Plastic Limit, and Plasticity Index of Soils, Annual Book of ASTM Standards: Volume 4 - Construction Section 8 Soil and Rock (I). American Society for Testing and Materials, D 4318-10.

Bovis, M.J., 1985. Earthflows in the Interior Plateau, southwest British Columbia. Canadian Geotechnical Journal, vol. 22, p. 313-334.

Brideau, M.-A., Stead, D., Roots, C., and Orwin, J., 2007a. Geomorphology and engineering geology of a landslide in ultramafic rocks, Dawson City, Yukon. Engineering Geology vol. 89, p. 171-194.

Brideau, M.-A., Stead, D., Stevens, V., Roots, C., Lipovsky, P., and VonGaza, P., 2007b. The Dawson City landslide (Dawson map area, NTS 116B/3), central Yukon. *In:* Yukon Exploration and Geology 2006, Emond, D.S., Lewis, L.L., and Weston, L.H. (Eds.), Yukon Geological Survey, Whitehorse, Yukon, p. 123-137.

Colpron, M. (compiler), 2006. Tectonic assemblage map of Yukon-Tanana and related terranes in Yukon and northern British Columbia (1:1 000 000 scale). Yukon Geological Survey, Open File 2006-1.

Craig, R.F., 2004. Craig's soil mechanics 7th Edition. Spon Press, 447 p.

Crosta, G.B. and Agliardi, F., 2003. Failure forecast of large rock slides by surface displacement measurements. Canadian Geotechnical Journal vol. 40, p. 176-191.

Duk-Rodkin, A., 1999. Glacial limits map of Yukon Territory. Geological Survey of Canada Open File 3694, scale 1:1 000 000.

Duk-Rodkin, A., 1996. Surficial geology, Dawson, Yukon Territory. Geological Survey of Canada Open File 3288, scale 1:250 000.

Environment Canada, 2011. National Climate Data and Information Archive, http://climate.weatheroffice.gc.ca/climateData/canada_e.html, accessed October 30, 2011.

Froese, D.G., Barendregt, R.W., Enkin, R.J., and Baker, J., 2000. Paleomagnetic evidence for multiple Late Pliocene - Early Pleistocene glaciations in the Klondike area, Yukon Territory. Canadian Journal of Earth Sciences, vol. 37, p. 863-877.

Fukuzono, T., 1990. Recent studies on time prediction of slope failure. Landslides News, vol. 4, p. 9-12.

Guglielmi, Y. and Cappa, F., 2010. Regional-scale relief evolution and large landslides: Insights from geomechanical analyses in the Tinee Valley (southern French Alps). Geomorphology, vol. 117, p. 121-129.

Holland, J.E. and Richards, J., 1982. Road pavements on expansive clays. Australian Road Research, vol. 12, p. 173-179.

Mortensen, J.K., 1988. Geology of southwestern Dawson map area, Yukon Territory. Geological Survey of Canada, Current Research, 88-1E, p. 73-78.

NZS, 1986. Test 2.6 Determination of the linear shrinkage, New Zealand Standards, Methods of testing soils for civil engineering purposes, NZS 4402:1986.

Natural Resources Canada, 1993. Canada-Permafrost [map]. Fifth Edition, National Atlas of Canada.

Petley, D.N., 2004. The evolution of slope failures: Mechanisms of rupture propagation. Natural Hazards and Earth System Sciences, vol. 4, p. 147-152.

Petley, D.N., Bulmer, M.H., and Murphy, W., 2002. Patterns of movement in rotational and translational landslides. Geology, vol. 30, p. 719-722.

Petley, D.N., Mantovani, F., Bulmer, M.H., and Zannoni, A., 2005. The use of surface monitoring data for the interpretation of landslide movement patterns. Geomorphology, vol. 66, p. 133-147.

Rose, N.D. and Hungr, O., 2007. Forecasting potential rock slope failure in open pit mines using the inverse-velocity method. International Journal of Rock Mechanics & Mining Sciences, vol., 44, p. 308-320.

Tyrrell, J.B., 1910. "Rock glaciers" or chrystocrenes. Journal of Geology, vol. 18, p. 549-553.

Voight, B., 1988. A method for prediction of volcanic eruptions. Nature, vol. 332, p. 125-130.

Voight, B., 1989. Material science law applies to time forecasts of slope failure. Landslide News, vol. 3, p. 8-10.

Zerathe, S. and Lebourg, T., 2011. Evolution stages of large deep-seated landslides at the front of a subalpine meridional chain (Maritime-Alps, France). Geomorphology, doi:10.1016/j.geomorph.2011.10.006.

Preliminary observations on the geology of the Rackla belt, Mount Ferrell map area (NTS 106C/3), central Yukon

Maurice Colpron[1]
Yukon Geological Survey, Whitehorse, YT

Colpron, M., 2012. Preliminary observations on the geology of the Rackla belt, Mount Ferrell map area (NTS 106C/3), central Yukon. *In:* Yukon Exploration and Geology 2011, K.E. MacFarlane and P.J. Sack (eds.), Yukon Geological Survey, p. 27-43.

ABSTRACT

The Mount Ferrell area straddles the Paleozoic platform-basin transition at the northern edge of Selwyn basin and the structural corridor of the Dawson thrust, a geological and metallogenic belt informally referred to as the Rackla belt. Main facies and structural domains are delimited by the Kathleen Lakes and Dawson faults. Paleozoic platformal rocks occur north of the Kathleen Lakes fault; their coeval slope deposits are bound by the Kathleen Lakes and Dawson thrust. Strata of Selwyn basin (Hyland Group) and overlying mid-Paleozoic Earn and Tsichu groups occur in the hanging wall of the Dawson thrust. Igneous rocks of probable Paleozoic age are restricted to the Dawson thrust zone. The Rackla belt is actively being explored for gold and silver occurrences, including possible Carlin-type gold mineralization, and has potential for base metal deposits.

[1] *maurice.colpron@gov.yk.ca*

INTRODUCTION

The 2008-2010 discoveries of gold mineralization, and particularly of potential Carlin-type carbonate replacement mineralization by ATAC Resources Ltd. in southern Nash Creek (106D) and Nadaleen River (106C) map areas has led to claim staking and intensive exploration activities in this part of central Yukon (Fig. 1). The new discoveries occur in carbonate rocks in the vicinity of the Dawson thrust, a WNW-striking structure that marks the northern edge of Selwyn basin (Abbott, 1997)(Fig. 2). The region is informally referred to as the Rackla belt.

Published bedrock maps for this region are primarily limited to 1:250 000 scale reconnaissance maps by Green (1972, for Nash Creek [106D]) and Blusson (1974, for Nadaleen River [106C]), with exception of the Mount Westman area (106D/1) which was mapped at 1:50 000 scale by Abbott (1990a; Fig. 2). In 2010, the Yukon Geological Survey initiated a regional mapping program of the Rackla belt in order to improve the geoscience knowledge of the area, and to provide the regional structural and stratigraphic context for mineralization along this belt. Results of mapping in the Mount Mervyn area (106C/4) in 2010 were presented by Chakungal and Bennett (2011). The present report summarizes observations made in the adjacent Mount Ferrell area (106C/3) during the summer 2011; it is companion to a 1:50 000 scale Open File map (Colpron, 2012). The goal for 2012 is to complete mapping of the Rackla belt to the east into southwest Bonnet Plume Lake map area (106B; Fig. 2) and produce a compilation of all 1:50 000 scale maps along the belt.

GEOLOGICAL FRAMEWORK

The Mount Ferrell area straddles the platform to basin transition at the northern edge of Selwyn basin (Figs. 2 and 3). The main facies belt and stratigraphic successions in the area are bounded by the Kathleen Lakes fault and the Dawson thrust (Figs. 3 and 4). Paleozoic carbonate assigned to the Bouvette Formation (Gordey and Makepeace, 1999; Morrow, 1999) occupies the northern part of the map area and overlies local exposures of Hyland Group (Fig. 4). The carbonate rocks form part of the Mackenzie platform in the southern Wernecke Mountains. The Paleozoic platform rocks are bound to the south by the Kathleen Lakes fault (Figs. 3 and 4).

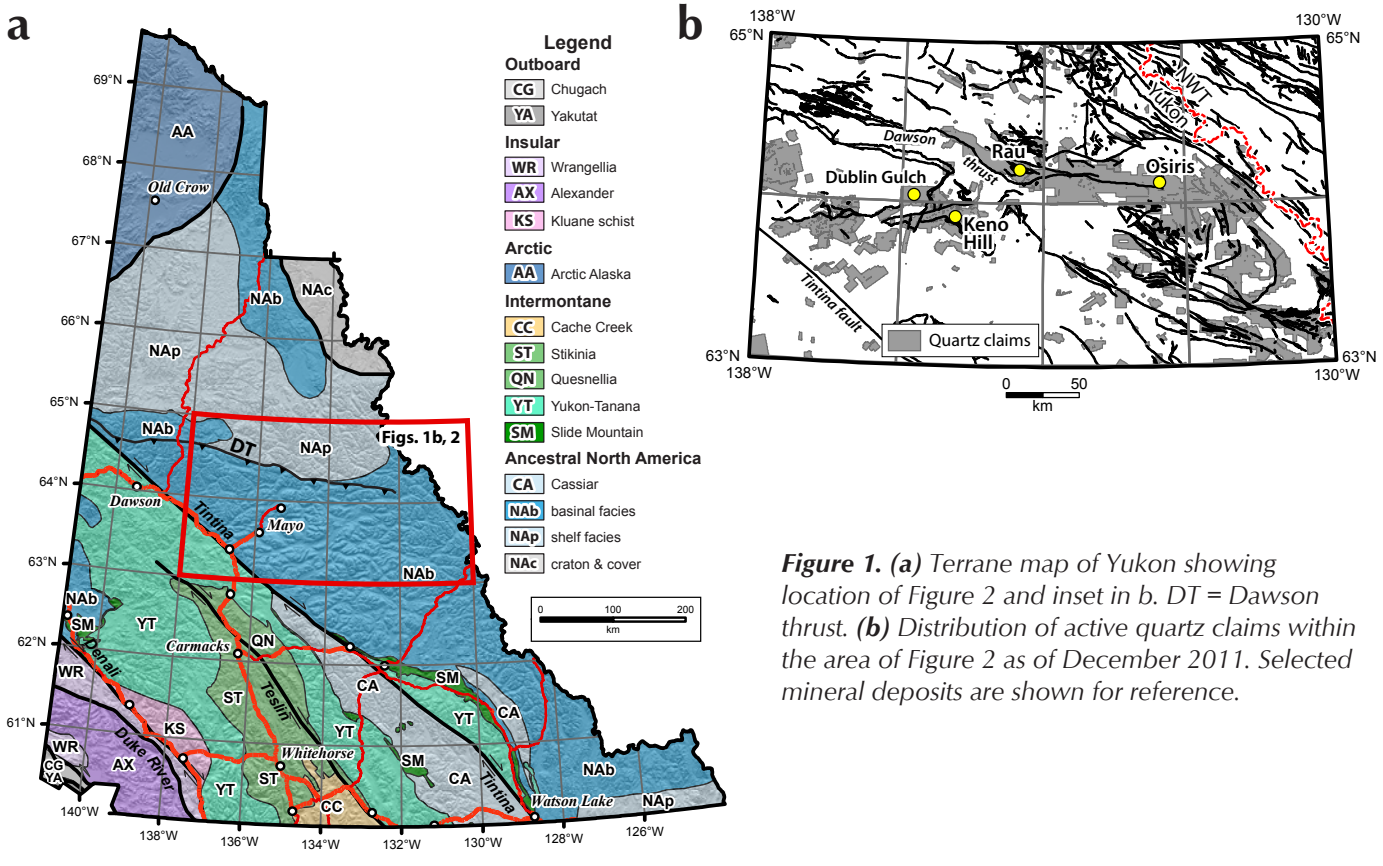

Figure 1. ***(a)*** *Terrane map of Yukon showing location of Figure 2 and inset in b. DT = Dawson thrust.* ***(b)*** *Distribution of active quartz claims within the area of Figure 2 as of December 2011. Selected mineral deposits are shown for reference.*

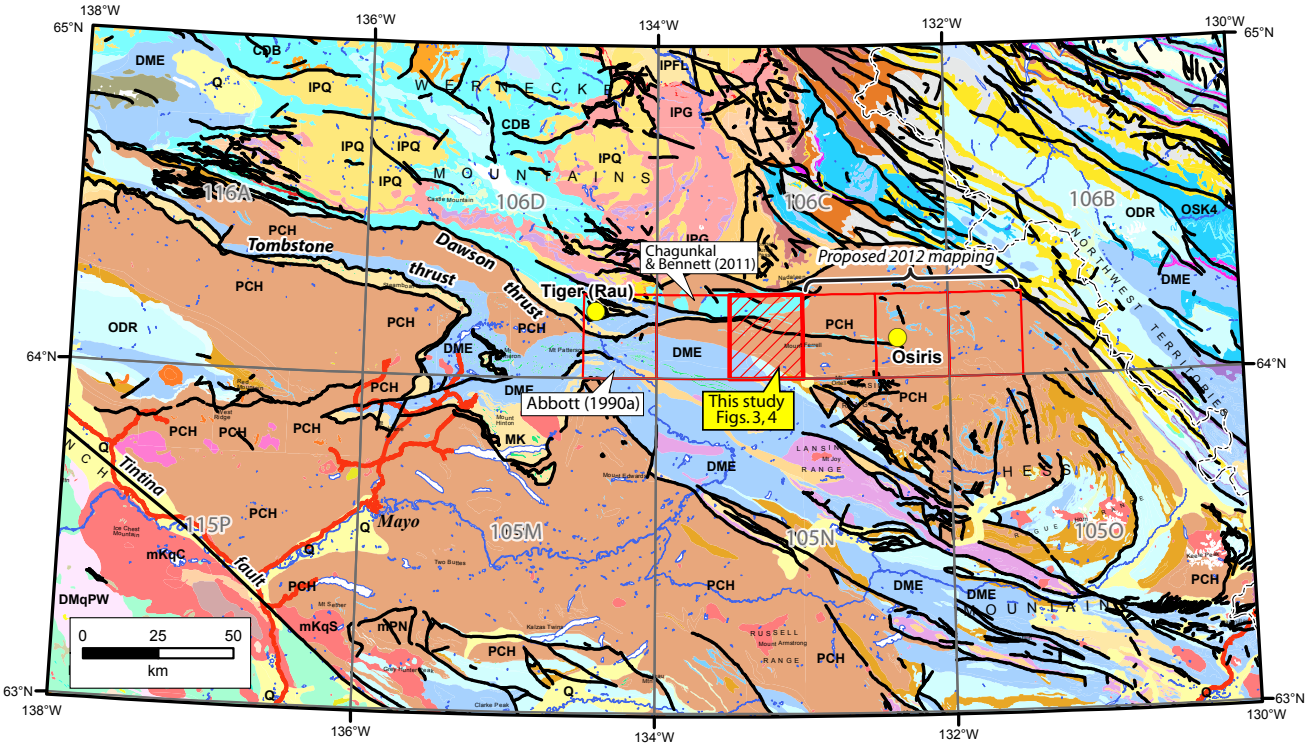

Figure 2. *Regional geology of the northern part of Selwyn basin (after Gordey and Makepeace, 1999) showing location of major mineral occurrences and of existing and proposed detailed geological mapping along the Rackla belt. Major map units along the Rackla belt include: CDB – Bouvette Formation; DME – Earn Group; ODR – Road River Group; PCH – Hyland Group. For complete legend and unit information refer to Gordey and Makepeace (1999, 2000).*

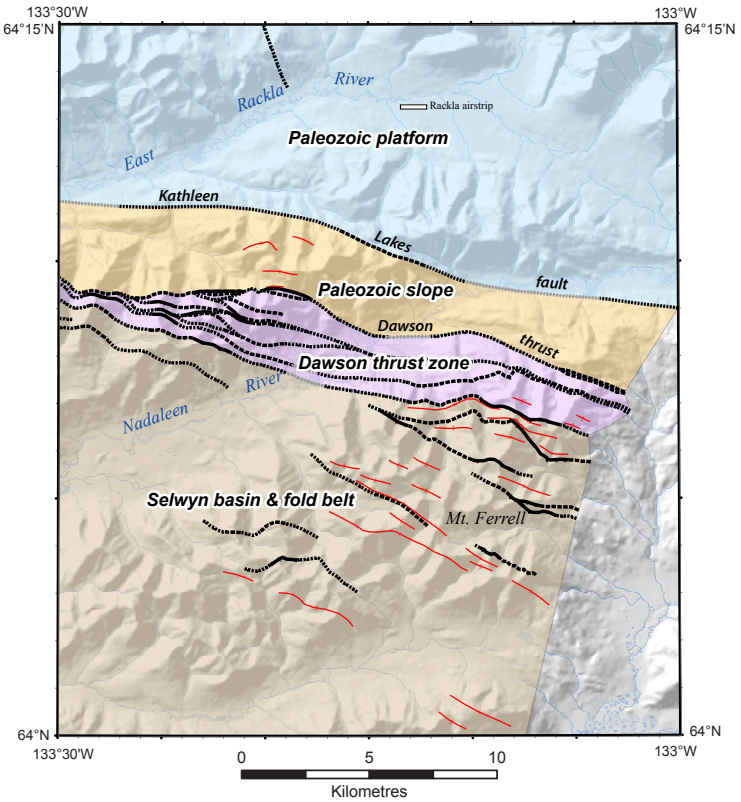

Figure 3. *Geological framework of the Mount Ferrell area (106C/3).*

South of the Kathleen Lakes fault, black shale with minor chert and carbonate debris-flow horizons represent Paleozoic slope to basinal clastic deposition and were assigned to the Road River Group by Blusson (1974)(Figs. 3 and 4). These rocks are bound to the south by the Dawson thrust.

Rocks in the hanging wall of the Dawson thrust to the south are primarily coarse sandstone, shale and carbonate rocks of the Neoproterozoic to Lower Cambrian Hyland Group, the oldest unit in Selwyn basin (Figs. 3 and 4). These are unconformably overlain to the south by Devonian and Mississippian rocks of the Earn and Tsichu groups (Fig. 4). Igneous rocks of inferred Paleozoic age occur exclusively in the Dawson thrust zone.

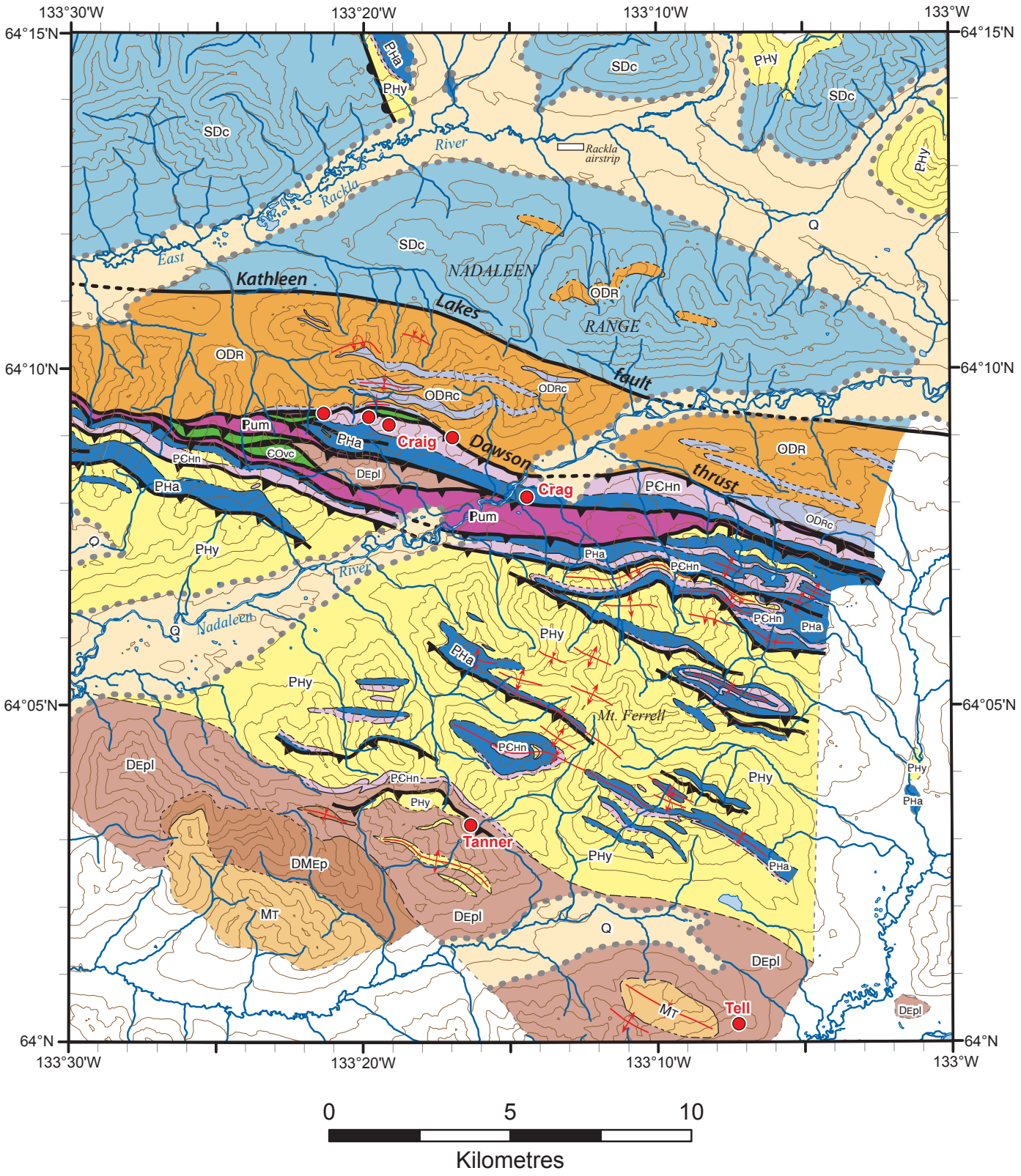

Figure 4. *Simplified geological map of the Mount Ferrell area (106C/3)(after Colpron, 2012). Geology north of the East Rackla River is mostly after Blusson (1974).*

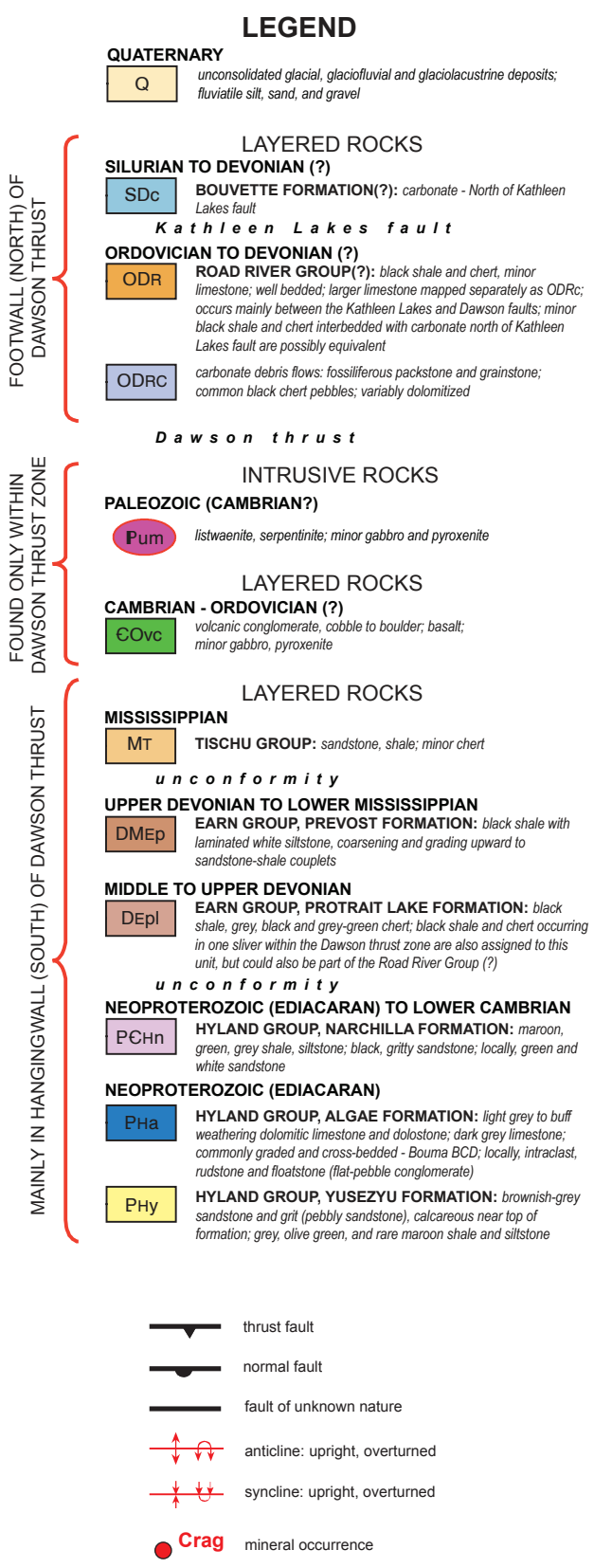

Figure 4 con'd

STRATIGRAPHY

PALEOZOIC PLATFORM

North of the Kathleen Lakes fault, the Mount Ferrell area is predominantly underlain by variably dolomitized carbonate rocks (Fig. 4). South of the East Rackla River these consist of light grey to yellowish-buff weathering dolostone and dolomitic limestone with common black chert nodules (Fig. 5a). The carbonate comprises mainly crudely bedded to massive fossiliferous wackestone to grainstone (Fig. 5b), with bed thickness ranging from 10-60 cm. Planar laminations are locally apparent. Fossil fragments include crinoids, echinoderms, colonial and solitary (rugose) corals. Local horizons of fossiliferous rudstone comprise a similar fossil assemblage but also contain black chert clasts up to 3 cm long. Coral bioherms are mainly developed at the crest of the Nadaleen Range, near the Kathleen Lakes fault, where they form cliffs (Fig. 5c,d). Chert locally make up beds up to 10-20 cm thick within dolostone, grading into intercalation of black argillite and chert, generally less than 5 m thick, but locally up to 75 m thick (labeled ODR in Fig. 4).

Limited observations north of the East Rackla River in 2011 indicate that much of the carbonate sequence in this region consist of generally finer grained, well-bedded micritic dolostone and dolomitic limestone capped by cliff-forming bioherms (Fig. 5e). Paleozoic carbonates unconformably overlie rocks of the Hyland Group in this region (Blusson, 1974; Fig. 4).

The carbonate rocks north of the Kathleen Lakes fault are assigned to the Cambrian-Devonian Bouvette Formation (Morrow, 1999; Gordey and Makepeace, 2000). Fossiliferous carbonates in the Mount Westman area to the west (106D/1) yielded Silurian and Devonian corals (Poulton *et al.*, 1999). Based on similar lithologies and fossils, carbonates in northern Mount Ferrell area (Fig. 4) are inferred to be Silurian-Devonian. However, occurrences of an Early Permian conodont fauna in carbonate from the intervening Mount Mervyn area (106C/4; Abbott and Orchard *in* Chakungal and Bennett, 2011) suggest that rocks in north Mount Ferrell could be this young as well.

Carbonate strata in the northern part of the Mount Ferrell area are generally gently folded north of the East Rackla River, with folds becoming tighter to the south near the Kathleen Lakes fault.

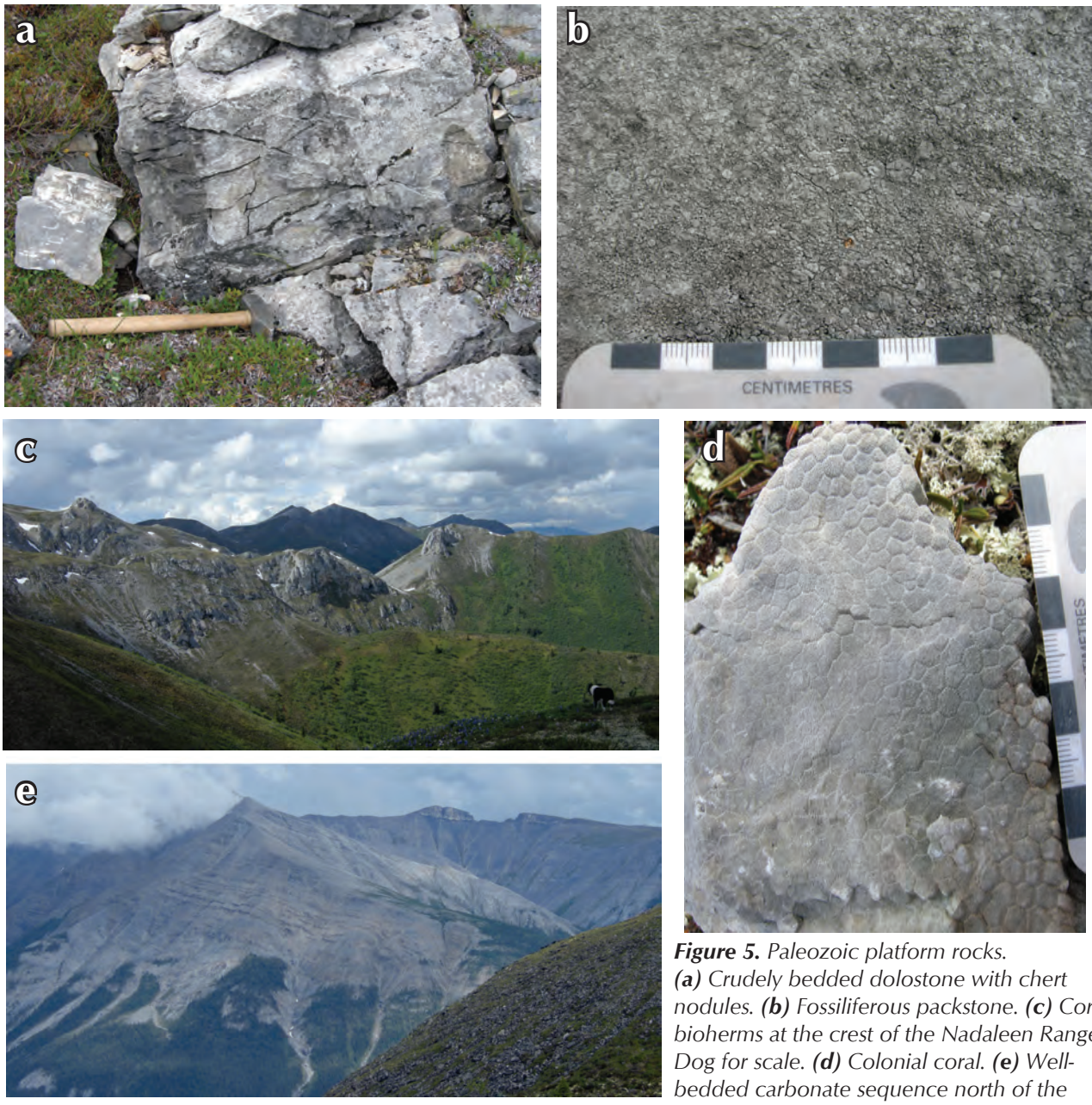

Figure 5. *Paleozoic platform rocks.* ***(a)*** *Crudely bedded dolostone with chert nodules.* ***(b)*** *Fossiliferous packstone.* ***(c)*** *Coral bioherms at the crest of the Nadaleen Range. Dog for scale.* ***(d)*** *Colonial coral.* ***(e)*** *Well-bedded carbonate sequence north of the East Rackla River. The distinct cliff along the background ridge is a coral bioherm.*

PALEOZOIC SLOPE DEPOSITS

The structural panel between the Kathleen Lakes fault and the Dawson thrust comprises a succession of tightly folded black shale and chert, with discontinuous light grey carbonate horizons (Fig. 6a). Chert occurs in beds up to 1 m thick and forms horizons up to 10-20 m within black shale (Fig. 6b). Chert represents approximately 20-30% of the black shale and chert unit.

Carbonate rocks occur as beds 5 cm to 1 m thick within the black shale (Fig. 6c). The carbonate rocks range from light grey weathering limestone and dolomitic limestone, to buff weathering, variably recrystallized dolostone. It is commonly associated with irregular chert bands up to 10 cm thick. Sections with more than 80% carbonate are up to 20-30 m thick and laterally discontinuous; they commonly have greater apparent thickness due to tight folding and dip slope exposures (Fig. 6a,c). The carbonate is typically a skeletal grainstone to rudstone with coral and crinoid fragments, and pebbles of chert, limestone and shale (Fig. 6d,e). It is commonly normally graded and planar laminated (Fig. 6e). These rocks are interpreted as carbonate debris flows emplaced in a slope environment. The similarity in lithologic types and fossil assemblages suggests that these debris flows may be derived from

platform carbonates like those exposed north of the Kathleen Lakes fault (Fig. 4). Correspondingly, minor black shale and chert intercalated with platform carbonates to the north are likely interfingering of slope deposits at the platform margin.

Blusson (1974) assigned the black shale-dominated sequence to the Ordovician-Devonian Road River Group; a reasonable interpretation pending better biostratigraphic control based on 2011 collections (Fig. 4). This map unit was omitted in the compilation of Gordey and Makepeace (1999; Fig. 2).

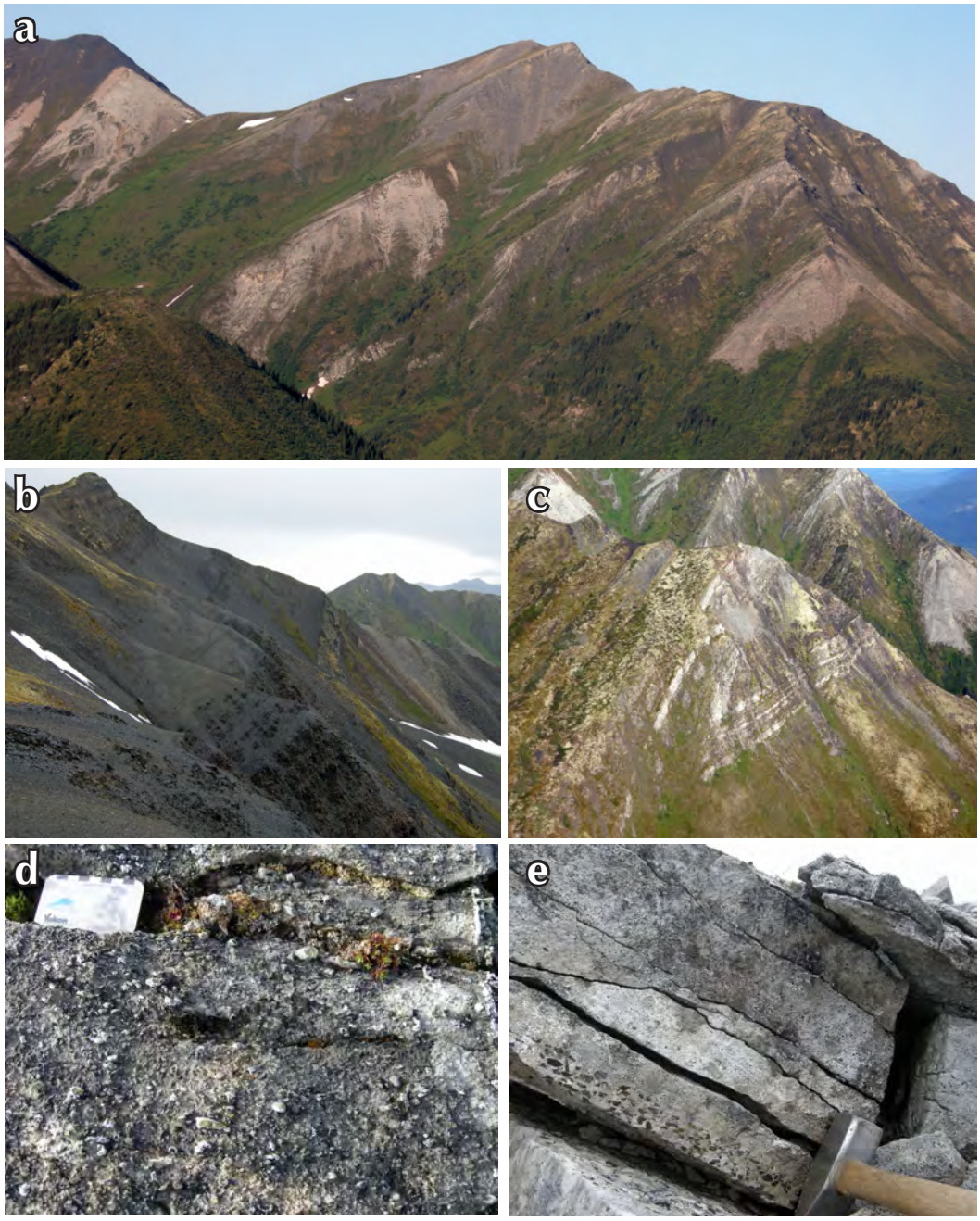

Figure 6. *Paleozoic slope deposits.* ***(a)*** *Intercalated black shale and chert (ODR), and discontinuous carbonate (ODRc).* ***(b)*** *Black shale (recessive) and chert (more resistant, at break in slope) of the Road River Group.* ***(c)*** *Tightly folded carbonate beds up to 1 m thick interbedded with black shale.* ***(d)*** *Fossiliferous packstone typical of carbonate in the slope facies.* ***(e)*** *Base of carbonate bed outlined by black chert pebbles. Chert pebbles are particularly evident due to strong dolomitization of fossil fragments in this outcrop.*

HYLAND GROUP

Rocks of the Hyland Group occur primarily in the central part of the Mount Ferrell area, in the hanging wall of the Dawson thrust, but also in valleys below the platform carbonate north of the East Rackla River (Figs. 2 and 4; Blusson, 1974). The Hyland Group is subdivided into three formations: 1) Neoproterozoic Yusezyu Formation, comprising mainly coarse clastic rocks; 2) carbonate of the Neoproterozoic Algae Formation; and 3) Neoproterozoic-Lower Cambrian Narchilla Formation, characterized by maroon shale (Gordey and Anderson, 1993; Cecile, 2000; Figs. 4 and 7a).

The Yusezyu Formation comprises mainly brown weathering sandstone and shale. The sandstone is brownish-grey, dark grey, or greenish-grey on fresh surfaces. It is fine to coarse grained, commonly "gritty" (granules to pebbles in a medium to coarse sand matrix; Fig. 7b), and generally poorly sorted and immature. It is generally well-bedded, with bed thickness up to 0.5-2 m, and locally displays rhythmic and graded bedding, loads and flute casts, and slump folds; sedimentary structures consistent with deposition in a submarine fan environment (Gordey and Anderson, 1993). Quartz is the most important detrital mode clast in Yusezyu sandstones, but feldspar, muscovite (and locally biotite), shale chips and more rarely carbonate clasts are also common. Limonite clasts are also locally common (Fig. 7b). The sandstone is locally calcareous, most notably near the top of the formation where it grades into carbonate of the Algae Formation.

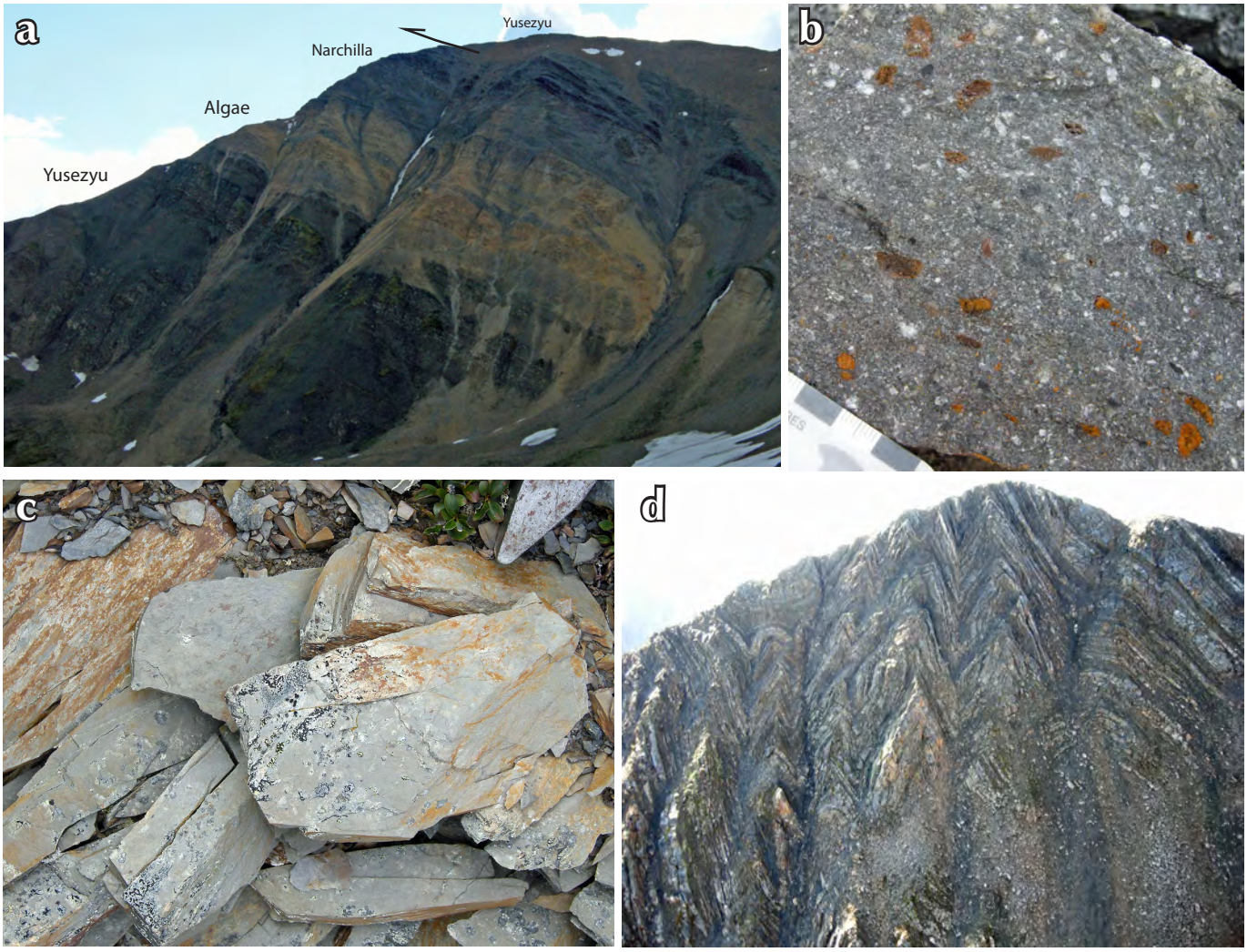

Figure 7. *Hyland Group.* ***(a)*** *Section of Hyland Group north of Mount Ferrell displaying the three main units. The Yusezyu Formation is repeated by a thrust fault at the top of the ridge.* ***(b)*** *Typical gritty sandstone of the Yusezyu Formation. Note shale chips and limonite clasts.* ***(c)*** *Brown-weathering, greenish-grey shale of the Yusezyu Formation.* ***(d)*** *Tightly folded, intercalated shale and sandstone of the Yusezyu Formation.*

Figure 7 con'd. ***(e)*** *Well-bedded, yellowish-buff weathering, dolomitic limestone of the Algae Formation.* ***(f)*** *Cross-bedding and planar laminations in dolomitic limestone of the Algae Formation.* ***(g)*** *Limestone breccia (floatstone), Algae Formation.* ***(h)*** *Flat-pebble, intraclast conglomerate (rudstone), Algae Formation.* ***(i)*** *Maroon shale of the Narchilla Formation.*

The sandstone and grit of the Yusezyu Formation are intercalated with grey, brown, olive green and locally maroon shale (Fig. 7c,d). Shale interbeds in sandstone are typically less than 40 cm thick, although shale-dominated sections up to 50-70 m occur. Dolomitic limestone beds less than 40 cm thick are locally present within the grey shale.

Carbonate of the Algae Formation is typically a light grey to yellowish-buff weathering, medium to dark grey dolomitic limestone (Fig. 7a,e). Gordey and Anderson (1993) considered this limestone as the uppermost member of the Yusezyu Formation. Cecile (2000) separated it out and elevated it to formation status. The limestone is well-bedded, with bed thicknesses varying from 1-20 cm, and intercalated with grey and green shale horizons up to 3 cm thick (Fig. 7e). Locally, dark grey chert nodules are present in the limestone. The dolomitic limestone is typically sandy to locally gritty, and commonly displays planar laminations, cross-bedding, flute casts, and locally graded beds (Fig. 7f). Intraclast conglomerate and breccia (rudstone and locally floatstone; Fig. 7g), including flat-pebble conglomerate (Fig. 7h), are made up of limestone clasts 1-10 cm long and typically occur in horizons 20-40 cm thick, but locally several metres thick.

Carbonate in the northernmost thrust slice of the Dawson thrust zone comprises a black silty limestone intercalated with dark grey to black shale. It is assigned to the Algae Formation because it appears gradational with shale and sandstone of the Narchilla Formation to the north (Fig. 4). The black limestone is typically finely laminated and locally cross-bedded, and occurs in beds 1-10 cm thick. This limestone is associated with, and locally hosts, mineralization at the Craig/Crag occurrences; it is usually strongly dolomitized and/or silicified where associated with mineralization.

The Algae Formation passes gradationally upward into maroon, green, and lesser grey and black shale of the Narchilla Formation (Fig. 7i). Although the Narchilla Formation is typically dominated by shale, it also includes white, greenish-grey and black siltstone to fine and medium-grained sandstone. Millimetre to 3 cm-thick, graded horizons of light grey siltstone and fine sandstone typically outline bedding in the Narchilla Formation. Greenish-grey and black sandstone is usually coarser-grained, locally gritty, and locally forms beds 40 cm to 2 m thick. Regionally, the Narchilla Formation is assigned an upper Neoproterozoic to Lower Cambrian age based on occurrence of the trace fossil *Oldhamia* sp. (Gordey and Anderson, 1993; Cecile, 2000); no trace fossils were observed in the Mount Ferrell area. It should also be noted that stratigraphic relationships between the Algae and Narchilla formations in the Mount Ferrell area are somewhat different than those described from their type sections (Cecile, 2000; Gordey and Anderson, 1993). In the Mount Ferrell area, maroon shale typical of the Narchilla Formation locally occurs stratigraphically below or within dolomitic limestone of the Algae Formation (Fig. 4); further stratigraphic studies are required to better characterize these relationships.

IGNEOUS ROCKS IN DAWSON THRUST ZONE

Occurrences of igneous rocks in the Mount Ferrell area are restricted to the Dawson thrust zone (Figs. 3 and 4). They are most prominently represented by altered ultramafic rocks (serpentinite and listwaenite; Fig. 8a), but also include gabbro sills and dikes (Fig. 8b), and fault-bounded slivers of mafic volcanic rocks (Fig. 8c,d).

Dikes and sills of gabbro (and lesser diorite) 1-3 m-wide intrude carbonate and shale in both footwall and hanging wall of the Dawson thrust. The gabbro is typically beige-weathering, black in fresh surface, and fine to medium-grained (Fig. 8b). It is locally pyroxene-phyric and weakly foliated. In the hanging wall of the Dawson thrust, gabbro dikes are spatially associated with serpentinite occurrences.

Ultramafic rocks were previously described by Tempelman-Kluit (1981) and Jutras (2003). They include serpentinite and more strongly altered listwaenite. The listwaenite is bright orange-weathering and the most distinctive rock unit in the Mount Ferrell area (Fig. 8a). It occurs within several fault-bounded panels in the Dawson thrust zone, the most prominent reaching up to ~1 km in width and extending laterally across the entire map area (Figs. 4, 8a). The listwaenite is a strongly carbonate and silica-altered ultramafic rock, locally containing traces of bright green chrome mica (fuschite). The rock is massive to strongly foliated and locally associated with serpentinite. The serpentinite is bottle green to black, composed mainly of antigorite and anthophyllite, strongly sheared, and occurs as pods within or along the margin of the more resistant listwaenite. Serpentinite is most common in the western part of the Mount Ferrell area, and the adjacent Mount Mervyn area (Chakungal and Bennett, 2011). Relict igneous textures in least altered exposures of ultramafic rocks suggest they may be derived from pyroxenite sills or dikes.

Figure 8. *Igneous rocks associated with the Dawson thrust zone.* ***(a)*** *Looking southwest at orange-weathering listwaenite within the Dawson thrust zone. The foreground vegetated slope is underlain by Paleozoic carbonate debris flow deposits (unit ODRc in Fig. 4). Background peaks are underlain by carbonate, shale, and sandstone of the Neoproterozoic to Lower Cambrian Hyland Group. The trace of the Dawson thrust is located in the notch in front of the listwaenite body.* ***(b)*** *Close-up of fresh and weathered surface of medium-grained gabbro in the footwall of the Dawson thrust. Hammer handle for scale.* ***(c)*** *Pillow basalt in the hanging wall of the Dawson thrust.* ***(d)*** *Volcanic breccia.*

Volcanic rocks include pillow basalt (Fig. 8c), and volcanic conglomerate and breccia (Fig. 8d). Pillow basalt is restricted to a single fault sliver in the immediate hanging wall of the Dawson thrust, near the Craig mineral occurrences (Fig. 4). It is a fine-grained, hornblende-phyric, vesicular basalt, with flattened pillows up to 30 cm long (Fig. 8c). Interpillow material includes hyaloclastite, green argillite, and local brown carbonate alteration. The volcanic conglomerate is brownish-green and composed mainly of pebbles and cobbles of mafic to intermediate volcanic rocks, locally plagioclase-phyric, but also including pebbles of brown-weathering dolostone and white quartz. The volcanic conglomerate is intercalated with brown-weathering, green shale with minor white quartz sandstone bands less than 1 cm thick.

The age of igneous rocks in the Mount Ferrell area is not precisely known. They are probably Paleozoic, but some dikes could also be Mesozoic. Abbott (1997) reports early (Cambrian?) and late Paleozoic ages (Permian?) from mafic and ultramafic dikes and sills in the vicinity of the Dawson thrust in the Upper Hart River area to the west (116A, Fig. 2). He also describes mafic volcanic rocks of Cambrian, Ordovician, and Silurian ages. Similarly, mafic volcanic rocks are intercalated with Silurian carbonate at the Tiger deposit, north of the Dawson thrust in the Mount Westman area (106D/1; Abbott, 1990a; M. Dumala, pers. comm., 2011). Triassic gabbro and diorite sills intrude mainly Earn Group strata to the south and west (Abbott, 1990a,b; 1997; Chakungal and Bennett, 2011; Roots, 1997; 2003). Finally, Cretaceous intrusions are widespread to the south in Selwyn basin (Gordey and Makepeace, 1999; 2000); some of the dikes in Mount Ferrell area could be related to Cretaceous magmatism as well. To date, Late Cretaceous magmatism has only been documented at one locality along the Rackla belt, in the vicinity of the Tiger deposit in southeast Nash Creek map area (106D, Fig. 2; Kingston *et al.*, 2010; V. Bennett, pers. comm., 2011).

EARN GROUP

Strata of the Earn Group unconformably overlie the Hyland Group south of Nadaleen River in the Mount Ferrell area (Fig. 4). The lower part of the Earn Group is dominated by medium to dark grey, greenish grey and black chert interbedded with lesser black shale and minor siltstone (Fig. 9a-c). The chert is well-bedded (Fig. 9a); beds are typically 2-5 cm but locally up to 50 cm thick. Chert is more dominant near the base of the Earn Group; shale becomes more predominant up-section. The dark grey to black shale is typically rusty brown weathering; locally it forms silvery grey-weathering scree. Rare dark grey limestone intervals up to 10 m thick occur near the base of this succession. These rocks are correlated with the Middle to Upper Devonian Portrait Lake Formation of Gordey and Anderson (1993).

In the southwest part of the Mount Ferrell area, the dark grey shale contains tan weathering, white siltstone, and fine-grained sandstone beds (Fig. 9d,e). The siltstone is laminated and forms millimetre to 1-3 cm horizons (Fig. 9d). Sandstone occurs as graded beds 1-5 cm thick (Fig. 9e). Chert only occurs locally as isolated beds less than 5 cm thick within this more sandy part of the Earn Group. These rocks are assigned to the Upper Devonian to Lower Mississippian Prevost Formation of Gordey and Anderson (1993).

Black shale and chert also occurs within one fault sliver in the Dawson thrust zone (Fig. 4). These rocks are also provisionally assigned to the Portrait Lake Formation (DEpl on the map); but they could also be a sliver of the Road River Group within the fault zone.

TSICHU GROUP

Well-bedded orthoquartzite intercalated with bluish-black argillite that cap ridges along the southern edge of the Mount Ferrell area are correlated with the Tsichu Group of Cecile (2000; Fig. 4). The quartz sandstone is light grey to white, fine to medium grained, and typically forms massive beds 10-40 cm thick, and locally up to 1-2 m thick (Fig. 10). Black shale interbeds are up to 10-20 cm thick. The sandstone is composed almost exclusively of well-rounded, moderately to well-sorted quartz grains in a silica cement. Rare beds of black chert sandstone and 3-4 mm-long shale chips are locally present.

STRUCTURE

Structures in the Mount Ferrell area are dominated by WNW-trending folds and thrust faults (Fig. 4). Paleozoic carbonates north of the Kathleen Lakes fault are generally gently folded (Fig. 5e) with folds becoming tighter towards the south. South of the Kathleen Lakes fault, shale, chert, and carbonate assigned to the Road River Group are tightly folded with folds overturned to the NNE (Fig. 6c). Folds are tight to isoclinal and overturned to the NNE in the hanging wall of the Dawson thrust; they become more opened and progressively more upright to the south (Fig. 7d). An axial plane cleavage is only well-developed

Figure 9. *Earn Group.* ***(a)*** *Well-bedded chert of the Portrait Lake Formation. Thicker beds are approximately 20 cm in this outcrop.* ***(b)*** *Dark grey shale, Portrait Lake Formation.* ***(c)*** *Grey chert, Portrait Lake Formation. Hammer head for scale.* ***(d)*** *White siltstone to fine sandstone laminae in black shale, Prevost Formation.* ***(e)*** *Rhythmically bedded sandstone and shale, Prevost Formation.*

Figure 10. *Well-bedded orthoquartzite of the Tsichu Group.*

in finer grained rocks in the hanging wall of the Dawson thrust (Fig. 9b,e). It is a pressure solution cleavage that generally dips moderately to steeply to the SSW.

Evidence for a younger generation of folds was only locally noted in the Mount Ferrell area. Both NW and NE-striking spaced cleavages were noted at a few localities, as well as broad warp folds with northerly trending axes and rare kink folds.

Thrust faults are generally identified by repetitions and/or truncations of marker units (mainly maroon shale of the Narchilla Formation or buff-weathering carbonate of the Algae Formation) in the hanging wall of the Dawson thrust (Fig. 4); they are also recognized locally in brown-weathering shale and sandstone of the Yusezyu Formation (Fig. 11). Thrust faults appear more closely spaced in the immediate hanging wall of the Dawson thrust and become more widely separated to the south (Fig. 4).

The Dawson thrust juxtaposed a thick succession of Neoproterozoic-Lower Cambrian Hyland Group in its hanging wall upon Paleozoic slope deposits in its footwall to the north (Fig. 12). The Dawson thrust zone comprises the zone of more pronounced deformation and close spacing of faults in the hanging wall of the main thrust; it is up to 3 km wide near the Nadaleen River and apparently narrows to the west (Figs. 3 and 4). Only limited occurrences of fault rocks were noted in 2011. West of the Nadaleen River, localized cataclastic breccia and brittle fault planes with step-fibres suggest reverse (top-to-the-N) dextral oblique displacement. To the east of the Nadaleen

Figure 11. *Hanging wall ramp in sandstone and shale of the Yusezyu Formation. View to the west.*

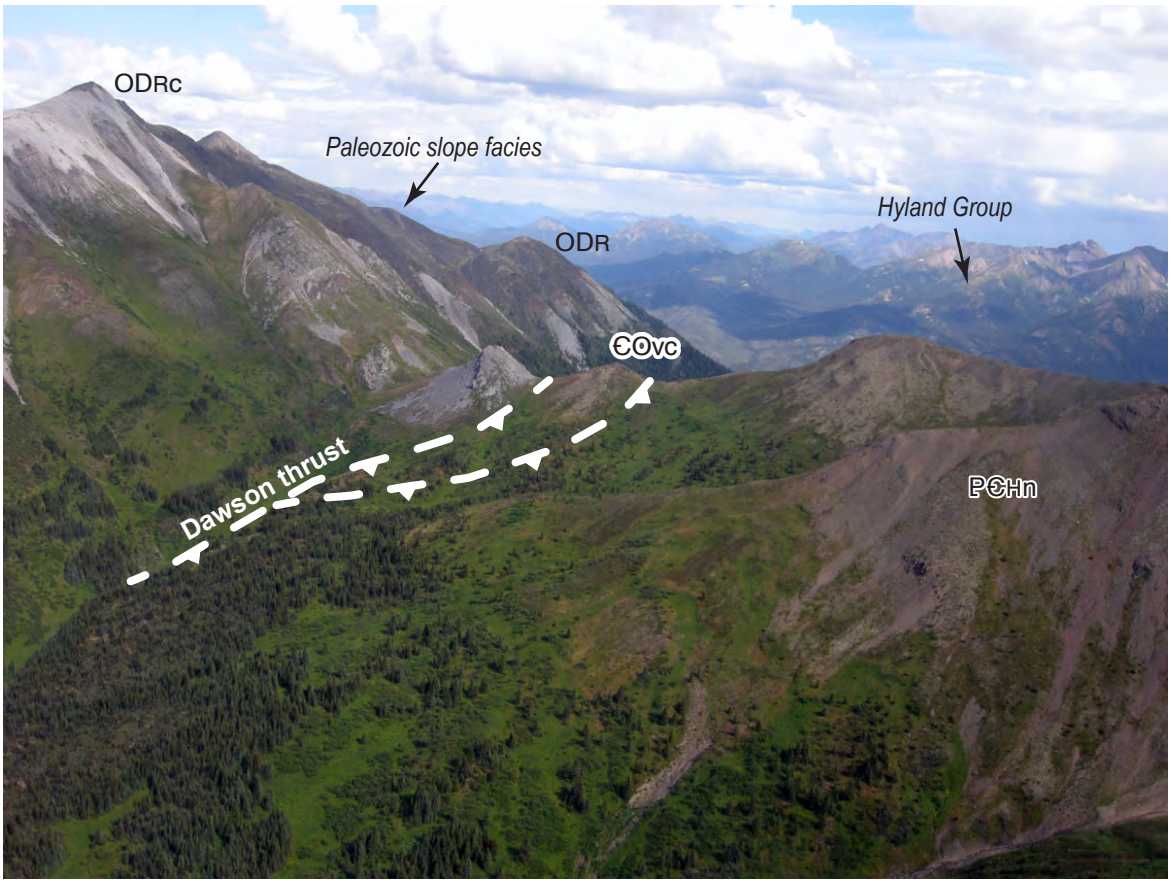

Figure 12. *View to the east at the Dawson thrust.*

River, shear bands in foliated fuschite-bearing listwaenite indicate an apparent top-to-the-N shear, although the lack of a pervasive lineation in this outcrop prevents definite interpretation.

The Kathleen Lakes fault in the Mount Ferrell area marks the boundary between Paleozoic carbonate platform strata to the north and Paleozoic clastic slope deposits to the south (Fig. 3). It has mainly been traced from mapping to the west (Abbott, 1990a; Chakungal and Bennett, 2011) and only has subtle expression in the Mount Ferrell area. Carbonate near the fault appears more fractured but does not provide information about the nature of the fault. The fault is traced at the sharp facies boundary and follows topographic lineaments.

It has been suggested that the Dawson and Kathleen Lakes faults are reactivated faults because of their apparent control on distribution of Middle Paleozoic and older sedimentary facies (Tempelman-Kluit, 1981; Abbott, 1990b; 1997). This may explain the local occurrences of Paleozoic mafic and ultramafic igneous rocks along the Dawson thrust zone in the Mount Ferrell area (Fig. 4).

MINERAL POTENTIAL

The Mount Ferrell area lies approximately half-way between ATAC Resources Ltd. two major gold discoveries along the Rackla belt: the Tiger deposit (indicated resources of 508,000 ounces averaging 2.21 g/t gold; www.atacresources.com, accessed January 3, 2012) to the west, and the Carlin-style gold occurrences at Osiris-Conrad and related zones to the east (Fig. 2). Both discoveries apparently lie in the footwall of the Dawson thrust. At Tiger, mineralization occurs as sulphide replacement in Silurian-Devonian carbonate and as oxidation zones along north-striking structures (Kingston *et al.*, 2010). Mineralization at Osiris-Conrad is more subtle, with varying concentrations of arsenic sulphide (realgar and orpiment) and very fine grained pyrite, and alteration comprising decalcification, clay alteration, and locally jasperoid. The mineralization is hosted in silty to sandy dolomitic limestone and carbonate debris flow. This latter style of mineralization is being compared to gold occurrences in the Carlin trend in Nevada.

Known occurrences in the Mount Ferrell area include a string of showings along the Dawson thrust zone (Craig; Yukon Occurrence 106C 073) and two potential sedimentary exhalative exploration targets in Earn Group strata to the south (Tell, Yukon Occurrence 106C 091; and Tanner, Yukon Occurrence 106C 098; Fig. 4). The Craig occurrences (recently renamed in part the Crag claims by Strategic Metals Ltd.) include 5 showings (over a strike length of 6.5 km) with galena and sphalerite mineralization, and minor pyrite, tetrahedrite and chalcopyrite; realgar and orpiment were reported from drillholes at the easternmost occurrence (Trent zone; labeled Crag on Fig. 4; Glifford, 1977). These occurrences were originally explored in the late 1970s for base metals and silver (Tempelman-Kluit, 1981). Jutras (2003) highlighted the potential of altered ultramafic rocks in the area for copper-nickel and gold mineralization. Drilling by Strategic Metals at the Crag (Trent zone) in 2011 confirmed occurrences of realgar and orpiment but only reported minor gold intersections (www.strategicmetalsltd.com, accessed December 21, 2011).

The Tell occurrence includes a number of gossan and kill zones with highly anomalous zinc and arsenic values in soils (Manson Creek Resources Ltd., www.manson.ca, accessed January 3, 2012). The Tanner occurrence also covers a gossanous spring underlain by Earn Group. The only mineralization reported from this occurrence consists of bedded barite and pyrite laminations.

ACKNOWLEDGEMENTS

Luke Bickerton provided assistance in the field. ATAC Resources Ltd. and Archer, Cathro & Associates (1981) Limited are thanked for logistical assistance at the Rackla airstrip and for making available their helicopters contracted through Fireweed Helicopters. Alkan Air and Great River Air provided fixed wing support. This paper benefited from critical reading by Lee Pigage and Don Murphy.

REFERENCES

Abbott, G., 1990a. Geological map of Mt. Westman map area (106D/1). Yukon Geological Survey, Open File 1990-1, 1:50 000.

Abbott, G., 1990b. Preliminary results of the stratigraphy and structure of the Mt. Westman map area, central Yukon. *In:* Current Research, Part E, Geological Survey of Canada, Paper 90-1E, p. 15-22.

Abbott, G., 1997. Geology of the upper Hart River area, eastern Ogilvie Mountains, Yukon Territory (116A/10, 116A/11). Yukon Geological Survey, Bulletin 9, 92 p.

Blusson, S.L., 1974. Five geological maps of northern Selwyn Basin (Operation Stewart), Yukon Territory and District of Mackenzie, N.W.T. Geological Survey of Canada, Open File 205, 1:250 000.

Cecile, M.P., 2000. Geology of the northeastern Niddery Lake map area, east-central Yukon and adjacent Northwest Territories. Geological Survey of Canada, Bulletin 553, 120 p.

Chakungal, J. and Bennett, V., 2011. New bedrock geology of Mount Mervyn map sheet (106C/04) and mineral potential for the South Wernecke mapping project. *In:* Yukon Exploration and Geology 2010, K.E. MacFarlane, L.H. Weston and C. Relf (eds.), Yukon Geological Survey, p. 55-87.

Colpron, M., 2012. Preliminary geological map of the Mount Ferrell area (106C/3), central Yukon. Yukon Geological Survey, Open File 2012-11, 1:50 000.

Glifford, R.G., 1977. Geological Report on Craig Property, McIntyre Mines Limited. Yukon Energy, Mines and Resources, Assessment Report 090307, 147 p.

Gordey, S.P. and Anderson, R.G., 1993. Evolution of the northern Cordilleran miogeocline, Nahanni map area (105I), Yukon and Northwest Territories. Geological Survey of Canada, Memoir 428, 214 p.

Gordey, S.P. and Makepeace, A.J., 1999. Yukon digital geology. Geological Survey of Canada, Open File D3826, *also Exploration and Geological Services Division, Yukon, Indian and Northern Affairs Canada, Open File 1999-1(D).*

Gordey, S.P. and Makepeace, A.J., 2000. Bedrock geology, Yukon Territory. Geological Survey of Canada, Open File 3754, 1:1 000 000. *also: Exploration and Geological Services Division, Yukon, Indian and Northern Affairs Canada, Open File 2001-1.*

Green, L.H., 1972. Geology of Nash Creek, Larsen Creek, and Dawson map-areas, Yukon Territory. Geological Survey of Canada, Memoir 364, 157 p.

Jutras, J.-P., 2003. Ultramafic nickel-bearing magmas of the Nadaleen River map area (106C/3) and associated listwaenites: New exploration targets in the Mayo Mining District, Yukon. *In:* Yukon Exploration and Geology 2002, D.S. Emond and L.L. Lewis (eds.), Yukon Geological Survey, p. 261-266.

Kingston, S., Mortensen, J.K., Dumala, M. and Gabites, J., 2010. Ar-Ar geochronology and Pb isotopic constraints on the origin of the Rau gold-rich carbonate replacement deposit, central Yukon. *In:* Yukon Exploration and Geology 2009, K.E. MacFarlane, L.H. Weston and L.R. Blackburn (eds.), Yukon Geological Survey, p. 213-222.

Morrow, D.W., 1999. Lower Paleozoic stratigraphy of northern Yukon Territory and northwestern District of Mackenzie. Geological Survey of Canada, Bulletin 538, 202 p.

Poulton, T., Orchard, M.J., Gordey, S.P. and Davenport, P., 1999. Selected Yukon fossil determinations. *In:* Yukon digital geology, S.P. Gordey and A.J. Makepeace (eds.), Geological Survey of Canada, Open File D3826; *also Exploration and Geological Services Division, Yukon, Indian and Northern Affairs Canada, Open File 1999-1(D)*.

Roots, C.F., 1997. Geology of the Mayo map area, Yukon Territory (105M). Exploration and Geological Services Division, Yukon, Indian and Northern Affairs Canada, Bulletin 7, 81 p.

Roots, C.F., 2003. Bedrock geology of Lansing Range map area (NTS 105N), central Yukon. Yukon Geological Survey, Geoscience Map 2003-1, 1:250 000; *also Geological Survey of Canada, Open File 1616*.

Tempelman-Kluit, D.J., 1981. Craig property summary. *In:* Yukon Geology and Exploration 1979-1980, Yukon Geological Survey, p. 225-230.

Shale gas potential of Devonian shale in north Yukon: Results from a diamond drillhole study in western Richardson Mountains

Tiffani A. Fraser[1], Tammy L. Allen
Yukon Geological Survey, Whitehorse, YT

Larry S. Lane, Julito C. Reyes
Geological Survey of Canada, Calgary, AB

Fraser, T.A., Allen, T.L., Lane, L.S., and Reyes, J.C., 2012. Shale gas potential of Devonian shale in north Yukon: Results from a diamond drillhole study in western Richardson Mountains. *In:* Yukon Exploration and Geology 2011, K.E. MacFarlane and P.J. Sack (eds.), Yukon Geological Survey, p. 45-74.

ABSTRACT

Fresh diamond drill core samples from Paleozoic shale of the Road River Group and Canol and Imperial formations in the Richardson Mountains, immediately east of Eagle Plain basin, were analysed for Rock-Eval pyrolysis and total organic carbon content, organic petrology, and vitrinite reflectance to assess organic matter quantity, quality, and thermal maturity. X-ray diffraction was conducted to assess quartz, clay, and carbonate mineralogy. Samples are from three areas located along a north-trending strike length of 110 km.

All samples are overmature with respect to oil generation (1.89 to 3.86 $\%Ro_R$). However, values systematically decrease southward along the mountain front through the dry gas window to the upper limit of the mixed wet/dry gas window (2.00 $\%Ro_R$). Organic petrology identified abundant amorphous kerogen with lesser amounts of alginite-derived macerals, and *Tasmanites* alginite in both the Road River Group and Canol Formation while the Imperial Formation was organically lean. Total organic carbon values for the Canol Formation are 0.3 to 20.1 wt % with most samples containing 2 to 5 wt % TOC. For the Road River Group, TOC values are 1.0 to 19.3 wt % with most less than 5 wt %. The Imperial Formation TOC values are mainly below 1 wt %.

X-ray diffraction analyses indicate the succession is highly siliceous, particularly the Canol Formation with quartz values from 91 to 100%. Samples of the Imperial Formation are generally 82 to 90% quartz, while Road River Group samples are more variable with 62 to 96% quartz.

This study suggests that these strata have the potential to host unconventional hydrocarbons in the region under favourable burial conditions. Canol Formation and Road River Group strata have high TOC values and contain identifiable Type I and II organic macerals suggesting they may have been richer source rocks in the past. All strata are highly siliceous and thus good candidates for hydraulic fracture stimulation, with the Canol Formation the most mineralogically consistent of all strata examined.

A 2010 study of subsurface Canol and Imperial formation shale west of the study area indicates these formations are within the oil window, less thermally mature than in the Richardson Mountains. These results highlight the potential for natural gas and liquids in Devonian shale in Eagle Plain basin.

[1] *tiffani.fraser@gov.yk.ca*

INTRODUCTION

In recent years, thick shale deposits have been the target of exploration efforts in many North American basins for their natural gas potential. As thick shale deposits are known to exist in many Yukon sedimentary basins, studies are being made by the Yukon Geological Survey and the Geological Survey of Canada to assess these rocks for their hydrocarbon potential. This paper presents the results of one such study in northern Yukon, immediately east of Eagle Plain basin on the western flank of the Richardson Mountains. The study was made possible by the successful collaboration of geologists from federal and territorial governments, and the minerals and oil and gas sectors.

In 2009, diamond drill core from a 2007-2008 mineral exploration program was retrieved from the field by staff from Northern Cross (Yukon) Limited, the Geological Survey of Canada, and the Yukon Geological Survey. This relatively 'fresh' core was collected for study as it penetrated three Devonian shale formations thought to be prospective for shale gas. Approximately 1500 metres of core was collected from three different localities spanning 110 km, all in the western flank of the Richardson Mountains, immediately east of Eagle Plain basin. Core samples were analysed for thermal maturity, source rock potential, mineralogy, and age. The collection of the core was made possible by donation from Archer, Cathro & Associates (1981) Limited, who conducted exploration activities including diamond drilling in the region on behalf of a third party mineral company.

Preliminary results were previously reported from one of the diamond drill properties, the Rich property, including a 600 m long composite section penetrating the uppermost Road River Group, Canol and lowermost Imperial formations (Allen *et al.*, 2011). This paper builds on the previous publication and includes data from two additional properties, Pe to the south and Fox to the north. Analytical work completed on the shale samples highlights the importance of Devonian shale as hosts for unconventional hydrocarbons in northern Yukon.

STUDY AREA

The diamond drill core assessed in this study was retrieved from the Fox, Rich, and Pe properties along the western flank of the southern Richardson Mountains (Fig. 1), immediately east of Eagle Plain basin. The southern Richardson Mountains are north-trending, extending roughly from the Peel River in the south to near where the Dempster Highway crosses the mountain trend adjacent the Northwest Territories/Yukon border (Fig. 1). Eagle Plain basin, an underdeveloped prospective hydrocarbon exploration area in north Yukon, lies between 65.5 and 67.5°N latitudes and 136 and 140°W longitudes (Osadetz *et al.*, 2005). North to south, the basin is approximately 170 km long and extends approximately 80 km east to west, covering an area of approximately 20 600 km^2. Tectonic uplift in the region immediately east of the basin exposes Devonian strata where mineral exploration, including diamond drilling, was conducted. The stratigraphic interval, exposed in the range, extends westward across Eagle Plain basin in the subsurface.

The Fox is the northernmost property located on NTS map sheet 116I/16 at 66°56'N latitude and 136°16'W longitude. The property is approximately 70 km northeast of Eagle Plains Hotel which is situated at km 369 of the Dempster Highway (Fig. 1). The Rich property is located on NTS map sheet 116I/08 at latitude 66°19'N and longitude 136°14'W. The property is 23 km southeast of the Eagle Plains Hotel and 65 km south of the Fox property. The Pe is the southernmost property located on NTS map sheets 106E/13 and 116H/16 at latitude 65°56'N and longitude 136°01'W. The property is located approximately 56 km southeast of the Eagle Plains Hotel. The distance between the Rich and Pe properties is approximately 43 km.

GEOLOGICAL SETTING

TECTONIC

Eagle Plain and Richardson Mountains are foreland elements of the Northern Yukon Fold Complex, which sits on the great arc of the Mackenzie Mountains of the northern Cordillera. The complex is a north-striking fold and thrust belt extending 500 km northward from the Ogilvie Mountains to the Beaufort Sea. The deformation that produced the complex culminated in Paleocene-Eocene time (Lane and Dietrich, 1995) in response to regional east-west shortening coeval with the northward-directed deformation that uplifted the Ogilvie Range (Lane, 1998).

The southern Richardson Mountains (Fig. 1) are a faulted anticlinorium that developed by tectonic inversion of the early Paleozoic Richardson trough, either by thick-skinned deformation localized at a felsic-to-mafic basement transition (Lane, 1996) or by thin-skinned deformation transmitted hundreds of kilometres eastward from a distant

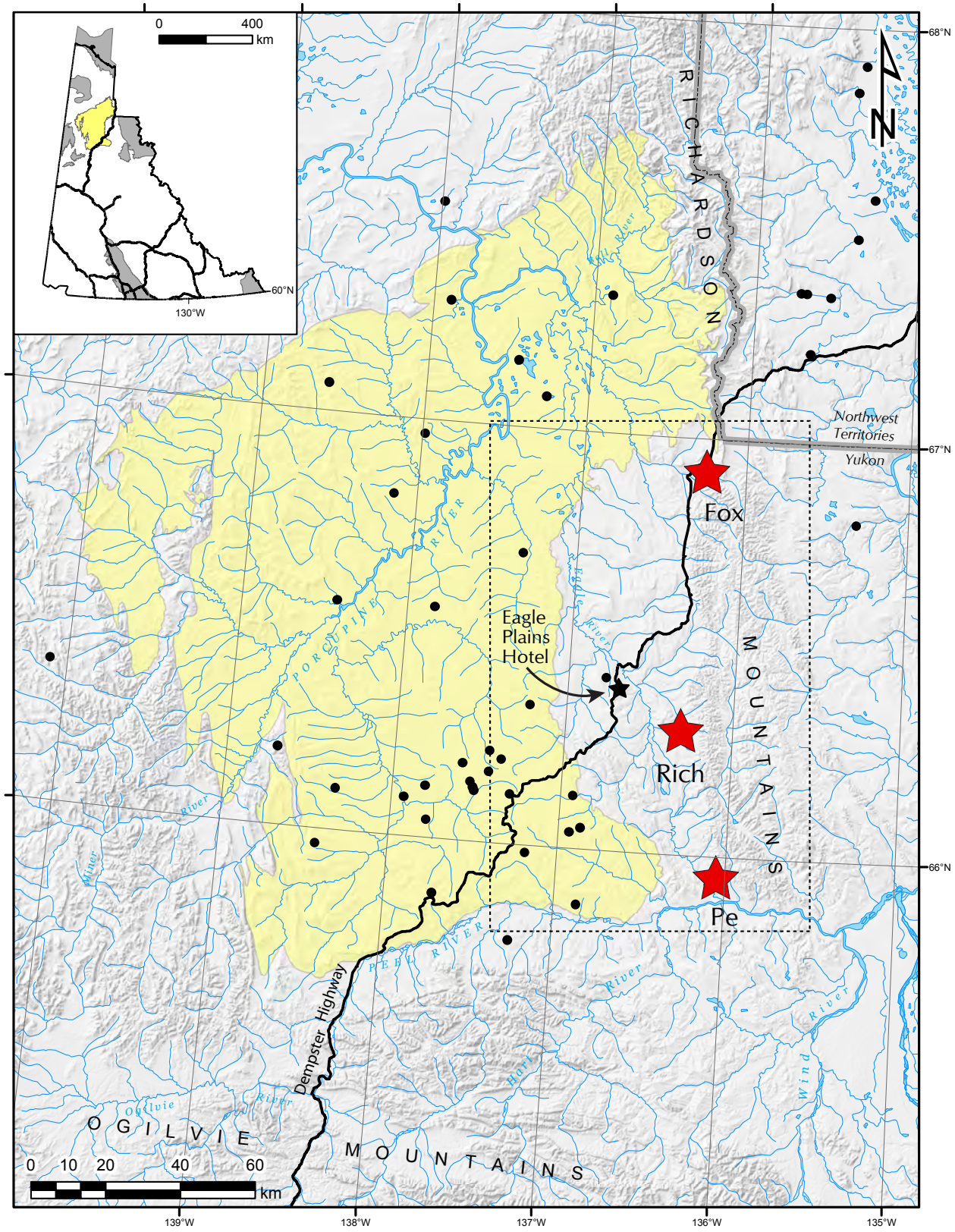

Figure 1. *Map of Eagle Plain basin exploration region (yellow polygon) and the location of the Fox, Rich and Pe properties. Black dots represent oil and gas exploration well locations. Inset map of Yukon with Eagle Plain exploration region in yellow and other oil and gas basins in grey. Dotted box is area displayed in Figure 7.*

hinterland (Hall and Cook, 1998). The eastern part of the anticlinorium has been partially dismembered on sub-vertical faults related to Neogene tectonics (Mazzotti *et al.*, 2008).

The adjacent Eagle Plain basin (Fig. 1) is a mildly deformed foreland-style intermontane basin dominated by gentle north-trending folds that are detached in Proterozoic strata at depth, and are commonly thrust-cored (Lane, 1996; Hall and Cook, 1998), although most of the faults do not project to the surface.

An earlier cycle of deposition and uplift is recorded in the Devonian and Carboniferous successions relevant to this contribution. Widespread carbonate banks on the Northern Interior Platform and Yukon Stable Block, as well as deeper water deposits comprising the Road River Group in the Richardson trough, were drowned abruptly in Middle Devonian time in an event that resulted in the deposition of the Canol Formation over a wide area of northwestern Canada (Morrow, 1999). Soon thereafter an aggregate thickness of several kilometres of turbiditic shale, siltstone, and sandstone of the Imperial and Tuttle formations were deposited through Late Devonian and Early Carboniferous time. These clastic wedge deposits were shed from the Ellesmerian orogen as it encroached into the northern margin of Eagle Plain, resulting in substantial burial (Lane, 2007, 2010). Subsequent uplift and denudation produced a widespread erosional unconformity across Eagle Plain and Peel Plateau that places Early Cretaceous strata directly onto Devonian and Carboniferous rocks in northern and central Eagle Plain; and onto Permian strata in the south.

STRATIGRAPHY

The regional stratigraphic setting is described in Allen *et al.* (2011). Descriptions of Middle Devonian to Carboniferous strata are re-iterated here as they pertain specifically to this study. Of interest is the uppermost Road River Group, Canol and lower Imperial formations. A stratigraphic column for the Silurian to Carboniferous section is shown in Fig. 2, displaying the relationship and ages of the units of interest.

The Road River Group (originally defined by Jackson and Lenz (1962) and elevated to group status by Fritz (1985)) was deposited during Late Cambrian to Middle Devonian time in the Richardson trough and on most of the Yukon Stable Block (Morrow, 1999). In outcrop, the upper portion of this unit is generally a graptolitic, black shale and shaly limestone, although the upper 50 m, and the stratigraphy pertinent to this study, is white weathering, siliceous shale, and chert (Fig. 3). Road River Group strata are thickest in the Richardson trough, at almost 3000 m, however it is thinner on the Yukon Stable Block (Morrow, 1999). Numerous early workers referred to a significant unconformity at the upper contact of the Road River Group with the overlying Canol Formation; more recent workers consider the contact conformable, with the Canol Formation being a condensed section possibly initiated by rapid sea level rise in Givetian time (see discussions in Pugh, 1983 and Morrow, 1999).

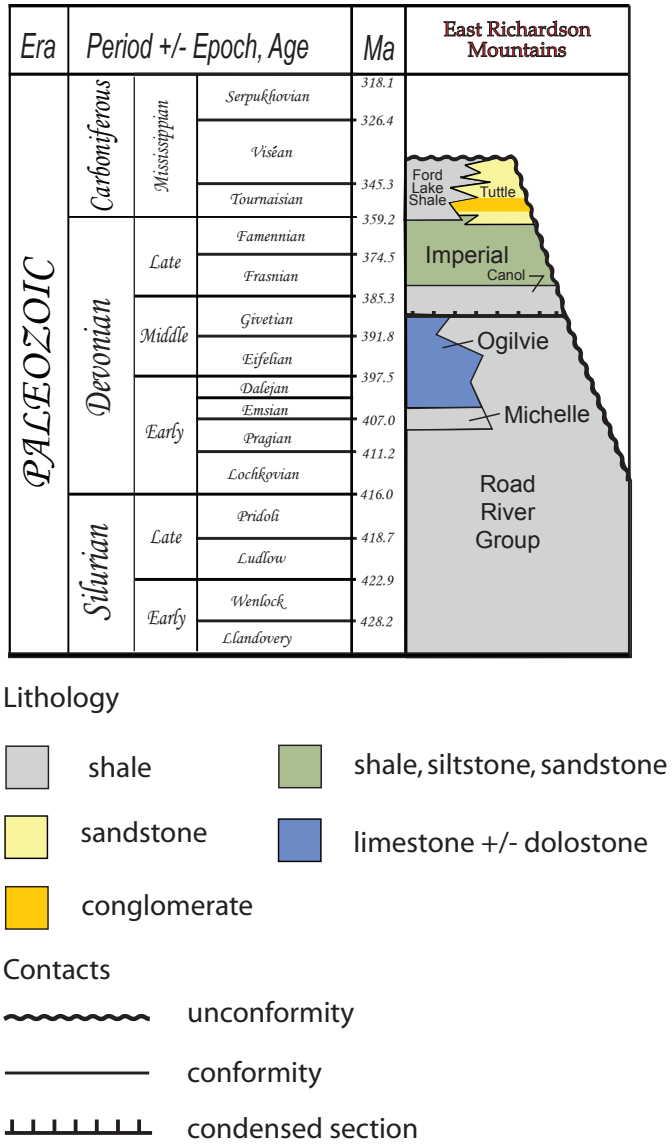

Figure 2. *Stratigraphic column of Silurian to Carboniferous geology of the east Richardson Mountains (modified from Morrow, 1999).*

Figure 3. *Black shale and chert interbedded with resistant, light grey weathered limestone of Road River Group, unnamed creek, NTS map sheet 116I/08.*

The Middle to Upper Devonian (late Givetian and early Frasnian) Canol Formation (Bassett, 1961) is a grey to black, siliceous, thin-bedded, fissile and predominantly non-calcareous shale (Bassett, 1961; Norris, 1985; Fig 4). The Canol Formation is widely distributed over much of Yukon and Northwest Territories. In the Eagle Plain basin it ranges in thickness from approximately 4 to 80 m, based on well intersections (Fraser and Hogue, 2007). It is highly organic and is considered a hydrocarbon source rock for the Norman Wells oil field which has been producing since the 1940s, and continues to be a prominent target for ongoing exploration in that region. In the Richardson Mountains, the Imperial Formation (A.W. Norris, 1997) conformably overlies the Canol Formation.

Figure 4. *Canol Formation as observed on an unnamed creek, NTS map sheet 116I/08. Note the fissile nature of the shale.*

The Upper Devonian Imperial Formation (originally defined by Link, 1921; formalized by Hume and Link, 1945) is a thick package of siliciclastic strata representing shelf, slope, and basin deposits derived from the Ellesmerian orogeny north of the study area (Pugh, 1983; Braman and Hills, 1992). In the western Richardson Mountains, the Imperial Formation consists of three lithologically different units: a lower rusty weathering, siliceous siltstone and shale with minor sandstone (Fig. 5), a middle unit dominated by siliceous siltstone, turbiditic sandstone and shale, and an upper portion of light grey weathering, laminated shale and siltstone with thin orange weathering pyritic sandstone beds. The lower portion has been dated in the study area as Frasnian to Famennian (*e.g.,* Braman and Hills, 1992; Dolby, 2010; Allen *et al.*, 2011). In the subsurface of Eagle Plain, the Imperial Formation attains a maximum thickness of 1229 m in well intersections; and is overlain, depending on location, either conformably by the Ford Lake Shale or Tuttle Formation, or, unconformably by Permian or Cretaceous strata (Fraser and Hogue, 2007; Norris, 1984).

Figure 5. *Imperial Formation strata observed above the Canol Formation on unnamed creek on 116I/08. Note the strata lack fissility and layering that is well established in the Road River Group and Canol Formation. Imperial strata are also lighter in colour.*

PREVIOUS STUDIES

Shale gas research in Yukon is in its infancy, however some published information exists on Upper Devonian shale units in north Yukon. Hamblin (2006), in a report offering a preliminary inventory of shale gas possibilities in Canada, identified Road River Group, Canol and Imperial formation shale units in Eagle Plain as having significant apparent geological potential. That report was compiled solely from existing published data and was meant to

encourage geological studies in certain areas of Canada. Other shale gas literature for Yukon strata includes preliminary results of the research presented in Allen *et al.* (2011) which provided Rock-Eval, mineralogical and palynological determinations of Road River Group, and Canol and Imperial formation strata from Rich property core.

Upper Devonian shale characteristics from field studies in north Yukon have been reported in a number of publications (*e.g.*, Norris, 1985; A.W. Norris, 1997; Richards *et al.*, 1997; Pugh, 1983; Morrow, 1999; Gal *et al., 2009*; Hadlari *et al.*, 2009; Allen, 2010). Rock-Eval/TOC results from Canol and Imperial formation shale (cuttings and/or core) from selected petroleum exploration wells in Eagle Plain basin are reported in Link *et al.* (1989), Snowdon (1988) and Lane *et al.* (2010).

Link *et al.* (1989) used Rock-Eval/TOC and organic petrology to evaluate the petroleum source rock potential of the Phanerozoic succession in northern Yukon and northwestern Northwest Territories (NWT), including Road River Group, Canol and Imperial formation shale. In that study, a substantial set of samples were analysed from outcrop samples collected along the Dempster Highway and from exploration well cuttings throughout the Eagle Plain and Mackenzie Delta region. Also, Link and Bustin (1989) investigated the thermal history and levels of organic maturation of Phanerozoic strata in northern Yukon and northwestern NWT by visual analyses including vitrinite reflectance and conodont alteration index.

Industry exploration for hydrocarbons has been ongoing in Eagle Plain basin from the 1950s to the present. To date, 34 wells have been drilled in the basin to evaluate conventional oil or gas targets, with several discoveries and multiple minor shows from various stratigraphic intervals. This exploration history is summarized in Osadetz *et al.* (2005).

Limited industry exploration for mineral deposits has occurred in the region. A few regional exploration programs targeting lead-zinc mineralization were undertaken in the area during the 1970s with very little of this work filed as assessment reports (Héon, 2006). The reader is directed to Héon (2006) for further details regarding mineral exploration and potential mineral occurrences.

Nickel-rich massive sulphide deposits hosted by Devonian black shale occur in the Richardson Mountains (Goodfellow, 2011). Exploration by Archer, Cathro in 2007 and 2008 resulted in bedrock mapping and a diamond drilling program targeting the strata bound nickel-molybdenum (NiMo) occurrence on the west flank of the Richardson Mountains (Rob Carne, pers. comm., 2010). The occurrence is described as a sheet-like massive sulphide layer enriched with nickel, molybdenum, and zinc located at the contact between the Road River Group and the overlying Canol Formation (Fig. 6). Individual holes penetrated the lowermost Imperial Formation, Canol Formation and uppermost Road River Group; however diamond drilling at the Pe property did not intersect the target (Rob Carne, pers. comm., 2010).

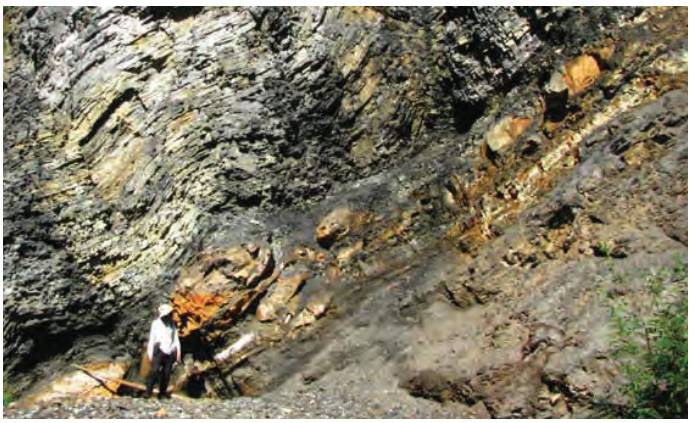

Figure 6. *Contact between the Road River Group and the overlying Canol Formation. The metre-scale iron-stained nodules are commonly observed between the two units. The NiMo zone occurs less than a metre above the nodule horizon. This photo is from an unnamed creek on NTS map sheet 116I/08.*

METHODS

CORE COLLECTION

In September 2009, approximately 1500 m of core was salvaged from the Fox, Rich and Pe properties in order to collect a representative suite of continuous core along the 110 km long north trend of the Canol and Imperial formations. From the Fox property, Road River Group and Canol Formation strata were collected from two drillhole locations (FX07-02 and FX-07-03). From the Rich property, core was collected from six drillhole locations (Rich 07-02, 07-7A, 07-16, 07-20, 08-24 and 08-25) which penetrated either the Imperial or Canol formations or Road River Group strata, or a subset thereof. At the Pe property, Canol Formation core was collected from one drillhole (PE-07-07). The core was slung by helicopter from each mineral property to the Eagle Plains Hotel. From the hotel, the core was transported by truck to the Geological Survey of Canada in Calgary, Alberta. Location information for all core is presented in Figs. 1 and 7 and Table 1.

ANALYTICAL WORK

Analytical work conducted on the shale drill cores includes Rock-Eval pyrolysis and total organic carbon content analysis (RE/TOC) to assess the quantity, quality, type, and thermal maturity of organic matter; vitrinite reflectance (VR) to also assess thermal maturity of organic matter; organic petrology to confirm the type of organic matter; x-ray diffraction (XRD) mineralogy to evaluate rock mineralogy and 'fracability'; and palynological studies to determine stratal age and relationships.

ROCK-EVAL /TOC

Core samples from the Road River Group, Canol and Imperial formations were analysed for organic richness and maturity of organic matter using a Rock-Eval 6 Turbo pyrolysis apparatus in the Organic Geochemistry Laboratory of the Geological Survey of Canada, Calgary. These analyses provide information on organic matter quantity or richness (TOC), quality (OI/HI cross plots), thermal maturity (T_{max}), and ultimately remaining hydrocarbon potential (all parameters combined). RE/TOC samples were selected at a constant spacing measured perpendicular to local bedding, with minor adjustments to ensure suitable lithologies were sampled, and with selective additional sampling near contacts. The core sample spacing was typically every 7-14 m for Fox core, 10-18 m for the Rich core, and typically 10-14 m for the Pe core. A bitumen sample was also included in the sample set.

VITRINITE REFLECTANCE AND ORGANIC PETROLOGY

Vitrinite reflectance (VR) and organic petrology were completed at the Organic Geochemistry Laboratory at GSC Calgary where standard procedures for organic petrology based on Mackowsky (1982) are generally followed. Samples are prepared for incident white and fluorescent light microscopy by crushing them into 1-5 mm particulates, with many also sized to up to 1 cm cubes. The samples were then mounted in an epoxy, ground, and finally polished. Organic petrography was conducted using incident light microscopes equipped with white (halogen; 546 nm) and fluorescent (HBO 100W) light sources, and oil immersion 50X objective. Percent reflectance in oil (%Ro; refractive index of immersion oil = 1.518) was measured with the Leitz MPV II – COMBI system. The number of reflectance measurements made on any given maceral within a sample generally varied from 5 to 50. Random percent reflectance in oil ($\%Ro_R$) was measured (n = 5 to 50) on huminite, primary bitumen, and vitrinite macerals. A Leitz MPM II microscope with a PC-controller system is used for %Ro data collection. Reflectance is calibrated using glass standards (0.506, 1.025, and 1.817 %Ro) of known refractive index.

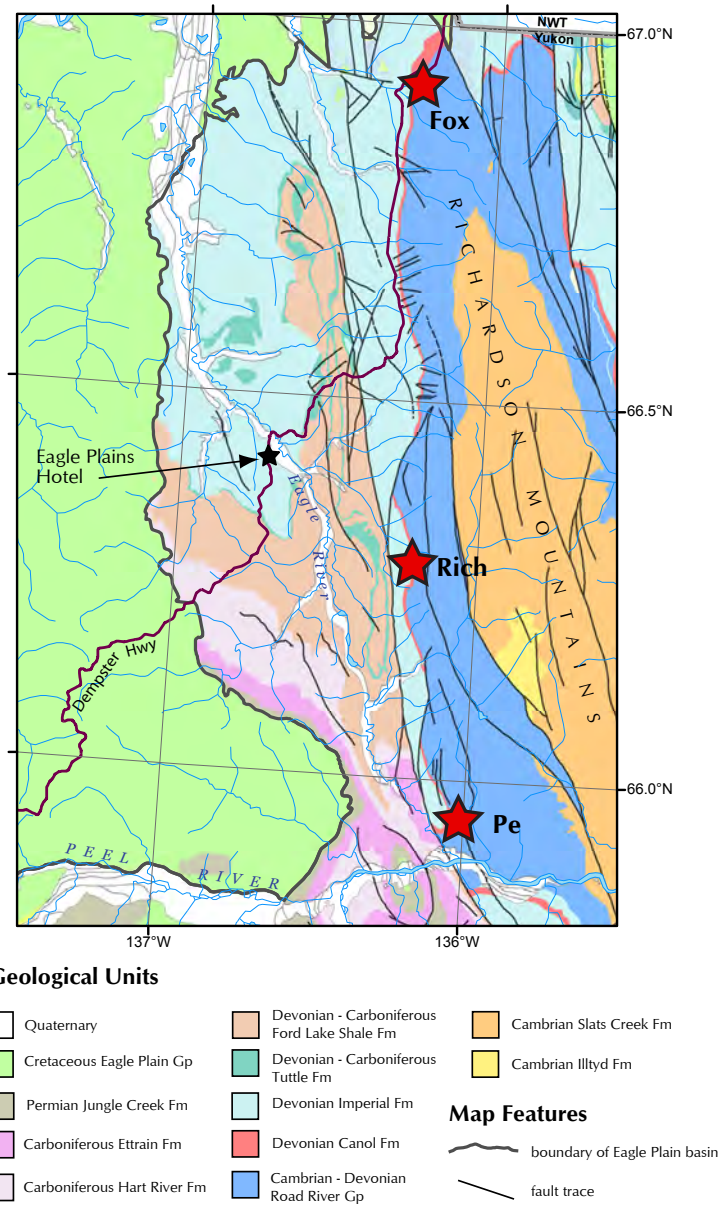

Figure 7. *Geological map showing mineral properties from which diamond drillhole core was retrieved. Geology after Gordey and Makepeace (1999). The location of this map with respect to Eagle Plain basin is displayed in Figure 1.*

Table 1. *Summary of diamond drillholes used in this study. Note that results from the Rich property (excluding vitrinite reflectance) were previously published in Allen et al. (2011). Fx = Fox property, RI = Rich property. The location of the drillhole indicates where the hole was collared.*

Diamond drillhole	Location* (UTM NAD83, Zone 8W)		Unit	Downhole depth		Downhole thickness (m)	Total depth drilled (m)	Core size	Azimuth	Dip
	Easting	Northing		from (m)	to (m)					
FX07-02	442197	7420757					106.68	BTW	110°	-75
			overburden	0	5.92	5.92				
			Imperial Fm	n/a	n/a	0				
			Canol Fm	5.92	68.37	62.45				
			Road River Gp	68.37	106.68	38.31				
FX07-03	442337	7423398					210.31	BTW	110°	-75
			Canol Fm	0	~95.0	~95.0				
			Road River Gp	~95.0	210.31	96.75				
PE07-07	452941	7314197					164.59	BTW	045°	-70
			overburden	0	7.58	7.58				
			Canol Fm	7.58	164.59	157.01				
RI07-02	445508	7353769					176.79	BTW	090°	-50
			overburden	0	24.8	24.8				
			Road River Gp	24.8	176.79	151.99				
RI07-07A	444283	7356805					170.69	BTW	070°	-60
			overburden	0	24.38	24.38				
			Canol Fm	24.38	158.67	134.29				
			Road River Gp	158.67	170.69	12.02				
RI07-16	443054	7359059					121.92	BTW	060°	-75
			overburden	0	16.02	16.02				
			Canol Fm	16.02	91.9	75.88				
			Road River Gp	91.91	121.92	30.01				
RI07-20	444880	7356092					189.28	BTW	060°	-75
			overburden	0	51.3	51.3				
			Canol Fm	51.3	189.28	137.98				
RI08-24	443753	7356495					565.71	HQ and NQ	090°	-70
			overburden	0	8.97	8.97				
			Imperial Fm	8.97	370	361.03				
			Canol Fm	370	565.71	195.71				
RI08-25	444390	7354600					343.50	HQ and NQ	090°	-70
			overburden	0	9.35	9.35				
			Imperial Fm	9.35	343.5	334.15				

*Location refers to where the hole was collared.

Sample spacing for vitrinite reflectance was a minimum of 50 to 60 m, measured perpendicular to bedding. Additional samples were analysed in some instances, particularly close to formational contacts.

XRD MINERALOGY

X-ray diffraction (XRD) is a common method used to determine the mineral composition of shale, which is important in determining a formation's brittleness or 'fracability' (mechanically-induced fracture development). Sampling for semi-quantitative XRD analyses was carried out on shale samples from the Road River Group, Canol and Imperial formations at a typical spacing of 25 m measured perpendicular to bedding, with some additional samples collected in the vicinity of contacts. The XRD analyses were run on a Philips PW1700 powder diffraction system with cobalt x-ray source. All analyses were run on powder mounted samples, and executed by the PANalytical X'Pert Quantify software. Mineral determination was processed by PANalytical's X'pert Highscore program, and the quantification of minerals within samples was calculated from their mineral peak intensities (or peak area). Whole rock results are semi-quantitative and are expressed in mineral ratio percent. Total quartz (including chert), total carbonate, and total clay percentages were summed and recalculated out of 100% based on the XRD analyses, and plotted as ternary diagrams.

ANALYTICAL RESULTS

ROCK-EVAL /TOC

Rock-Eval pyrolysis (RE/TOC) results from drill core samples from the Fox, Rich and Pe properties are summarized in Table 2a. Table 2b summarizes RE/TOC results from Rich property surface field samples. Guidelines for interpreting these data are provided in several publications including Espitalié *et al*. (1985), Peters (1986), Peters *et al.* (2005) and Lafargue *et al*. (1998).

At the Fox property TOC values for Road River Group strata range from 3.7 to 19.3 wt % with the average 10.2 wt %. The 19.3 wt % value is anomalous and by removing this value, the average TOC value lowers to 8.7 wt %. TOC values for the Canol Formation range from 1.5 to 20.1 wt %, with the average 7.5 wt %, and the majority in the 4.6 to 7.6 wt % range. The 20.1 wt % value is anomalous and removing this value results in an average TOC of 6.3 wt % for the Canol at this property.

At the Rich property TOC values for Road River Group strata range from 1.6 to 6.1 wt %, averaging 2.8 wt % with the majority between 1 and 3 wt %. TOC values for Canol Formation strata range from 0.3 to 7.3 wt %, averaging 3.3 wt % with the majority in the 2 to 5 wt % range. TOC values for Imperial Formation strata range from 0.7 to 3.1 wt % with almost 90% of samples containing less than 1 wt % TOC. All TOC contents obtained from outcrop samples collected on the Rich property for the Road River Group and the Canol Formation are within the above mentioned ranges obtained from the diamond drill core samples. The samples of the Imperial Formation from outcrop, range from 0.9 to 5.7 wt % or slightly higher than those from diamond drill core. A TOC value of 5.7 wt % is not typical of the Imperial Formation, however a similar phenomena was documented on Tetlit Creek and Trail River, Yukon where isolated intervals up to 1.65 m thick contained black, organic-rich shale with anomalously high TOC values up to 5.3 wt % (Allen, 2010).

At the Pe property, where only the Canol Formation was intersected, TOC values for all samples range from 1.0 to 5.1 wt %, averaging 2.7 wt % with the majority between 2 and 3 wt %.

Figure 8 summarizes the TOC values by geologic unit. The Road River Group strata range from 1.6 to 19.3 wt %, the Canol Formation ranges from 0.3 to 20.1 wt % with only one sample below 1 wt % and the Imperial Formation ranges from 0.7 to 5.7 wt %, with over 85% of the Imperial samples less than 1 wt %.

All samples in this study have S2 values less than 0.2 mg HC/g rock. When S2 values are this low, the Rock-Eval derived T_{max}, production index (PI) and hydrocarbon index (HI) are often unreliable and should be rejected (Peters, 1986). Low S2 values may be attributed to depletion by oxidation, high thermal maturity, or large amounts of Type IV kerogen present (Peters, 1986). With low S2 values, determination of thermal maturity via Rock-Eval is not possible. Further, determination of kerogen type (*e.g.*, I, II and III) is impossible to deduce from a modified van Krevelen cross plot as the hydrogen indices (HI) are very low. All HI values obtained in this study are below 22 mg HC/g C_{org}, with over 90% of the HI values below 6 mg HC/g C_{org}. With increasing temperature, kerogen loses hydrogen resulting in lower HI values. This results in high maturity samples plotting close to the x-axis of the modified van Krevelen diagram rendering it essentially impossible to determine the evolutionary pathway the samples followed, and therefore impossible to infer the original type of organic matter from Rock-Eval analyses (Fowler *et al.,* 2005).

Table 2a and 2b. *Summary of Rock-Eval/TOC data from diamond drillholes (2a) and outcrop data (2b). Parameters measured and derived from Rock-Eval pyrolysis include TOC = total organic carbon content as percent weight of whole rock; S1 = mg hydrocarbons/g rock; S2 = mg hydrocarbons/g rock; S3 = mg CO_2/g rock; PI = production index (S1/(S1+S2)); HI = hydrogen index ((S2/TOC)x100); OI = oxygen index ((S3/TOC)x100); T_{max} = maximum temperature (°C) at top of S2 peak. Note where S2 values are less than 0.2 mg HC/g rock, the PI and Tmax values are unreliable and should be rejected (Peters, 1986). Vitrinite reflectance (%Ro_R) values obtained from this study are included for reference. Unit RR=Road River Group. Highlighted sample is bitumen.*

Table 2a.

Sample	GSC curation #	Downhole depth (m)	Unit	S1	S2	PI	S3	T_{max}	HI	OI	%Ro_R
FX07-02-9	C-491544	18.0	Canol	0.01	0.03	0.22	0.40	611	1	9	
FX07-02-8	C-491543	25.8	Canol	0.01	0.01	0.62	1.75	343	1	114	
FX07-02-7	C-491542	40.2	Canol	0.01	0.02	0.27	0.75	611	0	12	
FX07-02-6	C-491541	52.7	Canol	0.00	0.01	0.37	0.57	291	0	8	3.24
FX07-02-5	C-491540	57.2	Canol	0.00	0.00	0.76	0.44	611	0	6	
FX07-02-4	C-491539	64.0	Canol	0.00	0.01	0.33	0.59	610	0	12	3.41
FX07-02-3	C-491538	79.0	RR	0.01	0.04	0.18	0.12	413	0	1	3.60
FX07-02-2	C-491537	92.2	RR	0.01	0.01	0.29	0.14	453	0	4	
FX07-02-1	C-491536	106.7	RR	0.01	0.03	0.27	0.23	611	0	1	3.85
FX07-03-9	C-491553	33.3	Canol	0.01	0.01	0.44	0.62	611	0	9	3.59
FX07-03-8	C-491552	47.2	Canol	0.01	0.01	0.41	0.34	611	0	5	
FX07-03-7	C-491551	60.7	Canol	0.01	0.03	0.24	0.18	394	0	2	
FX07-03-6	C-491550	74.0	Canol	0.01	0.07	0.17	0.36	396	0	2	
FX07-03-5	C-491549	87.5	Canol	0.00	0.01	0.28	0.23	423	0	5	3.87
FX07-03-4	C-491548	100.0	RR	0.00	0.02	0.18	0.12	611	0	1	
FX07-03-3	C-491547	111.5	RR	0.01	0.03	0.22	0.14	435	0	2	3.85
FX07-03-2	C-491546	128.6	RR	0.01	0.01	0.45	0.28	611	0	2	3.86
FX07-03-1	C-491545	139.0	RR	0.01	0.02	0.46	0.26	408	0	3	3.87
R107-02-6	C-491566	34.0	RR	0.02	0.08	0.19	0.43	607	4	19	
R107-02-5	C-491565	44.7	RR	0.02	0.08	0.19	0.78	606	3	31	2.21
R107-02-4	C-491564	58.7	RR	0.02	0.12	0.15	0.21	534	3	6	
R107-02-3	C-491563	75.8	RR	0.02	0.10	0.16	0.35	343	4	13	
R107-02-2	C-491562	90.0	RR	0.01	0.07	0.17	0.24	428	3	10	
R107-02-1	C-491561	105.6	RR	0.01	0.10	0.10	0.24	608	2	4	2.25
R107-07A-12	C-491526	37.8	Canol	0.01	0.02	0.26	0.18	389	0	4	2.00
R107-07A-11	C-491525	50.6	Canol	0.01	0.03	0.19	0.13	421	1	4	
R107-07A-10	C-491524	63.2	Canol	0.00	0.02	0.19	0.10	513	0	2	
R107-07A-7	C-491521	78.1	Canol	0.01	0.02	0.20	0.15	340	0	3	
R107-07A-6	C-491520	91.0	Canol	0.00	0.02	0.20	0.09	611	1	2	2.11
R107-07A-5	C-491519	102.3	Canol	0.00	0.01	0.26	0.07	343	0	3	2.18
R107-07A-4	C-491518	114.8	Canol	0.01	0.03	0.21	0.07	357	1	3	
R107-07A-3	C-491517	127.5	Canol	0.01	0.04	0.23	0.09	611	1	3	
R107-07A-2	C-491516	140.2	Canol	0.01	0.05	0.12	0.08	610	1	2	2.48
R107-07A-1	C-491515	166.5	RR	0.01	0.02	0.25	0.10	316	1	4	2.77
R107-16-7	C-491560	25.5	Canol	0.01	0.04	0.20	0.09	522	2	4	

Table 2a continued.

Sample	GSC curation #	Downhole depth (m)	Unit	S1	S2	P1	S3	T_{max}	HI	OI	$\%Ro_R$
R107-16-6	C-491559	42.0	Canol	0.01	0.05	0.19	0.13	606	1	3	
R107-16-5	C-491558	58.5	Canol	0.01	0.04	0.20	0.13	607	1	3	2.27
R107-16-4	C-491557	72.9	Canol	0.01	0.05	0.16	0.10	606	1	3	
R107-16-3	C-491556	86.0	Canol	0.01	0.02	0.29	0.11	606	1	4	2.43
R107-16-2	C-491555	103.1	RR	0.02	0.03	0.32	0.17	607	2	11	2.56
R107-16-1	C-491554	121.9	RR	0.01	0.04	0.19	0.14	607	3	9	2.43
R107-20-7	C-491573	85.9	Canol	0.00	0.02	0.16	0.12	489	1	5	
R107-20-6	C-491572	102.6	Canol	0.01	0.03	0.18	0.20	607	1	6	
R107-20-5	C-491571	119.3	Canol	0.01	0.04	0.14	0.11	607	1	3	2.33
R107-20-4	C-491570	135.9	Canol	0.02	0.11	0.13	0.24	606	3	7	
R107-20-3	C-491569	152.6	Canol	0.04	0.10	0.29	0.30	607	3	8	
R107-20-2	C-491568	169.3	Canol?	0.02	0.08	0.23	0.21	606	5	12	
R107-20-1	C-491567	185.9	Canol?	0.02	0.07	0.21	0.23	604	2	8	2.51
R108-24-47	C-491514	39.3	Imperial	0.00	0.01	0.15	0.11	609	1	15	
R108-24-46	C-491513	52.0	Imperial	0.00	0.02	0.15	0.03	610	3	5	
R108-24-45	C-491512	66.9	Imperial	0.00	0.03	0.13	0.00	609	4	0	2.33
R108-24-44	C-491511	86.2	Imperial	0.01	0.04	0.17	0.00	601	3	0	
R108-24-43	C-491510	96.3	Imperial	0.00	0.03	0.14	0.05	609	4	6	
R108-24-42	C-491509	111.4	Imperial	0.01	0.05	0.22	0.05	334	6	6	
R108-24-41	C-491508	129.6	Imperial	0.01	0.18	0.04	0.10	436	22	12	3.00
R108-24-40	C-491507	141.5	Imperial	0.01	0.03	0.15	0.01	607	4	1	
R108-24-39	C-491506	155.0	Imperial	0.00	0.02	0.11	0.09	609	3	12	
R108-24-38	C-491505	170.5	Imperial	0.00	0.03	0.10	0.06	608	4	8	
R108-24-37	C-491504	184.5	Imperial	0.01	0.04	0.12	0.33	609	5	40	2.68
R108-24-36	C-491503	199.0	Imperial	0.01	0.03	0.17	0.18	385	1	6	
R108-24-34	C-491501	214.3	Imperial	0.00	0.03	0.12	0.04	609	4	5	
R108-24-33	C-486500	230.0	Imperial	0.00	0.03	0.11	0.06	609	4	7	
R108-24-31	C-486498	236.2	Imperial	0.09	3.04	0.03	0.94	608	3	1	
R108-24-30	C-486497	244.1	Imperial	0.00	0.02	0.10	0.07	605	2	8	3.11
R108-24-29	C-486496	258.9	Imperial	0.01	0.06	0.10	0.21	499	8	29	
R108-24-28	C-486495	273.2	Imperial	0.00	0.02	0.10	0.06	607	3	8	
R108-24-27	C-486494	287.3	Imperial	0.00	0.03	0.11	0.00	607	4	0	
R108-24-26	C-486493	302.8	Imperial	0.01	0.03	0.13	0.09	609	3	10	2.89
R108-24-24	C-486491	316.0	Imperial	0.00	0.03	0.09	0.12	608	3	13	
R108-24-23	C-486490	330.9	Imperial	0.00	0.03	0.10	0.09	609	3	10	
R108-24-22	C-486489	345.7	Imperial	0.00	0.03	0.12	0.01	359	4	1	
R108-24-21	C-486488	360.0	Imperial	0.00	0.03	0.10	0.34	568	4	47	3.09
R108-24-20	C-486487	366.8	Imperial?	0.01	0.03	0.13	0.00	537	3	0	2.90
R108-24-19	C-486486	376.2	Canol	0.01	0.04	0.15	0.11	608	1	4	2.90
R108-24-18	C-486485	384.3	Canol	0.00	0.02	0.15	0.21	609	1	6	2.89
R108-24-17	C-486484	393.0	Canol	0.01	0.03	0.16	0.06	610	1	2	
R108-24-16	C-486483	401.7	Canol	0.01	0.03	0.17	0.25	609	0	4	2.77
R108-24-15	C-486482	408.8	Canol	0.01	0.04	0.13	0.11	394	2	4	

Table 2a continued.

Sample	GSC curation #	Downhole depth (m)	Unit	S1	S2	P1	S3	T_{max}	HI	OI	$\%Ro_R$
R108-24-14	C-486481	425.0	Canol	0.01	0.03	0.15	0.00	606	1	0	2.83
R108-24-13	C-486480	441.0	Canol	0.01	0.05	0.12	0.00	446	1	0	
R108-24-12	C-486479	458.8	Canol	0.00	0.02	0.10	0.00	609	1	0	
R108-24-10	C-486476	477.5	Canol	0.01	0.03	0.17	0.04	357	1	1	
R108-24-9	C-486475	483.3	Canol	0.00	0.04	0.08	0.15	609	13	48	
R108-24-8	C-486474	494.5	Canol	0.00	0.00	0.28	0.17	541	0	3	2.76
R108-24-7	C-486473	507.7	Canol	0.01	0.03	0.16	0.06	386	1	1	
R108-24-6	C-486472	511.7	Canol	0.01	0.04	0.17	0.49	383	1	13	
R108-24-5	C-486471	521.3	Canol	0.01	0.04	0.16	0.27	371	1	6	
R108-24-4	C-486470	531.3	Canol	0.01	0.02	0.17	0.11	608	0	2	
R108-24-3	C-486469	546.5	Canol	0.01	0.06	0.13	0.47	606	2	17	
R108-24-1	C-486467	565.0	Canol	0.01	0.03	0.17	0.04	420	2	2	2.88
R108-25-22	C-491595	49.5	Imperial	0.01	0.03	0.30	0.06	607	4	9	2.09
R108-25-21	C-491594	63.5	Imperial	0.01	0.02	0.23	0.08	606	3	13	
R108-25-20	C-491593	77.5	Imperial	0.01	0.02	0.43	0.16	607	4	28	
R108-25-19	C-491592	91.5	Imperial	0.06	0.09	0.41	0.14	271	12	19	
R108-25-18	C-491591	105.5	Imperial	0.11	0.08	0.59	0.10	334	11	14	2.08
R108-25-17	C-491590	120.5	Imperial	0.01	0.05	0.21	0.11	605	7	15	
R108-25-16	C-491589	134.5	Imperial	0.02	0.03	0.37	0.11	473	4	15	
R108-25-15	C-491588	148.5	Imperial	0.01	0.06	0.15	0.16	607	8	22	
R108-25-14	C-491587	163.8	Imperial	0.01	0.03	0.14	0.06	607	4	8	2.25
R108-25-13	C-491586	179.1	Imperial	0.01	0.04	0.23	0.12	434	5	16	
R108-25-12	C-491585	194.4	Imperial	0.01	0.04	0.17	0.08	606	2	4	
R108-25-11	C-491584	209.7	Imperial	0.01	0.02	0.27	0.09	607	3	12	
R108-25-10	C-491583	225.1	Imperial	0.01	0.03	0.25	0.14	422	4	16	2.41
R108-25-9	C-491582	240.4	Imperial	0.02	0.04	0.35	0.09	605	5	12	
R108-25-8	C-491581	255.7	Imperial	0.01	0.04	0.26	0.07	605	6	10	
R108-25-7	C-491580	271.0	Imperial	0.01	0.05	0.21	0.11	607	2	5	
R108-25-5	C-491578	286.5	Imperial	0.02	0.04	0.33	0.08	607	5	10	2.32
R108-25-4	C-491577	300.6	Imperial	0.01	0.03	0.26	0.08	607	3	9	
R108-25-3	C-491576	314.7	Imperial	0.01	0.04	0.15	0.06	606	6	8	
R108-25-2	C-491575	329.1	Imperial	0.02	0.04	0.35	0.10	292	5	12	
R108-25-1	C-491574	343.5	Imperial	0.01	0.04	0.23	0.09	605	5	12	2.47
PE07-07-9	C-491535	67.6	Canol	0.01	0.10	0.10	0.48	605	4	19	
PE07-07-8	C-491534	82.5	Canol	0.01	0.03	0.26	0.08	609	1	4	
PE07-07-7	C-491533	96.0	Canol	0.01	0.04	0.12	0.07	489	2	3	
PE07-07-6	C-491532	99.4	Canol	0.01	0.05	0.15	0.31	499	1	6	1.89
PE07-07-5	C-491531	109.7	Canol	0.01	0.10	0.11	0.09	608	4	3	1.97
PE07-07-4	C-491530	123.4	Canol	0.01	0.04	0.18	0.07	593	4	7	
PE07-07-3	C-491529	137.2	Canol	0.01	0.03	0.32	0.15	609	2	13	
PE07-07-2	C-491528	151.4	Canol	0.01	0.07	0.16	0.13	485	2	3	
PE07-07-1	C-491527	164.2	Canol	0.01	0.06	0.18	0.07	606	2	3	1.82

Table 2b.

Sample	GSC curation #	Unit	NAD 83 Zone 8 Easting	Northing	S1	S2	PI	S3	T_{max}	TOC	HI	OI
10TLA-RICH-09P		Imperial	443605	7357239	0.00	0.03	0.14	0.25	609	0.87	3	29
10TLA-RICH-09O		Imperial	443605	7357239	0.01	0.04	0.24	0.37	479	5.68	1	7
10TLA-RICH-09N		Imperial	443865	7357101	0.00	0.03	0.10	0.47	609	1.02	3	46
10TLA-RICH-09M	C-542085	Canol	443994	7357127	0.01	0.04	0.17	0.72	482	2.94	1	24
10TLA-RICH-09K	C-542084	Canol	444442	7357098	0.01	0.03	0.20	0.34	352	3.12	1	11
10TLA-RICH-09I	C-542083	RR	444611	7356939	0.01	0.03	0.16	0.26	610	2.65	1	10
10TLA-RICH-09G		RR	444927	7356821	0.00	0.05	0.08	1.01	609	4.96	1	20
10TLA-RICH-09F		RR	444944	7356815	0.01	0.04	0.12	2.14	609	4.66	1	46
10TLA-RICH-09D		RR	444967	7356804	0.01	0.04	0.15	1.04	609	2.42	2	43
10TLA-RICH-09B		RR	445304	7356761	0.01	0.03	0.15	0.58	610	1.02	3	57
10TLA-RICH-09A		RR	445902	7356439	0.01	0.08	0.07	1.71	522	3.22	2	53

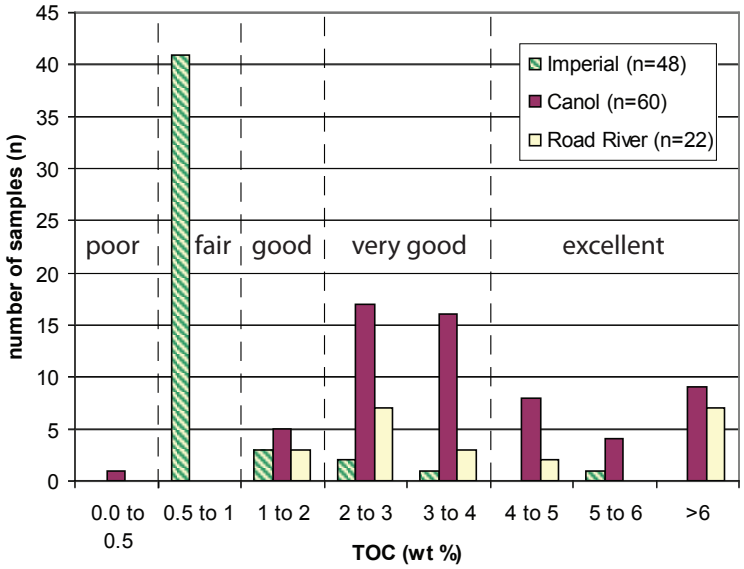

Figure 8. *Histogram summarizing the total organic carbon (TOC) content, expressed in weight percent (wt %), from samples of Road River Group, Canol and Imperial formations from both drill core and outcrop samples. The TOC categories (good to excellent) correspond to source rock generative potential (Peters et al., 2005). See Table 2 for corresponding dataset.*

VITRINITE REFLECTANCE AND ORGANIC PETROLOGY

In order to determine thermal maturity, vitrinite reflectance, a widely accepted method by the oil and gas industry (Fowler *et al.*, 2005; Peters *et al.*, 2005), is an especially important technique when the T_{max} values are rendered meaningless. Table 3 summarizes VR data collected from all drillholes. Appendix A is a detailed table which includes vitrinite reflectance values and comments about the organic material observed in each sample based on organic petrology. From shale samples collected at the Fox property, vitrinite reflectance values range from 2.99 to 3.86 $\%Ro_R$ for the Road River Group (n=5) and 2.91 to 3.59 $\%Ro_R$ for the Canol Formation (n=4). At the Rich property, VR data derived from diamond drill core samples of Road River Group strata range from 2.21 to 2.77 $\%Ro_R$ (n=5); for the Canol Formation from 2.07 to 2.90 $\%Ro_R$ (n=14); and for the Imperial Formation from 2.09 to 3.11 $\%Ro_R$ (n=13). VR values for Canol Formation strata at the Pe property range from 1.89 to 1.97 $\%Ro_R$ (n=3). Thermal maturity values from all samples are very high, with all samples from the Fox and the Rich properties in the dry gas zone (>2.00 $\%Ro_R$), and samples from the Pe property (Canol) near the upper limit of the mixed wet/dry gas zone (just below 2.00 $\%Ro_R$; Mukhopadhyay, 1994).

Organic petrology of the Road River Group samples identified mainly amorphous kerogen with rare to trace amounts of alginite derived vitrinite macerals, chitinozoans, radiolarians and *Tasmanites* alginite (refer to Appendix A for more detailed descriptions). The organic-rich black shale of the Canol Formation contains mainly amorphous kerogen, with minor alginite, alginite derived vitrinite and bitumen (pyrobitumen and migra-bitumen) macerals, negligible terrestrial plant derived inertinite macerals, trace *Tasmanites*, chitinozoans and radiolaria. Both the Road River Group and Canol Formation contain framboidal and tetrahedral pyrite. Imperial Formation

Table 3. *Summary of vitrinite reflectance data in random percent reflectance in oil (% Ro_R) from diamond drill holes. Grey cells represent vitrinite equivalent values for measured pyrobitumen macerals based on Jacob (1989). See Appendix A for more detail including descriptions of macerals.*

Sample #	Downhole depth (m)	Unit	$\%Ro_R$
FX07-02-6	52.7	Canol	2.91
FX07-02-4	64.0	Canol	3.00
FX07-02-3	79.0	Road River	3.09
FX07-02-1	106.9	Road River	3.11
FX07-03-9	33.3	Canol	3.59
FX07-03-5	87.5	Canol	3.13
FX07-03-3	111.5	Road River	3.14
FX07-03-2	128.6	Road River	3.86

Table 3 continued.

Sample #	Downhole depth (m)	Unit	$\%Ro_R$
FX07-03-1	139.0	Road River	2.99
RI07-02-5	44.7	Road River	2.21
RI07-02-1	105.6	Road River	2.25
RI07-07A-12	37.8	Canol	2.07
RI07-07A-6	91.0	Canol	2.28
RI07-07A-5	102.3	Canol	2.30
RI07-07A-2	140.2	Canol	2.48
RI07-07A-1	166.5	Road River	2.77
RI07-16-5	58.5	Canol	2.27
RI07-16-3	86.0	Canol	2.43
RI07-16-2	103.1	Road River	2.56
RI07-16-1	121.9	Road River	2.43
RI07-20-5	119.3	Canol	2.33
RI07-20-1	185.9	Canol?	2.51
R108-24-45	66.9	Imperial	2.33
R108-24-41	129.6	Imperial	3.00
R108-24-37	184.5	Imperial	2.68
R108-24-30	244.1	Imperial	3.11
R108-24-26	302.8	Imperial	2.89
R108-24-21	360.0	Imperial	3.09
R108-24-20	366.8	Imperial	2.90
R108-24-19	376.2	Canol	2.90
R108-24-18	384.3	Canol	2.89
R108-24-16	401.7	Canol	2.77
R108-24-14	425.0	Canol	2.83
R108-24-8	494.5	Canol	2.76
R108-24-1	565.0	Canol	2.88
RI08-25-22	49.5	Imperial	2.09
RI08-25-18	105.5	Imperial	2.08
RI08-25-14	163.8	Imperial	2.25
RI08-25-10	225.1	Imperial	2.41
RI08-25-5	286.5	Imperial	2.32
RI08-25-1	343.5	Imperial	2.47
PE07-07-6	99.40	Canol	1.89
PE07-07-5	109.70	Canol	1.97
PE07-07-1	164.20	Canol	1.89

samples are described as organically lean and as containing minor vitrinite and bitumen macerals and some inertinite macerals (see Appendix A for full details).

XRD MINERALOGY

XRD mineralogy ternary diagrams for percentage of quartz, carbonate, and clay for Road River Group and Canol and Imperial formation shale are provided in Figure 9. Table 4 lists the simplified XRD mineralogy data for each sample, re-calculated from raw data to enable plotting on quartz, carbonate, and clay ternary diagrams. Appendix B lists the XRD mineralogy raw data which includes other minerals not included on the ternary diagrams.

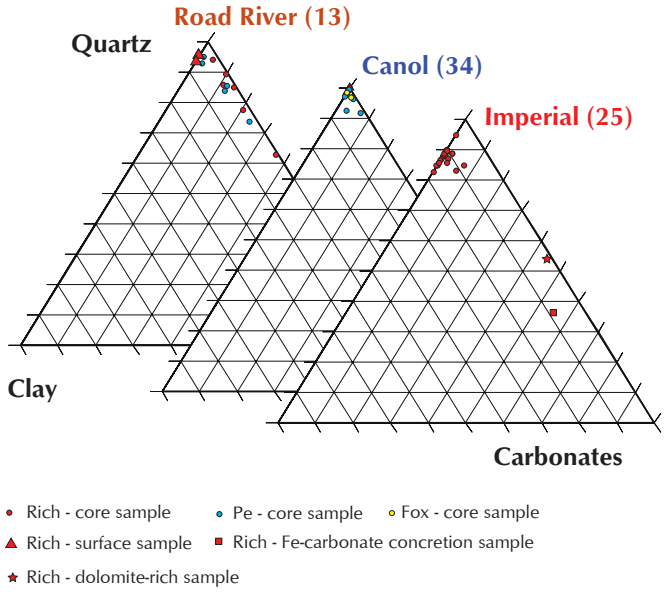

Figure 9. *Ternary diagram displaying the relative mineralogical compositions of Road River Group, Canol and Imperial formation drill core and surface field samples. The corresponding data are in Table 4.*

Road River Group shale samples were analysed from the Rich and Fox properties (n=6 and 5, respectively). In addition, two samples from Road River Group strata exposed at the surface of the Rich property were analysed. Road River shale has the most variable lithology observed, with quartz ranging between 62 and 96%, and carbonate between 0 to 37%. Carbonate is mainly calcite (up to 34%) with minor dolomite (typically ≤2%), except for two samples from the Fox property which had 8 and 11% dolomite. Percentage of clay in all samples was very low, ≤4% mica/illite.

Canol Formation shale was analysed from drill core at the Fox, Rich, and PE properties (n=6, 23, and 4, respectively). In addition, one sample from Canol Formation exposed at the surface of the Rich property was analysed. The Canol Formation, from all properties, is highly siliceous, in all instances exceeding 91% quartz, and typically ≥ 95% quartz. Carbonate and clay fractions are very minor in these samples, typically ≤2% except at the Fox property where higher values of carbonate (up to 7% calcite/dolomite) and up to 4% clay minerals (mica/illite) were found. Of note is one sample from the Fox property which had ~41% gypsum identified.

Twenty-three shale samples from the Imperial Formation were analysed from the Rich property drill core. The Imperial is less siliceous than the Canol Formation but is a more homogeneous lithology than the Road River Group shale sampled from the core. The quartz fraction in all instances of Imperial Formation is >82% with the clay fraction 5 to 17% (chlinochlore, mica/illite, and other mixed layer clays). The carbonate fraction is mainly dolomite (≤2%; n=5) with lesser calcite (2%; n=1), and siderite was found in three samples (≤2%). A number of Imperial samples had minor amounts of Na-feldspar. In addition to the shale samples, two carbonate-rich samples from the Imperial Formation including one dolomite-rich sample (45% total carbonate) and one siderite concretion (55% siderite) are included in Figure 9. Caution should be used with these results as the amount of quartz tends to be overestimated and clay underestimated in many shale samples using standard XRD techniques (Spencer *et al.*, 2010).

DISCUSSION

HYDROCARBON POTENTIAL

Determination of TOC values are used to evaluate source rock generative potential (Peters, 1986). In addition, quantity of TOC is critical in assessing potential shale gas reservoirs as organic matter provides necessary porosity and adsorptive sites for hydrocarbons (Faraj, 2009; Passey *et al.*, 2010). Based on TOC values, the Road River Group and the Canol Formation are organic-rich and demonstrate the most promising prospect as potential source rocks, with predominantly very good to excellent generative potential (Peters, 1986; Fig. 8). Road River Group and Canol Formation strata typically contain 2 to 5 wt % TOC, while the Imperial Formation generally has less than one weight per cent. Because of the high thermal maturity of

Table 4. *Summary of mineral compositions, recalculated from raw data, based on XRD semi-quantitative analysis (expressed in mineral ratio percent) of black shale core samples. Highlighted samples refer to carbonate-rich shale (R108-24-21) and a siderite nodule (R108-24-25). ** = surface samples; NAD83, Zone 8; 10TLA-RICH-09M (443994, 7357127), 10TLA-RICH-09I (444611, 7356939), 10TAL-RICH-09K (444442, 7357098).*

Sample	GSC curation #	Downhole Depth (m)	Formation	% quartz	% carbonate	% clay
RI08-25-22	C-491595	49.5	Imperial	85.4	0.0	14.6
RI08-25-20	C-491593	77.5	Imperial	82.7	6.1	11.2
RI08-25-18	C-491591	105.5	Imperial	89.5	0.0	10.5
RI08-25-16	C-491589	134.5	Imperial	89.7	0.0	10.3
RI08-25-14	C-491587	163.8	Imperial	85.4	2.1	12.5
RI08-25-12	C-491585	194.4	Imperial	88.4	2.1	9.5
RI08-25-10	C-491583	225.1	Imperial	88.7	0.0	11.3
RI08-25-8	C-491581	255.7	Imperial	85.7	0.0	14.3
RI08-25-5	C-491578	286.5	Imperial	86.7	0.0	13.3
RI08-25-3	C-491576	314.7	Imperial	86.5	0.0	13.5
RI08-25-1	C-491574	343.5	Imperial	86.7	0.0	13.3
RI08-24-47	C-491514	39.3	Imperial	89.4	0.0	10.6
RI08-24-45	C-491512	66.9	Imperial	87.5	1.0	11.5
RI08-24-43	C-491510	96.3	Imperial	88.5	2.1	9.4
RI08-24-41	C-491508	129.6	Imperial	84.5	0.0	15.5
RI08-24-39	C-491506	155.0	Imperial	87.8	0.0	12.2
RI08-24-37	C-491504	184.5	Imperial	82.7	0.0	17.3
RI08-24-34	C-491501	214.3	Imperial	88.8	0.0	11.2
RI08-24-30	C-486497	244.1	Imperial	85.7	0.0	14.3
RI08-24-28	C-486495	273.2	Imperial	84.7	0.0	15.3
RI08-24-26	C-486493	302.8	Imperial	86.7	2.0	11.2
RI08-24-25	C-486492	315.2	Imperial	36.0	55.0	9.0
RI08-24-23	C-486490	330.9	Imperial	84.4	7.3	8.3
RI08-24-21	C-486488	360.0	Imperial	52.9	44.7	2.4
RI08-24-20	C-486487	366.8	Imperial?	94.6	0.0	5.4
FX07-02-8	C-491543	25.8	Canol	96.4	0.0	3.6
FX07-02-6	C-491541	52.7	Canol	98.9	0.0	1.1
FX07-02-4	C-491539	64.0	Canol	98.9	0.0	1.1
FX07-03-9	C-491553	33.3	Canol	95.9	3.1	1.0
FX07-03-7	C-491551	60.7	Canol	92.4	3.3	4.3
FX07-03-5	C-491549	87.5	Canol	91.8	7.2	1.0
RI07-07A-12	C-491526	37.8	Canol	98.9	0.0	1.1
RI07-07A-10	C-491524	63.2	Canol	97.8	0.0	2.2
RI07-07A-6	C-491520	91.0	Canol	98.0	1.0	1.0
RI07-07A-5	C-491519	102.3	Canol	98.9	0.0	1.1
RI07-07A-4	C-491518	114.8	Canol	97.9	0.0	2.1
RI07-07A-2	C-491516	140.2	Canol	98.0	1.0	1.0

Table 4 continued.

Sample	GSC curation #	Downhole depth (m)	Formation	% Quartz	% Carbonate	% Clay
RI07-16-7	C-491560	25.5	Canol	97.9	0.0	2.1
RI07-16-5	C-491558	58.5	Canol	97.9	0.0	2.1
RI07-16-3	C-491556	86.0	Canol	99.0	0.0	1.0
RI07-20-7	C-491573	85.9	Canol	99.0	0.0	1.0
RI07-20-5	C-491571	119.3	Canol	99.0	0.0	1.0
RI07-20-3	C-491569	152.6	Canol	98.0	1.0	1.0
RI07-20-1	C-491567	185.9	Canol?	98.0	0.0	2.0
RI08-24-19	C-486486	376.2	Canol	96.9	2.0	1.0
RI08-24-18	C-486485	384.3	Canol	97.9	0.0	2.1
RI08-24-17	C-486484	393.0	Canol	98.0	0.0	2.0
RI08-24-16	C-486483	401.7	Canol	97.8	0.0	2.2
RI08-24-14	C-486481	425.0	Canol	98.9	0.0	1.1
RI08-24-12	C-486479	458.8	Canol	100.0	0.0	0.0
RI08-24-8	C-486474	494.5	Canol	99.0	0.0	1.0
RI08-24-7	C-486473	507.7	Canol	98.9	0.0	1.1
RI08-24-4	C-486470	531.3	Canol	98.9	0.0	1.1
RI08-24-1	C-486467	565.0	Canol	100.0	0.0	0.0
10TLA-RICH-09M**	C-542085		Canol	99.0	0.0	1.0
PE07-07-8	C-491534	82.5	Canol	95.8	3.1	1.0
PE07-07-5	C-491531	109.7	Canol	98.0	0.0	2.0
PE07-07-3	C-491529	137.2	Canol	97.8	0.0	2.2
PE07-07-1	C-491527	164.2	Canol	97.9	0.0	2.1
RI07-07A-1	C-491515	166.5	RR	93.9	4.1	2.0
RI07-16-2	C-491555	103.1	RR	62.2	36.7	1.0
RI07-16-1	C-491554	121.9	RR	88.9	10.1	1.0
RI07-02-5	C-491565	44.7	RR	85.3	11.6	3.2
RI07-02-3	C-491563	75.8	RR	77.3	20.6	2.1
RI07-02-1	C-491561	105.6	RR	84.4	14.6	1.0
10TLA-RICH-09I**	C-542083		RR	94.9	0.0	5.1
10TLA-RICH-09K**	C-542084		RR	93.8	0.0	6.2
FX07-02-3	C-491538	79.0	RR	95.7	1.1	3.3
FX07-02-1	C-491536	106.7	RR	93.7	2.1	4.2
FX07-03-3	C-491547	111.5	RR	84.2	12.6	3.2
FX07-03-2	C-491546	128.6	RR	73.2	24.7	2.1
FX07-03-1	C-491545	139.0	RR	85.7	13.3	1.0

these samples (≥1.89 %Ro_R), care should be taken when using TOC values to describe source rock potential. First, as a source rock matures, the amount of organic matter in the source rock will decrease as hydrocarbons are created, resulting in a decrease in TOC values as the amount of reactive kerogen gets consumed (Daly and Edman, 1987). Tissot and Welte (1984) suggest that for Type II organic matter, hydrocarbon utilizes roughly half of the initial TOC. Using this rule of thumb, and recognizing that the original type of organic matter in the samples may have been variable, the initial TOC of the samples could have been higher, for example in the 4-10 wt % range for the Canol Formation and Road River Group, and between 1 and 2 wt % for the Imperial Formation. Second, TOC by itself is not necessarily a good indicator of how much hydrocarbon a rock can generate (Dembicki, 2009). For organic matter to generate hydrocarbons, the carbon must have associated hydrogen. An indirect measure of hydrogen is the Rock-Eval derived S2 value which is a quantification of the hydrocarbons formed during the thermal decomposition of the kerogen in the rock (Dembicki, 2009). In this study, all strata have Rock-Eval S2 values below 0.2 mg HC/g rock, indicating that there is almost no hydrogen available for generating hydrocarbons, suggesting the source rock potential for the strata at these locations is poor. In other areas where the thermal maturity is not as high, for example in Eagle Plain basin where Canol and Imperial formation strata is in the oil window (Link and Bustin, 1989; Lane *et al*., 2010), the source rock potential is more favourable.

Organic petrology revealed the presence of mainly amorphous kerogen with minor amounts of alginite derived vitrinite and bitumen macerals and negligible amounts of recycled or reworked terrestrial plant derived inertinite macerals and *Tasmanites* algae in the Road River Group and Canol Formation. In contrast, organic matter within the Imperial Formation is described as organically lean, containing minor vitrinite, inertinite and bitumen macerals. Kerogen type is fundamental to the determination of what ranges of hydrocarbon will be produced and affects adsorptive capacity (Faraj, 2009). The type of organic matter within the Road River Group and Canol Formation can be categorized as consisting of a mix of types I and II kerogen which are oil-prone. Alginite, such as *Tasmanites,* is frequently a major contributor to type I kerogen (Peters *et al*., 2005).

VR data indicates that there is a regional trend of decreasing thermal maturity southward along the flank of the Richardson Mountains. This is in part due to differential uplift on major structures that strike sub-parallel to the anticlinorium axis (*e.g.*, Lane, 1996; Lane *et al*. 2007); as well as to presumed deeper burial in the north. No obvious trend exists between the level of thermal maturity and the stratigraphic interval. In the south, where vitrinite reflectance values for the Canol are 1.89-1.97 %Ro_R, the level of thermal maturity is at the upper limit of the wet/dry gas generation zone. Moving north to the Rich and Fox properties, where vitrinite reflectance values for all formations is >2.0 %Ro_R, the strata are within the dry gas generation zone. It is believed that strata with vitrinite reflectance values greater than 4 %Ro are barren of hydrocarbons (North, 1985), however post-mature thermogenic shale-gas has been produced from the Marcellus Formation in the eastern Pennsylvania at Ro_R values >3.0 (*e.g.,* Laughrey *et al*., 2011). To the west of the Richardson anticlinorium, in Eagle Plain basin, the maturity of the Canol and Imperial formations in the subsurface decreases from the dry gas window to the oil window (Link and Bustin, 1989; Lane *et al*., 2010). This trend probably reflects greater depth of burial at the level of Devonian shale in the former Richardson trough. However, variations in the paleogeothermal gradient in the region cannot be ruled out (Link and Bustin, 1989). These results highlight the potential for source rock generation and shale gas/liquids in Eagle Plain basin.

Mineralogical composition is an important property in characterizing the mechanical properties of shale in order to design optimal techniques for natural gas extraction, *e.g.*, hydraulic fracturing. Hydraulic fracturing increases the amount of shale reservoir contacted by a wellbore by creating an artificial fracture network through fluid stimulation. Brittle shale is more likely to respond to this type of stimulation by creating a complex fracture network (Clarkson *et al*., 2011). According to Passey *et al*. (2010), current producing shale-gas reservoirs tend to have <50% clay, and the reservoirs that contain >50% quartz or carbonate are more brittle and respond well to current stimulation practises. Using these guidelines, XRD results indicate that all strata examined can be characterized as brittle, with high silica components enhanced by variable carbonate contents, and minor to negligible clay contents. The Canol Formation and Road River Group are comparatively brittle, with the Canol consistently highly siliceous with greater than 91% quartz and low (typically <3%) carbonate and clay components. Road River Group shale has a more varied lithology with 62 to 96% quartz and up to 37% carbonate minerals (mostly calcite) and up to 4% mica/illite (in core samples). Imperial Formation

shale is overall less brittle than the Canol Formation or Road River Group as the clay component is generally higher (up to 17% mica, illite, mixed-layer clay and/or clinochore), however, the considerable quartz content (82 to 90%) characterizes it as brittle regardless. Further assessment using a scanning electron microscope (SEM) may provide more accurate mineralogical information than standard XRD techniques, removing the possibility of quartz overestimation and clay underestimation mentioned previously. SEM also provides further information about the rock fabric and natural fracture patterns used to assess mechanical and flow properties of shale (Spencer *et al*., 2010). In addition, further information about the quartz component would enhance this study, as it has been suggested that the most effective quartz component for reservoir stimulation is biogenic opaline silica (Jarvie *et al*., 2007) and that detrital quartz is less effective (Thyberg *et al*., 2009).

All strata analysed herein have the potential to host unconventional hydrocarbons under proper burial conditions. The Canol Formation is the most promising unit as it is extremely brittle due to its high silica contents, mineralogically consistent throughout the study region, has very good to excellent total organic carbon contents and has favourable thermal maturity in Eagle Plain basin. The Road River Group also has favourable TOC and XRD values, however, previous studies from limited well data suggest it has poor source rock potential regionally in northern Yukon (Link and Bustin, 1989). Imperial Formation strata has lower TOC contents than the other units, but it is brittle and found to be favourably thermally mature in some Eagle Plain wells.

SUMMARY AND CONCLUSIONS

Fresh diamond drill core samples from Paleozoic shale of the Road River Group and Canol and Imperial formations in the Richardson Mountains immediately east of Eagle Plain basin were analysed for Rock-Eval pyrolysis, organic petrology, and vitrinite reflectance to assess organic matter quantity, quality, and thermal maturity. X-ray diffraction was conducted to assess quartz, clay, and carbonate mineralogy.

Results of this study suggest that the strata examined have the potential to host unconventional hydrocarbons in the region, under favourable burial conditions. Based on TOC values, Canol Formation and Road River Group contain the most organic-rich strata of that studied, and may have been more organic-rich in the past. At the current sample locations, however, the high thermal maturity of strata suggests they have limited generative potential. Based on organic petrology, it was determined that the organic matter consists of a mix of types I and II which coincide with oil-prone kerogen. Vitrinite reflectance illustrates the levels of thermal maturation for all strata are very high, ranging from 1.89 to 3.86 $\%Ro_R$, with 93% of samples >2.0 $\%Ro_R$ indicating most of the strata have matured beyond the oil and wet gas windows into the dry gas generation zone. The maturity data also demonstrate a general trend of decreasing thermal maturity from the Fox property in the north to the Pe property in the south for all geological units assessed. X-ray diffraction results indicate that all strata are dominantly siliceous, and thus candidates for successful hydraulic fracturing programs, however, the Canol Formation is the most mineralogically consistent with over 91% quartz in all samples. Road River Group strata are slightly more mineralogically variable than Canol Formations samples, with silica content ranging from 62-96% and carbonate content up to 37%. The Imperial Formation contains over 82% quartz with up to 17% clay.

Initial results from this diamond drillhole study were presented in Allen *et al*. (2011) which presented Rock-Eval, XRD mineralogy, and palynological determinations of Road River Group, and Canol and Imperial strata from Rich property core. This study includes core data from two additional locations (Fox and Pe) and surface field samples from the Rich property. The inclusion of data from locations both south and north of the Rich property in this paper expands the geographic extent of these analyses and illustrates improved understanding of thermal maturity trends along strike. In addition, this study includes vitrinite reflectance data and a summary description of the organic petrology. The organic petrology results provide insight into the types of organic matter present in the strata as determination through geochemical techniques was not possible due to the advanced thermal maturity of the organic matter.

It is important to mention that this study would not have been possible without data sharing between the minerals and oil and gas sectors, specifically the prompt provision of diamond drill core that may otherwise have been subjected to weathering in the field. Further collaboration between these sectors is encouraged in advancing the understanding of Yukon geology.

ACKNOWLEDGEMENTS

This project, including field logistics and all analytical support, was funded by the Earth Sciences Sector, Natural Resources Canada, Geo-Mapping for Energy and Minerals (GEM-Energy) initiative. This project was also funded in part by YGS and Northern Cross (Yukon) Limited (NCY). Fireweed helicopters Ltd. provided reliable and safe helicopter support. Special acknowledgement is extended to Archer Cathro & Associates (1981) Limited who donated core for this project. The manuscript was reviewed by Lee Pigage, Yukon Geological Survey, and Mark Obermajer, Geological Survey of Canada. The manuscript is ESS Contribution No. 20110357.

REFERENCES

Allen, T.L., 2010. Field notes on the Upper Devonian Imperial Formation (NTS map sheet 106L), Tetlit Creek, east Richardson Mountains, Yukon. *In:* Yukon Exploration and Geology 2009, K.E. MacFarlane, L.H. Weston and L.R. Blackburn (eds.), Yukon Geological Survey, p. 1-21.

Allen, T.L., Fraser, T.A., and Lane, L.S., 2011. Preliminary results from a diamond drill hole study to assess shale gas potential of Devonian strata, Eagle Plain, Yukon. *In:* Yukon Exploration and Geology 2010, K.E. MacFarlane, L.H. Weston and C. Relf (eds.), Yukon Geological Survey, p. 1-17.

Bassett, H.G., 1961. Devonian stratigraphy, central Mackenzie River region, Northwest Territories, Canada. *In:* Geology of the Arctic, G.O. Raasch (ed.), Alberta Society of Petroleum Geologists and University of Toronto Press, vol. 1, p. 481-498.

Braman, D.R. and Hills, L.V., 1992. Upper Devonian and Lower Carboniferous miospores, western District of Mackenzie and Yukon Territory, Canada. Palaeontolographica Canadiana, no. 8, 97 p.

Clarkson, C.R., Aguilera, R., Pederson, P.K., and Spencer, R.J., 2011. Shale Gas Part 6 – Influence of Technology on Shale Gas Development. CSPG Reservoir, vol. 38, no. 2, p. 23-29.

Daly, A.R. and J.D. Edman, 1987. Loss of organic carbon from source rocks during thermal maturation. American Association of Petroleum Geologists Bulletin, vol. 71, p. 546.

Dembicki, H. Jr., 2009. Three common source rock evaluation errors made by geologists during prospect or play appraisals. American Association Petroleum Geologists Bulletin, vol. 93, no. 3, p. 341-356.

Dolby, G., 2010. Palynological analysis of core, cuttings and outcrop samples from the GEM Yukon Basins Project. Dolby and Associates Report # 2010.9. Internal report prepared for Natural Resources Canada, Calgary, Alberta, 21 p.

Espitalié, J., Deroo, G., and Marquis, F., 1985. Rock Eval Pyrolysis and Its Applications. Preprint; Institut Française du Petrole, Geologie No. 27299, 72 p. English translation of, La pyrolyse Rock-Eval et ses applications, Premiere, Deuxieme et Troisieme Parties, in Revue de l'Institut Francais du Petrole, vol. 40, p. 563-579 and 755-784; vol. 41, p. 73-89.

Faraj, B. 2009. Shale gas critical fundamentals, techniques and tools for exploration analysis. Canadian Society of Petroleum Geologists Short Course # SC0902, October 26, 2009.

Fowler, M., Snowdon, L., and Stasiuk, V., 2005. Applying petroleum geochemistry to hydrocarbon exploration and exploitation. American Association of Petroleum Geologists Short Course Notes, June 18-19, 2005, Calgary, Alberta, 224 p.

Fraser, T. and Hogue, B., 2007. List of Wells and Formation Tops, Yukon Territory, version 1.0. Yukon Geological Survey, YGS Open File 2007-5, 1 p., plus spreadsheet.

Fritz, W.H., 1985. The basal contact of the Road River Group - a proposal for its location in the type area and in other selected areas in the northern Canadian Cordillera. *In:* Current Research, Part B, Geological Survey of Canada, Paper 85-1B, p. 205-215.

Gal, L.P., Allen, T.L., Hadlari, T., and Zantvoort, W.G., 2009. Chapter 10 – Petroleum Systems Elements. *In:* Regional Geoscience Studies and Petroleum Potential, Peel Plateau and Plain, Northwest Territories and Yukon: Project Volume, L.J. Pyle and A.L. Jones (eds.), Northwest Territories Geoscience Office and Yukon Geological Survey, NWT Open File 2009-02 and YGS Open File 2009-25, p. 477-549.

Gordey, S.P. and Makepeace, A.J., 1999. Yukon digital geology. Geological Survey of Canada, Open File D3826.

Goodfellow, W.D., 2011. Devonian shale-hosted Ni-Zn-Mo-PGE sulfide deposits, Yukon. *In:* Abstracts with Program, GAC/MAC 2011, May 25-27, Ottawa, p. 77.

Hadlari, T., Gal, L.P., Zantvoort, W.G., Tylosky, S.A., Allen, T.L., Fraser, T.A., Lemieux, Y., and Catuneanu, O., 2009. Chapter 7 – Upper Devonian to Carboniferous Strata I – Imperial Formation Play. *In:* Regional Geoscience Studies and Petroleum Potential, Peel Plateau and Plain, Northwest Territories and Yukon: Project Volume, L.J. Pyle and A.L. Jones (eds.), Northwest Territories Geoscience Office and Yukon Geological Survey, NWT Open File 2009-02 and YGS Open File 2009-25, p. 337-364.

Hall, K.W. and Cook, F.A., 1998. Geophysical transect of the Eagle Plains foldbelt and Richardson Mountains anticlinorium, northwestern Canada. Geological Society of America Bulletin, vol. 110, no. 3, p. 311-325.

Hamblin, A.P., 2006. The "Shale Gas" concept in Canada: a preliminary inventory of possibilities. Geological Survey of Canada Open File 5384, 103 p.

Héon, D., 2006. Mineral Assessment of the Eagle Plain Study Area, Yukon. Yukon Geological Survey, Open File 2006-3. Includes 2 reports: original study (103 p. plus 1 map) and update (12 p. plus 4 maps).

Hume, G.S. and Link, T.A., 1945. Canol investigations in the Mackenzie River area, Northwest Territories and Yukon. Geological Survey of Canada, Paper 45-16, 87 p.

Jacob, H., 1989. Classification, structure, genesis and practical importance of natural solid oil bitumen ("migra-bitumen"). International Journal of Coal Geology, vol. **11**, p. 65–79.

Jackson, D.E. and Lenz, A.C., 1962. Zonation of Ordovician and Silurian graptolites of northern Yukon, Canada. American Association of Petroleum Geologists Bulletin, vol. 46, p. 30-45.

Jarvie, D.M., Hill, R.J., Ruble, T.E., and Pollastro, R.M., 2007. Unconventional shale-gas systems: The Mississippian Barnett Shale of north-central Texas as one model for thermogenic shale-gas assessment. American Association of Petroleum Geologists Bulletin, vol. 91, no. 4, p. 475–499.

Lafargue, E., Espitalié, J., Marquis, F., and Pillot, D., 1998. Rock-Eval 6 applications in hydrocarbon exploration, production and soil contamination studies. Revue de l'Insitut Français du Petrole vol. 53, p. 421-437.

Lane, L.S., 1996. Geometry and tectonics of early Tertiary triangle zones, northeastern Eagle Plain, Yukon Territory. Bulletin of Canadian Petroleum Geology, vol. 44, p. 337-348.

Lane, L.S., 1998. Late Cretaceous-Tertiary tectonic evolution of northern Yukon and adjacent Arctic Alaska. American Association of Petroleum Geologists Bulletin, vol. 82, p. 1353-1371.

Lane, L.S., 2007. Devonian-Carboniferous paleogeography and orogenesis, northern Yukon and adjacent Arctic Alaska. Canadian Journal of Earth Sciences, vol. 44, p. 679-694.

Lane, L.S., 2010. Phanerozoic Structural Evolution of Eagle Plain, Yukon. Canadian Society of Petroleum Geologists, Reservoir, vol. 37, no.1, p. 11.

Lane, L. S. and Dietrich, J.R., 1995. Tertiary structural evolution of the Beaufort Sea - Mackenzie Delta region, Arctic Canada. Bulletin of Canadian Petroleum Geology, vol. 43, p. 293-314.

Lane, L.S., Utting, J., Allen, T.L., Fraser, T., and Zantvoort, W., 2007. Refinements to Lithostratigraphy, Biostratigraphy and Structural Geometry of the Devonian and Carboniferous Imperial and Tuttle Formations, eastern Eagle Plain, northern Yukon. CSPG-CSEG Annual Meeting, Calgary AB, Program and Abstracts Volume, p. 316-317; CD-ROM: 214S0131.

Lane, L.S., Snowdon, L.R., and Obermajer, M., 2010. Rock-Eval/TOC and oil show analyzer data for selected Yukon borehole samples. Geological Survey of Canada, Open File 6652, 1 CD-ROM.

Laughrey, C.D., Ruble, T.E., Lemmens, H., Kostelnik, J., Butcher, A.R., Walker, G., and Knowles, W., 2011. Black shale diagenesis: insights from integrated high-definition analyses of post-mature Marcellus Formation rocks, northeastern Pennsylvania. American Association of Petrology Geologists, Search and Discovery Article #110150.

Link, T.A., 1921. Unpublished geological report on the Fort Norman area: Imperial Oil Ltd., Calgary, Alberta, 81 p.

Link, C.M. and Bustin, R.M., 1989. Organic maturation and thermal history of Phanerozoic strata in northern Yukon and northwestern District of Mackenzie. Bulletin of Canadian Petroleum Geology, vol. 37, p. 266-292.

Link, C.M., Bustin, R.M., and Snowdon, L.R., 1989. Petroleum Source Potential and Depositional Setting of Phanerozoic Strata in northern Yukon and northwestern District of Mackenzie. Bulletin of Canadian Petroleum Geology, vol. 37, p. 293-315.

Mackowsky, M. –Th., 1982. Methods and tools of examination. *In:* Stach's Textbook of coal Petrology, 3rd ed., E. Stach, M.-Th. Mackowsky, M. Teichmüller, G.H. Taylor, D. Chandra, and R. Teichmüller (eds.), Berlin: Gerbruder Borntraeger, p. 295-299.

Mazzotti, W., Leonard, L.J., Hyndman, R.D., and Cassidy, J.F., 2008. Tectonics, Dynamics, and Seismic Hazard in the Canada-Alaska Cordillera. *In:* Active Tectonics and Seismic Potential of Alaska; American Geophysical Union, Geophysical Monograph Series, no. 179, p. 297-319.

Morrow, D.W., 1999. Lower Paleozoic Stratigraphy of Northern Yukon Territory and Northwestern District of Mackenzie. Geological Survey of Canada, Bulletin 538, 202 p.

Mukhopadyhay, P.K., 1994. Vitrinite reflectance as maturity parameter: petrographic and molecular characterization and its applications to basin modeling. *In*: Vitrinite reflectance as a maturity parameter, applications and limitations, P.K. Mukhopadyhay and W.G. Dow (eds.), American Chemical Society Symposium Series 570, p. 1-25.

Norris, A.W., 1985. Stratigraphy of Devonian outcrop belts in northern Yukon Territory and northwestern District of Mackenzie. Geological Survey of Canada, Paper 67-53, 287 p.

Norris, A.W., 1997. Devonian (Chapter 7). *In:* Geology and Mineral and Hydrocarbon Potential of Northern Yukon Territory and Northwestern District of Mackenzie, D.K. Norris (ed.), Geological Survey of Canada, Bulletin 422, p. 163-200.

Norris, D.K., 1984. Geology of the northern Yukon and northwestern District of Mackenzie. Geological Survey of Canada, Map 1581A.

North, F.K., 1985. Petroleum Geology, Allen & Unwin, London, 607 p.

Osadetz, K.G., Zhuoheng, C., and Bird, T.D., 2005. Petroleum Resource Assessment, Eagle Plain Basin and Environs, Yukon Territory, Canada. Yukon Geological Survey Open File 2005-2/Geological Survey of Canada, Open File 4922, 88 p.

Passey, Q.R., Bohacs, K.M., Esch, W.L., Klimentidis, R., and Sinha, S., 2010. From oil-prone source rock to gas-producing shale reservoir – geological and petrophysical characterization of unconventional shale-gas reservoirs. Society of Petroleum Engineers, CPS/SPE International Oil & Gas Conference and Exhibition, Beijing, China, 8-10 June, 2010, SPE 131350, 29 p.

Peters, K.E., 1986. Guidelines for evaluating petroleum source rock using programmed pyrolysis. American Association of Petroleum Geologists Bulletin, vol. 70, no. 3, p. 318-329.

Peters, K.E., Walters, C.C., and Moldowan, J.M., 2005. The Biomarker Guide, Volume 1. Biomarkers and Isotopes in the Environment and Human History. Cambridge University Press, New York, 471 p.

Pugh, D.C., 1983. Pre-Mesozoic geology in the subsurface of Peel River Map area, Yukon Territory and District of Mackenzie. Geological Survey of Canada, Memoir 401, 61 p.

Richards, B.C., Bamber, E.W., and Utting, J., 1997. Upper Devonian to Permian. *In:* Geology and Mineral and Hydrocarbon Potential of Northern Yukon Territory and Northwestern District of Mackenzie, D.K. Norris (ed.); Geological Survey of Canada, Bulletin 422, p. 201-251.

Snowdon, L.R., 1988. Petroleum source rock potential and thermal maturation reconnaissance in Eagle Plain, Yukon Territory. Geological Survey of Canada, Open File 1720, 115 p.

Spencer, R.J., Pedersen, P.K., Clarkson, C.R., and Aguilera, R., 2010. Shale Gas Part 3 – Shale Properties. CSPG Reservoir, vol. 37, no. 10, p. 26-29.

Tissot, B.P. and Welte, D.H., 1984. Petroleum Formation and Occurrence. Springer-Verlag, Berlin, Heidelberg, New York, Tokyo, 699 p.

Thyburg, B., Jahren, J., Winje, T., Bjorlykke, K., and Faleide, J.I., 2009. From mud to shale: rock stiffening by microquartz cementation. European Association of Geoscientists and Engineers, First Break, vol. 27, issue 2, p. 53-39.

Appendix A. *Summary of vitrinite reflectance data including sample descriptions. SD = standard deviation and N = number of measurements for corresponding average %Ro. Grey cells represent vitrinite equivalent values for measured pyrobitumen macerals based on Jacob (1989).*

Sample #	GSC Curation #	Downhole depth (m)	Unit	$\%Ro_R$	SD	N	Comments
FX07-02-6	C-491541	52.7	Canol	2.91	0.12	15	Overmature organic-rich black shale with major amount of interconnected network of sieve like amorphous kerogen with minor amount of alginite and alginite derived vitrinite and bitumen macerals, and rare amount of framboidal and tetrahedral pyrite minerals. Trace amount of Tasmanites, chitinozoans and inertinite macerals.
FX07-02-4	C-491539	64.0	Canol	3.00	0.14	22	Overmature organic-rich black shale with major amount of interconnected network of sieve like amorphous kerogen with minor amount of alginite and alginite derived vitrinite and bitumen macerals, and rare amount of framboidal and tetrahedral pyrite minerals. Trace amount of Tasmanites, chitinozoans and inertinite macerals.
FX07-02-3	C-491538	79.0	Road River	3.09	0.09	15	Overmature organic-rich black shale with major amount of interconnected network of sieve like amorphous kerogen with minor amount of alginite and alginite derived vitrinite and bitumen macerals, and rare amount of framboidal and tetrahedral pyrite minerals. Trace amount of Tasmanites, chitinozoans and inertinite macerals.
FX07-02-1	C-491536	106.9	Road River	3.11	0.09	22	Overmature organic-rich black shale with major amount of interconnected network of sieve like amorphous kerogen with minor amount of alginite and alginite derived vitrinite and bitumen macerals, and rare amount of framboidal and tetrahedral pyrite minerals. Trace amount of Tasmanites, chitinozoans and inertinite macerals.
FX07-03-9	C-491553	33.3	Canol	3.59	0.11	18	Overmature organic-rich black shale with major amount of interconnected network of sieve like amorphous kerogen with minor amount of alginite and alginite derived vitrinite and bitumen macerals, and rare amount of framboidal and tetrahedral pyrite minerals. Trace amount of Tasmanites, chitinozoans and inertinite macerals.
FX07-03-5	C-491549	87.5	Canol	3.13	0.09	21	Overmature organic-rich black shale with major amount of interconnected network of sieve like amorphous kerogen with minor amount of alginite and alginite derived vitrinite and bitumen macerals, and rare amount of framboidal and tetrahedral pyrite minerals. Trace amount of Tasmanites, chitinozoans and inertinite macerals.
FX07-03-3	C-491547	111.5	Road River	3.14	0.15	28	Overmature organic-rich black silty shale with major amount of interconnected network of sieve like amorphous kerogen with minor amount of alginite and alginite derived vitrinite and bitumen macerals, and rare amount of framboidal and tetrahedral pyrite minerals. Trace amount of Tasmanites, chitinozoans, radiolaria and inertinite macerals.

Appendix A continued.

Sample #	GSC curation #	Downhole depth (m)	Unit	$\%Ro_R$	SD	N	Comments
FX07-03-2	C-491546	128.6	Road River	3.86	0.14	28	Overmature organic-rich black silty shale with major amount of interconnected network of sieve like amorphous kerogen with minor amount of alginite and alginite derived vitrinite and bitumen macerals, and rare amount of framboidal and tetrahedral pyrite minerals. Trace amount of Tasmanites, chitinozoans, radiolaria and inertinite macerals.
FX07-03-1	C-491545	139.0	Road River	2.99	0.08	21	Overmature organic-rich black silty shale with major amount of interconnected network of sieve like amorphous kerogen with minor amount of alginite and alginite derived vitrinite and bitumen macerals, and rare amount of framboidal and tetrahedral pyrite minerals. Trace amount of Tasmanites, chitinozoans, radiolaria and inertinite macerals.
RI07-02-5	C-491565	44.7	Road River	2.21	0.13	4	Framboidal pyrite-rich black shale with trace amount of bitumen and migrabitumen macerals (associated with carbonate minerals in pores or in fractures) brecciated within micrinite-rich spent amorphinite kerogen. Rare amount of alginite derived vitrinite macerals and Tasmanites alginite and trace of amount of calcite filled radiolaria microfossils, chitinozoans and Tasmanites alginite.
RI07-02-1	C-491561	105.6	Road River	2.25	0.12	22	Carbonate-rich black shale with minor of amount of calcite filled radiolaria microfossils and Tasmanites alginite. Mainly small alginite derived amorphinite lenses and bitumen macerals.
RI07-07A-12	C-491526	37.8	Canol	2.07	0.11	22	Framboidal pyrite-rich black shale with trace amount of bitumen and migrabitumen macerals (mainly granular and associated with carbonate minerals in pores or in fractures) brecciated within micrinite-rich spent amorphinite kerogen. Rare amount of alginite derived vitrinite macerals and trace of amount of calcite filled radiolaria microfossils, chitinozoans and Tasmanites alginite.
RI07-07A-6	C-491520	91.0	Canol	2.28	0.15	19	The microstratigraphy shows two distinct matrices consisting of organic and pyrite rich black shale with mostly sieve like amorphinite kerogen and organic-rich mostly amrphinite kerogen, pyrite lean black shale matrix. Trace amount of alginite macerals possibly from prosinophyte.
RI07-07A-5	C-491519	102.3	Canol	2.30	0.10	9	Framboidal pyrite-rich black shale with trace amount of bitumen and migrabitumen macerals (mainly granular and associated with carbonate minerals in pores or in fractures) brecciated within micrinite-rich spent amorphinite kerogen. Rare amount of alginite derived vitrinite macerals and trace of amount of calcite filled radiolaria microfossils, chitinozoans and Tasmanites alginite.

Appendix A continued.

Sample #	GSC curation #	Downhole depth (m)	Unit	%Ro_R	SD	N	Comments
RI07-07A-2	C-491516	140.2	Canol	2.48	0.11	17	Black shale with mostly sieve like amorphous amorphinite kerogen lenses and rare amount of alginite derived vitrinite and bitumen (mostly granular pore filling migrabitumen) macerals. Trace amount of chitinozoans and fracture filling dolomite mineral.
RI07-07A-1	C-491515	166.5	Road River	2.77	0.09	17	Black shale containing minor amount of framboidal pyrite with mostly amorphous amorphinite kerogen and rare amount of alginite derived vitrinite and bitumen macerals. Trace amount of Tasmanites alginite and chitinozoans were also observed together mostly small prosinophyte alginite.
RI07-16-5	C-491558	58.5	Canol	2.27	0.09	12	Framboidal pyrite-rich black shale with trace amount of bitumen and migrabitumen macerals (associated with carbonate minerals in pores or in fractures) within amorphinite-rich matrix. Rare amount of alginite derived vitrinite macerals and Tasmanites alginite.
RI07-16-3	C-491556	86.0	Canol	2.43	0.07	19	black shale with evidence of dolomitizing fluid intrusion. Mainly spent amorphinite kerogen with rare bitumen maceral and trace amount of alginite (possibly prasinophyte) derived vitrinite macerals and chitinozoans. Trace amount of bitumen macerals showing very fine grain and minor anisotropic morphology, and high pyrite inclusion indication of high sulphides.
RI07-16-2	C-491555	103.1	Road River	2.56	0.12	18	Black shale with evidence of dolomitizing fluid intrusion. Mainly spent amorphinite kerogen with rare bitumen maceral and trace amount of alginite (possibly prasinophyte) derived vitrinite macerals and chitinozoans. Rare amount of bitumen macerals proximal to the dolomite matrix shows granular and minor anisotropic morphology, and high pyrite inclusion indication of high sulphides.
RI07-16-1	C-491554	121.9	Road River	2.43	0.06	10	Black shale with evidence of dolomitizing fluid intrusion. Mainly spent amorphinite kerogen with rare bitumen maceral and trace amount of alginite (possibly prasinophyte and Tasmanites) derived vitrinite macerals. Some bitumen macerals proximal to the dolomite matrix shows granular and minor anisotropic morphology, and high pyrite inclusion indication of high sulphides.
RI07-20-5	C-491571	119.3	Canol	2.33	0.09	18	Framboidal pyrite-rich black shale with trace amount of bitumen and migrabitumen macerals (associated with carbonate minerals in pores or in fractures) brecciated within micrinite-rich spent amorphinite kerogen matrix. Rare amount of alginite derived vitrinite macerals, trace of amount of calcite filled radiolaria microfossils, chitinozoans and possibly Leiophaeridia alginite.

Appendix A continued.

Sample #	GSC curation #	Downhole depth (m)	Unit	%Ro_R	SD	N	Comments
RI07-20-1	C-491567	185.9	Canol?	2.51	0.13	15	Black shale with mainly spent amorphinite kerogen with minor amount small lenses of bitumen macerals and framboidal pyrite, and trace amount of alginite (possibly prasinophyte) derived vitrinite macerals. Trace amount of chitinozoans. Rare amount of bitumen macerals proximal to the dolomite matrix shows granular and minor anisotropic morphology, and high pyrite inclusion indication of high sulphides.
R108-24-45	C-486512	66.9	Imperial	2.33	0.22	6	Siltstone with minor amount amount organic and pyrite (framboidal and euhedral crystal). Presence of phosphatic nodules, inertinite. Rare isotropic vitrinite and bitumen lenses.
R108-24-41	C-486508	129.6	Imperial	3.00	0.13	17	Organic and pyrite (framboidal and euhedral crystal) rich silty shale. Presence of phosphatic nodules, inertinite. Rare isotropic vitrinite and bitumen lenses.
R108-24-37	C-486504	184.5	Imperial	2.68	0.08	2	Organic and pyrite (framboidal and euhedral crystal) rich silty shale. Presence of phosphatic nodules, inertinite. Rare isotropic vitrinite and bitumen lenses.
R108-24-30	C-486497	244.1	Imperial	3.11	0.19	12	Organic and pyrite (framboidal and euhedral crystal) rich silty shale. Presence of phosphatic nodules, inertinite. Rare isotropic vitrinite and bitumen lenses.
R108-24-26	C-486493	302.8	Imperial	2.89	0.18	38	Organic and pyrite (framboidal and euhedral crystal) rich silty shale. Presence of phosphatic nodules, inertinite. Rare isotropic vitrinite and bitumen lenses.
R108-24-21	C-486488	360.0	Imperial	3.09	0.14	8	Mainly limestone with minor amount of partially dolomitized siltstone containing minor dark amorphous styloccumulates kerogen and rare high reflecting isotropic pyrobitumen.
R108-24-20	C-486487	366.8	Imperial	2.90	0.13	14	Organic and pyrite (framboidal and euhedral crystal) rich silty shale. Presence of phosphatic nodules, inertinite. Rare anisotropic vitrinite and bitumen lenses evidence of thermal cracking.
R108-24-19	C-486486	376.2	Canol	2.90	0.16	20	Pyrite (mainly framboidal) rich shale. Mainly primary bitumen derived from the thin interconnected amorphinite lenses. Silicified radiolaria and corbonate filled forams and alginite, inertinite and phosphatic nodules were also observed.
R108-24-18	C-486485	384.3	Canol	2.89	0.23	14	similar to above sample
R108-24-16	C-486483	401.7	Canol	2.77	0.28	30	Pyrite (mainly framboidal) rich shale with mainly brown amorphous kerogen with small particle (lenses), rare pyrobitumen maceral observed between carbonates grains.
R108-24-14	C-486481	425.0	Canol	2.83	0.20	20	Pyrite (mainly framboidal) rich shale. Mainly primary bitumen derived from the thin interconnected amorphinite lenses. Silicified radiolaria and corbonate filled forams and alginite, inertinite and phosphatic nodules were also observed.
R108-24-8	C-486474	494.5	Canol	2.76	0.23	15	Pyrite (mainly framboidal and sulphide-rich organic coaly lenses) rich shale. Mainly primary bitumen derived from the thin interconnected amorphinite lenses.

Appendix A continued.

Sample #	GSC curation #	Downhole depth (m)	Unit	%Ro_R	SD	N	Comments
R108-24-1	C-486467	565.0	Canol	2.88	0.28	7	Amorphinite and pyrite (mainly framboidal) rich shale with rare vitrinite and pyrobitumen lenses. Thin interconnected amorphinite macerals.
RI08-25-22	C-491595	49.5	Imperial	2.09	0.07	3	Organically lean matrix minor amount of vitrinite and bitumen maceral brecciated between fine grain siltstone matrix. Some sporinite and semifusinite derived inertinite macerals are of the sample thermal maturity as the bitumen and vitrinite macerals.
RI08-25-18	C-491591	105.5	Imperial	2.08	0.16	3	Organically lean matrix minor amount of vitrinite and bitumen maceral brecciated between fine grain siltstone matrix. Some sporinite and semifusinite derived inertinite macerals are of the sample thermal maturity as the bitumen and vitrinite macerals.
RI08-25-14	C-491587	163.8	Imperial	2.25	0.03	4	Organically lean matrix minor amount of vitrinite and bitumen maceral brecciated between fine grain siltstone matrix. Some sporinite and semifusinite derived inertinite macerals are of the sample thermal maturity as the bitumen and vitrinite macerals.
RI08-25-10	C-491583	225.1	Imperial	2.41	0.03	7	Organically lean matrix minor amount of vitrinite and bitumen maceral brecciated between fine grain siltstone matrix. Some inertinite macerals are of the sample thermal maturity as the bitumen and vitrinite macerals.
RI08-25-5	C-491578	286.5	Imperial	2.32	0.04	4	Organically lean matrix minor amount of vitrinite and bitumen maceral brecciated between fine grain siltstone matrix. Some inertinite macerals are of the sample thermal maturity as the bitumen and vitrinite macerals.
RI08-25-1	C-491574	343.5	Imperial	2.47	0.09	3	Organically lean matrix minor amount of vitrinite and bitumen maceral brecciated between fine grain siltstone matrix. Some inertinite macerals are of the sample thermal maturity as the bitumen and vitrinite macerals.
PE07-07-6	C-491532	99.4	Canol	1.89	0.09	21	Framboidal pyrite-rich dominated black shale matrix with trace amount of bitumen and migrabitumen macerals (mainly granular and associated with carbonate minerals in pores or in fractures) brecciated within micrinite-rich spent amorphinite kerogen. Trace amount of alginite derived vitrinite macerals and terrestrial plant derived inertinite macerals.
PE07-07-5	C-491531	109.7	Canol	1.97	0.09	14	Framboidal pyrite-rich black shale with trace amount of bitumen and migrabitumen macerals (mainly granular and associated with carbonate minerals in pores or in fractures) brecciated within micrinite-rich spent amorphinite kerogen. Trace amount of alginite derived vitrinite macerals and terrestrial plant derived inertinite macerals.
PE07-07-1	C-491527	164.2	Canol	1.89	0.13	10	Framboidal pyrite-rich black shale with trace amount of bitumen and migrabitumen macerals (mainly granular and associated with carbonate minerals in pores or in fractures) brecciated within micrinite-rich spent amorphinite kerogen. Trace amount of alginite derived vitrinite macerals and terrestrial plant derived inertinite macerals.

Appendix B. *Mineral composition raw data based on XRD semi-quantitative analysis (expressed in mineral ratio percent) of black shale core samples and surface field samples. Highlighted samples refer to carbonate-rich shale (R108-24-21) and a siderite nodule (R108-24-25).* = mixed-layer clay; ** = surface field samples; and + = chlorite and/or kaolinite.*

Sample #	GSC curation #	Downhole depth (m)	Fm	M.L.C.*	Mica/ Illite	Clino-chlore	Gyp	Qtz	Fldspr	Cal	Dol	Sd	Py	Others	Qtz	Total Carb	Total Clay	Sum Qtz, Carb & Clay	% Qtz	% Carb	% Clay
RI08-25-22	C491595	49.5	Imperial	2.0	3.0	9.0		82.0	2.0(Na)				2.0		82.0	0.0	14.0	96.0	85.4	0.0	14.6
RI08-25-20	C491593	77.5	Imperial	2.0	3.0	6.0		81.0	tr			6.0	2.0	Siderite-6%	81.0	6.0	11.0	98.0	82.7	6.1	11.2
RI08-25-18	C491591	105.5	Imperial	2.0	3.0	5.0		85.0	3.0(Na)				2.0		85.0	0.0	10.0	95.0	89.5	0.0	10.5
RI08-25-16	C491589	134.5	Imperial	2.0	3.0	5.0		87.0					3.0		87.0	0.0	10.0	97.0	89.7	0.0	10.3
RI08-25-14	C491587	163.8	Imperial	2.0	3.0	7.0		82.0	2.0(Na)		2.0		2.0	Fe dolomite	82.0	2.0	12.0	96.0	85.4	2.1	12.5
RI08-25-12	C491585	194.4	Imperial	3.0	3.0	3.0		84.0			2.0		5.0	Fe dolomite	84.0	2.0	9.0	95.0	88.4	2.1	9.5
RI08-25-10	C491583	225.1	Imperial	2.0	3.0	6.0		86.0					3.0		86.0	0.0	11.0	97.0	88.7	0.0	11.3
RI08-25-8	C491581	255.7	Imperial	3.0	4.0	7.0		84.0	tr				2.0		84.0	0.0	14.0	98.0	85.7	0.0	14.3
RI08-25-5	C491578	286.5	Imperial	3.0	4.0	6.0		85.0	tr				2.0		85.0	0.0	13.0	98.0	86.7	0.0	13.3
RI08-25-3	C491576	314.7	Imperial	3.0	3.0	7.0		83.0	2.0(Na)				2.0		83.0	0.0	13.0	96.0	86.5	0.0	13.5
RI08-25-1	C491574	343.5	Imperial	3.0	4.0	6.0		85.0					2.0		85.0	0.0	13.0	98.0	86.7	0.0	13.3
RI08-24-47	C491514	39.3	Imperial	2.0	3.0	5.0	tr	84.0	4.0(Na)				2.0		84.0	0.0	10.0	94.0	89.4	0.0	10.6
RI08-24-45	C491512	66.9	Imperial	2.0	3.0	6.0		84.0	3.0(Na)		1.0		1.0		84.0	1.0	11.0	96.0	87.5	1.0	11.5
RI08-24-43	C491510	96.3	Imperial	2.0	2.0	5.0		85.0	2.0(Na)		2.0		2.0		85.0	2.0	9.0	96.0	88.5	2.1	9.4
RI08-24-41	C491508	129.6	Imperial	3.0	4.0	8.0		82.0					3.0		82.0	0.0	15.0	97.0	84.5	0.0	15.5
RI08-24-39	C491506	155.0	Imperial	3.0	4.0	5.0		86.0					2.0		86.0	0.0	12.0	98.0	87.8	0.0	12.2
RI08-24-37	C491504	184.5	Imperial	3.0	4.0	10.0		81.0					2.0		81.0	0.0	17.0	98.0	82.7	0.0	17.3
RI08-24-34	C491501	214.3	Imperial	3.0	4.0	4.0		87.0					2.0		87.0	0.0	11.0	98.0	88.8	0.0	11.2
RI08-24-30	C486497	244.1	Imperial	3.0	4.0	7.0		84.0					2.0		84.0	0.0	14.0	98.0	85.7	0.0	14.3
RI08-24-28	C486495	273.2	Imperial	3.0	5.0	7.0		83.0					2.0		83.0	0.0	15.0	98.0	84.7	0.0	15.3
RI08-24-26	C486493	302.8	Imperial	3.0	4.0	4.0		85.0				2.0	2.0	Siderite-2%	85.0	2.0	11.0	98.0	86.7	2.0	11.2
RI08-24-25	C486492	315.2	Imperial	2.0	2.0	5.0		36.0				55.0		Siderite-55%	36.0	55.0	9.0	100.0	36.0	55.0	9.0
RI08-24-23	C486490	330.9	Imperial	3.0	3.0	2.0		81.0	2.0(Na)		4.0	3.0	2.0	Siderite-3%	81.0	7.0	8.0	96.0	84.4	7.3	8.3
RI08-24-21	C486488	360.0	Imperial		2.0			45.0		2.0	36.0		15.0		45.0	38.0	2.0	85.0	52.9	44.7	2.4
RI08-24-20	C486487	366.8	Imperial?	tr	5.0			88.0	tr				7.0		88.0	0.0	5.0	93.0	94.6	0.0	5.4
FX07-02-8	C491543	25.8	Canol		2.0		41.0	53.0	1.0(K), 2.0(Na)					Anhydrite?-1%	53.0	0.0	2.0	55.0	96.4	0.0	3.6
FX07-02-6	C491541	52.7	Canol		1.0		5.0	90.0	3.0(K), 1.0(Na)						90.0	0.0	1.0	91.0	98.9	0.0	1.1

Fm = Formation *Qtz = Quartz* *Cal = Calcite* *Sd = Siderite* *Carb = Carbonate*

Gyp = Gypsum *Fldspr = Feldspars* *Dol = Dolomite* *Py = Pyrite*

Appendix B continued

Sample	GSC curation #	Downhole depth (m)	Fm	M.L.C.*	Mica/ Illite	Clino-clore	Gyp	Qtz	Fldspr	Cal	Dol	Sd	Py	Others	Qtx	Total Carb	Total Clay	Sum Qtz, Carb & Clay	% Qtz	% Carb	% Clay
FX07-02-4	C491539	64.0	Canol		1.0		4.0	92.0	2.0(K)					Augite-1%	92.0	0.0	1.0	93.0	98.9	0.0	1.1
FX07-03-9	C491553	33.3	Canol		1.0		2.0	93.0	1.0(k)	3.0					93.0	3.0	1.0	97.0	95.9	3.1	1.0
FX07-03-7	C491551	60.7	Canol		4.0		tr	85.0	3.0(K)	2.0	1.0		3.0	Sphalerite?-2%	85.0	3.0	4.0	92.0	92.4	3.3	4.3
FX07-03-5	C491549	87.5	Canol		1.0			89.0	1.0(K)	7.0			1.0	Sphalerite?-1%	89.0	7.0	1.0	97.0	91.8	7.2	1.0
RI07-07A-12	C491526	37.8	Canol		1.0		1.0	90.0					8.0		90.0	0.0	1.0	91.0	98.9	0.0	1.1
RI07-07A-10	C491524	63.2	Canol		2.0		2.0	88.0					8.0		88.0	0.0	2.0	90.0	97.8	0.0	2.2
RI07-07A-6	C491520	91.0	Canol		1.0		tr	96.0		tr	1.0		2.0		96.0	1.0	1.0	98.0	98.0	1.0	1.0
RI07-07A-5	C491519	102.3	Canol	tr	1.0			94.0					5.0		94.0	0.0	1.0	95.0	98.9	0.0	1.1
RI07-07A-4	C491518	114.8	Canol		2.0			95.0					3.0		95.0	0.0	2.0	97.0	97.9	0.0	2.1
RI07-07A-2	C491516	140.2	Canol		1.0			96.0	1.0(K)	1.0			1.0		96.0	1.0	1.0	98.0	98.0	1.0	1.0
RI07-16-7	C491560	25.5	Canol		2.0			95.0	tr				3.0		95.0	0.0	2.0	97.0	97.9	0.0	2.1
RI07-16-5	C491558	58.5	Canol		2.0			92.0	2.0(K)				4.0		92.0	0.0	2.0	94.0	97.9	0.0	2.1
RI07-16-3	C491556	86.0	Canol		1.0			98.0	tr				1.0		98.0	0.0	1.0	99.0	99.0	0.0	1.0
RI07-20-7	C491573	85.9	Canol		1.0		1.0	95.0					3.0		95.0	0.0	1.0	96.0	99.0	0.0	1.0
RI07-20-5	C491571	119.3	Canol		1.0		tr	98.0					1.0		98.0	0.0	1.0	99.0	99.0	0.0	1.0
RI07-20-3	C491569	152.6	Canol		1.0			96.0				1.0	2.0	Siderite?-1%	96.0	1.0	1.0	98.0	98.0	1.0	1.0
RI07-20-1	C491567	185.9	Canol?		2.0			96.0					2.0		96.0	0.0	2.0	98.0	98.0	0.0	2.0
RI08-24-19	C486486	376.2	Canol		1.0			95.0			2.0		2.0		95.0	2.0	1.0	98.0	96.9	2.0	1.0
RI08-24-18	C486485	384.3	Canol		2.0		tr	95.0					3.0	Hercynite?-tr	95.0	0.0	2.0	97.0	97.9	0.0	2.1
RI08-24-17	C486484	393.0	Canol		2.0			96.0					2.0		96.0	0.0	2.0	98.0	98.0	0.0	2.0
RI08-24-16	C486483	401.7	Canol		2.0			91.0					6.0	Anhydrite-1%	91.0	0.0	2.0	93.0	97.8	0.0	2.2
RI08-24-14	C486481	425.0	Canol		1.0			93.0					5.0	Gahnite(ferroan)?-1%	93.0	0.0	1.0	94.0	98.9	0.0	1.1
RI08-24-12	C486479	458.8	Canol		tr			95.0					4.0	Hercynite?-1%	95.0	0.0	0.0	95.0	100.0	0.0	0.0
RI08-24-8	C486474	494.5	Canol		1.0			95.0					4.0		95.0	0.0	1.0	96.0	99.0	0.0	1.0
RI08-24-7	C486473	507.7	Canol		1.0			93.0					6.0		93.0	0.0	1.0	94.0	98.9	0.0	1.1

Fm = Formation *Qtz = Quartz* *Cal = Calcite* *Sd = Siderite* *Carb = Carbonate*

Gyp = Gypsum *Fldspr = Feldspars* *Dol = Dolomite* *Py = Pyrite*

Appendix B continued

Sample	GSC curation #	Downhole depth (m)	Fm	M.L.C.*	Mica/ Illite	Clino-clore	Gyp	Qtz	Fldspr	Cal	Dol	Sd	Py	Others	Qtx	Total Carb	Total Clay	Sum Qtz, Carb & Clay	% Qtz	% Carb	% Clay
RI08-24-4	C486470	531.3	Canol		1.0			93.0					5.0	Rutile?-1%	93.0	0.0	1.0	94.0	98.9	0.0	1.1
RI08-24-1	C486467	565.0	Canol		tr			99.0					1.0		99.0	0.0	0.0	99.0	100.0	0.0	0.0
10TLA-RICH-09M**	C542085		Canol	trace	1	tr+		99							99	0.0	1.0	100.0	99.0	0.0	1.0
PE07-07-8	C491534	82.5	Canol		1.0		1.0	92.0			3.0		2.0	Kaolinite-1%	92.0	3.0	1.0	96.0	95.8	3.1	1.0
PE07-07-5	C491531	109.7	Canol	1.0	1.0			96.0					2.0		96.0	0.0	2.0	98.0	98.0	0.0	2.0
PE07-07-3	C491529	137.2	Canol		2.0			89.0					5.0	Fluorapatite-4%	89.0	0.0	2.0	91.0	97.8	0.0	2.2
PE07-07-1	C491527	164.2	Canol		2.0		tr	94.0	tr				4.0		94.0	0.0	2.0	96.0	97.9	0.0	2.1
FX07-02-3	C491538	79.0	RR		3.0			88.0	2(K)	1.0			4.0	Sphalerite?-2%, Augite-tr	88.0	1.0	3.0	92.0	95.7	1.1	3.3
FX07-02-1	C491536	106.7	RR		4.0		tr	89.0	2(K)	2.0			3.0		89.0	2.0	4.0	95.0	93.7	2.1	4.2
FX07-03-3	C491547	111.5	RR		3.0			80.0	3.0(K)	4.0	8.0		2.0		80.0	12.0	3.0	95.0	84.2	12.6	3.2
FX07-03-2	C491546	128.6	RR		2.0			71.0	2(K)	13.0	11.0		1.0		71.0	24.0	2.0	97.0	73.2	24.7	2.1
FX07-03-1	C491545	139.0	RR		1.0			84.0	1(K)	11.0	2.0		1.0		84.0	13.0	1.0	98.0	85.7	13.3	1.0
RI07-07A-1	C491515	166.5	RR		2.0			92.0		4.0			2.0		92.0	4.0	2.0	98.0	93.9	4.1	2.0
RI07-16-2	C491555	103.1	RR		1.0			61.0		34.0	2.0		2.0		61.0	36.0	1.0	98.0	62.2	36.7	1.0
RI07-16-1	C491554	121.9	RR		1.0			88.0		10.0			1.0		88.0	10.0	1.0	99.0	88.9	10.1	1.0
RI07-02-5	C491565	44.7	RR		3.0		3.0	81.0		11.0			2.0		81.0	11.0	3.0	95.0	85.3	11.6	3.2
RI07-02-3	C491563	75.8	RR		2.0			75.0		19.0	1.0		3.0		75.0	20.0	2.0	97.0	77.3	20.6	2.1
RI07-02-1	C491561	105.6	RR		1.0			81.0	1.0	14.0			1.0	Sphalerite?-2	81.0	14.0	1.0	96.0	84.4	14.6	1.0
10TLA-RICH-09I**	C542083		RR		5	tr+		93	2 (Na)						93	0.0	5.0	98.0	94.9	0.0	5.1
10TLA-RICH-09K**	C542084		RR		6			91	tr (K)					Gypsum-1%, Pyrite-2%	91	0.0	6.0	97.0	93.8	0.0	6.2

Fm = Formation *Qtz = Quartz* *Cal = Calcite* *Sd = Siderite* *Carb = Carbonate*

Gyp = Gypsum *Fldspr = Feldspars* *Dol = Dolomite* *Py = Pyrite*

Updated definition and correlation of the lower Fifteenmile Group in the central and eastern Ogilvie Mountains

Galen P. Halverson[1]
Department of Earth and Planetary Science/GEOTOP, McGill University, Montreal, QB

Francis A. Macdonald, Justin V. Strauss, Emily F. Smith
Department of Earth and Planetary Sciences, Harvard University, Cambridge, MA

Grant M. Cox, Lucie Hubert-Théou
Department of Earth and Planetary Science/GEOTOP, McGill University, Montreal, QB

Halverson, G.P., Macdonald, F.A., Strauss, J.V., Smith, E.F., Cox, G.M., and Hubert-Théou, L., 2012. Updated definition and correlation of the lower Fifteenmile Group in the central and eastern Ogilvie Mountains. *In:* Yukon Exploration and Geology 2011, K.E. MacFarlane and P.J. Sack (eds.), Yukon Geological Survey, p. 75-90.

ABSTRACT

Ongoing mapping, chemostratigraphy, geochronology, and stratigraphic analysis of Neoproterozoic successions in the Ogilvie Mountains requires redefinition and correlation of the Fifteenmile Group across the Proterozoic inliers in Yukon. Here we present new stratigraphic logs through the lower Fifteenmile Group in the Coal Creek and Hart River inliers. Based on these data and new observations, we propose redefinition of the lower Fifteenmile Group. A succession dominated by sandstone, mapped as unit PPD1 in the Hart River inlier, is now recognized at the base of the Fifteenmile Group in the Coal Creek inlier. These strata unconformably overlie the Pinguicula Group and transition upward into a distinctive carbonate interval; together, these comprise the informally defined Gibben formation. The shallowing-upward carbonate sequence contains abundant oolitic grainstone and packstone and microbial laminated dolostone. It is capped by a distinct interval of mud-cracked maroon mudstone, siltstone, and fine-grained sandstone that forms the base of what we informally define as the Chandindu formation. The mud-cracked shale transitions upwards into interbedded shale, coarse-grained sandstone, and minor carbonate. The overlying informally defined Reefal assemblage consists of up to 1 km of complexly interbedded carbonate and shale, with variable truncation beneath the major angular unconformity at the base of the Callison Lake Dolostone. The lower Fifteenmile Group (now informally PPD1 through the Chandindu formation) likely correlates with the Hematite Creek Group in the Wernecke Mountains.

[1] *galen.halverson@mcgill.ca*

INTRODUCTION

Proterozoic strata in Yukon are preserved in mountainous inliers that stretch between Alaska and Northwest Territories, north of the Dawson thrust (Fig. 1). Geologists have worked for decades to determine the age and correlation of these rocks in Yukon (*e.g.*, Abbott, 1997; Thorkelson *et al.*, 2005) and across the rest of northern Canada (*e.g.*, Gabrielse, 1972; Young, 1979; Rainbird *et al.*, 1996). Cryogenian–Ediacaran-aged strata of the Windermere Supergroup and the Mount Harper Group and its equivalents in the Ogilvie Mountains comprise the so-called 'Sequence C' in northwestern Canada, the base of which is the major unconformity below the Rapitan and Mount Harper groups. Early and mid-Neoproterozoic (Tonian) strata comprise 'Sequence B', which includes the Shaler Supergroup on Victoria Island, the Mackenzie Mountains Supergroup and Coates Lake Group in the Mackenzie and Wernecke mountains, and the Fifteenmile Group in the Ogilvie Mountains (Fig. 1)(Eisbacher, 1981; Young, 1981; Rainbird *et al.*, 1996; Long *et al.*, 2008; Macdonald and Roots, 2010). In the Coal Creek, Hart River, and Wernecke inliers, the enigmatic Pinguicula Group occurs between the significantly older Wernecke Supergroup (late Paleoproterozoic–early Mesoproterozoic) and Sequence B strata (Young, 1979; Eisbacher, 1981; Thorkelson *et al.*, 2005; Medig *et al.*, 2010; Turner, 2011). Its placement within the tectonostratigraphic framework of the Proterozoic successions of northwestern Canada is a subject of ongoing debate.

While the broad correlation of Neoproterozoic strata between Victoria Island and the Mackenzie Mountains is relatively straightforward and uncontroversial, the poor accessibility and greater degree of Cordilleran deformation in Yukon have hindered detailed correlation of the Neoproterozoic stratigraphy with regions to the east. However, recent mapping coupled with application of high precision U-Pb zircon dating and chemostratigraphy (Macdonald *et al.*, 2010a,b) have significantly improved correlations and clearly established that the Neoproterozoic successions in the Tatonduk,

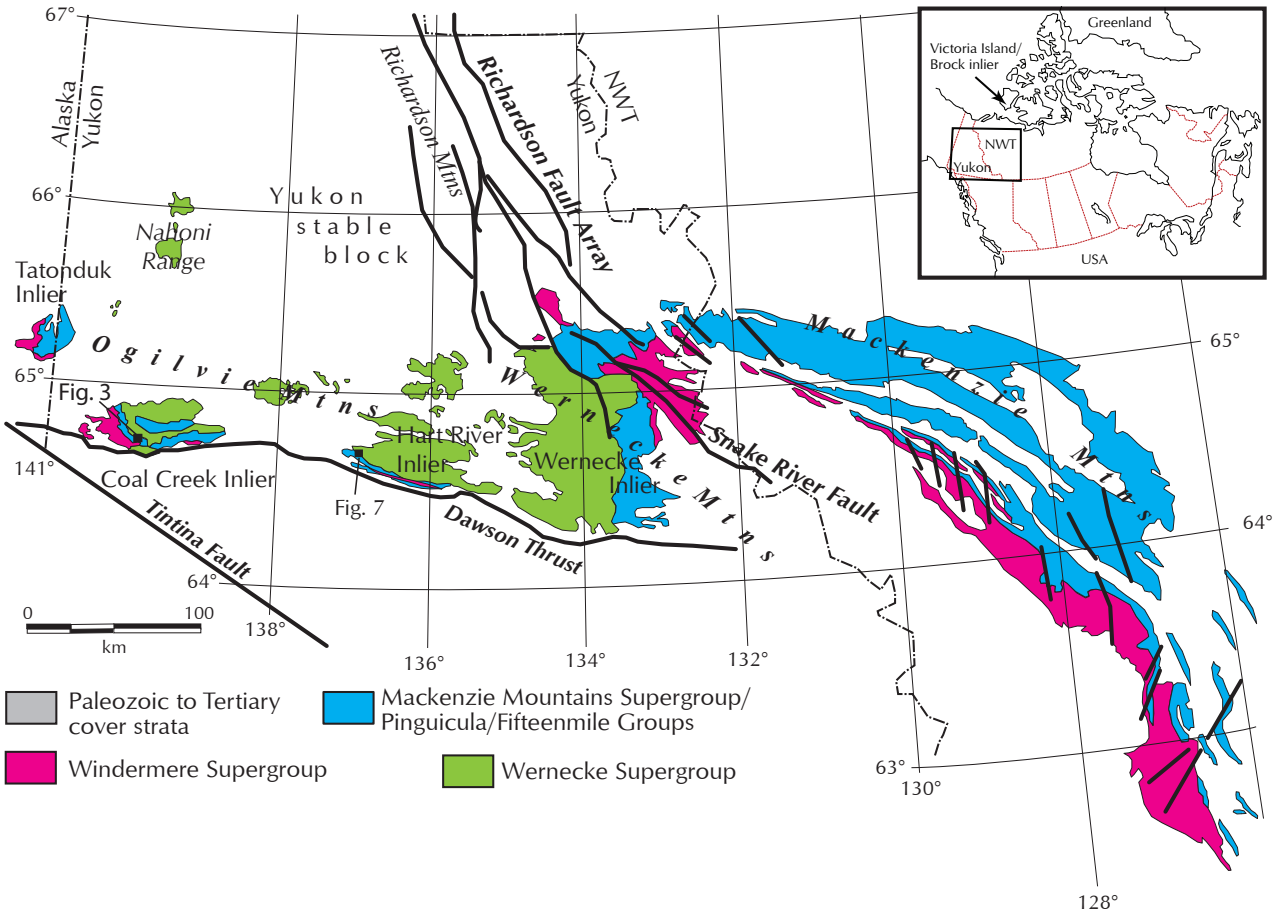

Figure 1. *Location and simplified geological map showing the Proterozoic inliers of the western Northwest Territories and Yukon and the distribution of Proterozoic strata. Black boxes in the Coal Creek and Hart River inliers show locations of maps and measured sections in subsequent figures. Modified from Macdonald et al. (2010).*

Coal Creek, and Hart River inliers (Fig. 1) are equivalent to Sequences B and C in the Mackenzie Mountains, albeit with a patchy and typically thin Cryogenian-Ediacaran succession. Macdonald and Roots (2010) and Macdonald *et al.* (2011) presented new correlations between the Tatonduk, Coal Creek, and Hart River inliers and preliminary revisions to the nomenclature in order to normalize stratigraphic names between these three regions. Our ongoing fieldwork in the inliers and complementary research by other groups (*e.g.*, Turner *et al.*, 2011; Medig *et al.*, 2010) continue to fill in remaining gaps in the Neoproterozoic stratigraphic framework for Yukon.

In this contribution we present new stratigraphic logs, mapping, and other field observations from the lower Fifteenmile Group in the Coal Creek and Hart River inliers. These results motivate a substantial revision to the definition of this heretofore poorly documented part of the Neoproterozoic stratigraphy in Yukon and its relationship to the Pinguicula Group in this region.

FIFTEENMILE GROUP

The Fifteenmile Group is named after Fifteenmile River, which drains the south-central Coal Creek inlier, between Mount Harper and Mount Gibben. As originally defined, the Fifteenmile Group comprises the strata between the late Paleoproterozoic Wernecke Supergroup below and the Mount Harper Group above (Thompson *et al.,* 1994; Mustard, 1991; Mustard and Roots, 1997), and hence represents Sequence B (Young *et al.*, 1979; Rainbird *et al.*, 1996) in the central Ogilvie Mountains. Thompson *et al.* (1994) subdivided the Fifteenmile Group into informal lower and upper subgroups, comprising five (PR1–PR5) lower map units and three (PF1–PF3) upper map units. Abbott (1993) extended the upper Fifteenmile Group nomenclature to the Hart River inlier and assigned an additional unit (PF4). Subsequently, Abbott (1997) renamed PF4 the Callison Lake Dolostone and reassigned all strata between the Wernecke Supergroup and Callison Lake Dolostone to the Pinguicula Group, which had previously been defined in the Wernecke Mountains as a distinct, mixed carbonate-siliciclastic succession overlying the Wernecke Supergroup (Eisbacher, 1981; Thorkelson *et al.*, 2005). The relationship between the Fifteenmile and Pinguicula groups remained vague.

Recent mapping, stratigraphy, chemostratigraphy, and U-Pb zircon dating of volcanic units and tuffs in the Coal Creek inlier have revealed major discrepancies in previous mapping and resulted in progressive revision to nomenclature and correlation of Fifteenmile Group strata both within the Coal Creek inlier and with neighboring inliers. A new U-Pb zircon age of 717.43±0.14 Ma on a rhyolitic flow in the Mount Harper volcanic complex (Macdonald *et al.*, 2010a) places a firm minimum age constraint on the Fifteenmile Group. An 811.51±0.25 Ma U-Pb zircon age on a tuff in the middle Fifteenmile Group is the first direct age on this succession (Macdonald *et al.*, 2010a). In combination with chemostratigraphy, these new ages provide a basis for correlation of the Fifteenmile Group with the lower Tindir Group in the Tatonduk inlier and refined correlation with the Hart River inlier (Macdonald and Roots, 2010). In an attempt to reconcile the stratigraphy of the Fifteenmile Group with major revisions to the mapping in the Coal Creek inlier, including elimination of many inferred thrust faults in the lower Fifteenmile Group, Macdonald *et al.* (2011) proposed a new subdivision of the Fifteenmile Group into an informal "Lower Assemblage" of mixed shale and variably stromatolitic dolostone, overlain by the informal "Craggy Dolostone." This thick and heavily recrystallized dolostone is unconformably overlain by the Callison Lake Dolostone in the Coal Creek inlier.

In this subdivision, Macdonald *et al.* (2011) ascribed what had previously been mapped as the lower Fifteenmile Group (PR1-PR4) to the Pinguicula Group, consistent with recent observations described by Medig *et al.* (2010). The latter authors observed that Pinguicula unit A (PPA) in the Hart River inlier post-dates the 1.38 Ga Hart River sills and highlighted similarities between units PR1 and PR2 in the Coal Creek inlier and Pinguicula units A–C.

NEW SECTIONS THROUGH THE LOWER FIFTEENMILE GROUP

In 2010 and 2011 we measured a series of new stratigraphic sections spanning the lower Fifteenmile Group in the central Coal Creek inlier and eastern Hart River inlier (Table 1). Based on these new sections and our correlations with the Hart River inlier, we define three new informal formations in what we regard as the lower Fifteenmile Group and revise a fourth map unit (PPD1 in the Hart River inlier; Abbott, 1997) to the Fifteenmile Group. Here we describe two key sections that underpin these new definitions and our proposed correlations.

Table 1. *Section names and locations of new stratigraphic logs in the Coal Creek (CC) and Hart River (HR) inliers that form the base of our proposed new nomenclature and correlation scheme for the lower Fifteenmile Group is this region.*

Measured Section	Inlier	Units measured	Latitude	Longitude	Comments
GO130	CC	Gibben fm (including lower sandstone), lower Chandindu fm	N64°44′36.1″	W139°48′34.8″	Proposed type section for the Gibben fm, which is superbly exposed
GO131	CC	Chandindu fm, lower Reefal ssemblage	N64°44′18.4″	W139°49′59.4″	Good exposure of siltstones in Chandindu fm; little exposure of overlying lower Reefal assemblage
GO133	CC	middle Reefal assemblage	N64°43′52.5″	W139°50′08.4″	Overall poor exposure, but some excellent exposure of silty black shale in creek
GO134	CC	middle Reefal assemblage	N64°43′46.1″	W139°50′18.5″	Intervals of no exposure, but some excellent exposures of black shales and carbonates
GO132	CC	middle Reefal assemblage	N64°43′15.4″	W139°49′52.8″	Top of section=base of F833 section; poorly exposed and tectonically thickened
GO137	HR	lower Gibben fm	N64°38′8.2″	W136°53′26.1″	Base of section in fault contact with PPD1; top of section folded
GO138	HR	Lower Gibben fm, Chandindu fm	N64°37′52.9″	W136°53′52.7″	Continuation of GO137; excellent exposure through upper Chandindu fm

COAL CREEK INLIER

We measured a series of new sections spanning the lower Fifteenmile Group, including a composite stratigraphic section starting from the Pinguicula-Fifteenmile contact through the base of the extraordinarily well-exposed section (F833; Figures 3 and 4 in Macdonald and Roots, 2010) that contains the 811 Ma ash bed (Macdonald *et al.*, 2010a) just north of the Mount Harper volcanic edifice (Figs. 2–4). Mapping of this lower Fifteenmile Group outcrop belt demonstrated that a series of minor thrust faults mapped by Thompson *et al.* (1994) as placing PR4 dolostone on PR5 shale are in fact conformable contacts, with each of the dolostone deposits representing distinct stratigraphic units interbedded with shale. Although the section is clearly affected by minor folding and tectonic thickening, in particular in the substantial intervals of shale, it represents a continuous stratigraphic section.

NEW MEASURED SECTION (GO130-131-132-133-134)

The base of the section (G0130; Fig. 3) is an unconformable contact with a wedge of large, domal, locally brecciated, and heavily cemented gold and grey dolomitic stromatolites below. The stromatolite unit is 10.2 m thick, but it thins to the east, where the Fifteenmile Group rests directly on cleaved shale and siltstone of the Gillespie Lake Group. To the west, the stromatolite unit thickens dramatically: approximately 3 km to the west, it is over 600 m thick. Above this contact, the basal Fifteenmile Group is composed of medium-grained, moderately sorted sandstone with abundant lithic fragments (carbonate and slate) and wavy, medium-bedding. In this section, the poorly exposed sandstone is only 13.5 m thick and transitions upwards into carbonate (Fig. 4a); to the west, the sandstone thickens and an unmeasured interval of shale separates the sandstone from the overlying carbonate unit.

This carbonate unit (Figs. 3 and 4) comprises 217 m of predominantly blue-grey, medium bedded dolostone with abundant ooid and intraclast grainstone and packstone, wavy laminated, dark grey ribbonites with molar tooth structures, microbial laminite, and associated rudites arranged in an overall shallowing-upward sequence. Rounded quartz grains are abundant in the lower part of the unit, indicating that the base of the carbonate is transitional from the sandstone below. Three recognizable but minor subaerial exposure surfaces occur within this interval (Fig. 3). The top of the dolostone unit consists of ~24 m of distinct, cream-coloured microbial laminite with minor grainstone capped by a prominent exposure surface.

This exposure surface marks a sharp transition into a prominent mud-cracked maroon shale and siltstone facies that is approximately 35 m thick. Interbedded silt and shale form flaser-like couples and couplets, and some beds are slightly dolomitic. The mud-cracked facies gives way to shoaling-upwards, 1 to 10 m-scale cycles consisting of shale and siltstone passing upward into dolomitic

grainstone, stromatolites, and stromatolitic breccias. The stromatolites are columnar to biohermal (up to 3 m thick) grey dolomite, commonly with egg-carton morphology in plan view, and in places canted and displaying significant inherited relief (Fig. 5).

The interval of carbonate-capped cycles passes upward into maroon and olive-coloured silty shale within interbedded fine-quartz wackestone and thin, fine-grained quartz arenite beds. This section eventually gives way to a dipslope on the ridge and non-exposure. The composite section was continued in a drainage 1 km to the west using the exposure at the top of the carbonate unit (Fig. 4b) as a correlation datum. Featureless siltstone and dolomitic wackestone with minor interbedded fine quartz arenite continue to a stratigraphic height of 171 m above the base of the carbonate, marked by a distinct shift to monotonous shale. A long interval of poor exposure follows, although where exposed, the lithology is exclusively dark grey to black shale with minor siltstone beds. Mapping of the unit indicates no apparent lithological variation. Where decent exposure resumes in a ravine, the lithology comprises black shale with minor black marl, transitioning upward to muddy carbonate. The carbonate begins as black limestone rhythmites with fine grey turbidites and grades upwards into a 12.7 m-thick rhythmite plus stromatolite breccia that marks the first major, resistant carbonate bed above the thick shale-dominated section. Flaggy marls with distinct wavy black limestone concretions occur above the breccia and continue upward into marl, black limestone rhythmite, and black rhythmite breccia. The breccias become silicified and dolomitic, in places forming clearly distinct coarse breccia sheets separated by lenses of black marl and rhythmite. This heavily altered, dolomitic breccia forms a prominent resistant cap to the ridge on which it occurs.

This dolomitic unit is separated from the next major carbonate buildup, the base of which is the lower part of section F833 (Fig. 2; Figure 4 in Macdonald and Roots, 2010; Macdonald *et al.*, 2010a,b). Exposure along the continuation of the measured section (through a saddle) was limited, but float consisted entirely of dark grey to black siltstone and shale. Steep gullies on either side of the saddle afford excellent exposures of black shale. This shale interval is likely several hundred metres thick, but due to local folding and potential repetition, an accurate stratigraphic thickness cannot be determined.

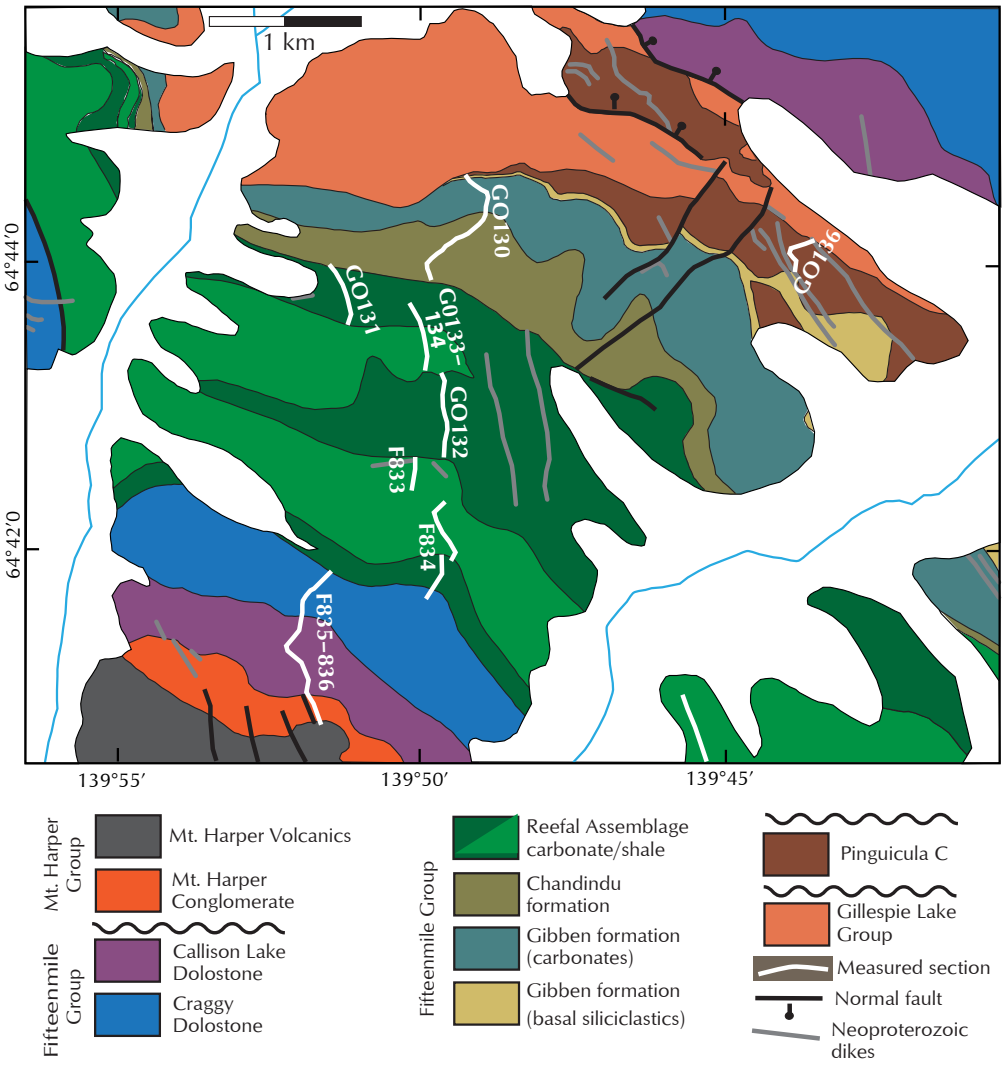

Figure 2. *Geological map for the NE flank of Mount Harper in the southwestern Coal Creek inlier (Fig. 1) showing the location of a key composite stratigraphic section through the Fifteenmile Group (see Figure 3). Based on our own mapping and previous mapping by Thompson et al. (1994).*

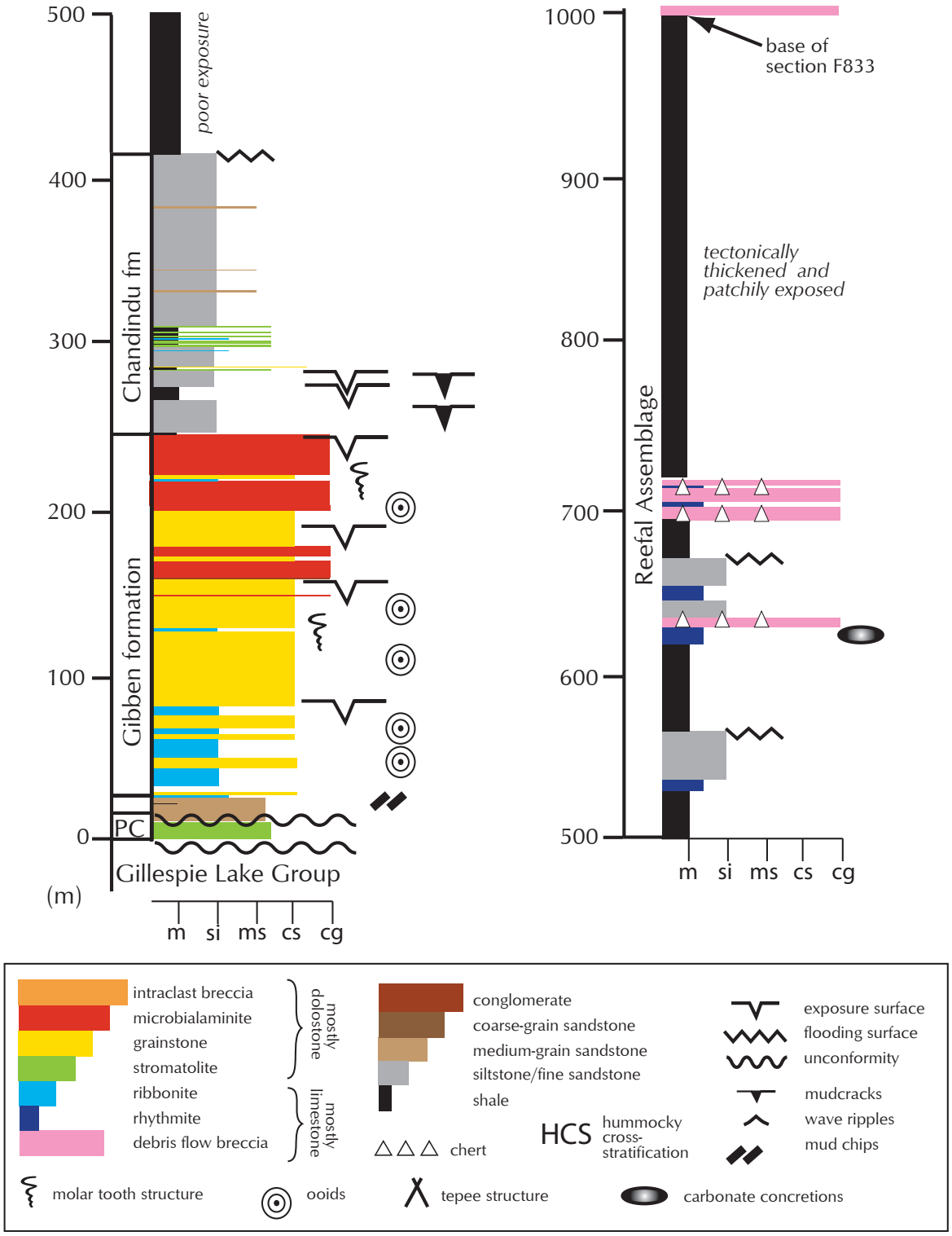

Figure 3. *Composite stratigraphic log (GO130/GO131/GO133-134/GO132) through the lower Fifteenmile Group NE of Mount Harper. Note the log ends at the base of section F833, which is the continuation of this composite Fifteenmile Group plotted in Macdonald and Roots (2010). Grain size scale: m = mud; si = silt; ms = medium sand; cs = coarse sand; cg = coarse gravel.*

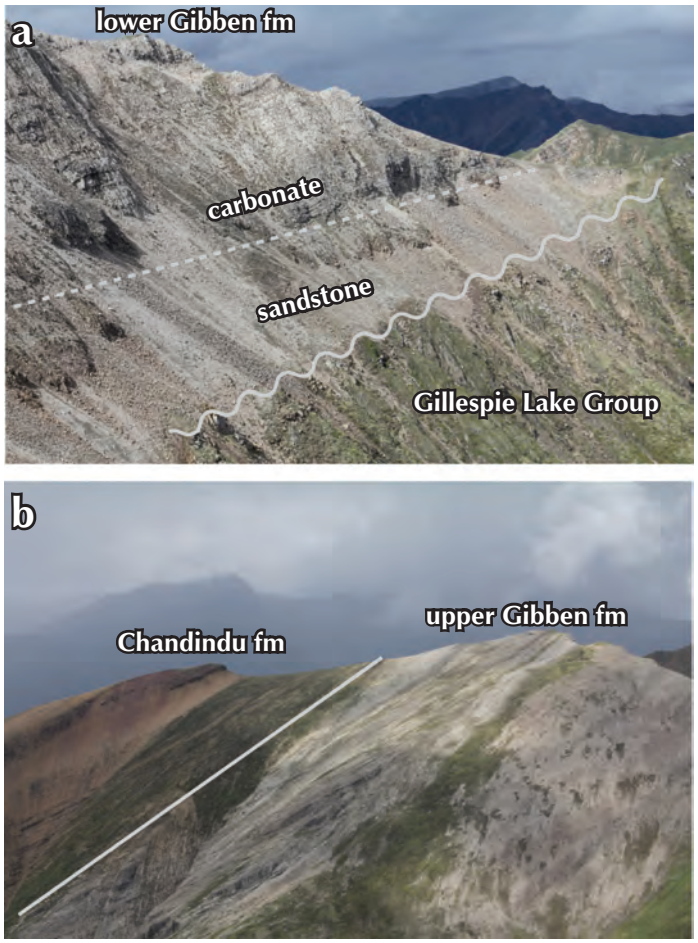

Figure 4. *Views of the lower Fifteenmile Group at section GO131, north of Mount Harper (Fig. 3).* ***(a)*** *Poorly exposed, northward-tapering sandstone interval here assigned to the basal Gibben formation unconformably overlies the Gillespie Lake Group and grades upward into ribbonite and grainstone of the lower Gibben formation.* ***(b)*** *Contact between dolomitic grainstone and microbial laminite of the upper Gibben formation and distinctive mud-cracked siltstone of the lower Chandindu formation.*

Figure 5. *Distinct, pseudo-columnar, canted grey limestone stromatolites in the middle Chandindu formation of the Coal Creek inlier and capping a shale-carbonate parasequence. Hammer, for scale, is 37 cm tall.*

HART RIVER INLIER

We measured stratigraphic sections through the lower Fifteenmile Group in the Hart River inlier (Figs. 6–8) in 2009, 2010, and 2011, building upon the detailed mapping of Abbott (1997) in the western part of the inlier and complementary work focused on the Pinguicula Group (*e.g.*, Medig *et al.*, 2010). The Fifteenmile Group is relatively incomplete in the Hart River inlier due to major erosional unconformities beneath both the Callison Lake Dolostone and the Cambrian–Devonian Bouvette Formation (Fig. 8). However, there are well-exposed sections of what has variably been included in the Fifteenmile (Abbott, 1993) and Pinguicula (Abbott, 1997) groups and what we regard here as lower Fifteenmile Group. Here we describe a key new section measured in 2011 (Fig. 7) that permits confident correlation of the upper Pinguicula and Fifteenmile groups between the Hart River and Coal Creek inliers.

NEW MEASURED SECTION (GO137-138)

This section lies along Abbott's (1997) Section 1 and follows a north-south ridge ~1.5 km east of Marc Creek in the eastern Hart River inlier (Figs. 6–8). Our section starts in maroon to purple shale that Abbott (1997) included as the upper member (above medium-grained quartz arenite) in map unit PPD1. The contact between the quartz arenite and shale is disturbed by a pair of north-dipping normal

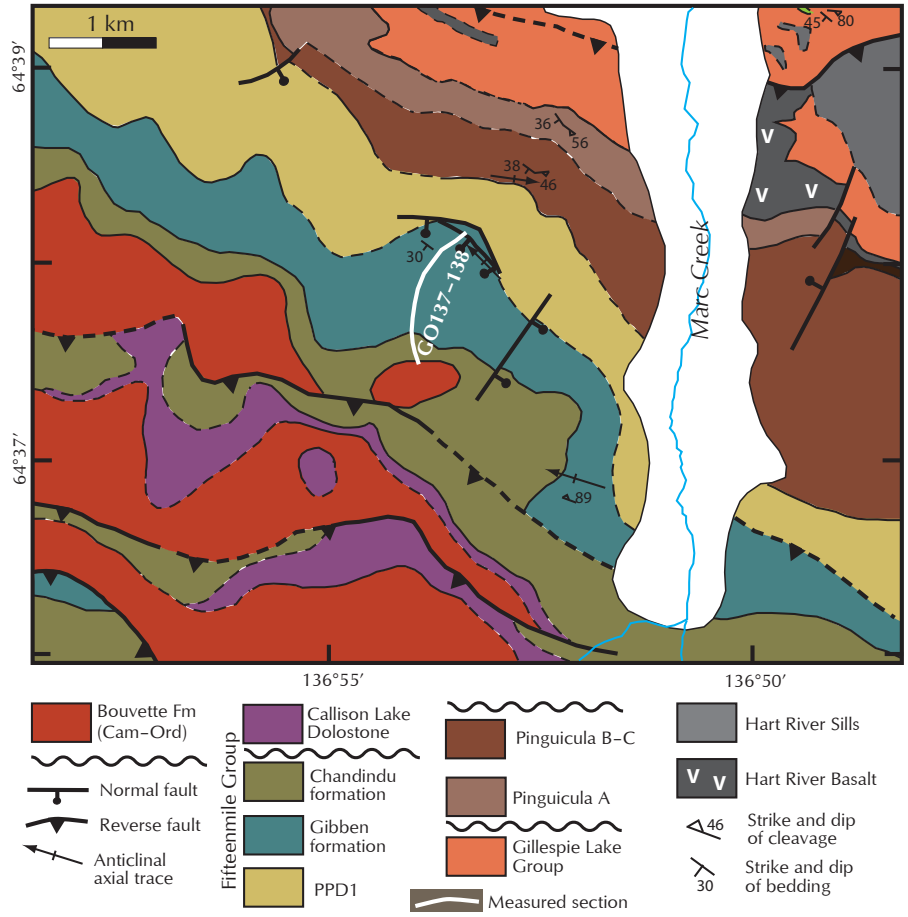

Figure 6. *Geological map in the eastern Hart River inlier (Fig. 1), showing the location of our new stratigraphic log through the Fifteenmile Group (Section 1 in Abbott, 1997) shown in Figure 7. Map is modified from Abbott (1997).*

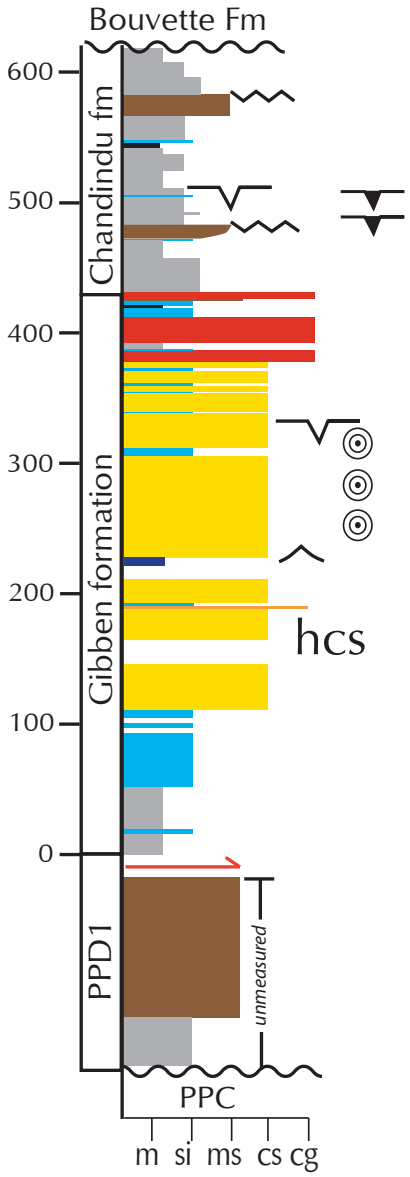

Figure 7. *Stratigraphic log in the lower Fifteenmile Group (PPD1, Gibben formation, and Chandindu formation) in the eastern Hart River inlier (Fig. 6). Grain size scale: m = mud; si = silt; ms = medium sand; cs = coarse sand; cg = coarse gravel. See Figure 3 for legend.*

faults and folds in the basal shale. However, along strike, it is clear that the quartz arenite transitions upwards into the shale, even if the transition is rather abrupt. These lower purple shales contain abundant lenses and thin beds of pink limestone through at least 55 m of section. They transition gradationally into flaggy to wavy pink and white limestone with minor hummocky cross-stratification (HCS) and abundant purple shale partings. The limestone-dominated interval is ~35 m thick, but because it is heavily folded and becomes poorly exposed upsection, its exact thickness is impossible to determine.

Whereas the contact with the much thicker, blue-grey carbonate unit above (Fig. 8) is somewhat obscured by cover, it appears gradational and likely reflects upward shoaling of the depositional sequence. This blue-grey dolomite unit measures 335 m thick and consists predominantly of grainstone and packstone, with abundant ooids, coated grains, and flat pebble intraclasts, arranged in mainly tabular, medium beds (Fig. 9a). Coarser-grained intraclast conglomerates also occur, and parallel to ribbony-laminated dark grey dolostones with minor HCS and molar tooth structures are also common (Fig. 9b). Rare exposure, flooding, and obviously scoured surfaces occur, and through most of the interval, there is no apparent cyclicity. However, in the upper 50 m of

Figure 8. *East-facing view of the measured section spanning the lower Fifteenmile Group in the Hart River inlier (equivalent to Abbott's [1997] section 1). Note that the section is top-truncated here by the Cambrian–Devonian Bouvette Formation. Elsewhere, the upper contact with the Chandindu formation is an angular unconformity beneath the Callison Lake Dolostone.*

the section, microbial laminite with tepee structures (Fig. 9c) becomes the dominant carbonate facies and occurs in beds separated variably by shale, marl, and dolomite ribbons, giving rise to apparent metre-scale cyclicity. The abundance of mud within this part of the section is noticeably diminished in outcrops approximately 2 km to the southeast, where the microbial laminite facies (Fig. 9c) is conversely more pronounced.

The top of the carbonate unit is marked by an abrupt shift to dominantly fine-grained siliciclastic rocks. The succeeding 186 m form 20 m-scale cycles that consist mainly of dark shale gradationally transitioning into grey to white siltstone or fine-grained quartz arenite. The cycles are separated by flooding and exposure surfaces. The cycles become somewhat coarser-grained upsection and the uppermost fine-grained sandstones below the Bouvette unconformity contain low angle cross-beds. Mud-cracks are also common in the upper part of the lower cycles (Fig. 9d). Tan to orange, flaggy dolomitic interbeds occur in the middle of several of the cycles and are more prominent upsection. In exposures ~2 km to the southeast, some of these thin and laminated dolomitic intervals are replaced by poorly developed, stromatolite beds (Fig. 9e).

CORRELATIONS AND UPDATED NOMENCLATURE FOR THE FIFTEENMILE GROUP

Two key observations in the Coal Creek inlier underlie the major revision to the correlation and nomenclature of the lower Fifteenmile Group (previously referred to as the "Lower assemblage"; *e.g.*, Macdonald *et al.*, 2011) that we propose here. First, the lowermost Fifteenmile Group is highly variable in thickness and appears to fill small fault-bounded sub-basins, resulting in wedge-shaped stratal geometries (Fig. 10). Second, a series of south-directed

Figure 9. *Lithofacies characteristic of the Gibben and Chandindu formations in the Hart River inlier.* ***(a)*** *Coated grain packstone in the middle Gibben formation.* ***(b)*** *Ribbon facies dolostone in the middle Gibben formation.* ***(c)*** *Microbial laminite with small tepee structures in the upper Gibben formation.* ***(d)*** *Mud-cracks in the lower Chandindu formation siltstone and shale.* ***(e)*** *Stromatolites in the upper Chandindu formation.*

thrust faults mapped as duplicating sections of carbonate-shale in the upper part of the lower Fifteenmile Group (Thompson *et al.* 1994) appear instead to be conformable stratigraphic contacts. Resolution of these problems paints a new picture of the stratigraphic evolution of the lower Fifteenmile Group and motivates new formation names that can be extended to the Hart River inlier. We propose below an informal tripartite division of the lower Fifteenmile Group comprising the Gibben formation (including unit PPD1), the Chandindu formation, and the Reefal assemblage.

THE GIBBEN FORMATION (INCLUDING UNIT PPD1)

The base of the Fifteenmile Group in Section 3 (Fig. 10) consists of hundreds of metres of shale, grading upward into pink limestone ribbonites. This distinct interval of the lower Fifteenmile Group tapers out laterally over a distance of kilometres; it is entirely absent in nearby Section 4 (Fig. 10). To the north (Sections 1 and 2), the Pinguicula Group is unconformably overlain by <10 m of coarse sandstone on paleo-highs and hundreds of metres of shale to siltstone in the axes of newly formed grabens. In Section 2, the sandstone is succeeded by the distinct pink limestone ribbons, which grade upward into ooid grainstones then microbial laminites with tepees, reflecting subaerial exposure. Hence this succession comprises a characteristic shoaling-upward sequence. It is overlain by distinct, maroon, mud-cracked shale and siltstone. In our new section north of Mount Harper (Fig. 4 and Section 2 in Fig. 10), an analogous shoaling-upward sequence occurs, albeit with a relatively condensed interval of ribbonites and a thicker interval of ooid-rich grainstone (Fig. 5). This sequence is similarly bound above by an exposure surface and overlain by mud-cracked maroon shale and siltstone at Section 2 and everywhere else we have mapped it (Fig. 10). We propose to name this succession, which includes the basal siltstone-sandstone and the carbonate sequence, the Gibben formation (informal) after Mount Gibben (Section 5), in the south-central Coal Creek inlier, but recommend that Section 2 be the reference section because the base of the section near Mount Gibben is truncated, lacking the lower ribbonites. Based on this definition, the base of the Gibben formation is a sandstone in unconformable contact with underlying Pinguicula or Gillespie Lake Group (Fig. 4A). The nature of this contact and the significance of the sandstone will be discussed further below. The Gibben formation varies in thickness from <20 to >600 m in the Coal Creek inlier. As defined, it is broadly equivalent to units PR3, PR4, and PR5a in Thompson *et al.* (1994).

THE CHANDINDU FORMATION

The top of the Gibben formation is an exposure surface developed on top of an interval of interbedded microbial laminites and grainstones (Fig. 4b). This contact marks an abrupt transition to fine-grained, mud-cracked, maroon shale and siltstone that form the base of what we have named the Chandindu formation, after the Chandindu River which drains the region east and south of Mount Gibben. This distinctive mud-cracked facies is more widespread than the underlying Gibben formation and has been recognized in all of our measured sections in the lowermost Fifteenmile Group (Fig. 10). The remainder of what we have identified as the Chandindu formation is rather variable between sections, but is typically dominated by shale or siltstone, in places arranged in cycles capped by carbonates (grainstone, stromatolite, or interclast breccia). In some sections, stromatolites are relatively abundant (Fig. 6), forming distinct bioherms surrounded by shale. Poorly-sorted, thin, granular sandstone beds also occur in some sections. We have placed the upper boundary of the Chandindu formation as the first major flooding surface above the mud-cracked shale and siltstone, which effectively separates this heterogeneous sequence from the overlying shale and dolomite-dominated informal "Reefal assemblage" described below. As defined, the Chandindu formation is approximately equivalent to Thompson *et al.* (1994) map unit PR5 and varies in thickness from ~150–400 m where we have mapped it in the Coal Creek inlier.

THE REEFAL ASSEMBLAGE

The removal of many of the minor thrust faults from the unpublished maps of the lower Fifteenmile Group in the Coal Creek inlier has important implications for understanding the stratigraphic evolution of the sedimentary basin in which the Fifteenmile Group was deposited. For example, we interpret the contact between heavily silicified, coarse breccia and shale (at approximately the 1300 m level in composite Section 2 in Fig. 10) previously mapped as a north-directed thrust fault that places "PR4" on "PR5" (Thompson *et al.*, 1994) to record instead a transition from deepwater rhythmites to talus breccias at the toe of a prograding carbonate platform. This and similar revisions to the mapping portray the upper part of the lower Fifteenmile Group as a thick (>1000 metres in our composite Section 1; Fig. 10) complex framework of interwoven carbonate and shale (Figs. 3 and 10). We interpret this stratigraphy to reflect a series of northwest-prograding stromatolite-cored reef tracts that grade distally into grey and black-shale dominated deep basinal deposits. Sections from within the carbonate platform are dominated by stromatolitic bioherms (Section 4) and shallow intertidal to supratidal facies (Section 5). To the northwest, stromatolites are rare and the succession is dominated by shale and gravitationally redeposited carbonate sediments (Section 2 in Fig. 10). In recognition of the importance of stromatolite reefs throughout this interval, we propose to name it the "Reefal assemblage," which is roughly equivalent to

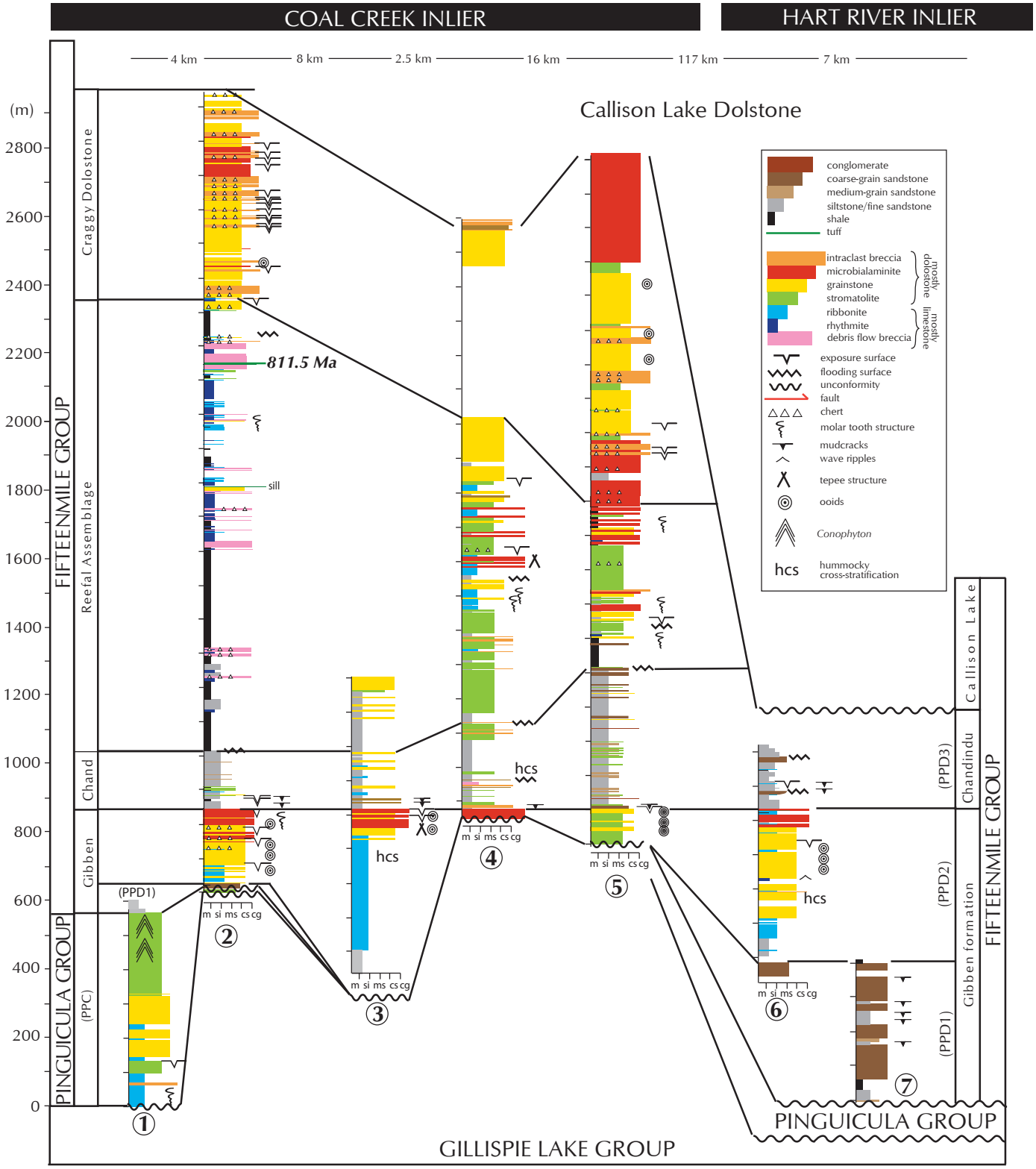

Figure 10. *Selected stratigraphic columns through the upper Pinguicula Group and lower Fifteenmile Group in the Coal Creek and Hart River inliers with suggested correlations and updated nomenclature. Note that the equivalent of map unit PPD1 in the Hart River inlier is included within the Gibben formation in the Coal Creek inlier. Grain size scale: m = mud; si = silt; ms = medium sand; cs = coarse sand; cg = coarse gravel.*

map unit "PF1a" of Thompson *et al.* (1994). The top of the Reefal assemblage is recorded by a distinct subaerial exposure surface overlain by the heavily silicified Craggy Dolostone ("PF1"), which comprises mainly shallow-water dolostone facies and appears to mark the progradation of a broad carbonate platform over the basin.

PPD1 AND CORRELATION WITH THE HART RIVER INLIER

In our proposed reference section (Fig. 3), the basal Gibben formation comprises several metres of medium-grained, moderately-sorted sandstone with rounded quartz grains and variable lithic clasts. This sandstone pinches out to the west and significantly thickens to the east (Fig. 2), where a dark grey siltstone is exposed beneath the sandstone. The contact between this siltstone-sandstone unit and the recrystallized stromatolitic dolostone below (previously mapped as "PR2"; Thompson and Roots, 1994) is an unconformity (Fig. 10). This overall sequence of siltstone grading up into sandstone and capped by a thick, shoaling-upward, medium-bedded, bluish-grey carbonate sequence replete with ooids and overlain by mud-cracked muddy siltstone is nearly identical to our measured section in the Hart River inlier (Figs. 7 and 8). Abbott (1997) referred to the siltstone–sandstone unit, along with the overlying maroon-purple shale as "PPD1", the carbonate sequence as "PPD2", and the upper interval of shale and siltstone with minor dolostone as unit "PPD3". We correlate PPD2 and PPD3 with the Gibben and Chandindu formations, respectively and interpret the siltstone-sandstone sequence at the base of the Fifteenmile Group in the Coal Creek inlier to be equivalent to PPD1 (Fig. 10). Because the equivalent of PPD1 is relatively poorly preserved in the Coal Creek inlier and transitional with overlying carbonates of the Gibben formation, we include PPD1 in the Gibben formation. However, pending identification of an appropriate reference section, PPD1 as a whole, or the lower shale-siltstone interval, should be separated as a distinct formation comprising the base of the Fifteenmile Group.

Abbott (1997) placed PPD1, PPD2, and PPD3 in the Pinguicula Group. However, we have recognized a prominent unconformity beneath PPD1 elsewhere in the Hart River inlier (Section 7; Fig. 10), consistent with Abbott (1993) and our observations in the Coal Creek inlier. Consequently, as originally proposed by Abbott (1993) and in agreement with Medig *et al.* (2010), we suggest including these units within the lower Fifteenmile Group. Correlation between the Coal Creek and Hart River inliers implies that a large portion of the Fifteenmile Group (upper Chandindu formation through the Craggy Dolostone) is missing in the Hart River inlier (Fig. 10). This conclusion is consistent with the documentation of a prominent angular unconformity beneath the Callison Lake Dolostone in the Hart River inlier (Abbott, 1997; Macdonald and Roots, 2010).

CONTACT WITH THE PINGUICULA GROUP

In Abbott's (1997) Section 1 in the Hart River inlier (Figs. 7 and 8), what we recognize as the base of the Fifteenmile Group unconformably overlies orange-weathering muddy dolostone and green shale of unit B of the Pinguicula Group (PPB). Further east in the inlier, the uppermost Pinguicula Group is composed of a cream-coloured, massive to thick-bedded dolostone (PPC; Abbott, 1997), which conformably overlies PPB (Medig *et al.*, 2010) and is intensely brecciated and karstified beneath PPD1. In our reference section for the Gibben formation (Fig. 3), PPD1 rests unconformably atop a unit of cream-coloured dolomitic stromatolites, this is truncated beneath the contact to the west. To the east, this dolostone thickens to over 600 m, the upper part of which is composed of a spectacular exposure (Fig. 10) of large, reef-forming *Minjaria* and *Conophyton* stromatolites (Fig. 11) and stromatolite breccias. We correlate this thick stromatolitic dolostone unit with PPC in the Hart River inlier. Notably, just as PPC appears to have been rotated and eroded beneath PPD1 in the Hart River inlier (Abbott, 1997), our upper Pinguicula Group stromatolites form a wedge-shaped map unit beneath the Fifteenmile Group (Fig. 2), implying rotation and truncation. This observation is consistent with mapping of the Gibben formation, which indicates that the onset of Fifteenmile Group deposition resulted from an extensional episode post-dating the Pinguicula Group but significantly earlier than 811 Ma.

DISCUSSION AND CONCLUSIONS

Figure 12 presents an updated but still incomplete revision of the informal nomenclature and stratigraphic framework for the Fifteenmile Group and its correlation between the Coal Creek and Hart River inliers. This new stratigraphic scheme builds upon recent revisions to the nomenclature in the Coal Creek and Tatonduk inliers (Macdonald and Roots, 2010; Macdonald *et al.*, 2011) and dispenses with the former PR and PF subdivision of the

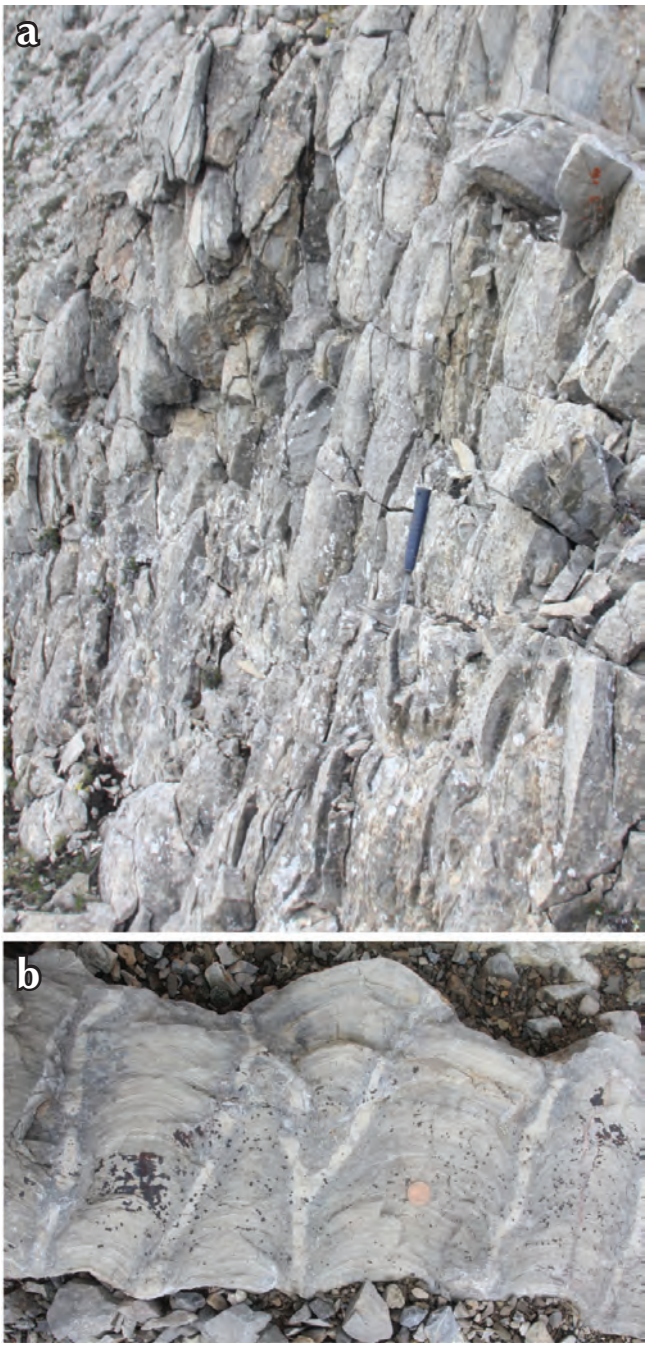

Figure 11. *Stromatolites in the upper Pinguicula Group in the Coal Creek inlier (section GO136; Fig. 3). A thick stromatolitic succession in the upper part of PPC(?) comprises mainly Conophyton* ***(a)*** *and Minjaria* ***(b)****.*

Fifteenmile Group. Given the recognition of an angular unconformity separating the Callison Lake Dolostone from the underlying Fifteenmile Group in the Hart River inlier, we suggest that the Callison Lake Dolostone more appropriately belongs with the lower Mt. Harper Group (Fig. 11), or perhaps even separate from both the Fifteenmile and Mt. Harper groups. The Fifteenmile Group is now tentatively subdivided, from oldest to youngest, into PPD1 (in the Hart River inlier), the Gibben formation, the Chandindu formation, the Reefal assemblage, and the Craggy Dolostone (Fig. 11). PPD1 is a residual name from when it was assigned to the Pinguicula Group (Abbott, 1997) and should be replaced by a proper formation name pending identification of an appropriate reference section, most likely in the Hart River inlier where it is best developed.

PPD1 and the Gibben and Chandindu formations correlate unambiguously between the Coal Creek and Hart River inliers (Fig. 10). In the former, where we have measured more sections, all three are highly variably in thickness, reflecting the opening of small, fault-bound sub-basins during deposition of the lowermost Fifteenmile Group. This faulting, which appears to have been active at least until early Chandindu times, is evident in the significant lateral variations in thickness of PPD1 and the Gibben formation and in the lateral facies variations in the Chandindu formation (Fig. 10). In the Coal Creek inlier, the thickness of the lower Gibben formation is clearly linked to the extent of erosional truncation of the underlying stromatolite unit (Fig. 2), suggesting block rotation related to normal faulting.

Medig *et al.* (2010) had previously suggested that former map units PR1 and PR2 in the Coal Creek inlier belong to the Pinguicula Group and our mapping bears this interpretation out. Hence, the unconformity separating PPB and PPC from PPD1 in the Hart River inlier is the same unconformity we have mapped atop the rotated stromatolitic dolostone in the Coal Creek inlier. We further suggest that the stromatolitic unit in the upper Pinguicula Group in the Coal Creek inlier (Fig. 10) is most likely equivalent to unit PPC, as identified in the Hart River (Abbott, 1997) and Wernecke (Eisbacher, 1981; Thorkelson *et al.*, 2005; Medig *et al.*, 2010) inliers.

ACKNOWLEDGMENTS

This paper is a product of collaborative research between McGill and Harvard universities, with support from the Yukon Geological Survey, NSERC, and the American Chemical Society (PRF). Erik Sperling and Andrei Popescu assisted with fieldwork in the Coal Creek inlier. Charlie Roots has been instrumental in guiding our fieldwork and interpretations. We thank Mo Colpron for a constructive review of the manuscript.

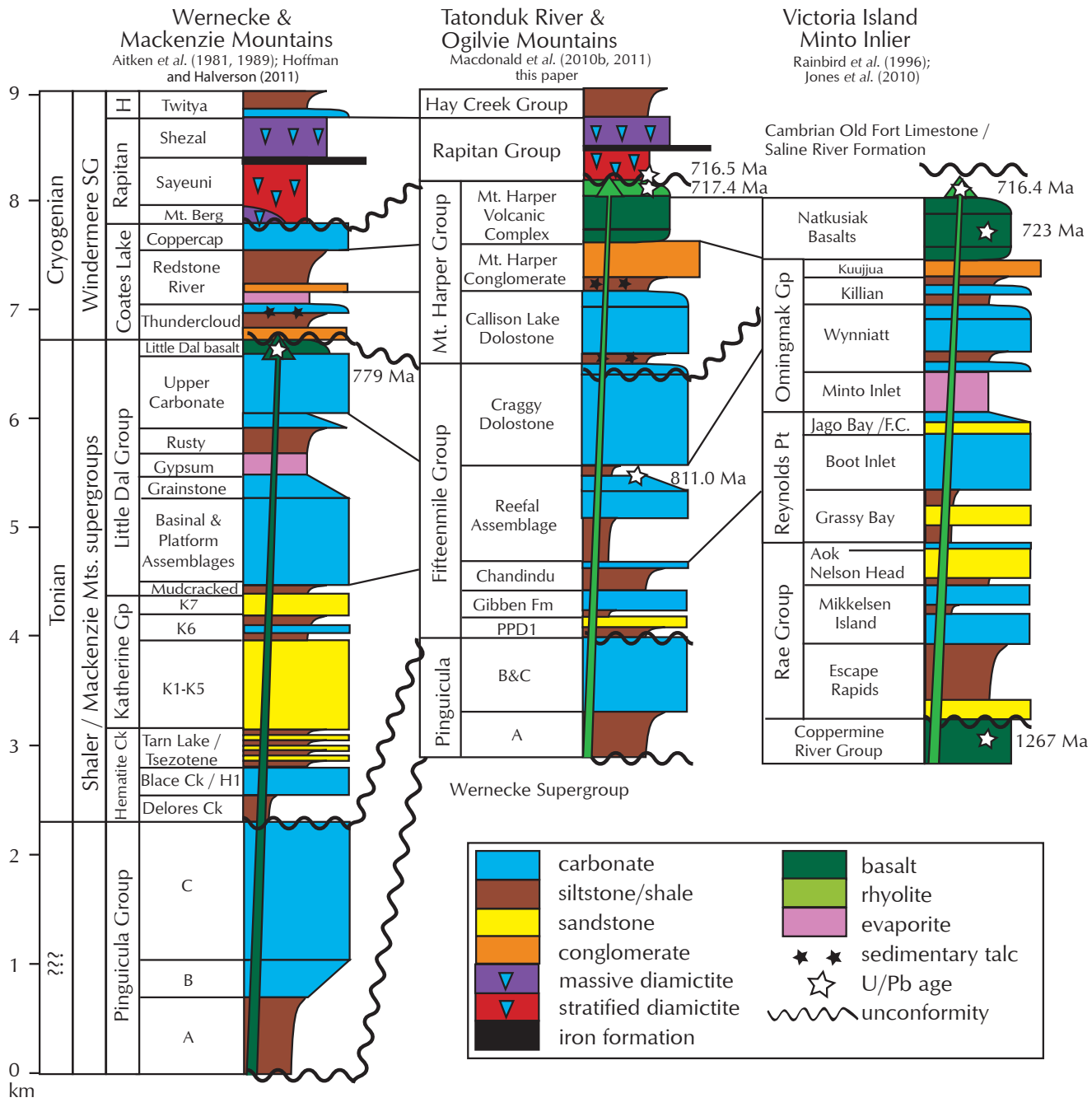

Figure 12. *Schematic columns of the Sequence B (plus Pinguicula) and lower Sequence C (Cryogenian) stratigraphy across northern Canada, showing available U-Pb zircon age constraints and our proposed correlations and new nomenclature for the lower Fifteenmile Group in the Ogilvie Mountains. U-Pb ages: 779 Ma (Harlan et al., 2003); 716.5, 717.4, 811.0, 716.4 Ma (Macdonald et al., 2010); 723 Ma (Heaman et al., 1992); 1267 Ma (LeCheminant and Heaman, 1989).*

REFERENCES

Abbott, J.G., 1993. Revised stratigraphy and new exploration targets in the Hart River Area (116A/10, 116A/11), southeastern Yukon. *In:* Yukon Exploration and Geology 1992, Exploration and Geological Sciences Division, Yukon, Indian and Northern Affairs Canada, p. 13-23.

Abbott, J.G., 1997. Geology of the upper Hart River area eastern Ogilvie Mountains, Yukon Territory (116A/10, 11). Exploration and Geological Services Division, Yukon Region, Indian and Northern Affairs Canada, Bulletin 9, 92 p.

Eisbacher, G.H., 1981. Sedimentary tectonics and glacial record in the Windermere Supergroup, Mackenzie Mountains, northwestern Canada. Geological Survey of Canada, Paper 80-27, 40 p.

Gabrielse, H., 1972. Younger Precambrian of the Canadian cordillera. American Journal of Science, vol. 272, p. 521–536.

Harlan, S.S., Heaman, L.M., LeCheminant, A.N., and Premo, W.R., 2003. Gunbarrel mafic magmatic event: a key 780 Ma time marker for Rodinia plate reconstructions. Geology, vol. 31, p. 1053-1056.

Heaman, L. M., LeCheminant, A. N., and Rainbird, R. H., 1992. Nature and timing of Franklin igneous events, Canada: Implications for a Late Proterozoic mantle plume and the break-up of Laurentia. Earth and Planetary Science Letters, vol. 109, p. 117–131.

LeCheminant, A. N. and Heaman, L. M., 1989, Mackenzie igneous events, Canada: Middle Proterozoic hotspot magmatism associated with ocean opening. Earth and Planetary Science Letters, vol. 96, p. 38–48.

Long, D.G.F., Rainbird, R.H., Turner, E..C., and MacNaughton, R.B., 2008. Early Neoproterozoic strata (Sequence B) of mainland northern Canada and Victoria and Banks islands: a contribution to the *Geological Atlas of the Northern Canadian Mainland Sedimentary Basin*; Geological Survey of Canada, Open File 5700, 24 p.

Macdonald, F.A. and Roots, C.F., 2010. Upper Fifteenmile Group in the Ogilvie Mountains and correlations of early Neoproterozoic strata in the northern Cordillera. *In:* Yukon Exploration and Geology 2009, K.E. MacFarlane, L.H. Weston and L.R. Blackburn (eds.), Yukon Geological Survey, p. 237-252.

Macdonald, F.A., Cohen, P.A., Dudás, F.O., and Schrag, D.P., 2010a. Early Neoproterozoic scale microfossils in the Lower Tindir Group of Alaska and the Yukon Territory. Geology, vol. 38, p. 143-146.

Macdonald, F.A., Schmitz, M.D., Crowley, J.L., Roots, C.F., Jones, D.S., Maloof, A.C., Strauss, J.V., Cohen, P.A., Johnston, D.T., and Schrag, D.P. 2010b. Calibrating the Cryogenian. Science, vol. 327, p. 1241-1243.

Macdonald, F.A., Smith, E.F., Strauss, J.V., Cox, G.M, Halverson, G.P., and Roots, C.F., 2011. Neoproterozoic and early Paleozoic correlations in the western Ogilvie Mountains, Yukon. *In:* Yukon Exploration and Geology 2010, K.E. MacFarlane, L.H. Weston and C. Relf (eds.), Yukon Geological Survey, p. 161-182.

Medig, K.P.R., Thorkelson, D.J., and Dunlop, R.L., 2010. The Proterozoic Pinguicula Group: Stratigraphy, contact relationships and possible correlations. *In:* Yukon Exploration and Geology 2009, K.E. MacFarlane, L.H. Weston and L.R. Blackburn (eds.), Yukon Geological Survey, p. 265-278.

Mustard, P.S. and Roots, C.F., 1997. Rift-related volcanism, sedimentation, and tectonic setting of the Mount Harper Group, Ogilvie Mountains, Yukon Territory. Geological Survey of Canada, Bulletin 492, 92 p.

Rainbird, R.H., Jefferson, C.W., and Young, G.M., 1996. The early Neoproterozoic sedimentary succession B of northwestern Laurentia: Correlations and paleogeographic significance. Geological Society of America Bulletin, vol. 108, no. 4, p. 454-470.

Thompson, R.I., Roots, C.F., and Mustard, P.S., 1994. Geology of Dawson map area 116B, C, northeast of Tintina Trench. Geological Survey of Canada, Open File 2849, scale 1: 50 000.

Thorkelson, D.J., Abbott, J.G., Mortensen, J.K., Creaser, R.A., Villeneuve, M.E., McNicoll, V.J., and Layer, P.W., 2005. Early and Middle Proterozoic evolution of Yukon, Canada. Canadian Journal of Earth Sciences, vol. 42, no. 6, p. 1045-1071.

Turner, E.C., 2011. Stratigraphy of the Mackenzie Mountains supergroup in the Wernecke Mountains, Yukon. *In:* Yukon Exploration and Geology 2010, K.E. MacFarlane, L.H. Weston and C. Relf (eds.), Yukon Geological Survey, p. 207-231.

Young, G.M., Jefferson, C.W., Delaney, G.D., and Yeo, G.M., 1979. Middle and Upper Proterozoic evolution of the northern Canadian Cordillera and Shield. Geology, vol. 7, p. 125-128.

New U-Pb geochronology of Early Cretaceous porphyry and skarn mineralization in southwest Yukon

Steve Israel[1]
Yukon Geological Survey, Whitehorse, YT

Rosie Cobbett
Archer Cathro and Associates (1981) Ltd.

Jim Mortensen
University of British Columbia, Vancouver, BC

Israel, S., Cobbett, R., and Mortensen, J., 2012. New U-Pb geochronology of Early Cretaceous porphyry and skarn mineralization in southwest Yukon. *In:* Yukon Exploration and Geology 2011, K.E. MacFarlane and P.J. Sack (eds.), Yukon Geological Survey, p. 91-102.

ABSTRACT

New U-Pb geochronological analyses of zircon and garnet found within intrusive rocks and skarn indicate that porphyry copper-gold and gold-copper skarn mineralization is associated with the Early Cretaceous Kluane Ranges suite in southwest Yukon. The Nikki porphyry property, located ~25 km south of Beaver Creek, is characterized by Paleozoic to Triassic rocks of Wrangellia intruded by *ca.* 125 Ma intermediate intrusions of the Kluane Ranges suite. High copper and anomalous gold values associated with intrusions are considered to be related to high-level porphyry-style mineralization. The Arn property, located ~15 km to the southeast of the Nikki, is characterized by gold and copper mineralization associated with skarn developed at the margin of intrusions thought to be the Kluane Ranges suite and Triassic carbonate of the Chitistone Limestone. No ages for the intrusions exist and age of mineralization was not well constrained. New U-Pb analyses of garnet and titanite from the skarn indicate that the skarn mineralization occurred at *ca.* 123 Ma.

The new data suggests that skarn mineralization is associated with Early Cretaceous intrusion of the Kluane Ranges suite and that porphyry mineralization at the Nikki property is the same age as skarn mineralization at the Arn. This indicates that the Kluane Ranges suite is highly prospective for both porphyry and skarn type mineralization elsewhere in southwest Yukon.

[1] *steve.israel@gov.yk.ca*

INTRODUCTION

Southwest Yukon is well-endowed with placer gold mineralization and native copper found in creeks and in fractures within rocks, as well as elevated values of copper and gold in regional geochemical surveys. Some of these anomalous values have been associated with Triassic mafic-ultramafic intrusions and their volcanic equivalents; however, these rocks cannot account for all the mineralization known in southwest Yukon. The Early Cretaceous Kluane Ranges suite, which consists mainly of diorite, quartz-diorite and granodiorite, is another possible mineralizer in the region; however, the possible relationship to mineralization in southwest Yukon is not very well understood. Two properties in southwest Yukon, near the Alaska border south of Beaver Creek, include mineralization that is thought to be related to the Kluane Ranges suite. One of these occurrences (Arn; Yukon occurrence 115K 048) comprises skarn mineralization, and the other (Nikki; Yukon occurrence 115K 082) includes porphyry copper mineralization. A regional Early Cretaceous emplacement age for the Kluane Ranges suite is mainly defined by K-Ar ages from hornblende and biotite found within the intrusive bodies, and by one TIMS age on zircon. These ages range from *ca.* 124 to 112 Ma, with a 122 Ma U-Pb TIMS date (Dodds and Campbell, 1988; Israel, unpublished data).

The Arn property (Fig. 1) is characterized by a copper-gold skarn developed within rocks of Wrangellia. Skarn mineralization at the Arn occurs near the intrusive contact between Triassic carbonate of the Chitistone Limestone and the Kluane Ranges suite. On the Nikki property (Fig. 1) porphyry copper mineralization is related to a quartz-diorite of the Kluane Ranges suite. The relationships between the two mineralizing systems have not been assessed previously, although it has been suspected they are of similar age.

This paper presents new mapping and zircon ages from the Nikki property and titanite and garnet ages from the skarn mineralization at the Arn property. The new data indicates that mineralization at the Arn and Nikki are both related to Kluane Ranges suite intrusions and occurred between 123 and 125 Ma. The new U-Pb data also shows the effectiveness of using garnet for dating skarn systems.

REGIONAL GEOLOGY

The region around the Nikki and Arn properties is characterized by Mississippian through to Triassic volcanic and sedimentary strata of Wrangellia, which are overlain by Jura-Cretaceous sedimentary rocks of the Dezadeash Formation (Israel *et al.*, 2007). The area is dissected by the Miles Creek fault, which separates the Jura-Cretaceous rocks to the south from the main Wrangellian sequence to the north (Fig. 2). This fault likely has some normal displacement associated with it and is probably linked to deformation along the Denali fault in the Cenozoic. North of the Miles Creek fault, rocks of Wrangellia are folded and cut by northeast directed thrust faults. Folds are tight and in places overturned towards the northeast. South of the Miles Creek fault, the geology is not as well understood and is broadly divided into Paleozoic volcaniclastic rocks of the Station Creek Formation, Triassic volcanic rocks of the Nikolai formation, Triassic carbonates of the Chitistone Limestone and Jura-Cretaceous turbidites of the Dezadeash Formation. Much of the geology has been compiled from existing 1:250 000 scale mapping and does not show the detailed structural and stratigraphic relationships north of the fault. The rocks south of the fault are intruded by large bodies of the Kluane Ranges suite; north of the fault smaller intrusive bodies of both Triassic and Cretaceous ages are found (Fig. 2).

Figure 1. *Location of the Nikki and Arn properties shown by red dots, black box indicates location of Figure 2. HJ-Haines Junction; BC-Beaver Creek.*

NORTHWEST ARN PROPERTY GEOLOGY

The approximate location of the Arn claims is shown in Figure 2. Mapping for this project covered the western part of the claim block. The geology of this study area is similar to that described for the rest of the property (Eaton, 2003; 2004; Fig. 3).

The lowermost stratigraphic unit within the Arn property is a dark green to black, fine-grained, locally vesicular or amygdaloidal, and locally pillowed, strongly magnetic basalt (unit mTRb) (Fig. 4) that crops out along a knife-edged ridge on the west side of the mapped area. Sitting above this, and to the north, is a horizon of grey, laminated to thin-bedded limestone (unit lTRl) that is locally converted to marble (unit lTRm) near the contact with intrusive rocks (Fig. 5). The limestone appears to dip shallowly to the north and is at most a few hundred metres thick. Above, and to the north of the limestone, is a relatively flat laying package of thin bedded, very fine grained, green and beige, banded tuffs (Fig. 6). The tuffs make up the highest part of the mountain in the northwest corner of the property. Contacts between the basalt, limestone, and tuff are inferred to be conformable; however the abundance of dikes and sills intruding this package obscures most of the exposed contacts. To the north and east of the layered rocks a grey, medium-grained diorite intrudes the layered rocks (unit Kd).

Of significance are the numerous intermediate to mafic dikes and sills that cut through the layered rocks. Textures of these bodies vary from fine grained to very coarsely porphyritic (hornblende, pyroxene and plagioclase phenocrysts). Intermediate, fine-grained dikes and feldspar porphyry dikes both cut hornblende ± pyroxene porphyry dikes. Both porphyritic dikes and intermediate composition dikes cut the diorite pluton, as does a light green, sugary felsite dike. Xenoliths of mafic and intermediate blocks, similar to the dikes in outcrop, occur within a medium-grained diorite, but are only recognized in float.

Lens shaped, discontinuous skarn horizons are common throughout the Arn property. Skarn horizons are commonly spatially associated with limestone, are rarely found within the basalt, and are always associated with intermediate or mafic dikes and sills believed to be associated with the Kluane Ranges suite intrusions. Within the mapped area, skarn minerals consist of varying amounts of garnet, epidote, pyroxene, magnetite, pyrite, and pyrrhotite.

To the east of the mapped area, still within the Arn property boundary, previous workers have recorded a wide variety of skarn minerals associated with grey, bedded limestone, and basalt, cut by intermediate dikes. Skarn assemblages in this area are typically made up of varying amounts of garnet, epidote, magnetite-amphibole, pyrrhotite and pyrite (Eaton, 2004). Copper and gold mineralization is found within pyrrhotite and pyrite rich skarns that occur within the basalts and less commonly within intermediate dikes near limestone bodies (Eaton, 2004).

NIKKI PROPERTY GEOLOGY

The Nikki property is characterized by layered sedimentary rocks of probable Permian age that have been intruded by Triassic Maple Creek gabbro and Early Cretaceous intrusions (Fig. 7).

Layered rocks mapped within the Nikki property boundary comprise banded tuffs, sandstone, siltstone and shale. The tuffs are made up of beige, light and dark green bands and are interlayered with green, volcaniclastic sandstone and siltstone. The volcaniclastic rocks grade upwards into dark grey siltstone with interbeds of fossiliferous shale. This becomes shale-rich and then finally passes up into shale interbedded with medium-grained arkose and lithic sandstone. Rare fining upwards sequences within the sandstone beds indicate this package of rocks is structurally upright (Fig. 8). This entire succession has been assigned to the Permian Hasen Creek Formation based on lithological similarities to Hasen Creek rocks mapped nearby (Fig. 2; Israel *et al.*, 2007).

The Hasen Creek Formation has been intruded by granodiorite that has been divided into three sub-units based on mineralogical variability within the mapped area. Salt and pepper, medium-grained, biotite-hornblende granodiorite to diorite (unit EKK, Fig. 7) crops out in the southeast corner of the map area and appears to be relatively unaltered. In the southwest corner of the map sheet a pinkish, medium-grained granodiorite is composed of quartz and plagioclase with biotite and hornblende altered to chlorite and what appears to be interstitial potassium feldspar (unit EKK2, Fig. 7). A band of purplish-grey, medium to coarse-grained, highly magnetic gabbro to diorite crops out north of the altered granodiorite. This body contains varying amounts of magnetite and locally significant amounts of secondary (?) biotite (unit EKK1, Fig. 7).

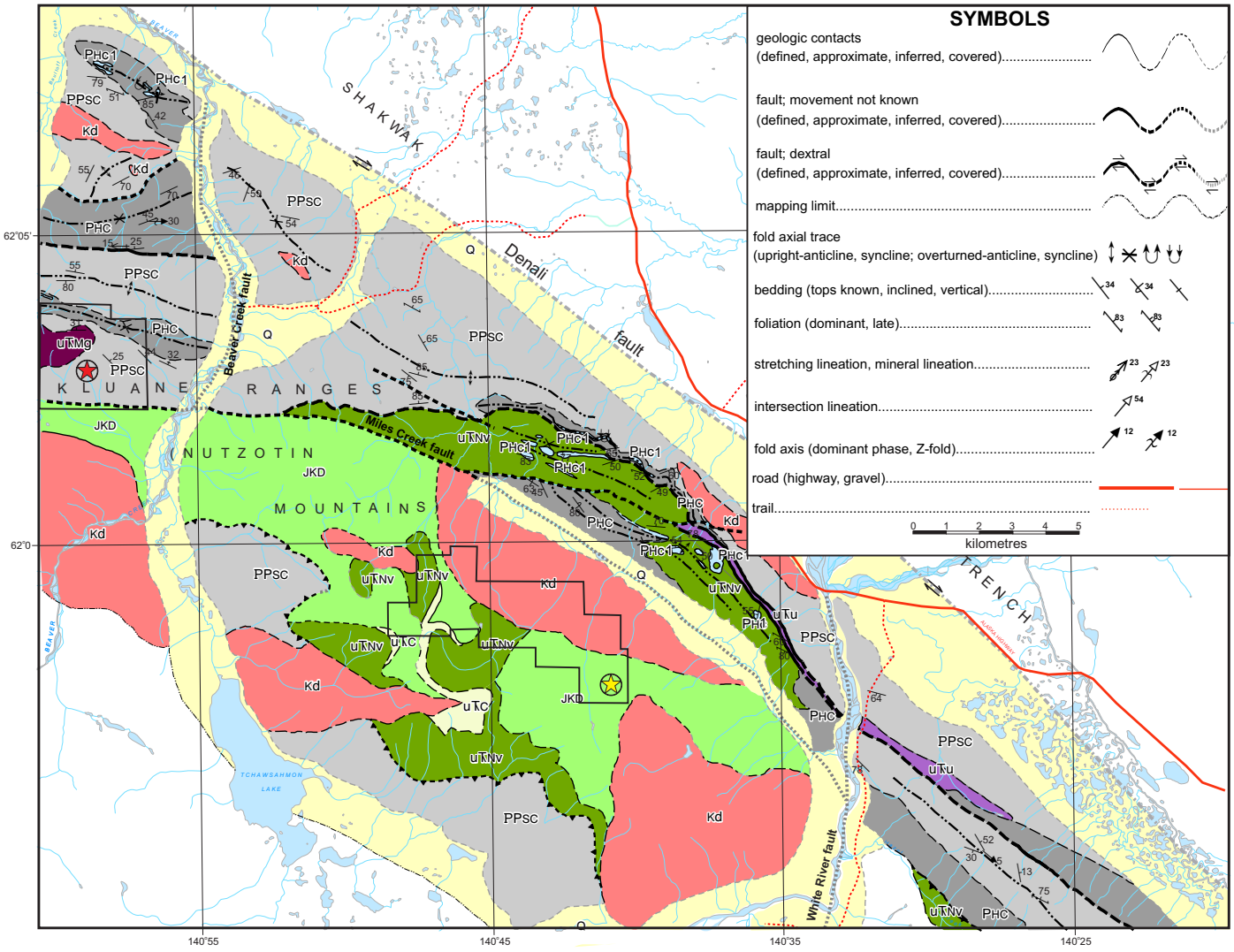

LEGEND

QUATERNARY

Q — unconsolidated glacial, glaciofluvial and glaciolacustrine deposits; fluviatile silt, sand and gravel, and local volcanic ash, in part with cover of soil and organic deposits

INTRUSIVE ROCKS

EARLY CRETACEOUS

Kd — KLUANE RANGES SUITE: medium to coarse-grained, unfoliated, hornblende-biotite, diorite to biotite granodiorite; salt and pepper appearance

LATE TRIASSIC

uTrMg — MAPLE CREEK GABBRO: medium to coarse-grained, massive to foliated, dark-grey weathered and fresh, pyroxene gabbro; rare olivine phenocrysts

uTru — KLUANE MAFIC-ULTRAMAFIC COMPLEX: fine to medium-grained, dark-grey weathered pyroxene gabbro; dark-green/black weathered peridotite, pyroxenite and rare dunite, locally strongly serpentinized and altered

LAYERED ROCKS

UPPER TRIASSIC(?) - JURASSIC

Dezadeash Formation

JKD — interbedded light to dark buff-grey lithic greywacke, sandstone and siltstone, thin dark grey shale, argillite, phyllite and conglomerate; rare tuff horizons; may include Late Triassic McCarthy Formation, well bedded calcareous mudstone and black fetid carbonate

TRIASSIC

uTrC — CHITISTONE LIMESTONE: light beige to light grey carbonate; massive to brecciated and locally bedded; noticeable absence of macrofossils distinguishes this unit from Paleozoic limestones; includes abundant dark green/maroon basalt clasts near contact with underlying Nikolai formation; may include Late Triassic McCarthy Formation, well bedded calcareous mudstones and black fetid carbonate

Nikolai formation

uTrNv — dark green/maroon weathered and fresh, massive to locally foliated, amygdaloidal and vesicular basalt flows; rare pillows, volcanic breccia and conglomerate locally developed near base of unit; breccia and conglomerate contain clasts of sedimentary and volcanic rocks of underlying Hasen Creek and Station Creek formations as well as rounded volcanic clasts typical of the Nikolai basalts

PENNSYLVANIAN - PERMIAN

Skolai Group

Hasen Creek Formation

PHc1 — light to medium grey, massive to bedded fossiliferous limestone; fossils include corals and crinoids

PHC — interbedded, dark-grey and brown weathered siltstone, mudstone and medium to coarse-grained sandstone; lower part contains volcaniclastic sandstones, tuffs and rare basaltic flows; rare dark-grey to black chert beds and pebble conglomerate

Station Creek Formation

PPSC — interbedded volcanic breccia, agglomerate and volcaniclastic sandstone; intercalated light-grey weathered, dark-green to black fresh, pyroxene-phyric basalt flows; dark grey to black siltstone and light to dark-grey limestone found near contact with Hasen Creek Formation

Figure 2. *Regional geological map of the area surrounding the Nikki (red star) and Arn (yellow star) properties, modified from Israel et al., (2007).*

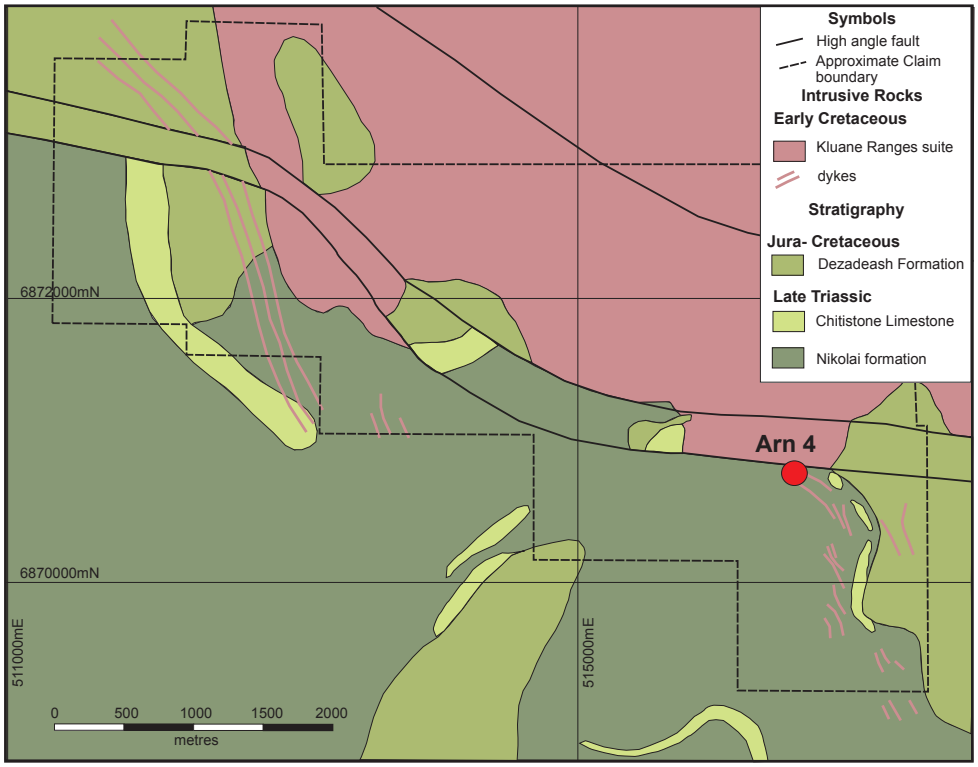

Figure 3. *Simplified geology of the Arn property, modified from Eaton (2004).*

Figure 4. *Basalt from the Arn property.*

Figure 5. *Layered limestone/marble found on the Arn property.*

Figure 6. *Banded tuff found at the stratigraphically highest level at the Arn property.*

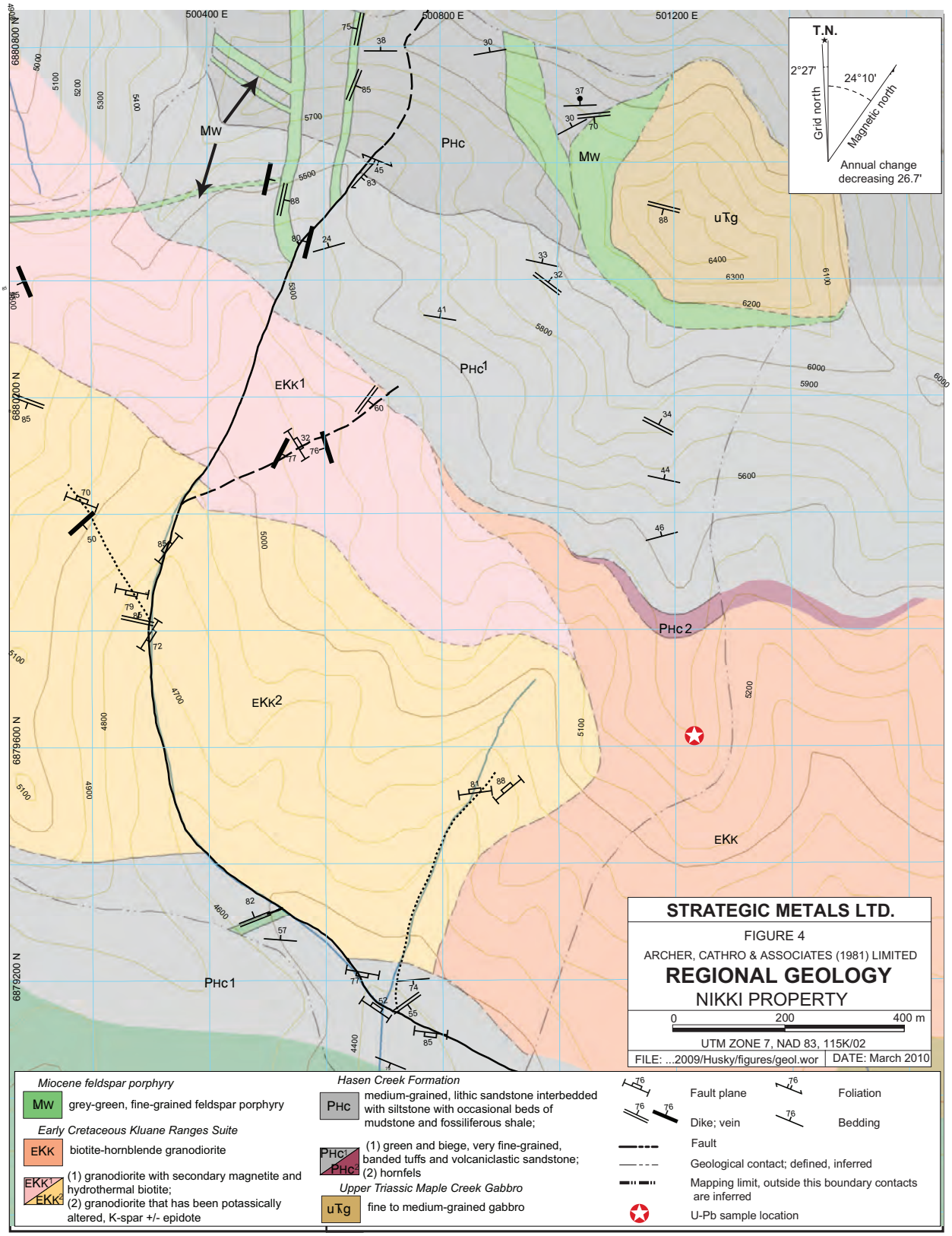

Figure 7. *Simplified geology of the Nikki property.*

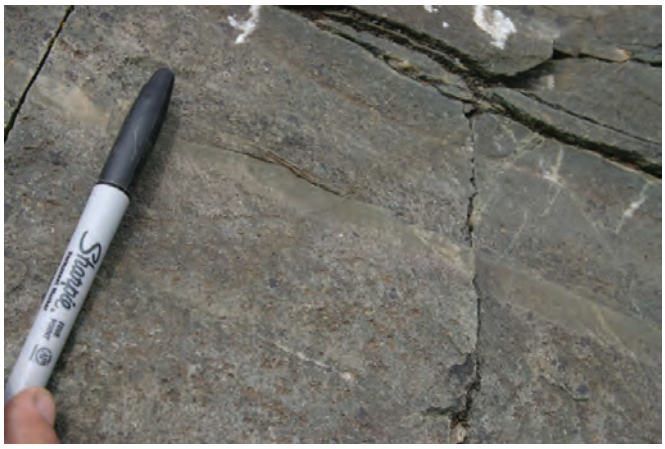

Figure 8. *Fining upwards graded beds in arkosic/lithic sandstone at the Nikki property.*

Figure 9. *Orange weathered clay within a brittle fault on the Nikki property.*

In the northeast corner of the Nikki property a rugged mountain peak is composed of fine to medium-grained gabbro that has not been dated but has been assigned to the upper Triassic Maple Creek Gabbro based on regional geology (Fig. 2).

Both the layered rocks and the plutons are commonly cut by feldspar ± quartz porphyry dikes that range in thickness from 2 to 40 m, intermediate to mafic composition, pyroxene-porphyry dikes and grey-green, fine-grained, intermediate composition dikes. The age of these dikes is unknown; they either represent a later phase of the Kluane Ranges suite or younger, possibly Oligocene or Miocene intrusions similar to those that have been found elsewhere in the region.

The main gully that runs north-south through the centre of the property follows the trace of a steeply dipping brittle fault. Where exposed, the fault comprises zones of crushed rock and clay that range in thickness from 20 to 50 cm (Fig. 9). Splays off the main fault occur both to the northwest and northeast, but cannot be traced for very long distances. This fault appears to have a component of dextral strike slip motion because contacts are offset by as much as 150 metres. The orientation of gouge and crushed rock zones measured at a variety of locations can be grouped into two orientations, suggesting they may form a conjugate set. The dominant set of fault plane measurements strikes northeast and dips steeply to the southeast. A minor set of faults strikes east-southeast and dips steeply to the south. Exposures of the fault zone exhibit very rusty weathered rock and locally contain copper carbonate staining (Fig. 10).

Figure 10. *Moderately mineralized brittle fault on the Nikki property.*

Mineralization at the Nikki property is believed to be porphyry copper-gold, with some anomalous molybdenum, and probably associated with high level intrusions of the Kluane Ranges suite (Eaton, 2005). A large copper and gold soil geochemical anomaly on the Nikki property was identified during work in 2004 and was subsequently followed up in this study with bedrock geological mapping.

GEOCHRONOLOGY

Samples from the Nikki and Arn properties were analysed using U-Pb zircon techniques at Memorial University of Newfoundland (MUN) and U-Pb titanite and garnet techniques at the Pacific Centre for Isotopic and Geochemical Research (PCIGR) at the University of British Columbia, in order to test the age of mineralization. Analytical techniques employed at MUN followed Bennett and Tubrett (2010), and at PCIGR methods used followed Mortensen *et al.* (1995).

NIKKI

A sample of hornblende, quartz-diorite from the Nikki property, associated with mineralization, was obtained during mapping. This sample was analysed at MUN using LAM-ICPMS to obtain an age for the intrusions at the property and the age of mineralization. Analytical data are shown in Appendix A. Zircons from the sample were imaged using cathodoluminescence and display oscillatory zoning and no cores or metamorphic rims. A total of 24 zircons were analysed with the best 17 returning a mean average age of 125.08±0.77 Ma (Fig. 11). We interpret this age as the crystallization age of the intrusion and also the age of the porphyry style mineralization associated with the intrusion.

ARN

Precisely dating mineralized skarns is hampered by the fact that minerals amenable to ^{40}Ar-^{39}Ar dating are commonly absent, and in many cases, as at the Arn, the temporal relationship between the mineralization and intrusive rock phases that could be dated by ^{40}Ar-^{39}Ar or U-Pb methods is unclear. However, Meinert *et al.* (2001) successfully employed U-Pb methods to directly date inclusion-free garnets from several copper skarns. In this study we have used U-Pb dating of both garnet and titanite from within mineralized skarn at the Arn property to establish the age of skarn formation. Garnet in mineralized skarn at the Arn

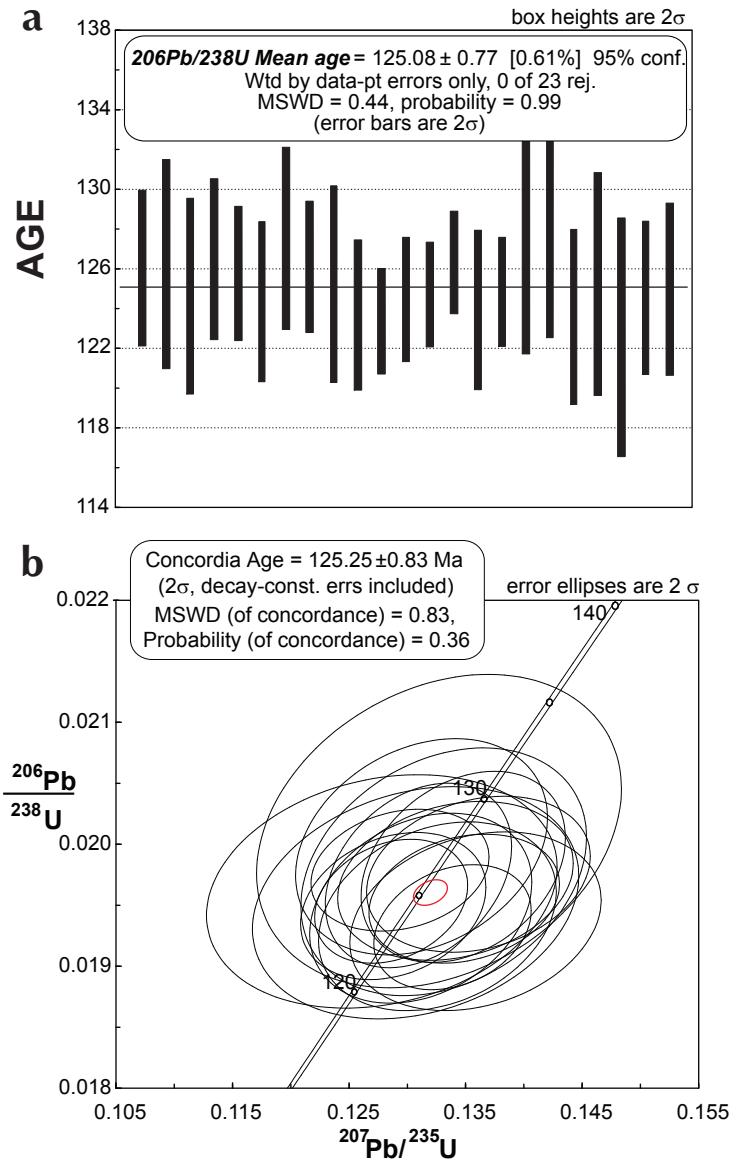

Figure 11. *U-Pb zircon ages from quartz-diorite samples at the Nikki property,* ***(a)*** *weighted mean of zircon ages,* ***(b)*** *U-Pb zircon concordia diagram.*

property is typically compositionally zoned from grossular-rich cores to more andraditic rims (Miller, 2004). Titanite occurs together with prismatic hornblende grains within calcite.

Selected samples of skarn material from diamond drillhole Arn 4, drilled adjacent to the Arn fault (Eaton, 2003; 2004; Fig. 3), were crushed and ground to fine sand size, and then garnet and/or titanite was concentrated using a combination of heavy liquids and magnetic separation methods. The best, clearest, inclusion-free grains available

were carefully hand-picked under a binocular microscope. Analytical data are reported in Appendix B. All errors in interpreted ages are given at the 2 sigma level.

Sample JM-14. Two fractions of clear, pinkish-brown garnet were analysed. Both yield concordant analyses with overlapping error envelopes (Fig. 12a). The interpreted age of 123.3±0.9 Ma is based on the total range of $^{206}Pb/^{238}U$ ages for the two garnet fractions.

Sample JM-28B. Two fractions of pinkish-brown garnet were analysed. Although both analyses are concordant there is a greater range of $^{206}Pb/^{238}U$ ages for the two fractions (Fig. 12b). An age of 122.9±0.8 Ma is assigned based on the total range of $^{206}Pb/^{238}U$ ages for the two fractions.

Sample ARN-16. Two fractions of clear, very pale pink garnet were analysed. Both yield slightly discordant analyses with a total range of $^{206}Pb/^{238}U$ ages of 123.6±0.8 Ma. The sample also yielded abundant clear, very pale yellow fragments of originally relatively large, subhedral to euhedral titanite. Two fractions of titanite were also analysed; one fraction yielded a concordant analysis and the second yielded a somewhat reversely discordant analysis (Appendix B; Fig. 12c). A $^{238}U/^{206}Pb$ isochron age of 124.0±0.8 Ma was obtained for the garnet and titanite analyses, with a MSWD of 4.1 and a calculated initial $^{206}Pb/^{204}Pb$ ratio of 18.0 (Fig. 13a).

Sample JM-16. Both garnet and titanite were analysed from this sample. The garnet was pale pinkish-brown. Two fractions of garnet and three fractions of titanite yield a considerable scatter in $^{206}Pb/^{238}U$ ages (Table 2; Fig. 12d); however a relatively imprecise $^{238}U/^{206}Pb$ isochron age of 125.5±4.2 Ma was obtained for the garnet and titanite analyses. The calculated regression has a MSWD of 219 and a calculated initial $^{206}Pb/^{204}Pb$ ratio of 19.7 (Fig. 13b).

The ages obtained for the four samples of Arn skarn material are in excellent agreement and collectively indicate that the skarn formed at about 123 Ma.

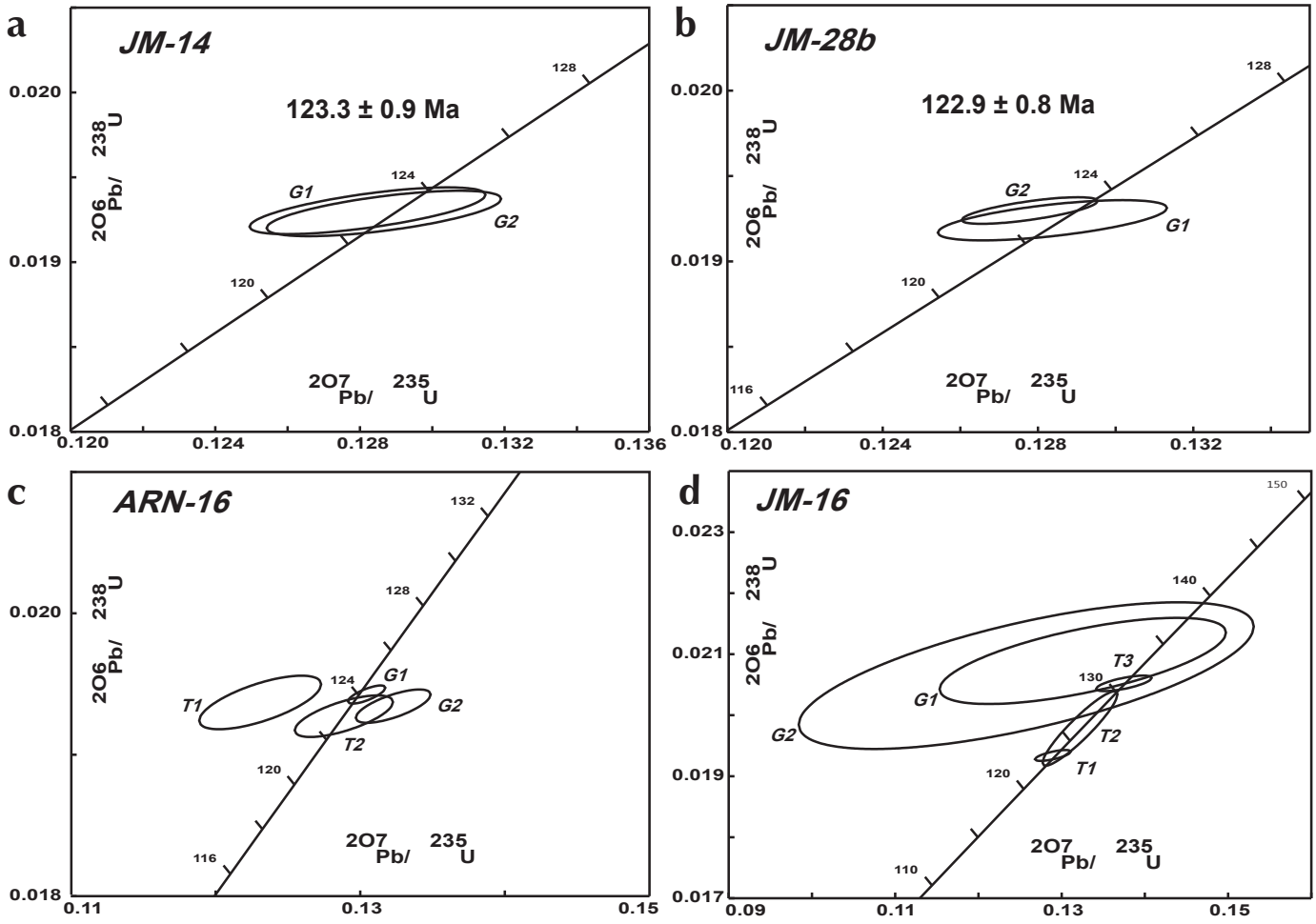

Figure 12. *U-Pb concordia diagrams for garnet and titanite from the Arn skarn samples;* ***(a)*** *JM-14,* ***(b)*** *JM-28b,* ***(c)*** *ARN-16, and* ***(d)*** *JM-16.*

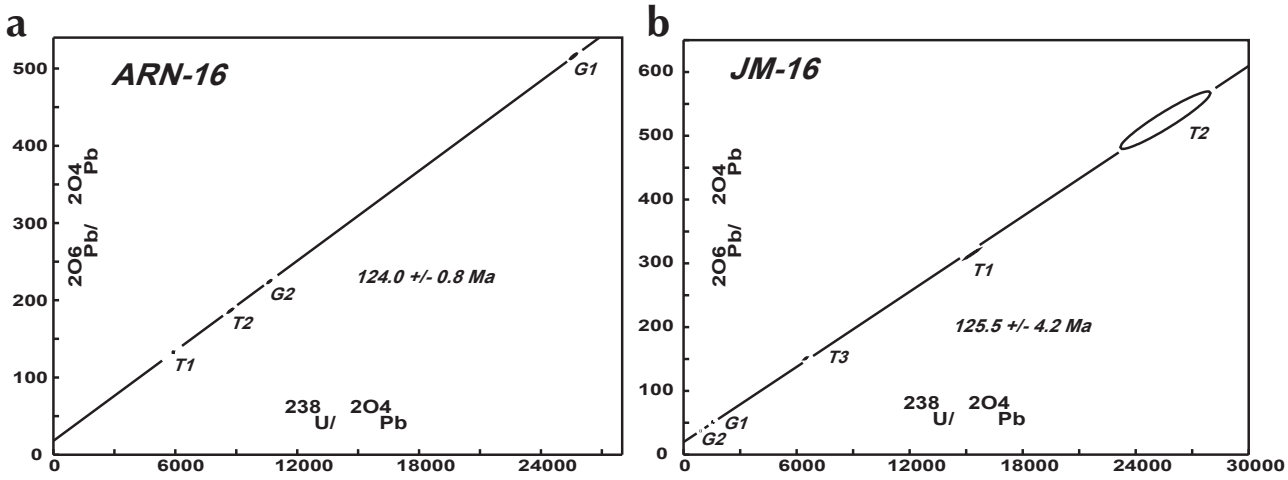

Figure 13. *U-Pb isochron diagrams for samples* ***(a)*** *ARN-16 and* ***(b)*** *JM-16.*

DISCUSSION

Geochronological results described here demonstrate that the porphyry style mineralization associated with intrusions at the Nikki property is the same age, within statistical error, as the skarn mineralization at the Arn property ~15 km to the southeast. We believe that intrusions responsible for both types of mineralization are associated with the Early Cretaceous Kluane Ranges suite. It is likely that both skarn and porphyry style mineralization is likely to be found associated with the Kluane Ranges suite elsewhere in southwest Yukon.

REFERENCES

Bennett, V. and Tubrett, M., 2010. U-Pb isotopic age dating by LAM ICP-MS, INCO Innovation Centre, Memorial University: Sample preparation methodology and analytical techniques. *In:* Yukon Exploration and Geology 2009, K.E. MacFarlane, L.H. Weston and L.R. Blackburn (eds.), Yukon Geological Survey, p. 47-55.

Dodds, C.J. and Campbell, R.B., 1988. Potassium-argon ages of mainly intrusive rocks in the Saint Elias Mountains, Yukon and British Columbia. Geological Survey of Canada, Paper 87-16, 43 p.

Eaton, W.D., 2003. Diamond drilling, prospecting and soil sampling on the Arn property. Yukon Territorial Assessment Report 094374.

Eaton, W.D., 2004. Geological mapping, soil sampling, prospecting and hand trenching on the Arn property. Yukon Territorial Assessment Report 094476.

Eaton, W.D., 2007. Prospecting, geological mapping, soil sampling and geophysical surveys at the Nikki property. Yukon Territorial Assessment Report 094527.

Israel, S., Cobbett, R. and Fozard, C., 2007. Bedrock geology of the Miles Ridge area, Yukon (parts of NTS 115F/15, 16 and 115K/1, 2) (1:50 000 scale). Yukon Geological Survey, Open File 2007-7.

Meinert, L.D., Nicolescu, S., Mortensen, J.K. and Cornell, D.H., 2001. U-Pb dating of hydrothermal garnets from skarn deposits – implications for petrogenesis and ore deposits. Geological Society of America, Abstracts with Program, v. 33.

Miller, J.L.P., 2004. U-Pb age and petrography of the ARN skarn occurrence in southwestern Yukon and the nature of contained gold. Unpublished B.A.Sc. thesis, University of British Columbia, 30 p.

Mortensen, J.K., Ghosh, D. and Ferri, F., 1995. U-Pb age constraints of intrusive rocks associated with copper-gold porphyry deposits in the Canadian Cordillera. *In:* Porphyry deposits of the northwestern Cordillera of North America, T.G. Shroeter (ed.), Canadian Institute of Mining and Metallurgy, Special Volume 46, p. 142-158.

Appendix A. *U-Pb analyses for sample 10-RC-038.*

								2 s %	2 s %	2 s %	AGES Ma						
Analysis	207/235	7/5 err	206/238	6/8 err	Rho	207/206	7/6 err	207/235	206/238	207/206	7/5 age	1 sigma	6/8 age	1sigma	Th_ppm	U_ppm	Th/U
no06a76	0.13095	0.00326	0.01974	0.00031	0.31388	0.04921	0.00131	4.99	3.13	5.33	125.0	2.9	126.0	2.0	86.2	241.3	0.36
no06a77	0.13312	0.00501	0.01977	0.00041	0.27889	0.04983	0.00197	7.52	4.20	7.89	126.9	4.5	126.2	2.6	181.2	328.6	0.55
no06a79	0.13071	0.00572	0.01952	0.00039	0.22766	0.04998	0.00245	8.75	3.98	9.82	124.7	5.1	124.6	2.5	86.2	178.3	0.48
no06a80	0.13480	0.00358	0.01981	0.00032	0.30414	0.05033	0.00154	5.31	3.23	6.10	128.4	3.2	126.5	2.0	119.8	297.9	0.40
no06a82	0.13414	0.00413	0.01970	0.00027	0.21940	0.04985	0.00132	6.16	2.70	5.29	127.8	3.7	125.8	1.7	150.1	361.8	0.41
no06a83	0.13115	0.00389	0.01948	0.00032	0.27523	0.05014	0.00175	5.94	3.27	6.98	125.1	3.5	124.3	2.0	123.4	231.4	0.53
no06a85	0.13122	0.00441	0.01998	0.00036	0.26934	0.04854	0.00170	6.73	3.62	7.00	125.2	4.0	127.5	2.3	83.6	225.3	0.37
no06a93	0.13610	0.00392	0.01975	0.00026	0.22939	0.05101	0.00169	5.76	2.64	6.61	129.6	3.5	126.1	1.7	110.7	357.0	0.31
no06a94	0.12781	0.00614	0.01961	0.00039	0.20727	0.04784	0.00215	9.62	3.99	8.97	122.1	5.5	125.2	2.5	197.1	318.0	0.62
no06a95	0.13585	0.00441	0.01937	0.00030	0.23826	0.05166	0.00164	6.49	3.09	6.37	129.3	3.9	123.7	1.9	190.6	420.0	0.45
no06a96	0.13388	0.00276	0.01932	0.00021	0.26323	0.05093	0.00111	4.12	2.17	4.36	127.6	2.5	123.4	1.3	473.2	547.6	0.86
no06a97	0.12880	0.00325	0.01949	0.00025	0.25057	0.04860	0.00135	5.04	2.53	5.57	123.0	2.9	124.5	1.6	520.4	576.3	0.90
no06a98	0.12861	0.00268	0.01953	0.00021	0.25488	0.04857	0.00119	4.17	2.13	4.92	122.9	2.4	124.7	1.3	474.0	548.3	0.86
no06a99	0.12937	0.00312	0.01979	0.00020	0.21369	0.04820	0.00124	4.82	2.06	5.13	123.5	2.8	126.3	1.3	420.4	503.7	0.83
no06a100	0.13258	0.00417	0.01941	0.00032	0.25913	0.05012	0.00182	6.28	3.26	7.25	126.4	3.7	123.9	2.0	684.1	635.4	1.08
no06a103	0.13488	0.00334	0.01955	0.00022	0.22294	0.05072	0.00125	4.96	2.21	4.94	128.5	3.0	124.8	1.4	440.6	559.4	0.79
no06a104	0.13272	0.00640	0.02011	0.00052	0.27081	0.04892	0.00235	9.64	5.22	9.63	126.5	5.7	128.3	3.3	53.2	133.0	0.40
no06a70*	0.11116	0.00465	0.01999	0.00040	0.23915	0.04170	0.00203	8.37	4.00	9.74	107.0	4.3	127.6	2.5	88.5	195.6	0.45
no06a78*	0.12202	0.00314	0.01935	0.00035	0.35008	0.04661	0.00124	5.14	3.60	5.34	116.9	2.8	123.6	2.2	94.2	271.8	0.35
no06a81*	0.11138	0.00419	0.01962	0.00044	0.30044	0.04210	0.00186	7.52	4.52	8.82	107.2	3.8	125.2	2.8	207.3	312.0	0.66
no06a84*	0.12489	0.00863	0.01919	0.00047	0.17862	0.04761	0.00332	13.82	4.94	13.93	119.5	7.8	122.5	3.0	91.8	278.1	0.33
no06a101*	0.11298	0.00362	0.01951	0.00030	0.24323	0.04278	0.00135	6.41	3.12	6.31	108.7	3.3	124.5	1.9	92.7	187.2	0.50
no06a102*	0.11752	0.00447	0.01957	0.00034	0.22970	0.04449	0.00177	7.61	3.50	7.94	112.8	4.1	125.0	2.2	124.1	237.0	0.52
no06a105*	0.12246	0.00595	0.01826	0.00041	0.22951	0.04955	0.00246	9.72	4.46	9.92	117.3	5.4	116.6	2.6	493.5	479.6	1.03

Note: samples with (*) were only used for 206Pb/238U mean age (Fig. 11 a)

Appendix B. *Arn U-Pb data.*

Sample Description[1]	Wt (mg) (mg)	U content (ppm)	Pb^2 content (ppm)	$^{206}Pb/^{204}Pb$ (meas.)[3]	total common Pb (pg)	$\%^{208}Pb^2$	$^{206}Pb/^{238}U^4$ (± % 1s)	$^{207}Pb/^{235}U^4$ (± % 1s)	$^{207}Pb/^{206}Pb^4$ (± % 1s)	$^{206}Pb/^{238}U$ age (Ma; ± % 2s)	$^{207}Pb/^{206}Pb$ age (Ma; ± % 2s)
Sample JM-14 (depth 47.6m)											
G1	0.688	11.9	0.21	179	60	0.89	0.01930(0.36)	0.1282(1.27)	0.04817(1.06)	123.3(0.9)	107.8(50.5)
G2	0.324	12.1	0.21	197	26	0.37	0.01929(0.35)	0.1287(1.26)	0.04838(1.07)	123.2(0.9)	118.0(50.6)
Sample JM-28 B (depth 12.5 m)											
G1	0.971	8.7	0.15	256	42	0.58	0.01924(0.31)	0.1284(1.15)	0.04839(0.99)	122.9(0.7)	118.3(46.5)
G2	0.588	20.2	0.35	344	37	0.01	0.01930(0.20)	0.1278(0.68)	0.04802(0.56)	123.2(0.5)	100.5(26.4)
Sample ARN-16											
G1	0.362	299	7.68	512	260	31.7	0.01943(0.17)	0.1304(0.50)	0.04870(0.39)	124.0(0.4)	133.5(18.1)
G2	0.213	87.9	2.27	220	109	32.1	0.01934(0.30)	0.1323(0.98)	0.04960(0.80)	123.5(0.7)	176.1(37.0)
T1	0.123	39.2	0.92	125	30	25.7	0.01937(0.50)	0.1231(1.71)	0.04609(1.43)	123.7(1.2)	2.1(69.1)
T2	0.067	75.5	1.88	182	67	30	0.01927(0.38)	0.1289(1.32)	0.04850(1.10)	123.1(0.9)	123.5(51.3)
Sample JM-16 (depth 45.0 m)											
G1	0.459	12.2	0.23	50.7	221	0.01	0.02089(1.69)	0.1324(6.49)	0.04602(5.52)	133.3(4.5)	-2(268.0)
G2	0.499	11.6	0.21	37.1	394	0.01	0.02065(2.91)	0.1257(10.9)	0.04417(9.18)	131.8(7.6)	-101(466)
T1	0.117	79.9	1.4	300	39	0.47	0.01934(0.23)	0.1289(0.83)	0.04835(0.69)	123.5(0.6)	116.6(32.5)
T2	0.056	69.1	1.24	434	11	0.58	0.01978(1.54)	0.1322(1.70)	0.04847(0.66)	126.3(3.9)	122.4(31.3)
T3	0.252	33.2	0.62	148	81	0.43	0.02052(0.31)	0.1375(1.21)	0.04859(1.02)	131.0(0.8)	127.9(48.2)

[1] G = garnet; T = titanite

[2] radiogenic Pb; corrected for blank, initial common Pb, and spike

[3] corrected for spike and fractionation

[4] corrected for blank Pb and U, and common Pb

Geology and mineral potential of the northwestern Aishihik Lake map area, parts of NTS 115H/12 and 13

Steve Israel[1] and Elizabeth Westberg
Yukon Geological Survey, Whitehorse, YT

Israel, S. and Westberg, E., 2012. Geology and mineral potential of the northwestern Aishihik Lake map area, parts of NTS 115H/12 and 13. *In:* Yukon Exploration and Geology 2011, K.E. MacFarlane and P.J. Sack (eds.), Yukon Geological Survey, p. 103-113.

ABSTRACT

Bedrock geological mapping in the northwestern Aishihik Lake map sheet in the summer of 2011 extended previous 1:50 000 scale geology mapping towards the Nisling River to the north. Mapping identified a complex of Paleocene volcanic and high-level intrusions assigned to the Rhyolite Creek complex, overlying polydeformed schist, quartzite, and gneiss of the Yukon-Tanana terrane. The youngest phase of deformation is characterized by north to northwest striking high-angle faults that are likely, in part, syn-eruption of the Rhyolite Creek complex and likely control some of the deposition of the volcanic rocks. Paleocene intrusions associated with both the Ruby Range batholith and the Rhyolite Creek complex have mutual crosscutting relationships with each other and with overlying volcanic rocks.

The area is most prospective for copper-gold porphyry and epithermal gold mineralization. Samples obtained during 2011 fieldwork returned some anomalous values for sliver, arsenic, mercury, zinc, copper and gold. Mineralization observed during mapping, is structurally controlled along late brittle faults and fractures.

[1] *steve.israel@gov.yk.ca*

INTRODUCTION

Bedrock mapping in the northwestern Aishihik Lake map sheet in 2011continued geological field work begun under the Coast Belt project in the 2010 (Fig. 1). Nearly two 1:50000 scale map sheets (NTS 115H/12 and 13) were completed in the summer of 2011, with the aim of extending new mapping towards the north and east of previous work.

The project area was first described during reconnaissance mapping by Cockfield (1927) and Templeman-Kluit (1974); however, no detailed bedrock mapping has taken place prior to this study. Fieldwork in 2011 overlaps slightly with work completed in 2010 (Israel *et al.*, 2011a,b) and includes some revision to the interpreted geology from that mapping (Israel and Westberg, 2011).

Access to the northwestern Aishihik project area is mainly by helicopter, staged out of a decommissioned airstrip near the old town site of Aishihik (Fig. 1). The project area is characterized by broad, rounded ridges separated by wide, vegetated valleys. Topography generally slopes towards the north and becomes quite gentle near the Nisling River, the northern boundary of the project area.

Figure 1. *Location of 2011 northwestern Aishihik Lake project area, outlined by black box. Fieldwork in 2010 is labeled and outlined. HJ-Haines Junction.*

Outcrop exposure is moderate to poor, with the general trend of becoming poorer to the north. A few, higher, rugged peaks north of Albert Creek offer the best outcrop exposures in the project area.

This paper reports on general lithologic relationships and observed mineralization within the project area. It is intended as companion text for Yukon Geological Survey, Open File 2011-31 (Israel and Westberg, 2011). For a more comprehensive description of regional structure and metallogeny see Israel *et al.* (2011a).

LITHOLOGY

The project area is underlain by Proterozoic to Mississippian schist, marble, and metavolcanic rocks of the Yukon-Tanana terrane, intruded and overlain by the Paleocene Ruby Range batholith and Rhyolite Creek complex, respectively (Figs. 2 and 3). Volcanic and intrusive rocks make up the majority of the high ground in the project area, particularly in the central portion; the metamorphic rocks outcrop in valleys and on lower slopes.

YUKON-TANANA TERRANE

SNOWCAP ASSEMBLAGE

The Snowcap assemblage is abundant north of Albert Creek and is found in less extensive exposures northeast and northwest of Stevens Lake (Fig. 2). It is structurally interleaved with the Finlayson assemblage and intruded and overlain by Paleocene igneous rocks. The Snowcap assemblage, in the project area, is characterized by quartz-muscovite ± garnet schist, beige to white and grey quartzite, and cream-coloured marble. Schist and quartzite make up the majority of the assemblage and are found interlayered with one another on the centimetre to metre-scale (Fig 4a). The schist is psammitic in composition with abundant quartz and shows a strong internal foliation. Quartzite varies from 'dirty' (*i.e.*, some micas and feldspars) to a massive, nearly pure orthoquartzite. Layering in the quartzite is characterized by thin mica-rich zones up to a few millimetres wide. Cream-weathered marble is found locally as thin (less than 2 m) layers within schist and quartzite, and rarely in bands several metres thick. Amphibolite was not observed within the project area but is known to occur within the Snowcap assemblage further south and west (Murphy *et al.*, 2009; Israel *et al.*, 2011a). Rare metaplutonic rocks are found within the Snowcap assemblage, just north of Albert Creek (Fig. 2). These metaplutonic rocks are strongly deformed,

hornblende-biotite- quartz-diorite to granodiorite in composition. The age of the metaplutonic rocks is not well constrained, they are tentatively correlated with the Mississippian Simpson Range suite, found elsewhere in the Yukon-Tanana terrane (Murphy *et al.*, 2006). Alternatively, it is possible that the metaplutonic rocks are Permian in age and correlate with the Sulphur Creek plutonic suite found in the Klondike region (Mortensen, 1990). The age of the Snowcap assemblage is Proterozoic to Devonian based on work elsewhere in the Yukon-Tanana terrane (Colpron *et al.*, 2006).

FINLAYSON ASSEMBLAGE

The Finlayson assemblage outcrops in the southern and northern portions of the project area (Fig. 2). The relationship between the Finlayson assemblage and the underlying Snowcap assemblage is interpreted as a structurally modified unconformity (Murphy *et al.*, 2009). The mapped contacts between the two assemblages reflect this complex relationship and in places it is difficult to determine the true geologic boundary. The Finlayson assemblage in the project area is characterized by carbonaceous quartzite and schist, marble and amphibolite (Fig. 4b). Schists are mainly psammitic in composition with locally abundant interlayered pelitic material. The schist almost ubiquitously weathers a dark grey to black, owing to the high carbon content. Quartzite is fine to medium grained and weathers a dark to light grey. Marble is found as interlayered units within the schist and quartzite, generally on the metre-scale, but can be up to several metres thick. The marble weathers white to light grey. It is massive to banded and shows varying amounts of deformation and recrystallization. Amphibolite is only locally observed, usually in association with the marble. The amphibolite probably represents strongly deformed and metamorphosed basalt or basaltic intrusions. It is fine grained, dark green to black, and locally contains abundant centimetre-scale garnet. The age of the Finlayson assemblage is Upper Devonian to Lower Mississippian (Murphy *et al.*, 2006).

RUBY RANGE BATHOLITH

The Ruby Range batholith, in the current project area, includes intrusive rocks of quartz diorite, tonalite and granodiorite compositions. They are mapped separately from the porphyritic rocks of the Rhyolite Creek complex (see below) but are likely comagmatic with respect to the complex. The Ruby Range batholith rocks are generally equigranular, fine to medium grained and include biotite and/or hornblende (Fig. 4c). Magnetite is a common accessory mineral, making some of the intrusions strongly magnetic in character. Miarolitic cavities are found throughout indicating emplacement at high crustal levels. The age of the batholith is *ca.* 64-57 Ma (Murphy and Israel, *unpublished data*).

RHYOLITE CREEK COMPLEX

The Rhyolite Creek complex is here defined as including Paleocene mafic to felsic volcanic rocks and age equivalent high-level porphyritic intrusions. The complex is named for exposures of volcanic rocks and porphyries found near Rhyolite Creek with preliminary Paleocene (*ca.* 57 Ma) U-Pb zircon ages (Murphy, *unpublished data*). Regionally the complex includes rocks assigned to the Mount Creedon volcanics (Johnston and Timmerman, 1994), rocks south of the Nisling River previously included in the Mount Nansen Group, and varicoloured acid tuffs east of Aishihik Lake described by Tempelman-Kluit (1974). Extensive exposures of the complex occur throughout the study area, with a concentration near the centre of the area (Fig. 2). The Rhyolite Creek complex is comagmatic with the younger phases of the Ruby Range batholith exhibited by mutual crosscutting relationships between the high-level porphyry and the granodiorite to quartz diorite intrusive bodies.

VOLCANIC ROCKS

Volcanic rocks within the Rhyolite Creek complex range in composition from felsic to mafic with the majority being of intermediate composition. Felsic volcanic rocks include rhyolite flows, tuffs, and breccias. Flows are generally light grey, green or maroon, often flow-banded, and variably quartz±feldspar phyric (Fig. 4d). Where flows are quartz phyric, the quartz is smokey grey in colour and up to 2 mm in diameter. Tuffs are aphanitic and banded with smokey quartz phenocrysts. Breccias are characterized by angular clasts of rhyolite flows and tuffs up to several centimetres in width, within a crystal-rich matrix of the same composition. Isolated, small (up to tens of metres) exposures of black to dark grey obsidian are found in several localities where it is spatially associated with larger rhyolitic deposits. The obsidian is often flow-banded and variably devitrified and/or recrystallized.

Volcanic rocks of intermediate composition are spatially the most common within the Rhyolite Creek complex. They consist of dacite to andesite breccias, flows, and dikes (Fig. 4e,f). Breccias vary from pumice fragments up to 2 cm in diameter within a crystal-rich, fine-grained

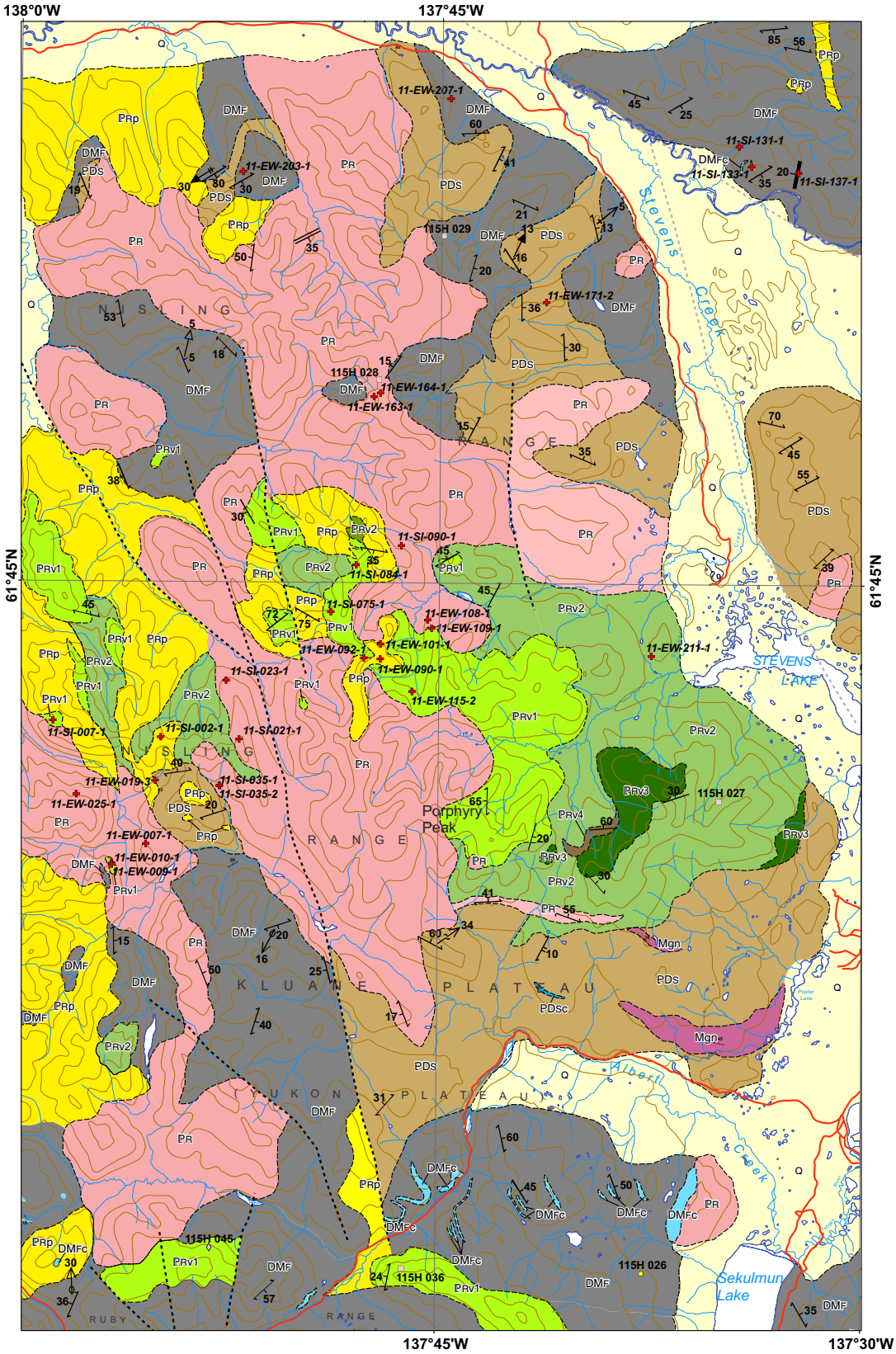

Figure 2. *Preliminary geology map of the northwestern Aishihik Lake area, parts of NTS 115H/12 and 13.*

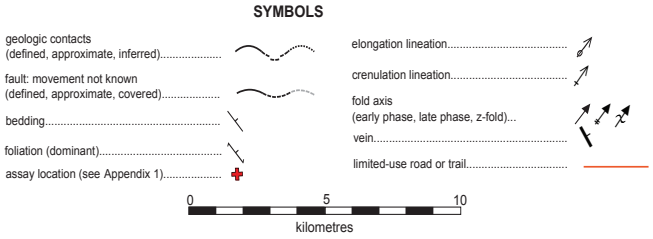

MINFILE Occurrences
(November, 2011)

Number	Name	Deposit Type	Commodity/Status
115H045	AI	Au-Quartz Veins	Au, Ag, Showing
115H036	Bilquist	Porphyry	Cu, Mo/Unknown
115H029	Occident	Porphyry	Cu, Mo/Anomaly
115H028	Canopus	Porphyry	Cu, Mo/Anomaly
115H027	Poplar	Porphyry	Mo, Zn/Anomaly
115H026	Thatch	Skarn	Au, Ag, Cu/Drilled prospect

Figure 2 con'd.

matrix to boulder-sized clasts of porphyritic andesite within a fine to medium-grained crystal-rich matrix. Compositionally the breccias do not vary too much, appearing to be dacitic to andesitic. Colour changes do occur within the clasts themselves and the matrix, mainly from greenish grey to maroon. The breccias represent both pyroclastic and autoclastic deposits, likely formed near a volcanic centre. Intermediate flows are only locally preserved and are dominated by dacitic flow banded, plagioclase ± quartz-phyric flows or plagioclase ± hornblende-phyric andesite. It is difficult to separate out plagioclase porphyry dikes of andesitic composition from the flows, mainly because of the lack of exposure and the similarity between the two rock types. Where dikes can be observed, they are generally one to two metres in width, nearly vertical and crosscut the breccia deposits.

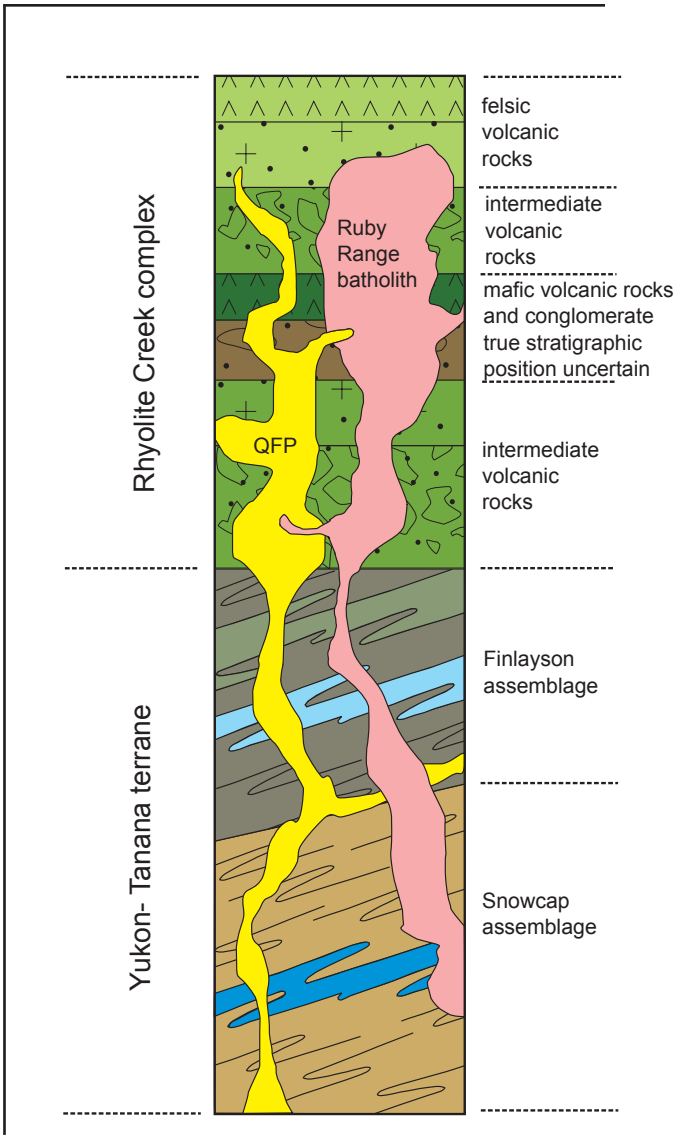

Figure 3. *Generalized stratigraphic column for the northwestern Aishihik Lake area. QFP-quartz-feldspar porphyry of the Rhyolite Creek complex.*

Figure 4. *Photographs of lithologic units from the northwestern Aishihik Lake area:* ***(a)*** *interlayered quartzite and psammitic schist typical of the Snowcap assemblage;* ***(b)*** *structurally interleaved marble, carbonaceous schist and amphibolite of the Finlayson assemblage;* ***(c)*** *massive, equigranular granodiorite to tonalite of the Ruby Range batholith;* ***(d)*** *flow-banded rhyolite of Rhyolite Creek complex.*

Mafic volcanic rocks are the least represented in the study area and are restricted to outcrops east of Porphyry Peak in the central part of the map sheet (Fig. 2). They are characterized by massive, brown weathered pyroxene-phyric basalt (Fig. 4g). Pyroxenes are up to 1 mm wide, black, and make up to 2-3% of the rock. Devitrified glassy black fragments are found throughout the basalt and can be up to 2-3 mm in length. The basalt is moderately to strongly magnetic.

Spatially associated with the basalt is a package of conglomerate/breccia up to several metres thick. Outcrops of the conglomerate/breccia are restricted to an area just west of Porphyry Peak where it overlies and is interlayered with the basalt. The unit is characterized by angular to rounded clasts of all compositions of volcanic rocks as well as metamorphic rocks from the underlying Yukon-Tanana terrane. Clasts range in size from less than one centimetre up to one metre across. The largest clasts appear to be of basalt.

INTRUSIVE ROCKS

Intrusive rocks of the Rhyolite Creek complex include distinctive quartz-feldspar porphyry that outcrops throughout the project area, but is concentrated in the western portions (Fig. 2). The porphyry occurs as both large intrusive bodies and smaller, metre-scale dikes. It intrudes into and is overlain by the volcanic rocks and has mutual crosscutting relationships with the Ruby Range batholith rocks. In the most common form, the porphyry is orange to beige weathering, beige on fresh surfaces, with smokey grey quartz and creamy white feldspar phenocrysts up to 3 mm in length in a fine-grained matrix

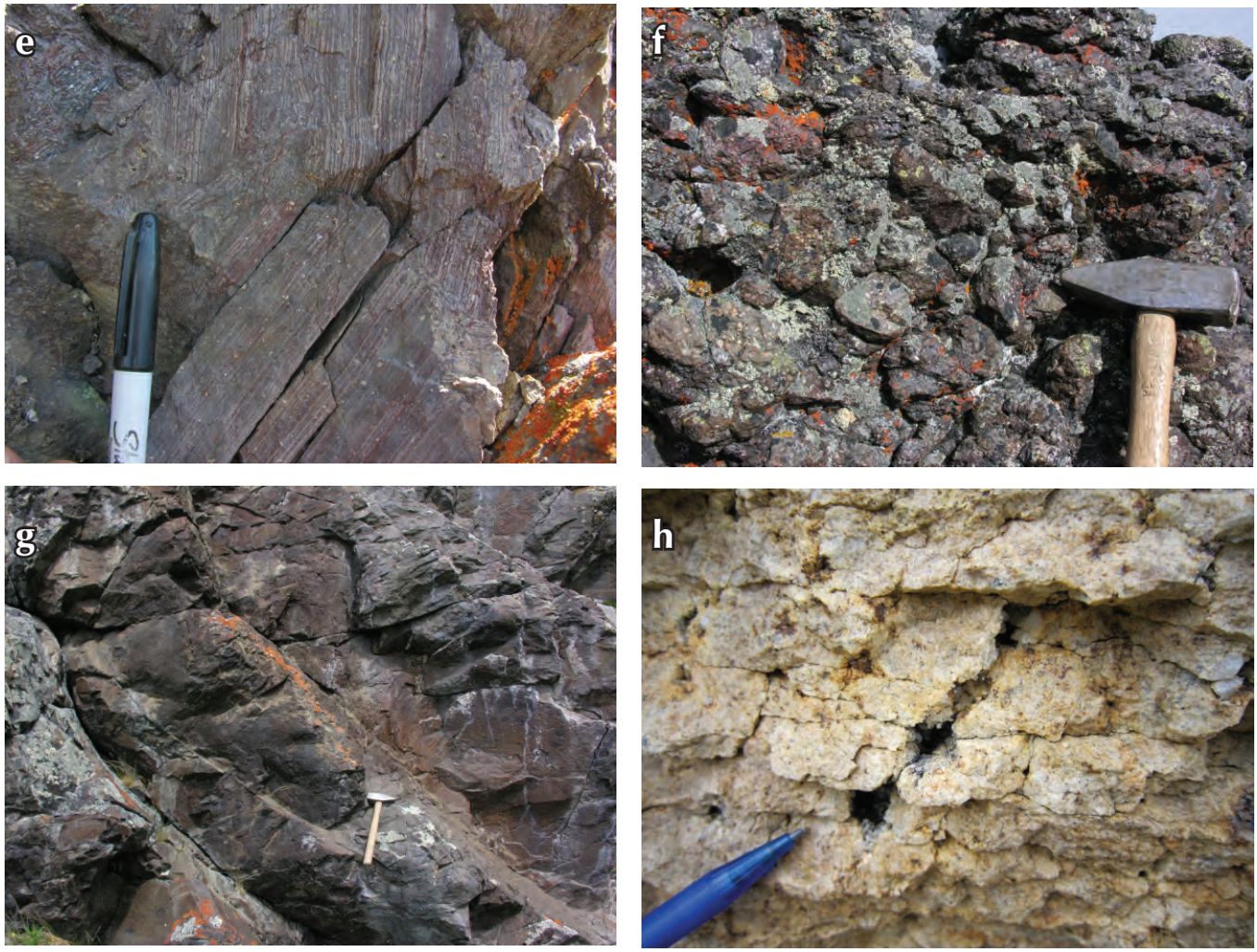

Figure 4 con'd. ***(e)*** *plagioclase and quartz phyric, flow-banded dacite of the Rhyolite Creek complex;* ***(f)*** *andesite breccia of the Rhyolite Creek complex;* ***(g)*** *massive, pyroxene-phyric basalt of the Rhyolite Creek complex;* ***(h)*** *miarolitic cavity within quartz-feldspar porphyry of the Rhyolite Creek complex.*

of quartz and feldspar. Locally the feldspar phenocrysts are up to 1 cm in length and the abundance of quartz decreases to near absence. In other places the porphyry is almost aphanitic with only a slight increase in size of feldspar and quartz crystals from the matrix. Miarolitic cavities are found throughout the intrusive bodies, and occur as open spaces up to 1-2 cm in length with quartz crystals formed along the edges of the openings (Fig. 4h). The mutual crosscutting nature of the porphyry with the Ruby Range batholith and the overlying volcanic rocks suggests the age of the porphyry is likely *ca.* 57 Ma.

MINERAL POTENTIAL

Mineral potential in the project area is likely related to either porphyry or epithermal deposit types. The general lithologic relationships observed in the northwestern Aishihik Lake area suggests that intrusive rocks of both the Ruby Range batholith and the Rhyolite Creek complex were intruded at high crustal levels, within the top few kilometres to near surface. This is the geologic setting where porphyry and epithermal mineralization would be expected. Porphyry occurrences do occur in the uppermost portion of the Ruby Range batholith, elsewhere in the region. No large alteration systems were identified during the mapping program; however, structurally controlled alteration and mineralization was observed, characterized by zones of weathered sulphides within brittle shear zones (Fig. 5a-d). Some large quartz veins were found in the northeastern portion of the map area; however, the depth at which these formed and their regional structural context is not yet known. Values for standard assays of rock samples taken throughout the project area, including anomalous arsenic, mercury, lead,

zinc, silver and minor gold in a few of the samples are provided in Appendix A (see Fig. 2 for sample locations).

DISCUSSION

The northwestern Aishihik Lake map area is characterized by Proterozoic to Mississippian metamorphosed basement rock, overlain by Paleocene volcanic and intrusive rocks. The lithologic relationships suggest that the area is likely the site of a Paleocene volcanic centre. Some of the north to northwest-striking structures observed in the field (Fig. 2) are likely syn-volcanic faults. The distribution of volcanic and intrusive rocks suggest a central zone of felsic material, likely defining rhyolite domes, flanked by more intermediate pyroclastic and autoclastic deposits (Fig. 6). The restricted distribution of the basalt may, in part, be related to an association with a fault off the side of the main volcanic axis that allowed the last gasp (volumetrically small) of volcanic material to flow out of the magma chamber. The central portion of the volcanic complex was intruded by its own magma chamber, likely near the end of the eruptive cycle.

Mineralization associated with volcanic centres can include porphyry and epithermal styles (Fig. 6). The main porphyry occurrences may be somewhat deeper in the system in the project area, and may outcrop lower in the valleys rather than up on ridges. The strong structural control on mineralization observed in the project area, may indicate epithermal systems associated with syn-volcanic structures were active during eruption.

Figure 5. *Structurally controlled mineralization within the northwestern Aishihik Lake area:* ***(a)*** *limonitic alteration of volcanic rocks of the Rhyolite Creek complex, 11-SI-084-1;* ***(b)*** *rusty weathered and fractured quartz-feldspar porphyry of the Rhyolite Creek complex, 11-SI-005-1;* ***(c)*** *weathered sulphides within fracture cutting through felsic volcanic rocks of the Rhyolite Creek complex, 11-SI-007-1;* ***(d)*** *quartz vein within carbonaceous schist of the Finlayson assemblage, 11-SI-137-1. See Figure 2 for sample location and Appendix 1 for assay values.*

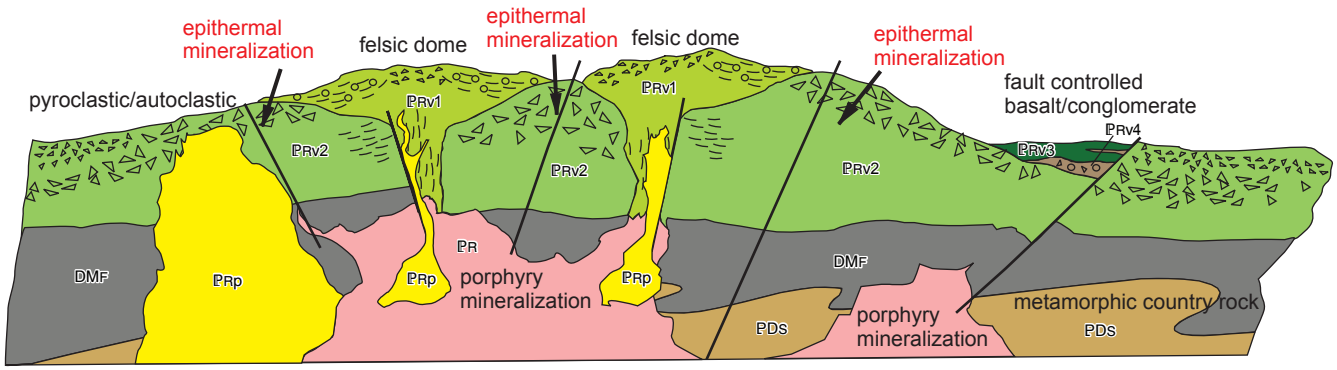

Figure 6. *Conceptual diagram illustrating the depositional setting for the Rhyolite Creek complex and location for possible related mineralization (labels same as Figure 2, for rock descriptions see Figure 2 legend).*

REFERENCES

Cockfield, W.E., 1927. Aishihik Lake District, Yukon. Geological Survey of Canada, Summary Report, 1926, part A, 1-13 p.

Colpron, M., Nelson, J.L., and Murphy, D.C., 2006. A tectonostratigraphic framework for the pericratonic terranes of the northern Cordillera. *In:* Paleozoic Evolution and Metallogeny of Pericratonic Terranes at the Ancient Pacific Margin of North America, Canadian and Alaskan Cordillera, M. Colpron and J.L. Nelson (eds.), Geological Association of Canada, Special Paper 45, p. 1-23.

Israel, S., Murphy, D.C., Bennett, V., Mortensen, J.K., and Crowley, J., 2011a. New insights into the geology and mineral potential of the Coast Belt in southwestern Yukon. *In:* Yukon Exploration and Geology, K.E. MacFarlane, L.H. Weston and C. Relf (eds.), Yukon Geological Survey, p. 101-123.

Israel, S., Cobbett, R., Westberg, E., Stanley, B. and Hayward, N., 2011b. Preliminary bedrock geology of the Ruby Ranges, southwest Yukon (Parts of NTS 115G, 115H, 115A and 115B) (1:150 000-scale). Yukon Geological Survey, Open File 2011-2.

Israel, S. and Westberg, E., 2011. Preliminary geological map of the northwestern Aishihik Lake area, parts of NTS 115H/12 and 13 (1:50 000-scale). Yukon Geological Survey Open File 2011-31.

Johnston, S.T. and Timmerman, J.R., 1994. Geology of the Aishihik Lake and Hopkins Lake map areas (115H6/7), southwestern Yukon. *In:* Yukon Exploration and Geology 1993, S.R. Morison (ed.), Indian and Northern Affairs Canada, Exploration and Geological Services Division, p. 93-110.

Mortensen, J.K., 1990. Geology and U-Pb geochronology of the Klondike District, west-central Yukon Territory. Canadian Journal of Earth Sciences, vol. 27, no. 7, p. 903-914.

Murphy, D.C., Mortensen, J.K. and van Staal, C.R., 2009. 'Windy-McKinley' terrane, western Yukon: new data bearing on its composition, age, correlation and paleotectonic settings. *In:* Yukon Exploration and Geology, L.H. Weston, L.R. Blackburn and L.L. Lewis (eds.), Yukon Geological Survey, p. 195-209.

Murphy, D.C., Mortensen, J.K., Piercey, S.J., Orchard, M.J. and Gehrels, G.E., 2006. Mid-Paleozoic to early Mesozoic tectonostratigraphic evolution of Yukon-Tanana and Slide Mountain terranes and affiliated overlap assemblages, Finlayson Lake massive sulphide district, southeastern Yukon. *In:* Paleozoic Evolution and Metallogeny of Pericratonic Terranes at the Ancient Pacific Margin of North America, Canadian and Alaskan Cordillera, M. Colpron and J.L. Nelson (eds.), Geological Association of Canada, Special Paper 45, p. 75-105.

Tempelman-Kluit, D.J., 1974. Reconnaissance geology of Aishihik Lake, Snag and part of Stewart River map areas, west-central Yukon. Geological Survey of Canada, Paper 73-21.

Appendix A. *Table of assay values.*

Sample	UTMNorth	UTMEast	Mo	Cu	Pb	Zn	Ag	Ni	Co	Mn	Fe	As	U	Au	Th	Sr	Cd	Sb	Bi
			ppm	ppm	ppm	ppm	ppb	ppm	ppm	ppm	%	ppm	ppm	ppb	ppm	ppm	ppm	ppm	ppm
11-EW-002-1	630825	6790218	1.55	86.89	15.44	90.0	188	57.4	23.4	720	4.26	15.6	1.0	0.8	3.3	56.9	0.12	0.14	0.11
11-EW-007-1	345358	6841628	3.73	3.93	11.73	50.3	47	0.5	0.2	30	0.58	0.5	4.8	<0.2	24.4	1.1	0.22	0.07	0.05
11-EW-009-1	344268	6841051	3.66	5.22	9.63	30.5	216	1.1	0.6	112	1.70	0.2	2.3	<0.2	12.6	6.5	0.15	0.15	0.26
11-EW-010-1	344267	6841015	2.84	7.10	6.60	38.1	149	0.4	0.4	377	1.83	0.1	1.8	<0.2	13.2	9.4	0.26	0.09	0.14
11-EW-019-3	345717	6843592	1.33	18.91	5.88	104.6	80	3.2	19.0	1284	5.72	2.4	0.5	<0.2	3.2	226.2	0.21	0.15	0.02
11-EW-023-1	343228	6342797	2.01	3.24	10.81	77.1	118	0.3	0.1	70	0.64	0.7	4.1	<0.2	17.9	1.1	0.10	0.09	0.07
11-EW-025-1	343239	6843257	0.46	1.06	15.22	29.7	28	0.7	0.5	95	0.79	0.1	1.9	<0.2	10.2	7.3	0.05	0.03	0.02
11-EW-090-1	352888	6847132	1.58	2.72	6.44	75.9	48	0.2	0.3	253	1.27	0.3	6.4	<0.2	21.5	2.6	0.18	0.03	0.47
11-EW-092-1	352370	6847180	0.32	2.82	22.90	57.4	97	0.1	0.1	39	0.73	3.1	5.5	<0.2	11.6	6.1	0.10	0.06	0.23
11-EW-101-1	352911	6847600	0.26	2.35	2.65	28.4	47	0.3	0.2	115	0.63	0.2	0.5	<0.2	1.7	2.9	0.12	<0.02	0.02
11-EW-108-1	354409	6848297	3.01	2.68	8.72	23.6	66	0.6	0.2	107	1.36	3.1	2.7	<0.2	12.2	1.8	0.03	0.21	0.06
11-EW-109-1	354522	6848028	0.98	21.49	6.84	108.3	93	38.9	17.7	552	4.09	0.7	1.4	<0.2	3.8	61.5	0.28	0.12	0.05
11-EW-115-2	353840	6846080	4.55	2.48	4.68	53.6	105	0.8	0.3	29	0.96	1.7	1.5	0.6	9.1	1.6	0.15	0.29	1.14
11-EW-163-1	352983	6855332	0.45	8.14	9.00	64.4	41	0.7	0.4	54	1.98	24.3	1.5	<0.2	13.5	5.4	0.09	0.36	0.22
11-EW-164-1	353185	6855438	0.79	7.08	1.77	2.3	87	2.8	0.7	24	0.45	20.4	0.3	2.2	0.1	1.5	<0.01	0.23	0.74
11-EW-171-2	358472	6858077	1.41	22.93	12.63	13.8	117	3.3	2.6	91	1.55	6.2	1.7	<0.2	6.1	38.0	0.05	2.08	0.15
11-EW-203-1	349142	6862505	0.27	38.13	3.94	1.6	128	1.6	0.5	41	1.15	139.1	0.3	6.4	2.5	9.9	0.05	1.25	0.30
11-EW-207-1	355713	6864552	1.21	28.21	6.86	11.3	624	2.6	0.9	154	1.01	1.5	2.7	<0.2	2.5	24.5	0.05	4.83	0.10
11-EW-211-1	361355	6846915	0.56	19.99	4.55	89.5	86	12.6	22.1	683	4.84	4.7	0.4	0.9	2.2	167.9	0.22	0.93	<0.02
11-SI-002-1	345945	6844943	0.24	1.32	11.47	63.1	56	0.7	0.3	82	0.64	0.4	3.2	<0.2	17.5	4.7	0.09	0.05	0.11
11-SI-005-1	343051	6345052	8.51	15.72	12.34	126.7	166	0.4	0.3	42	0.95	24.0	8.5	<0.2	17.9	3.2	0.16	0.30	0.39
11-SI-007-1	342595	6845586	8.68	142.24	4.26	119.8	320	47.1	19.0	263	4.54	2.6	1.8	0.4	1.7	155.2	0.54	0.51	0.10
11-SI-021-1	348385	6844785	1.35	3.22	11.20	91.0	70	0.5	0.2	98	1.02	0.9	2.6	<0.2	17.0	1.9	0.10	0.07	0.32
11-SI-023-1	348050	6846639	2.00	3.03	11.49	71.0	105	1.0	0.4	373	0.94	0.4	6.2	1.5	23.4	2.5	0.85	0.05	0.06
11-SI-035-2	347721	6843356	3.31	5.36	16.07	79.0	226	1.5	3.6	318	1.83	7.5	5.0	<0.2	17.1	7.9	0.78	0.37	0.27
11-SI-035-1	347721	6843356	2.54	15.14	20.43	23.2	234	0.9	0.3	40	0.75	111.7	2.7	1.8	15.6	4.1	1.07	0.21	0.83
11-SI-075-1	351394	6848660	5.29	2.81	4.22	60.6	146	0.4	0.1	160	0.66	84.8	6.4	<0.2	18.7	3.0	0.09	0.59	1.46
11-SI-084-1	352234	6850102	18.68	15.18	15.72	40.4	197	12.3	10.4	414	3.31	436.4	2.2	1.5	4.8	22.6	0.11	1.82	0.09
11-SI-090-1	353670	6850647	0.76	9.86	10.49	71.2	23	2.5	2.0	90	1.37	1.6	2.7	<0.2	16.8	7.6	0.06	0.07	0.08
11-SI-131-1	364662	6862732	0.90	13.70	1.99	15.4	237	13.2	4.4	60	0.75	2.8	0.7	0.6	2.4	19.4	0.10	0.07	0.03
11-SI-133-1	365025	6862091	0.43	30.81	0.89	44.2	131	7.1	1.2	170	3.59	1.6	0.9	0.3	0.4	4.1	0.03	0.37	<0.02
11-SI-137-1	366480	6861837	0.42	9.61	0.41	1.6	46	2.9	0.6	28	0.27	1.3	<0.1	0.4	<0.1	<0.5	<0.01	0.41	<0.02

Note: coordinates are NAD 83 UTM Zone 8

Appendix A con'd

Sample	V	Ca	P	La	Cr	Mg	Ba	Ti	B	Al	Na	K	W	Sc	Tl	S	Hg	Se	Te	Ga
	ppm	%	%	ppm	ppm	%	ppm	%	ppm	%	%	%	ppm	ppm	ppm	%	ppb	ppm	ppm	ppm
11-EW-002-1	67	1.28	0.113	5.7	88.2	1.86	90.6	0.013	1	2.58	0.008	0.14	<0.1	4.8	<0.02	0.03	<5	0.8	0.05	6.5
11-EW-007-1	<2	0.07	0.001	16.9	4.2	<0.01	40.0	0.003	<1	0.22	0.048	0.11	0.4	0.3	0.05	<0.02	<5	0.2	<0.02	1.8
11-EW-009-1	<2	0.18	0.012	29.5	6.2	0.03	131.1	0.084	<1	0.33	0.064	0.11	0.4	3.3	0.06	0.13	<5	1.2	0.08	4.1
11-EW-010-1	<2	0.50	0.010	47.4	3.5	0.07	161.0	0.125	<1	0.31	0.106	0.15	0.7	5.3	0.03	<0.02	<5	0.2	0.09	3.3
11-EW-019-3	90	4.65	0.210	22.8	14.7	0.90	168.5	0.061	<1	3.59	0.438	0.22	<0.1	16.3	0.12	0.08	7	0.3	0.03	9.7
11-EW-023-1	<2	0.03	0.001	29.0	2.6	<0.01	29.8	0.036	<1	0.21	0.055	0.12	0.8	0.4	0.08	<0.02	<5	0.2	<0.02	2.9
11-EW-025-1	<2	0.09	0.016	34.5	2.7	0.02	156.7	<0.001	<1	0.32	0.049	0.19	<0.1	1.2	0.05	<0.02	<5	0.1	<0.02	1.7
11-EW-090-1	<2	0.17	0.005	44.8	1.8	0.03	32.1	0.026	<1	0.56	0.056	0.18	<0.1	2.5	0.09	<0.02	<5	0.2	<0.02	5.1
11-EW-092-1	<2	0.93	0.001	44.0	0.9	<0.01	12.9	0.020	<1	1.03	1.231	0.22	<0.1	1.1	0.08	<0.02	<5	<0.1	<0.02	5.7
11-EW-101-1	<2	0.11	0.004	9.0	1.0	0.01	33.1	0.016	<1	0.15	0.445	0.19	<0.1	0.5	0.04	<0.02	<5	<0.1	<0.02	0.9
11-EW-108-1	<2	0.01	0.003	5.2	2.4	<0.01	23.3	0.025	<1	0.32	0.071	0.17	<0.1	0.4	0.04	<0.02	<5	<0.1	<0.02	1.8
11-EW-109-1	69	1.24	0.256	37.6	67.5	1.38	91.7	0.230	<1	1.63	0.158	0.17	0.2	4.0	<0.02	<0.02	<5	0.2	<0.02	6.7
11-EW-115-2	<2	0.02	0.002	25.9	3.2	<0.01	22.2	0.007	<1	0.24	0.035	0.19	0.2	0.2	0.10	0.62	13	0.1	<0.02	1.4
11-EW-163-1	<2	0.06	0.006	2.4	2.8	0.03	50.7	0.002	<1	0.39	0.058	0.08	0.4	1.1	0.03	<0.02	<5	0.5	<0.02	3.4
11-EW-164-1	<2	<0.01	0.008	<0.5	19.8	<0.01	46.3	<0.001	<1	0.02	0.002	<0.01	<0.1	0.1	<0.02	<0.02	<5	0.6	0.07	0.3
11-EW-171-2	39	0.33	0.083	14.9	14.2	0.43	71.9	0.109	<1	1.45	0.079	0.08	0.3	2.6	0.03	0.04	<5	0.2	0.05	6.4
11-EW-203-1	7	<0.01	0.008	9.6	13.5	<0.01	208.7	0.004	<1	0.17	0.002	0.06	0.1	0.8	0.06	<0.02	11	0.7	0.21	1.9
11-EW-207-1	100	0.18	0.227	11.2	37.4	0.35	1442.7	0.014	<1	0.68	0.006	0.30	0.1	1.7	0.14	0.13	7	5.1	0.07	3.4
11-EW-211-1	71	3.17	0.159	18.2	46.7	2.22	254.9	0.171	<1	3.78	0.295	0.10	0.1	8.0	0.03	<0.02	<5	0.2	<0.02	10.1
11-SI-002-1	<2	0.08	<0.001	11.3	2.5	0.01	18.8	0.003	<1	0.48	0.035	0.26	<0.1	0.2	0.12	<0.02	<5	0.2	<0.02	4.0
11-SI-005-1	<2	0.04	0.005	43.9	2.6	0.02	44.9	0.010	<1	0.58	0.058	0.11	0.1	2.2	0.07	<0.02	<5	0.5	0.02	4.8
11-SI-007-1	225	1.17	0.107	5.2	36.2	1.28	103.7	0.058	1	3.80	0.159	0.61	<0.1	10.1	0.67	0.98	<5	9.6	0.09	9.8
11-SI-021-1	<2	0.02	0.001	18.2	2.3	<0.01	39.9	0.030	<1	0.33	0.053	0.13	0.9	0.5	0.15	<0.02	<5	0.2	<0.02	3.6
11-SI-023-1	<2	0.07	0.001	16.4	4.3	<0.01	39.3	0.003	<1	0.40	0.039	0.14	0.4	0.4	0.06	<0.02	<5	0.3	<0.02	2.4
11-SI-035-2	12	0.13	0.038	40.6	6.5	0.19	120.9	0.041	<1	0.74	0.052	0.12	0.2	3.7	0.10	0.31	<5	0.3	<0.02	5.8
11-SI-035-1	<2	0.01	0.003	20.3	4.6	<0.01	43.3	<0.001	<1	0.17	0.068	0.15	0.1	0.6	0.06	0.19	<5	0.4	<0.02	1.1
11-SI-075-1	<2	0.04	<0.001	13.0	8.0	0.01	21.3	0.019	<1	0.45	0.054	0.20	0.3	0.5	0.20	<0.02	<5	0.2	<0.02	4.6
11-SI-084-1	65	0.69	0.131	24.5	34.2	0.45	112.1	0.003	<1	1.03	0.055	0.16	<0.1	3.5	0.38	0.54	3328	0.1	<0.02	5.9
11-SI-090-1	<2	0.03	0.003	16.1	1.4	0.02	62.1	0.014	<1	0.68	0.066	0.14	0.3	1.0	0.06	<0.02	12	0.2	<0.02	6.2
11-SI-131-1	7	0.45	0.021	7.7	14.0	0.14	51.4	0.041	1	0.56	0.013	0.05	0.2	0.8	<0.02	<0.02	23	0.4	0.04	1.9
11-SI-133-1	11	<0.01	0.032	2.3	14.1	<0.01	19.8	<0.001	<1	0.03	0.003	0.03	<0.1	0.2	<0.02	0.06	<5	1.0	<0.02	0.2
11-SI-137-1	<2	<0.01	<0.001	<0.5	19.4	<0.01	9.3	<0.001	<1	0.01	<0.001	<0.01	<0.1	<0.1	<0.02	<0.02	<5	<0.1	0.02	0.1

Note: coordinates are NAD 83 UTM Zone 8

Contrasting structural settings of mafic and ultramafic rocks in the Yukon-Tanana terrane

Doug MacKenzie[1] and Dave Craw
Geology Department, University of Otago, Dunedin, New Zealand

MacKenzie, D. and Craw, D., 2012. Contrasting structural settings of mafic and ultramafic rocks in the Yukon-Tanana terrane. *In:* Yukon Exploration and Geology 2011, K.E. MacFarlane and P.J. Sack (eds.), Yukon Geological Survey, p. 115-127.

ABSTRACT

Four different suites of mafic and ultramafic rocks occur in the Yukon-Tanana terrane between the Klondike goldfield and Stewart River area. Greenschist facies chloritic schist of mafic to intermediate composition is interlayered with quartzofeldspathic schist in the Klondike Schist. Amphibolite facies mafic gneisses, a major component of basement between Indian River and Stewart River, were emplaced with granitoids during Paleozoic metamorphism as gabbro and pyroxenite intrusions. These greenschist and amphibolite facies gneisses were subsequently sliced into kilometre-thick slabs and stacked by Jurassic thrust faults. This thrust stacking was accompanied by emplacement of discontinuous slices (~100 m thick) of variably serpentinized harzburgites and associated mafic and ultramafic rocks. The thrust stacking occurred under greenschist facies conditions and formed regionally continuous retrogressive shear zones in the amphibolite facies basement. Pyroxenite plutons with little or no deformation or alteration were emplaced in association with Mesozoic granitoids. Recognition of these different mafic/ultramafic rocks facilitates regional mapping.

[1] *doug.mackenzie@otago.ac.nz*

INTRODUCTION

The western Yukon region, from the Klondike goldfield to the Stewart River area, is currently the focus of intense exploration activity. This modern day gold rush is the result of recent discoveries of gold-bearing hydrothermal systems hosted in local metamorphic basement lithologies. Despite much of the regional geology having been mapped at 1:50 000 scale (Mortensen, 1996; Ryan and Gordey, 2001, 2004; Gordey and Ryan, 2005), the structural setting and inter-relationships among the different basement lithologies are still being unravelled (*e.g.*, Berman *et al.*, 2007; MacKenzie *et al.*, 2008a,b, 2010; MacKenzie and Craw, 2010); of particular difficulty are the various mafic and ultramafic rocks.

Pyroxenites and gabbros in the White River area were originally mapped as Jurassic intrusive rocks, similar to those at Pyroxene Mountain that were controlled by Jurassic D_3 structures (MacKenzie and Craw, 2010). However, the White River pyroxenites generally have incipient amphibolite facies foliations on their margins (MacKenzie and Craw, 2010), and are now thought to be part of the Paleozoic basement on the basis of mapping during the 2011 field season in the Black Hills Creek and Barker Creek areas. This incipient foliation is related to the metamorphic D_2 event and is referred to herein as late metamorphic foliation (Table 1). Recognition of relict primary metagabbro and pyroxenite mineralogy and textures in the mafic orthogneisses in the Paleozoic basement distinguishes these from the greenschist facies Jurassic D_3 shear zones. These Jurassic shear zones can also contain tectonically emplaced ultramafic rocks of the Slide Mountain terrane, which further complicates the interpretation of ultramafic rocks in the area.

Table 1. *Summary of the principal geological events affecting mafic and ultramafic rocks (in bold type) in the Yukon-Tanana terrane (modified after MacKenzie et al., 2008a; 2010).*

Age	Unit or event	Structural elements	Tectonics	Associated intrusions	Metamorphism	Gold
Pliocene-Recent	White Channel and modern gravels		Regional uplift and erosion			Placer
Eocene		Faults	Regional extension	Dykes	Hydrothermal alteration	?
Late Cretaceous	Carmacks Gp/ andesitic volcanism	Faults			Hydrothermal alteration	Epithermal
Middle Cretaceous	Indian River/fluvial	Faults		Ignimbrites and feeders	Hydrothermal alteration?	Epithermal, paleoplacer?
Jurassic-Cretaceous?	White River, Klondike Au mineralisation	F_4 folds & fractures; N & W trending faults	Collision	?	Hydrothermal alteration	Orogenic veins; disseminated Au with sulphides
Jurassic	Slide Mountain Terrane/ collision and thrusting	**Serpentinite emplacement,** D_3, phacoidal cleavage, local S_3 shear fabric	Thrust stacking	**Pyroxenite,** granitoid plutons;	Localized greenschist facies	
Permian	Late metamorphic deformation	Local late metamorphic foliation (D_2 continuation)	Assembly, Yukon-Tanana & Slide Mountain terranes	**Gabbro & pyroxenite;** granitoids	Greenschist facies (Klondike); amphibolite facies (Indian River-Stewart River)	
Mid-late Paleozoic	Metamorphic deformation	Pervasive S_1 & S_2 foliations		**Gabbro & pyroxenite;** granitoids		
Early Paleozoic?	**Mafic tuffaceous sediments,** quartzofeldspathic sediments, quartzite, marble	Bedding (S_0)		Minor **gabbro**		

Airborne magnetic maps (*e.g.*, Shives *et al.*, 2002a,b) have proven useful for delineating the mafic and ultramafic lithologies on the ground and our new interpretations are based on the combination of this geophysical data and our on-going structural mapping between the Klondike goldfield and the Stewart River area (Figs. 1 and 2). We recognize four different types of mafic and ultramafic rocks in the area, in different structural settings. Our focus in the 2011 summer field season was on basement structure and the four types of mafic and ultramafic rocks near Stewart River, as part of gold exploration in the vicinity of White River prospects (*e.g.*, MacKenzie *et al.*, 2010; Wainwright *et al.*, 2011). Herein we link the new results from the Stewart River area with our previous work (MacKenzie *et al.*, 2007, 2008a,b) in the White River area and the Klondike goldfield.

REGIONAL GEOLOGY

The metamorphic basement rocks in the Klondike goldfield-Stewart River area form part of the Yukon-Tanana terrane and consist primarily of pervasively foliated and recrystallized schists and gneisses that were deformed and metamorphosed during the Paleozoic, ending with the Klondike Orogeny in the Late Permian (Mortensen, 1992,1996; Mortensen *et al.*, 2007; Berman *et al.*, 2007; Beranek and Mortensen, 2011). Metamorphic grades of these basement rocks range from greenschist facies in the Klondike area to amphibolite facies in the Stewart and White River areas. Three generations of premetamorphic and synmetamorphic granitoids were intruded into gneisses in the Stewart River area in the Devonian, Mississippian, and Permian (Ruks *et al.*, 2006), and synmetamorphic plutonism occurred in the Klondike area in the Permian (Mortensen, 1990, 1996). Granitoids and host schists and gneisses have seen development of at least two metamorphic foliations, the second of which (S_2; Table 1) dominates at most outcrops. The basement rocks were locally redeformed during Jurassic thrust stacking, resulting in the development of narrow shear zones (D_3; Table 1).

As the metamorphic pile was exhumed in the Jurassic and Cretaceous, regional compression (F_4) gave way to regional extension and the region was cut by a set of north and west trending high angle normal faults (Table 1). Extension continued through the Late Cretaceous to the Eocene, when transcurrent displacement along the Tintina fault was initiated (Fig. 1; Gabrielse *et al.*, 2006). The emplacement of Cretaceous to Paleogene igneous rocks is controlled by this phase of extension and associated normal faults (Gabrielse *et al.*, 2006; Mortensen, 1996).

MAFIC AND ULTRAMAFIC ROCKS

CHLORITIC KLONDIKE SCHIST

The central and southern portion of the Klondike goldfield is underlain by medium to dark green chloritic schist, which is mineralogically distinct from other, nearby, Klondike Schist lithologies (Figs. 1 and 3). The schist has mafic to intermediate composition with the greenschist facies mineral assemblage quartz-actinolite-chlorite±epidote (Figs. 1 and 3; Mortensen, 1990, 1996). The chloritic schist is pervasively foliated (S_1+S_2) and this foliation, as well as the thrust contact at the base of the unit dip shallowly west to southwest (Fig. 1). There are gradational and interlaminated contacts between chloritic schist and adjacent micaceous and quartzose metasedimentary schists. There is also a close spatial association between chloritic schist and small bodies of well foliated medium-grained metagabbro. The overall composition, volcanic textures and morphology of the chloritic schist suggest derivation from intermediate to mafic igneous rocks (Mortensen, 1990), possibly as tuffaceous or volcanogenic sediments.

METAGABBROS AND METAPYROXENITES

Much of the basement schist and gneiss in the Yukon-Tanana terrane occurs as interlayered quartzite, micaceous schists, and minor marble derived from Paleozoic clastic sedimentary rocks. These metasedimentary gneisses are interlayered with metamorphosed granitoid orthogneisses, especially in the Stewart River area (Figs. 1 and 2). In addition, the metasedimentary and granitoid orthogneiss sequence was intruded by synmetamorphic mafic igneous rocks that are now variably foliated metagabbros and metapyroxenites (Figs. 1 and 2; Mortensen, 1990). All these gneisses are interlayered on the 1 to 1000 m scale. Most of the metagabbros and metapyroxenites have, with their host gneisses, a well developed foliation that is a composite of a first penetrative foliation (S_1) and an overprinting second foliation (S_2). Many of the amphibolite facies metagabbros and metapyroxenites in the Stewart River area have late metamorphic ductile folds of S_2, with a local, weakly developed, late metamorphic axial planar parallel cleavage (Fig. 4). This phase of late metamorphic ductile folding is an extension of D_2 deformation in these amphibolite facies rocks (Table 1), and is not recognizable in lower grade (greenschist facies) rocks.

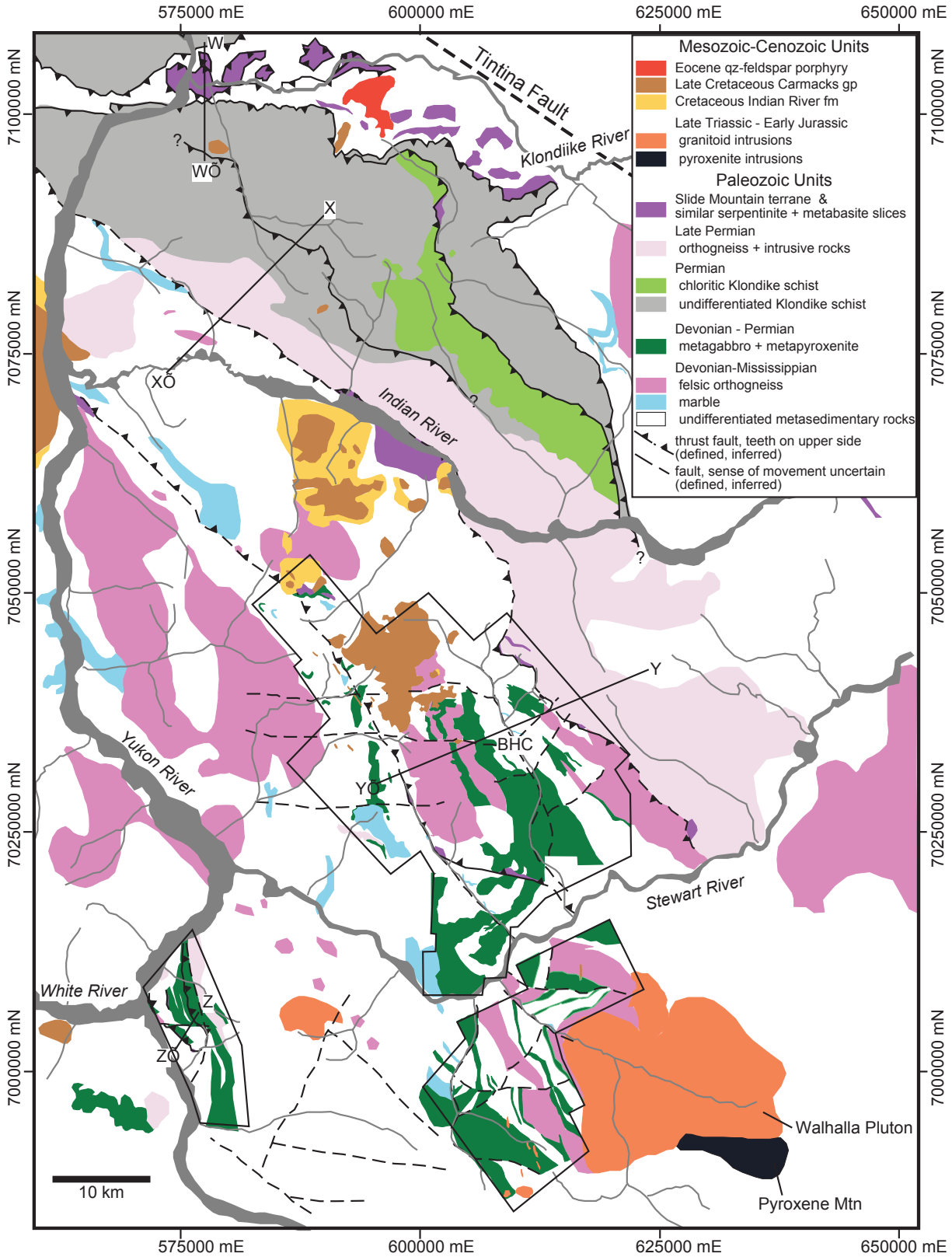

Figure 1. *Geological map of the Klondike – Stewart River area, central western Yukon (modified after Ryan and Gordey, 2004; MacKenzie et al., 2008a,b, 2010 and MacKenzie and Craw, 2010). Outlined areas have been mapped in more detail at 1:10000 and 50000 scale. Labelled lines mark locations of cross sections in Figure 2. BHC = Black Hills Creek.*

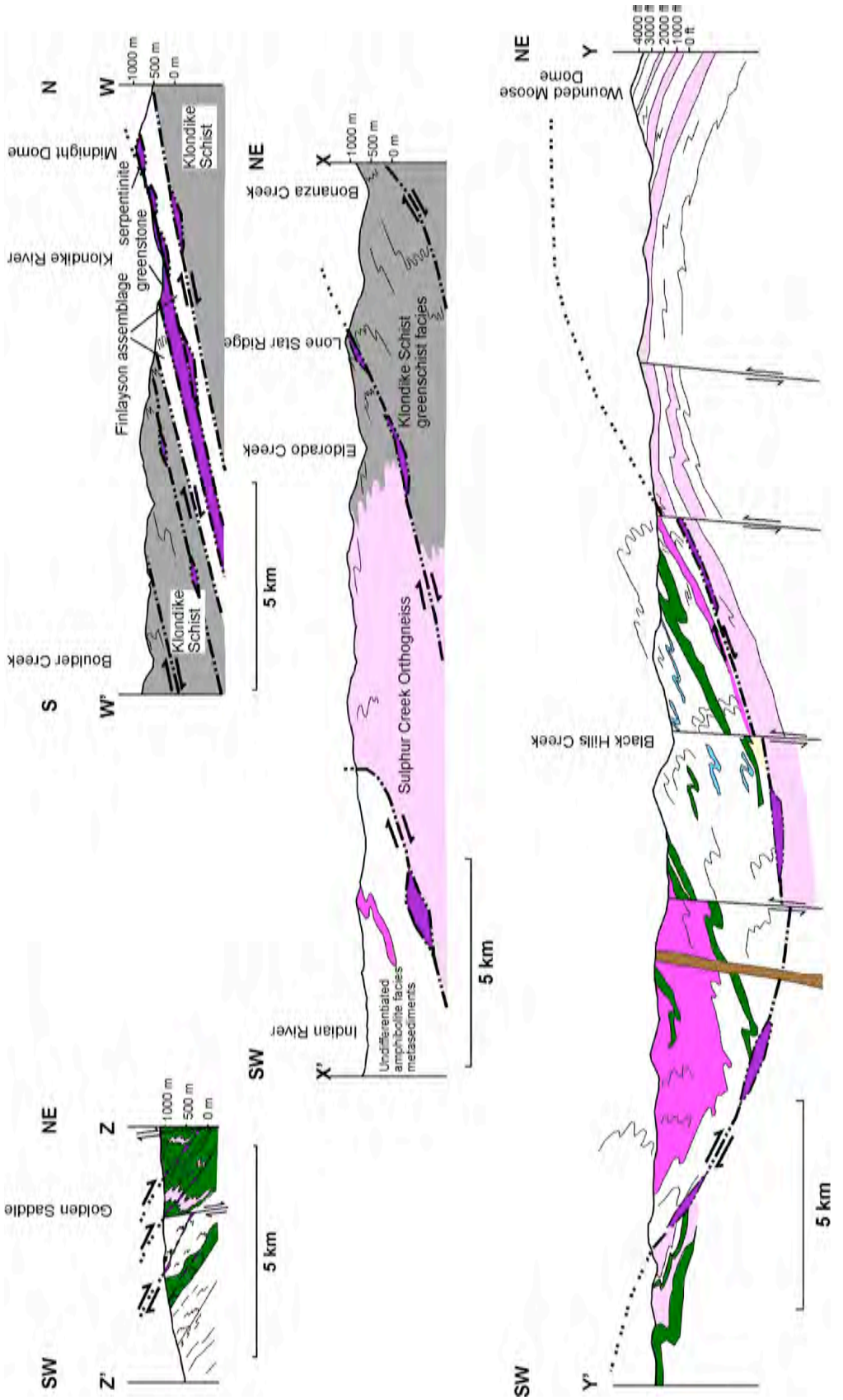

Figure 2. *Cross sections through the Klondike-Stewart River area as located by section lines in Figure 1.*

Figure 3. *Gold-bearing quartz vein cuts chloritic schist in the Klondike goldfield with an alteration halo of disseminated pyrite cubes up to 1 cm across.*

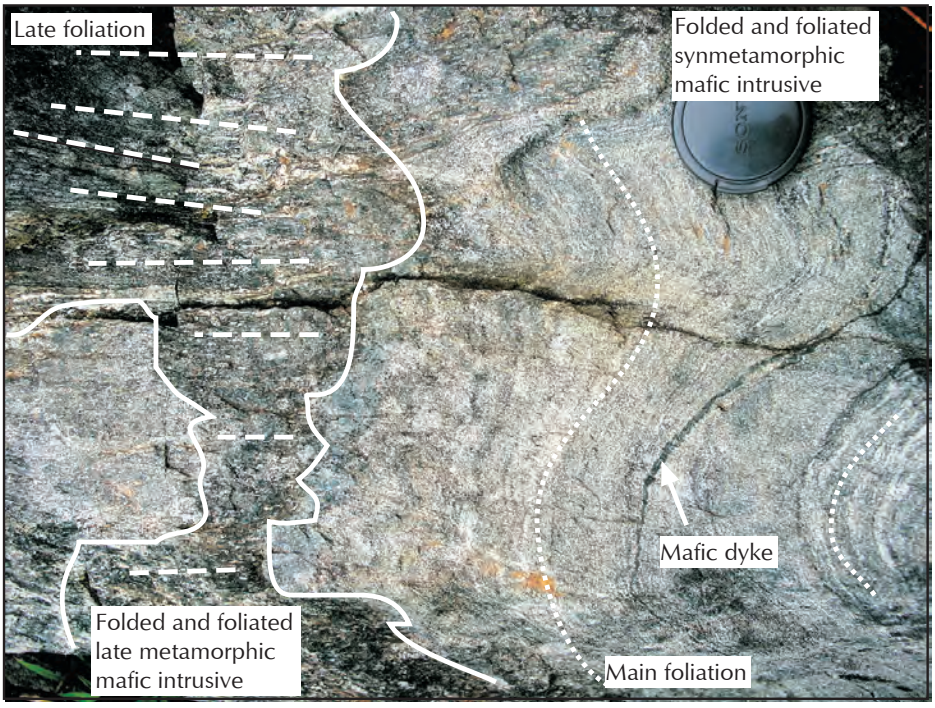

Figure 4. *Late metamorphic foliation (thick white dashed lines, left) weakly developed in a late metamorphic mafic dike cutting a well-foliated (light white dotted lines) and metamorphosed mafic orthogneiss (right). Both bodies have been folded by late metamorphic folds, and the late metamorphic foliation has formed parallel to the fold axial surface of these late metamorphic folds.*

Despite the metamorphic overprint, primary magmatic minerals and textures are locally preserved in less deformed parts of the metagabbros and metapyroxenites (Figs. 5 and 6). For example, intrusion breccias are interpreted on the basis of angular clasts of earlier gabbro and granitoid host rocks within a mafic to intermediate matrix (Fig. 5). We also see xenoliths or rafts of the surrounding metasedimentary rocks (0.1-10 m scale) near margins of metagabbro and metapyroxenite bodies and in some of the mafic rocks a relict coarse-grained texture is discernible. We interpret these rocks as plutonic pyroxenites, probably cumulates (Fig. 6). No primary olivine has been observed in these rocks. The primary mafic minerals have mostly been recrystallized to variably aligned metamorphic hornblende (Fig. 7), and biotite. Most mafic bodies are essentially completely recrystallized to hornblende-rich gneisses with S_2 foliation, but some appear to be controlled by, or cut, the S_2 foliation and have only the incipient late metamorphic foliation imposed on them (Fig. 4). Therefore, at least two generations of mafic intrusions were emplaced during metamorphism.

SERPENTINITE AND METABASITE SLICES

Between Indian River and Stewart River, serpentinite bodies occur sporadically along greenschist facies shear zones that cut the amphibolite facies basement gneisses (Fig. 1). Deformation along the shear zones is primarily ductile (D_3; Table 1), but some late-stage brittle shearing has occurred as well, in zones up to 100 m wide. The shear zones are traceable for tens of kilometres with this combination of serpentinites

Figure 5. *Intrusion breccia from Black Hills Creek area. Unfoliated leucocratic metagabbro encloses angular xenoliths of more mafic metagabbro.*

and localized greenschist facies overprint (Fig. 1). Ultramafic contacts are typically at a low to moderate angle (20-50°) to the adjacent gneiss foliation (Fig. 2). Serpentinites are locally affected by D_3 structures, principally semiductile, tight to angular folds with weak axial planar cleavage. Where D_3 deformation was intense, the ultramafic rocks form lenticular pods or phacoids that are cut by anastomosing semiductile shears (Fig. 8). Locally a new S_3 greenschist facies foliation developed parallel to shears and on the margins of individual phacoids. Serpentine is commonly accompanied by magnetite, talc, chlorite, and actinolite in metasomatic zones. Hence, the ultramafic rocks show up as prominent highs in published aeromagnetic images (*e.g.*, Shives *et al.*, 2002a,b).

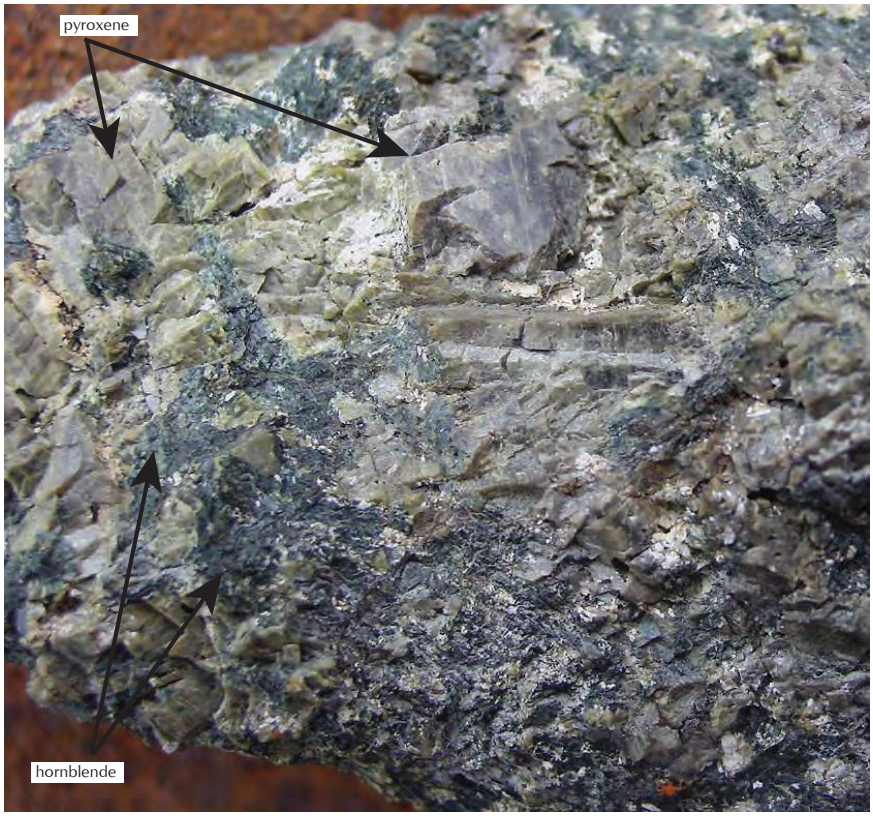

Figure 6. *Unfoliated coarse pyroxenite south of Stewart River. Coarse (up to 2 cm) pale brown pyroxenes (centre, protruding crystals) have been partially replaced by finer grained hornblende (black, recessive).*

POST-METAMORPHIC PYROXENITE INTRUSIONS

Some pyroxenite plutons, including dikes and sills associated with Late Triassic to Early Jurassic granitoid intrusions, intrude the metamorphic sequence (Gordey and Ryan, 2005). The Pyroxene Mountain pyroxenite intrusion associated with the Walhalla granite (Gordey and Ryan, 2005; Mortensen, unpublished data) is the most significant such feature in the Stewart River area (Fig. 1). This pyroxenite is massive and coarse grained, with no metamorphic overprint (Fig. 9), although minor shearing has occurred along pluton margins. The lack of foliation and metamorphic overprint in these rocks is important for distinguishing them in the field from the relict pyroxenites that occur in the Paleozoic metagabbro/metapyroxenite intrusive rocks within the gneiss basement (Figs. 6 and 7). However, both these types of pyroxenites have minor localized epidote-chlorite alteration.

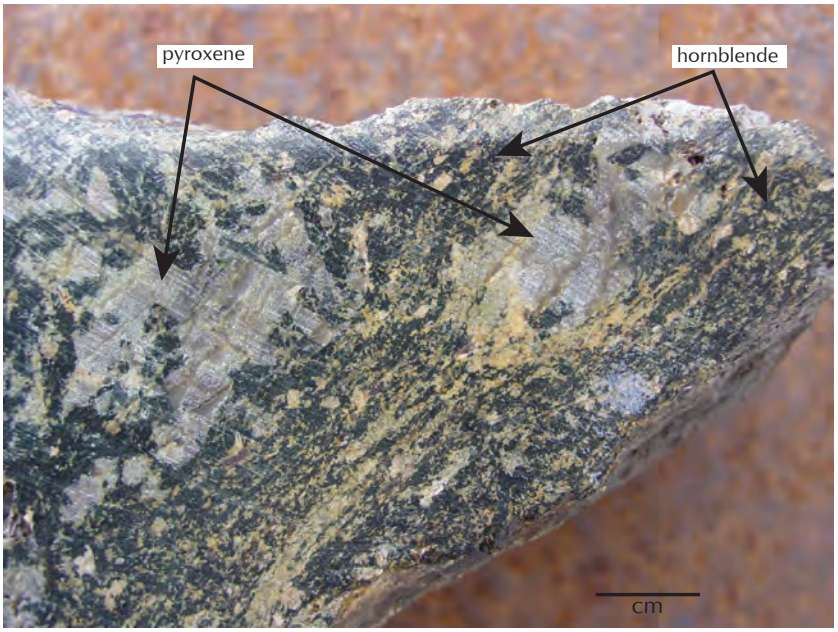

Figure 7. *Variably foliated pyroxenite with hornblende, from the Barker Creek area, south of Stewart River (Fig. 1). Coarse (up to 15 mm) pale brown pyroxenes (centre left and centre right) have been cut and partially replaced by finer grained black hornblendes that define a strong foliation on the right margin of the sample.*

DISTINCTIONS BETWEEN PALEOZOIC MAFIC AND ULTRAMAFIC GNEISSES AND SLIDE MOUNTAIN TERRANE SLICES

Some synmetamorphic to late metamorphic (Paleozoic) mafic metagabbros and pyroxenites resemble the ultramafic rocks emplaced in Jurassic D_3 shear zones, and distinction in the field can be difficult. The following points of distinction have been used to interpret outcrops and construct the maps and sections in Figures 1 and 2.

a. Paleozoic mafic and ultramafic rocks apparently have intrusive contacts with metasedimentary rocks. In contrast, Slide Mountain ultramafic rocks were structurally emplaced along shear zones that are traceable for kilometres or tens of kilometres (Fig. 1)

b. Paleozoic mafic and ultramafic rocks are invariably associated with mafic metagabbros and mafic gneisses, some of which are leucocratic. In contrast, Slide Mountain ultramafic rocks are not closely associated with mafic gneisses, although some are in structural contact with felsic orthogneisses.

c. No olivine has been seen in the Paleozoic metagabbros or pyroxenites. Slide Mountain ultramafic rocks are generally olivine-rich or at least olivine-bearing to some degree, which led to the production of abundant serpentine during greenschist facies metamorphism.

d. Paleozoic synmetamorphic to late metamorphic mafic and ultramafic rocks all have some degree of amphibolite facies metamorphic overprint, although this may be subtle in the case of late metamorphic intrusions. Principal features include localized hornblende±biotite foliation; replacement of pyroxene by hornblende; hornblende-rich lineation; and garnet-hornblende assemblages. Greenschist facies retrogression has occurred locally, but relict amphibolite facies assemblages can normally be found in close proximity to these mafic/ultramafic bodies. In contrast, Slide Mountain ultramafic rocks have only greenschist facies overprint and shear foliation development.

e. Paleozoic mafic and ultramafic rocks have some retrograde alteration to greenschist facies assemblage epidote-actinolite-chlorite. No serpentine has been seen in the Paleozoic rocks. Slide Mountain ultramafic rocks are typically serpentinized to varying degrees, commonly with talc and magnesite and only subordinate actinolite and chlorite.

REGIONAL STRUCTURE

Recognition of the above distinctive features of the four different types of mafic/ultramafic rocks over the whole Klondike-Stewart River portion of the Yukon-Tanana terrane has helped us to interpret outcrops and map patterns, and to compile the regional structural map (Fig. 1) coupled with the cross sections (Fig. 2). The key large-scale structural feature is that the metamorphic basement rocks consist of mappable thrust sheets that are stacked one upon another from the Stewart River area to the Klondike goldfield (Figs. 1 and 2). Thrust sheets that are part of this regional structural feature have been previously mapped in detail in the Klondike goldfield (Mortensen, 1990, 1996; MacKenzie *et al.*, 2008a,b), and we have been able to extend this overall structure to the Stewart River as part of the present study (Figs. 1 and 2).

Ultramafic rocks mainly consisting of serpentinized harzburgites and serpentinites occur as fault bounded slices separating distinct lithological units and thrust

Figure 8. (a) *Outcrop of deformed serpentinite from Black Hills Creek area (Fig. 1). Metre-scale lenses (phacoids) of less-deformed serpentinite have foliated and altered zones (cm to m scale) anastomosing around them to define a crude shear fabric dipping gently SE to left and away from the camera.* ***(b)*** *Close-up showing anastomosing cleavage surfaces and crosscutting white serpentine-magnetite veins running top to bottom.*

slices (Figs. 1 and 2; Mortensen, 1996; MacKenzie *et al.* 2008a,b). These ultramafic rocks are locally accompanied by massive to weakly foliated metabasaltic rocks. In the Klondike goldfield, the serpentinite and associated metabasites are considered to be part of a dismembered Permian Slide Mountain, and were tectonically emplaced in the Yukon-Tanana terrane during Jurassic thrusting (Fig. 1; Mortensen, 1990; MacKenzie *et al.*, 2008a,b). This thrust emplacement was accompanied by localized ductile and brittle shearing under greenschist facies conditions (D_3, Table 1). Some of the ultramafic lithologies are variably altered to talc-carbonate±magnesite schist and quartz-carbonate-fuchsite listwaenite (*e.g.*, MacKenzie *et al.*, 2008b).

In the Klondike goldfield, the Klondike Schist is thrust over several slices of Paleozoic (Nasina facies) metasedimentary rocks and mafic and ultramafic rocks of the Slide Mountain terrane (section W-W', Fig. 2). An imbricated package of

Figure 9. ***(a)*** *Massive outcrop of unfoliated and unsheared pyroxenite intrusive on Pyroxene Mountain (Fig. 1).* ***(b)*** *Close-up showing coarse unaltered euhedral pyroxene crystals (photo is 3 cm across).*

at least three different slices of Klondike Schist is stacked on top of two lower grade thrust slices of Finlayson assemblage (Nasina facies) and an intervening slice of relatively undeformed greenstone and discontinuous lenses of serpentinite (section W-W′, Fig. 2; MacKenzie *et al.*, 2008b). All these slices overlie another slice of Klondike Schist that crops out north of the Klondike River (Figs. 1 and 2). The chloritic schist unit, described above, sits in the upper Klondike Schist package and its lower contact is a low-angle thrust over-riding another slice of Klondike Schist in the southeastern portion of the Klondike goldfield. The thrust contact is marked by discontinuous fault bounded slices of serpentinite that are considered part of the Slide Mountain terrane (Fig.1; Mortensen, 1990, 1996).

South of Indian River, a package of amphibolite facies metasedimentary rocks is thrust over greenschist facies Sulphur Creek orthogneiss and Klondike Schist (Figs. 1 and 2, section X-X′). The underlying schist package is in turn thrust over another slice of Klondike Schist at Lone Star Ridge (section X-X′, Fig. 2). Both the Lone Star Ridge thrust (Fig. 2; MacKenzie *et al.*, 2007, 2008b) and the thrust bounding the Sulphur Creek orthogneiss (Fig. 1) are marked intermittently along strike by deformed lenses of serpentinite and ultramafic rocks.

In the Black Hills Creek area, a slice of amphibolite facies metasedimentary rocks and orthogneiss is thrust over a similar, but possibly younger, package of metasedimentary rocks containing Late Permian orthogneiss (Figs. 1 and 2, section Y-Y′). The thrust fault is gently folded, so that it has an apparent normal displacement along its NE dipping limbs (section Y-Y′, Fig. 2). In the White River area, a series of thrust slices are juxtaposed along NE dipping thrusts that may be similarly folded (section Z-Z′, Fig. 2; MacKenzie *et al.*, 2010; MacKenzie and Craw, 2010).

Thrust imbrication in all the above examples resulted in semiductile shearing and macroscopic folding on the 10-50 m scale by tight to isoclinal folds (F_3) with an axial planar spaced cleavage (MacKenzie *et al.*, 2008a, b). Tabular bodies of ultramafic rocks and serpentinites that were emplaced along the faults acted as loci for D_3 deformation and greenschist facies retrogression and metasomatism. A new S_3 greenschist facies foliation is locally developed, particularly next to, and within, these ultramafic bodies. These D_3 structures are locally overprinted by semibrittle folds, angular kinks, and fractures associated with a late compressional phase of regional scale warping and upright folding (F_4; Table 1; MacKenzie *et al.*, 2008a,b). This latter deformation also resulted in larger-scale folding and warping of regional S_2 foliation and D_3 thrust faults (Fig. 2).

CONCLUSIONS AND SIGNIFICANCE FOR GOLD MINERALIZATION

Four different types of mafic/ultramafic rocks have been recognized in the Yukon-Tanana terrane. Chloritic schists in the greenschist facies Klondike Schist are interlayered with metasedimentary rocks. Amphibolite facies metagabbros and metapyroxenites were intruded, in at least two stages, during Paleozoic metamorphism of basement metasedimentary rocks. Permian Slide Mountain terrane mafic and ultramafic rocks were dismembered in the Jurassic and emplaced along regionally extensive thrusts and associated shear zones, mainly as serpentinite bodies. These thrusts were formed under greenschist facies conditions with retrograde mineralogy that overprints amphibolite facies gneissic fabrics. Finally, massive, unaltered and unfoliated Jurassic pyroxenite intrusions were emplaced in association with granitoids.

Recognition and distinction of the four types of mafic and ultramafic rocks and their structural settings has enabled these features to be used as mappable units for construction of the regional map and cross sections (Figs. 1 and 2), and this aspect may be useful for gold exploration. Gold-bearing veins in the Klondike goldfield are largely controlled by F_4 structures at the outcrop scale, and perhaps regional-scale as well (MacKenzie *et al.*, 2008a). The broad F_4 folds and warps shown on a regional-scale in Figure 2 may help to define zones and orientations of more localized and more intense F_4 folding that may host orogenic gold south of Indian River (Fig. 1). In contrast, gold mineralization in the White River area is partially controlled by composite late metamorphic and D_3 shear zones, and is partially controlled by crosscutting faults (MacKenzie *et al.*, 2010; MacKenzie and Craw, 2010). Recognition and mapping of these structural features, as done on the regional-scale in Figure 1, is therefore of potential exploration significance for that deposit type.

At the outcrop-scale, the mafic and ultramafic rocks described above have varying significance to gold mineralization, depending on their structural settings as described above. Chloritic schists in the Klondike

goldfield act as hosts for orogenic gold-bearing veins, in a similar manner to adjacent quartzofeldspathic schists. However, chloritic schists were apparently more reactive to hydrothermal fluids than the quartzofeldspathic schists, and there are significant (metre-scale) hydrothermal alteration zones in chloritic schists adjacent to many veins. These alteration zones have variable amounts of disseminated pyrite (Fig. 3) and iron-bearing carbonate, and some disseminated gold (MacKenzie *et al.* 2008c). Some hydrothermal alteration of pyroxenites and associated mafic gneisses accompanied gold mineralization in the White River area, but this alteration was limited in extent (MacKenzie *et al.*, 2010; MacKenzie and Craw, 2010). Foliated margins of mafic gneiss bodies have had minor gold-bearing vein emplacement (MacKenzie *et al.*, 2010; MacKenzie and Craw, 2010). However, the weakly foliated hornblende-rich mafic gneisses and unfoliated pyroxenites appear to have been impermeable barriers to hydrothermal fluid flow (MacKenzie *et al.*, 2010). Ultramafic rocks in D_3 thrust zones have had some hydrothermal alteration but no significant gold mineralization has been detected as yet, in either White River area or the Klondike goldfield (MacKenzie *et al.* 2008a, 2010; MacKenzie and Craw, 2010). Pyroxenite intrusions at Pyroxene Mountain show no evidence for associated hydrothermal alteration or Au mineralization.

ACKNOWLEDGEMENTS

This research was supported financially by Smash Minerals Corporation, the NZ Foundation for Research, Science and Technology, and the University of Otago. Discussions with Adrian Fleming, Chris Siron, Chris Pennimpede, Phil Smerchanski, Rob Mackie, Dennis Arne, Colin Brodie, Mike Cooley, Lamont Leatherman, Kristy Long and Mike Young helped clarify our geological ideas. Constructive reviews by Jim Mortensen and Patrick Sack helped improve the manuscript.

REFERENCES

Beranek, L.P. and Mortensen, J.K., 2011. The timing and provenance record of the Late Permian Klondike orogeny in northwestern Canada and arc-continent collision along western North America. Tectonics (*in press*).

Berman, R.G., Ryan, J.J., Gordey, S.P., and Villeneuve, M., 2007. Permian to Cretaceous polymetamorphic evolution of the Stewart River region, Yukon Tanana Terrane, Yukon, Canada: P-T evolution linked with insitu SHRIMP monazite geochronology. Journal of Metamorphic Geology, vol. 25, p. 803-827.

Gabrielse, H., Murphy, D.C., and Mortensen, J.K., 2006, Cretaceous and Cenozoic dextral orogen-parallel displacements, magmatism, and paleogeography, north-central Canadian Cordillera. *In:* Paleogeography of the North American Cordillera: Evidence For and Against Large-Scale Displacements, J.W. Haggart, R.J. Enkin, and J.W.H. Monger (eds.), Geological Association of Canada, Special Paper 46, p. 255-276.

Gordey, S.P. and Ryan, J.J., 2005. Geology map, Stewart River area (115 N, 115-O and part of 115 J), Yukon Territory. Geological Survey of Canada, Open File 4970, 1:250 000 scale.

MacKenzie, D., Craw, D., Mortensen, J.K., and Liverton, T., 2007. Structure of schist in the vicinity of the Klondike goldfield, Yukon. *In:* Yukon Exploration and Geology 2006, D.S. Emond, L.L. Lewis, and L.H. Weston (eds.), Yukon Geological Survey, p. 197-212.

MacKenzie, D., Craw, D., and Mortensen, J.K., 2008a. Structural controls on orogenic gold mineralisation in the Klondike goldfield, Canada. Mineralium Deposita, vol. 43, p. 435-448.

MacKenzie, D., Craw, D., and Mortensen, J.K., 2008b. Thrust slices and associated deformation in the Klondike goldfield, Yukon. *In*: Yukon Exploration and Geology 2007, D.S. Emond, L.R. Blackburn, R.P. Hill, and L.H. Weston (eds.), Yukon Geological Survey, p. 199-213.

MacKenzie, D., Craw, D., Mortensen, J.K., and Liverton, T., 2008c. Disseminated gold mineralization associated with orogenic veins in Klondike Schist, Yukon. *In*: Yukon Exploration and Geology 2007, D.S. Emond, L.R. Blackburn, R.P. Hill and L.H. Weston (eds.), Yukon Geological Survey, p. 215-224.

MacKenzie, D., Craw, D., Cooley, M., and Fleming, A., 2010. Lithogeochemical localisation of disseminated gold in the White River area, Yukon, Canada. Mineralium Deposita vol. 45, p. 683-705.

MacKenzie, D.J. and Craw, D., 2010. Structural controls on hydrothermal gold mineralization in the White River area, Yukon. *In:* Yukon Exploration and Geology 2009, K.E. MacFarlane, L.H. Weston and L.R. Blackburn (eds.), Yukon Geological Survey, p. 253-263.

Mortensen, J.K., 1990. Geology and U-Pb chronology of the Klondike District, west-central Yukon. Canadian Journal of Earth Sciences, vol. 27, p. 903-914.

Mortensen, J.K., 1992. Pre-mid-Mesozoic tectonic evolution of the Yukon-Tanana Terrane, Yukon and Alaska. Tectonics, vol. 11, p. 836-853.

Mortensen, J.K., 1996. Geological compilation maps of the northern Stewart River map area, Klondike and Sixtymile Districts (115N/15, 16; 1150/13,14; and parts of 115O/15, 16). Exploration and Geological Services Division, Yukon region, Indian and Northern Affairs Canada, Open File 1996-1 (G), 43 p.

Mortensen, J.K., Beranek, L., and Murphy, D.C., 2007. Permo-Triassic Orogeny in the Northern Cordillera: Sonoma North? Geological Society of America, Abstracts with Programs, 103rd Annual Meeting, Cordilleran Section, Bellingham , WA, USA, Paper No. 28-5.

Ruks T.W., Piercey S.J., Ryan J.J., Villeneuve M.E., and Creaser R.A., 2006. Mid to late Paleozoic K-feldspar augen granitoids of the Yukon-Tanana Terrane, Yukon, Canada: Implications for crustal growth and tectonic evolution of the northern Cordillera. GSA Bulletin 118, p. 1212-1231.

Ryan, J.J. and Gordey, S.P., 2001. Geology, Thistle Creek Area, Yukon Territory (115O/3). Geological Survey of Canada, Open File 3690, scale 1:50000.

Ryan, J.J. and Gordey, S.P., 2004. Geology, Stewart River Area (Parts of 115N/1,2,7,8 and 115-O/2-12), Yukon Territory. Geological Survey of Canada, Open File 4641, scale 1:100000.

Shives, R.B.K., Carson, J.M., Ford, K.L., Holman, P.B., Gordey, S., and Abbott, G., 2002a. Magnetic Anomaly Map (Residual Total Field), Stewart River Area – 115O/6, 1:50000 scale. Geological Survey of Canada, Open File 4307; Exploration and Geological Services Division, Yukon, Indian and Northern Affairs Canada, Open File 2002-13.

Shives, R.B.K., Carson, J.M., Ford, K.L., Holman, P.B., Gordey, S., and Abbott, G., 2002b. Magnetic First Vertical Derivative Map, Stewart River Area – 115O/6, 1:50 000 scale. Geological Survey of Canada, Open File 4307; Exploration and Geological Services Division, Yukon, Indian and Northern Affairs Canada, Open File 2002-13.

Wainwright, A.J., Simmons, A.T., Finnigan, C.S., Smith, T.R., and Carpenter, R.L., 2011. Geology of new gold discoveries in the Coffee Creek area, White Gold District, west-central Yukon. *In:* Yukon Exploration and Geology 2010, K.E. MacFarlane, L.H. Weston and C. Relf (eds.), Yukon Geological Survey, p. 233-247.

The Proterozoic Pinguicula Group, Wernecke Mountains, Yukon: A siliciclastic and carbonate slope to basin succession with local and exotic sediment provenance

K.P.R. Medig[1], D.J. Thorkelson
Department of Earth Sciences, Simon Fraser University, Burnaby, BC

E.C. Turner
Department of Earth Sciences, Laurentian University, Sudbury, ON

W.J. Davis
Geological Survey of Canada, Ottawa, ON

H.D. Gibson
Department of Earth Sciences, Simon Fraser University, Burnaby, BC

R.H. Rainbird
Geological Survey of Canada, Ottawa, ON

D.D. Marshall
Department of Earth Sciences, Simon Fraser University, Burnaby, BC

Medig, K.P.R., Thorkelson, D.J., Turner, E.C., Davis, Gibson, H.D., Rainbird, R.H., and Marshall, D.D., 2012. The Proterozoic Pinguicula Group, Wernecke Mountains, Yukon: A siliciclastic and carbonate slope to basin succession with local and exotic sediment provenance. *In:* Yukon Exploration and Geology 2011, K.E. MacFarlane and P.J. Sack (eds.), Yukon Geological Survey, p. 129-149.

ABSTRACT

The late Meso or early Neoproterozoic Pinguicula Group, Wernecke Mountains, Yukon, is a siliciclastic and carbonate succession deposited on an angular unconformity developed on the Wernecke Supergroup. The group consists of three units. Unit A consists of a fining-upward conglomerate and sandstone unit overlain by a monotonous siltstone succession. Unit B is a dolostone and limestone succession in which shallower-water facies, deposited above storm wave-base, grade up-section into slope facies with intraclast rudstones and turbidites. Unit C is a deep-water dolostone and limestone succession that has been pervasively altered by carbonate veins, zebra dolomite, and coarsely crystalline dolostone.

Detrital zircon geochronology from the Pinguicula Group provides information on provenance and age of the sediment deposited in the Pinguicula basin. A distinctive population from the Mesoproterozoic, between 1610 and 1490 Ma (North American Magmatic Gap), suggests that sediment may have been derived from Australia. In addition, detrital zircon $^{207}Pb/^{206}Pb$ ages from the Wernecke inlier are as young as 1144±25 Ma (one grain), which raises the possibility that the Pinguicula Group is younger than *ca.* 1150 Ma. The reliability of this finding will be addressed by additional geochronology.

[1] *kmedig@gmail.com*

INTRODUCTION

The Meso or early Neoproterozoic Pinguicula Group is a siliciclastic and carbonate bearing succession in the Wernecke Mountains, Northern Yukon (Fig. 1a,b,c, herein referred to as the study area). Beyond this area it has poorly known distribution, but has been mapped in the Hart River inlier (Abbott, 1997). The group comprises three units (A, B, and C), which have not previously been described in detail.

Possible correlatives of the Pinguicula Group have been identified in the Hart River (also referred to as the Pinguicula Group) and Coal Creek (lower Fifteenmile Group) inliers in the Ogilvie Mountains (Thompson *et al.*, 1992; Abbott, 1997; Medig *et al.*, 2010). More distant correlatives have also been proposed, such as the Dismal Lakes Group in the Coppermine Homocline (Cook and MacLean, 1995; Thorkelson, 2000; Long *et al.*, 2008) and the lower Tindir Group in Alaska (Abbott, 1997; Macdonald *et al.*, 2011). The lack of detailed stratigraphic work in the type area combined with the lack of refined ages for the group have made definitive correlations difficult.

Between 2009 and 2011, detailed sections were measured in units A, B, and C of the Pinguicula Group. Samples were collected from a sandstone bed at the base of unit A and detrital zircon grains were extracted for U-Pb geochronologic analysis. Results of the analysis and the implications for proposed correlations, as well as the stratigraphy of the Pinguicula Group, are discussed in detail below.

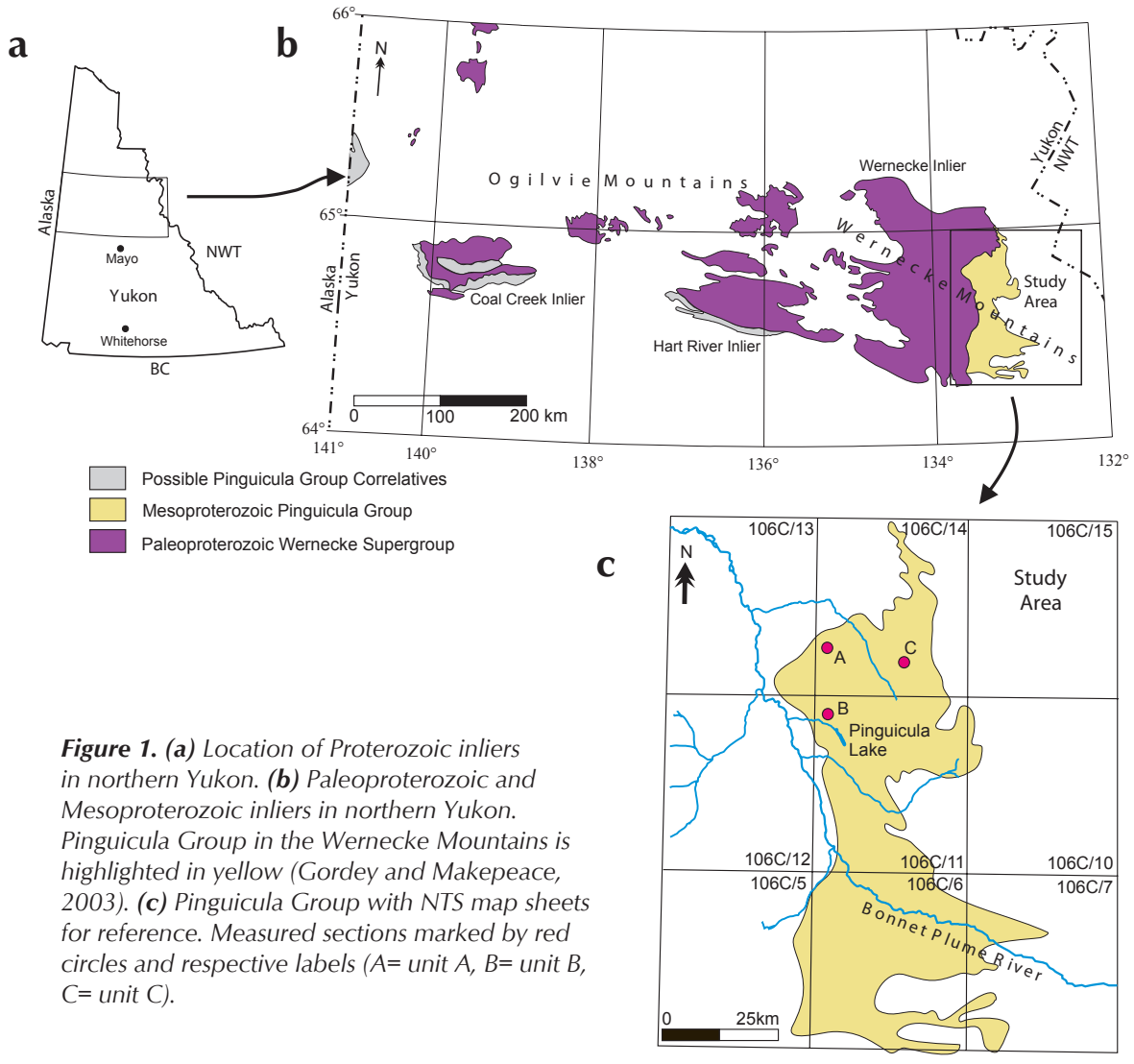

Figure 1. ***(a)*** *Location of Proterozoic inliers in northern Yukon.* ***(b)*** *Paleoproterozoic and Mesoproterozoic inliers in northern Yukon. Pinguicula Group in the Wernecke Mountains is highlighted in yellow (Gordey and Makepeace, 2003).* ***(c)*** *Pinguicula Group with NTS map sheets for reference. Measured sections marked by red circles and respective labels (A= unit A, B= unit B, C= unit C).*

REGIONAL GEOLOGY

The oldest exposed strata in the Wernecke and Ogilvie mountains are the Wernecke Supergroup. This includes (from oldest to youngest) the Fairchild Lake Group, the Quartet Group, and the Gillespie Lake Group (Thompson *et al.*, 1992; Abbott, 1997; Thorkelson, 2000). Detrital zircon ages from the Wernecke Supergroup indicate that the group is younger than 1610±30 Ma (Furlanetto *et al.*, 2009). The Wernecke Supergroup was affected by three generations of deformation, referred to collectively as the Racklan Orogeny, prior to intrusion of the Wernecke breccia at *ca.* 1595 Ma (Brideau *et al.*, 2002; Thorkelson *et al.*, 2005). The Wernecke Supergroup in both the eastern Ogilvie Mountains (Hart River inlier) and Wernecke Mountains (Wernecke inlier) is crosscut by the 1380 Ma Hart River sills (Abbott, 1997; Thorkelson *et al.*, 2005). In the *ca.* 200 Ma interval between the hydrothermal event forming the Wernecke breccia and the emplacement of the Hart River sills, there was either little activity in the area or the rock record has not been preserved. Deposition of the Pinguicula Group occurred well after emplacement of the Hart River sills. The erosional interval between emplacement of the Hart River sills and deposition of the Pinguicula Group may represent a significant time interval, as it is marked by a major gap in the rock record. Unconformably overlying the Pinguicula Group are strata of the Mackenzie Mountains supergroup strata (also known locally as the Hematite Creek Group) in the Wernecke inlier, unit D in the Hart River inlier, and lower Fifteenmile Group units PR3 to PR5 in the Coal Creek inlier (Medig *et al.*, 2010; MacDonald *et al.*, 2011; Turner, 2011).

PINGUICULA GROUP STRATIGRAPHY, WERNECKE MOUNTAINS

The Pinguicula Group was established in the Pinguicula Lake area by Eisbacher (1978), who described the group as unconformably overlying the Wernecke Supergroup and comprising six informal units (A through F; Eisbacher, 1978, 1981). Thorkelson (2000) and Thorkelson *et al.* (2003) identified a disconformity between units C and D and reassigned the upper three units to the Hematite Creek Group. Units D to F were correlated with the Tsezotene Formation and Katherine Group of the Mackenzie Mountains supergroup. Turner (2011) revised and subdivided the Hematite Creek Group into three formations: the Dolores Creek Formation, Black Canyon Creek Formation, and Tarn Lake Formation. Turner (2011) proposed correlation of the Black Canyon Creek formation of the Hematite Creek Group with the "H1 unit" of the Mackenzie Mountains supergroup. The Tarn Lake Formation was correlated with the Tsezotene Formation, also of the Mackenzie Mountains supergroup. The three new formations constitute the former unit 'D' of the Pinguicula Group. Former unit 'E' of the Pinguicula Group is now correlated with the Katherine Group, and former unit 'F' of the Pinguicula Group was identified as the lower part of the Little Dal Group. Units A through C, however, are internally conformable and remain part of the Pinguicula Group.

PINGUICULA GROUP

UNIT A

Description

Unit A is a siliciclastic succession that overlies the Gillespie Lake and Quartet groups of the Wernecke Supergroup, including zones of Wernecke breccia, with angular unconformity. Where Wernecke breccia underlies unit A, a pale, crumbly regolith is present at the erosional top of the breccia zones and extends downwards to as much as 12 metres in some areas (Thorkelson, 2000). In some locations, in both the Wernecke and Hart River inliers, the Pinguicula Group unconformably overlies the Hart River sills (Abbott, 1997; Medig *et al.*, 2010). This observation contrasts with a previous interpretation (Thorkelson, 2000; Thorkelson *et al.*, 2005) in which the Hart River sills in the Wernecke Mountains were thought to crosscut the Pinguicula Group. An unconformable rather than an intrusive contact relationship is supported by an apparent lack of metamorphism imposed by the Hart River sills on the Pinguicula Group. This relationship is in contrast to the Wernecke Supergroup and clasts within Wernecke breccia which are both affected by thermal metamorphism (Thorkelson, 2000). The upper contact between units A and B is gradational, and is marked by increased carbonate content in the siltstone immediately below the contact with unit B, as well as the appearance of bedding-parallel layers of carbonate nodules in the siltstone.

A detailed section through unit A was measured on an exposure in a creek bed at the PIKA mineral occurrence (Figs. 2 and 3; Yukon MINFILE, 106C 071; base at 573576E 7191036N NTS 106C/14[1]). This location was chosen because it is easily accessible (by helicopter and by foot) and exposes both a lower, unconformable

[1] *UTM coordinates are zone 8W and NAD 27 unless otherwise noted.*

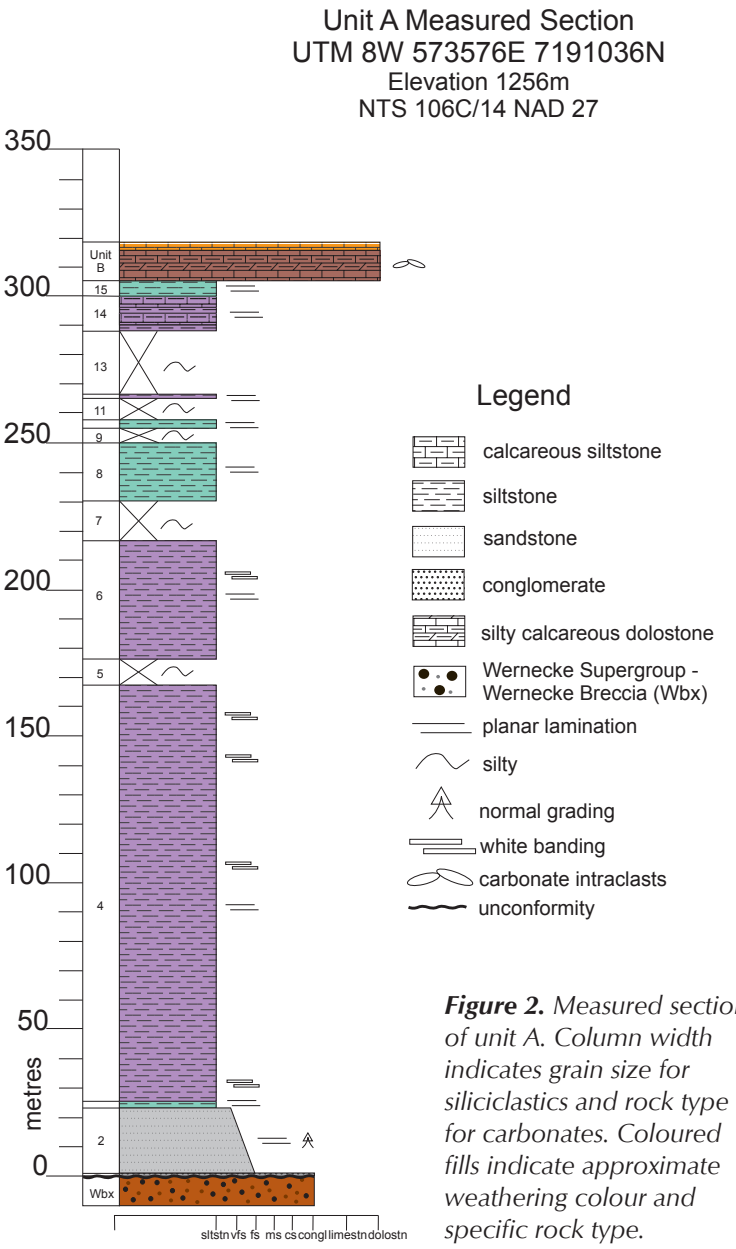

Figure 2. *Measured section of unit A. Column width indicates grain size for siliciclastics and rock type for carbonates. Coloured fills indicate approximate weathering colour and specific rock type.*

contact with the Wernecke breccia and an upper gradational contact with unit B. This location also has conglomerate and sandstone at the base of unit A: rock types that are commonly not exposed or not present in other locations in the study area.

At the measured section, unit A is 306 m thick. It consists predominantly of siltstone with minor conglomerate, and sandstone (Fig. 2). The base of unit A overlies a zone of Wernecke breccia. The lowest unit (unit 1) is an ~50 cm-thick layer of polymictic pebble conglomerate. The conglomerate is matrix-supported with a matrix of predominantly fine-sand grade quartz and carbonate grains. The clasts are predominantly of small to medium pebble grade. They are typically well-rounded and consist mainly of grey, hematitic red, and black siltstone, yellow-weathering, grey, and red carbonate, and rare clasts of Wernecke breccia. Within the conglomerate are 1-2 cm-thick beds of fine-sand grade quartz arenite (Fig. 4a). Overlying the conglomerate from 0.5 to 23 m is a succession of parallel-laminated to thin bedded rusty orange to grey-weathering sandstone layers (unit 2; Fig. 4b). The sandstone grades from a well-sorted fine-grained sandstone, texturally mature quartz arenite, with a minor lithic component and calcite cement, to a very fine-sand grade lithic wacke. Sandstone beds are typically from 3 to 10 cm-thick, but are locally up to 50 cm (Fig. 4c). Dark grey to black, planar-parallel laminae are present in the sandstone at a mm to cm-scale. The sandstone unit fines up-section and displays a transition in colour from grey to pale grey at the base to dark grey at the top. Pyrite is disseminated throughout the sandstone, resulting in a rusty orange-weathering surface.

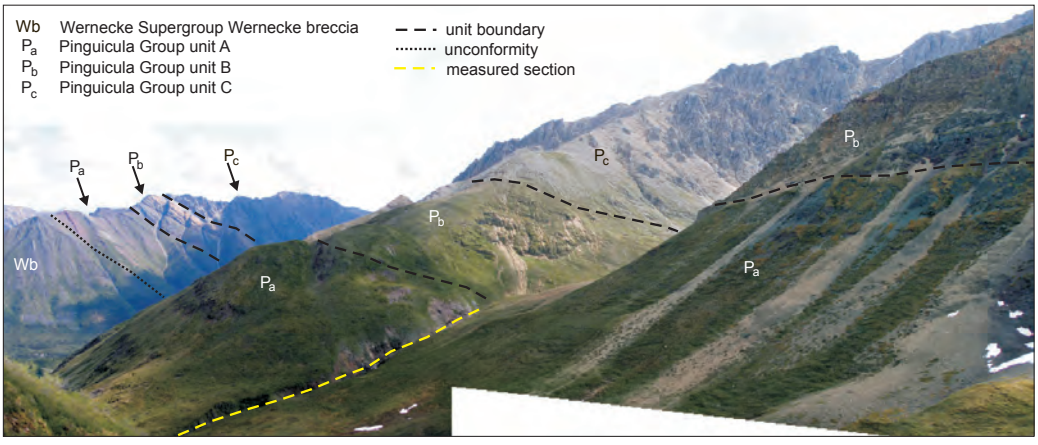

Figure 3. *Pinguicula units A, B, and C overlying the Wernecke breccia at the Pika occurrence. View to the northeast. Measured section of unit A was established along the creek. NTS map sheet 106C/14 UTM 8 W 573381E 7190576N NAD 27.*

The sandstone grades into a predominantly maroon and green-weathering (with some yellow to brown-weathering) siltstone that extends from 23 to 289 m (units 3-13 and 15), with intermittent covered intervals (Fig. 4d). The siltstone is planar, parallel-laminated and lacks other sedimentary structures and variation in grain size. The colour of much of the siltstone alternates between maroon and green, in units that are generally layer-parallel. In some locations, however, these colours form a cm to dm-scale mottled pattern, with patches of colour that cut across lamination. Distinct, continuous to discontinuous cm-thick white layers are present at several stratigraphic levels (Fig. 4e). The discontinuous to mottled appearance of the white, green and maroon layers suggests that the pattern of colours in unit A is diagenetic in origin, and is not strictly related to or derived from primary compositional differences among the siltstone layers. Just below the contact with unit B, the siltstone becomes increasingly calcareous (unit 14; Fig. 4f).

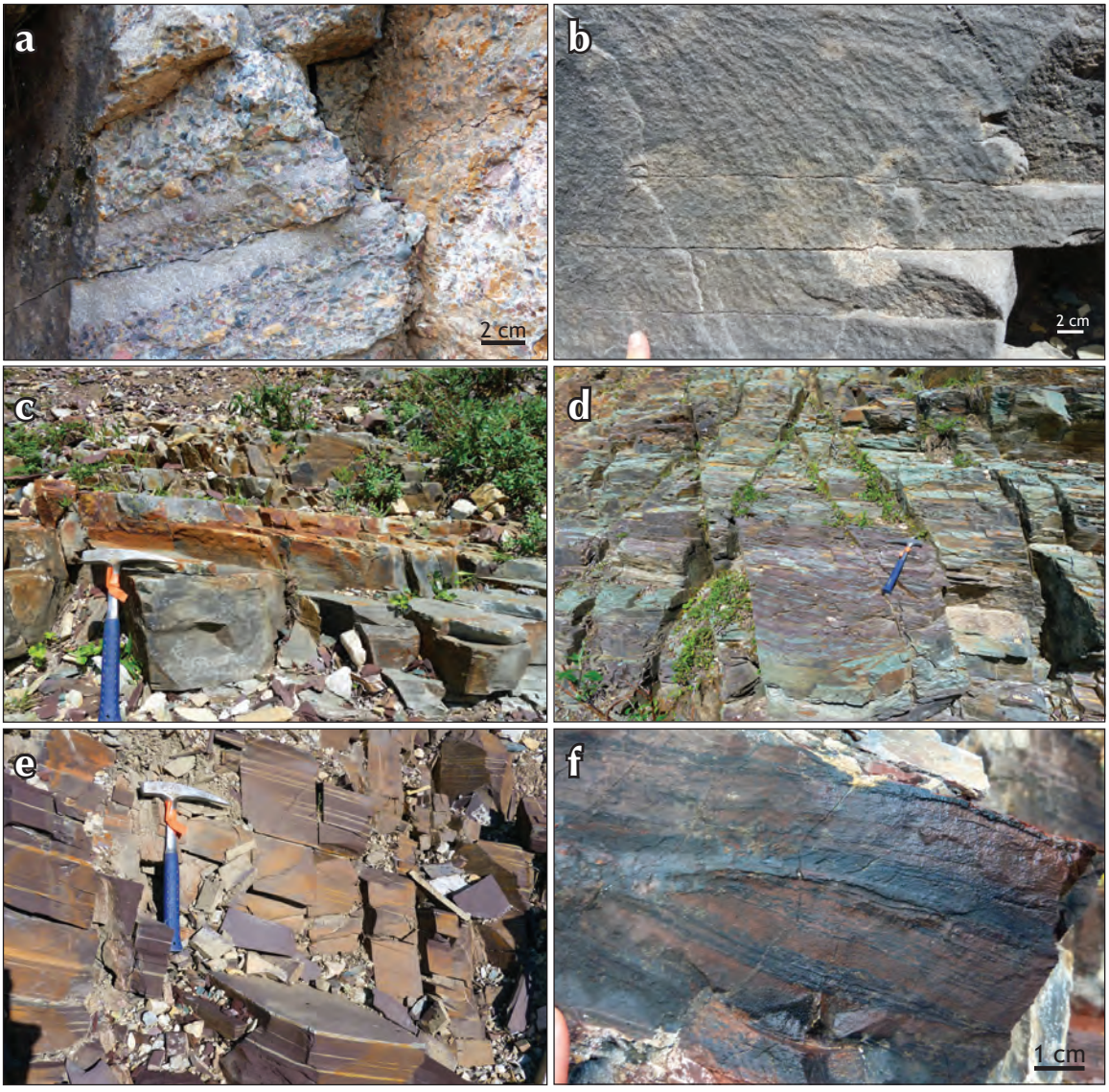

Figure 4. *Lithofacies of Pinguicula Group unit A in the Wernecke inlier.* ***(a)*** *Basal conglomerate with sandstone interbeds at the base of the measured section. Clasts are composed of limestone and siltstone.* ***(b)*** *Typical thinly bedded quartz arenite overlying the basal conglomerate.* ***(c)*** *Outcrop of orange-weathering, planar-laminated sandstone beds. Orange weathering colour is from pyrite disseminated in the sandstone weathering to limonite.* ***(d)*** *Outcrop of typical maroon and green siltstone.* ***(e)*** *Maroon, planar-laminated siltstone with distinctive discontinuous white banding.* ***(f)*** *Calcareous siltstone 6 m below the contact with unit B. Carbonate content in the siltstone increases before the transition to unit B.*

Regional Variation

Unit A extends from the northern part of NTS sheet 106C/14 southward to map sheet 106C/6, and farther south, beyond the extent of existing map coverage included in this study's mapping of 106C/6 (Fig. 1c). The thickness of unit A increases from north to south in the study area to approximately 1400 m, a phenomenon that has been attributed to a southward-deepening basin (Thorkelson, 2000). Weathering colours in the north are predominantly maroon and green (Fig. 5), and contrast with those in the south, which are dark grey, dark purple, and black. Weathering colour also varies stratigraphically. For example, at one location above the Gillespie Lake Group, unit A is orange-weathering at the base and dark grey-weathering up-section. The unit is recessive in the north and resistant in the south, where it forms steep cliffs and peaks. Unit A tends to be more ductile than overlying units B and C. Greater deformation is particularly apparent in the south, where tightly folded strata of unit A are overlain by unfolded, nearly horizontal beds of unit B. However, unit A grades stratigraphically upward into unit B, and the contrast in the amount of deformation cannot be interpreted as an angular unconformity. Instead, the difference in the degree of deformation is interpreted as an outcome of stress applied to rock units of different competence; unit A recorded more strain than the stronger, overlying carbonate units of units B and C.

Conglomerate, and conglomerate–sandstone assemblages are absent from the base of unit A in some locations in the study area. In these cases, either siltstone or sandstone directly overlies Wernecke Supergroup strata or Hart River sills. In other locations, conglomerate and sandstone are interbedded with siltstone lower in the unit.

Carbonate nodules in unit A are locally abundant within tens of metres of the contact with unit B at a number of locations (*e.g.*, northeast of the PIKA occurrence UTM 579053E 7193988N). Nodules are typically elongate with aspect ratios >20:1. Malachite stained pyrite nodules, having diameters of less than 1 to 3 cm, are also present south of the PIKA mineral occurrence along the Bonnet Plume River (UTM 563803E 7184575N).

UNIT B

Description

Unit B is a carbonate succession that is predominantly orange-weathering, with maroon weathering at the base and grey weathering toward the top. Unit B is exposed in cliffs that are crosscut by numerous gullies (Figs. 3, 5, and 7). Unit B gradationally overlies unit A and grades upward into unit C. Unit B thickens from approximately 150 m in the northern part of the study area (UTM 577907E 7193694N) to >450 m at the measured section described here and appears thicker beyond the southern limit of mapping in NTS 106C/6.

The detailed section for unit B was measured on an unnamed mountain west of Pinguicula Lake and south of Pinguicula Creek (Figs. 6 and 7; UTM 573055E 7175671N NTS 106C/11). Units A through C are easily accessible in a gully and along the ridgeline. The top and bottom of the unit are both exposed at this location.

In the measured section, the basal contact is placed at the transition from dominantly siliciclastic (calcareous siltstone) to dominantly calcareous beds (silty dolomudstone). Above the basal contact, siltstone-dominated lithologies are present, but the predominant rock type is dolomudstone.

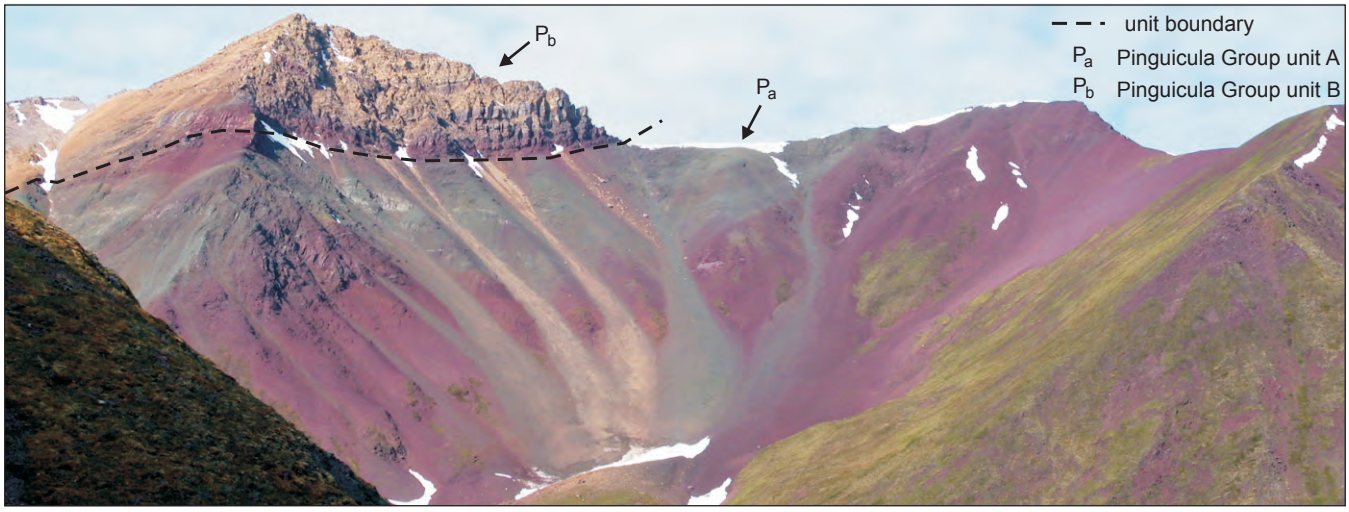

Figure 5. *Pinguicula units A and B in the northern part of the study area at the Pika occurrence. View to the southwest. NTS map sheet 106C/14 UTM 8W 573381E 7190576N NAD 27.*

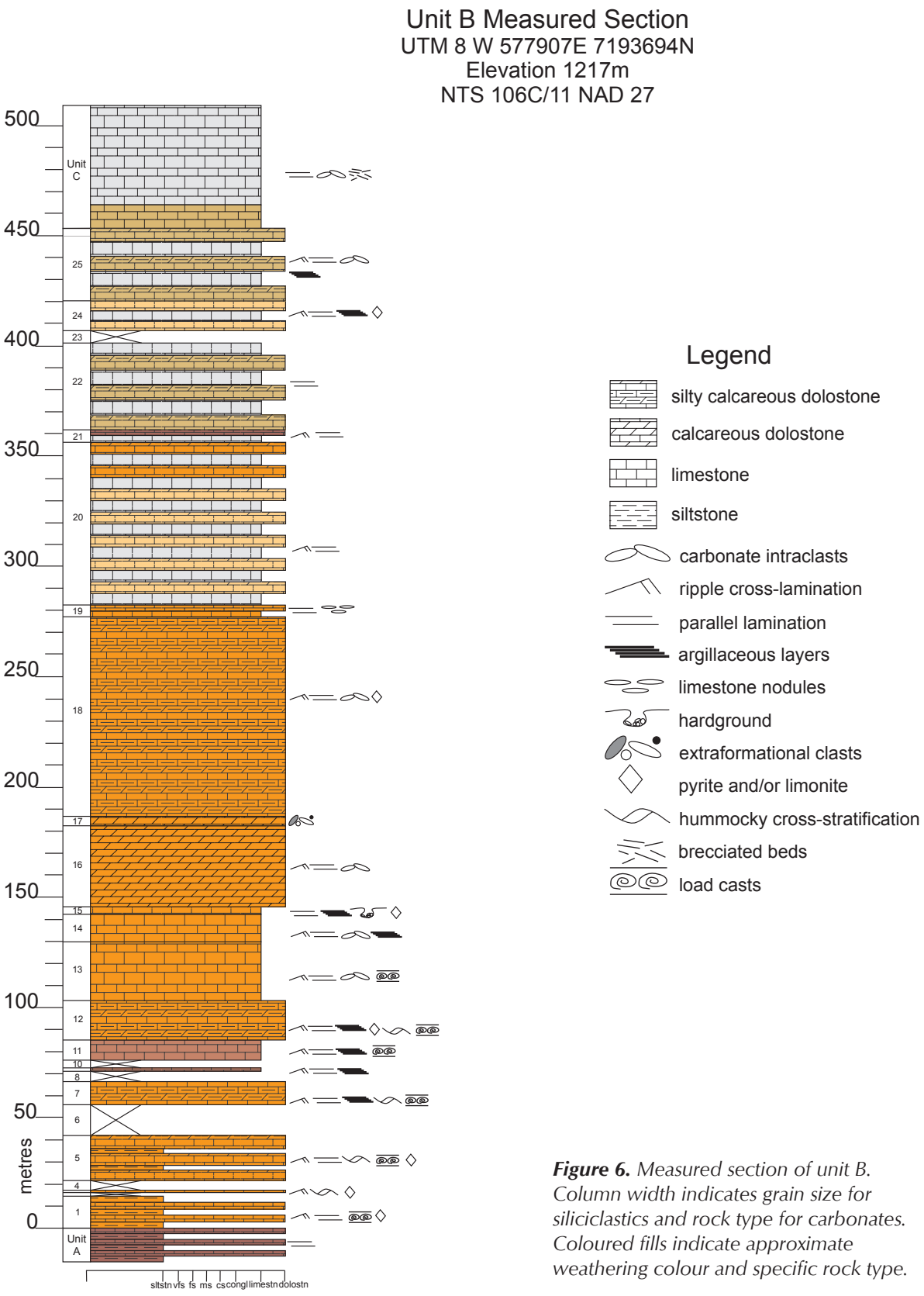

Figure 6. *Measured section of unit B. Column width indicates grain size for siliciclastics and rock type for carbonates. Coloured fills indicate approximate weathering colour and specific rock type.*

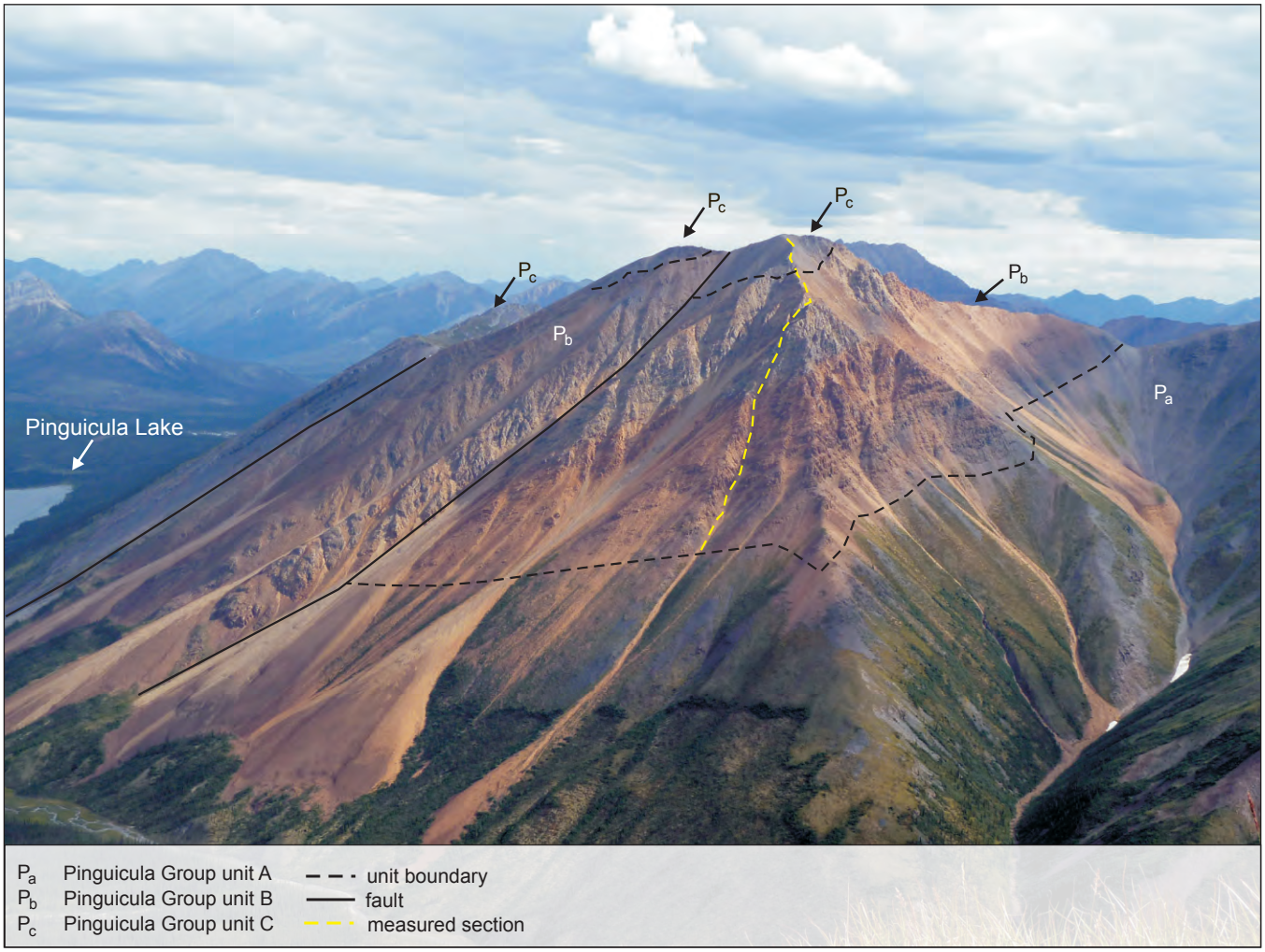

Figure 7. *Pinguicula units A, B, and C west of Pinguicula Lake and measured section. View to the southeast. NTS map sheet 106C/11 UTM 8W 573055E 7175671N NAD 27.*

The distinctive orange weathering colour cannot be used to define the boundary between units A and B because the lower part of unit B is maroon-weathering.

At base of the section, from 0 to 15 m (unit 1), is a rusty orange to maroon-weathering silty calcareous dolomudstone with interbeds of planar-laminated, maroon to grey siltstone. The silty calcareous dolostone contains abundant, disseminated, millimetric limonite-after-pyrite pseudomorphs. Discontinuous layers of carbonate mud, interlaminated with larger, sub-millimetric carbonate particles and organic matter form a wispy-laminated texture on the weathered surfaces. This wispy texture is present in most unit B dolostone and has been generated by differing degrees of pressure solution. Wispy-textured dolostone is interbedded with massive dolomudstone layers lacking any visible structures. In the overlying units 3 and 5, similar wispy lamination is present in the silty calcareous dolostone, but terrigenous silt and limonite pseudomorphs are also present. Unit 7 has similar characteristics, with the exception of disseminated limonite. Load casts, hummocky and swaley cross-stratification (HCS/SCS), ripple cross-lamination, and planar lamination are prominent in the lower 130 m of the section (Figs. 8a,b,c,d respectively). From 55 to 147 m (units 7-15), recessive, black, argillaceous, planar-laminated layers are interbedded with limestone and silty calcareous dolostone (Fig. 8e). Ripple cross-lamination and parallel lamination appear throughout the section. Units 9 and 11 (71 to 85 m) are composed of maroon-weathering, planar-laminated lime mudstone and wispy laminations are notably absent. Orange-weathering, silty calcareous dolomudstone in unit 12 (85 to 105 m) resembles the underlying dolomudstone units with black wispy laminations and millimetric limonite pseudomorphs. Units 13 through 15 (105 to 147 m) are

composed of orange-weathering lime mudstone with intermittent intraclast rudstone layers and lenses that are approximately 20 cm thick (Fig. 8f). Up-section in unit 16, intraclast rudstone layers are up to 1.5 m thick and are interbedded with dolomudstone. These layers consist of matrix and clast-supported tabular limestone clasts <1 cm to 15 cm long in a dolostone matrix. Some clasts maintained their tabular form during deposition whereas others did not and are slightly folded. Clasts are ungraded and are locally imbricated. Intraclast rudstone layers are intermittent in the section from 100 to 450 m; in total six intraclast rudstones are present in the section. In unit 16, small-scale, granular intraclast rudstone and floatstone are also present. Clasts are rounded and in a dolomudstone matrix. These intraclast rudstones are typically 1 to 3 cm-thick, and are overlain by dolomudstone. Some layers of

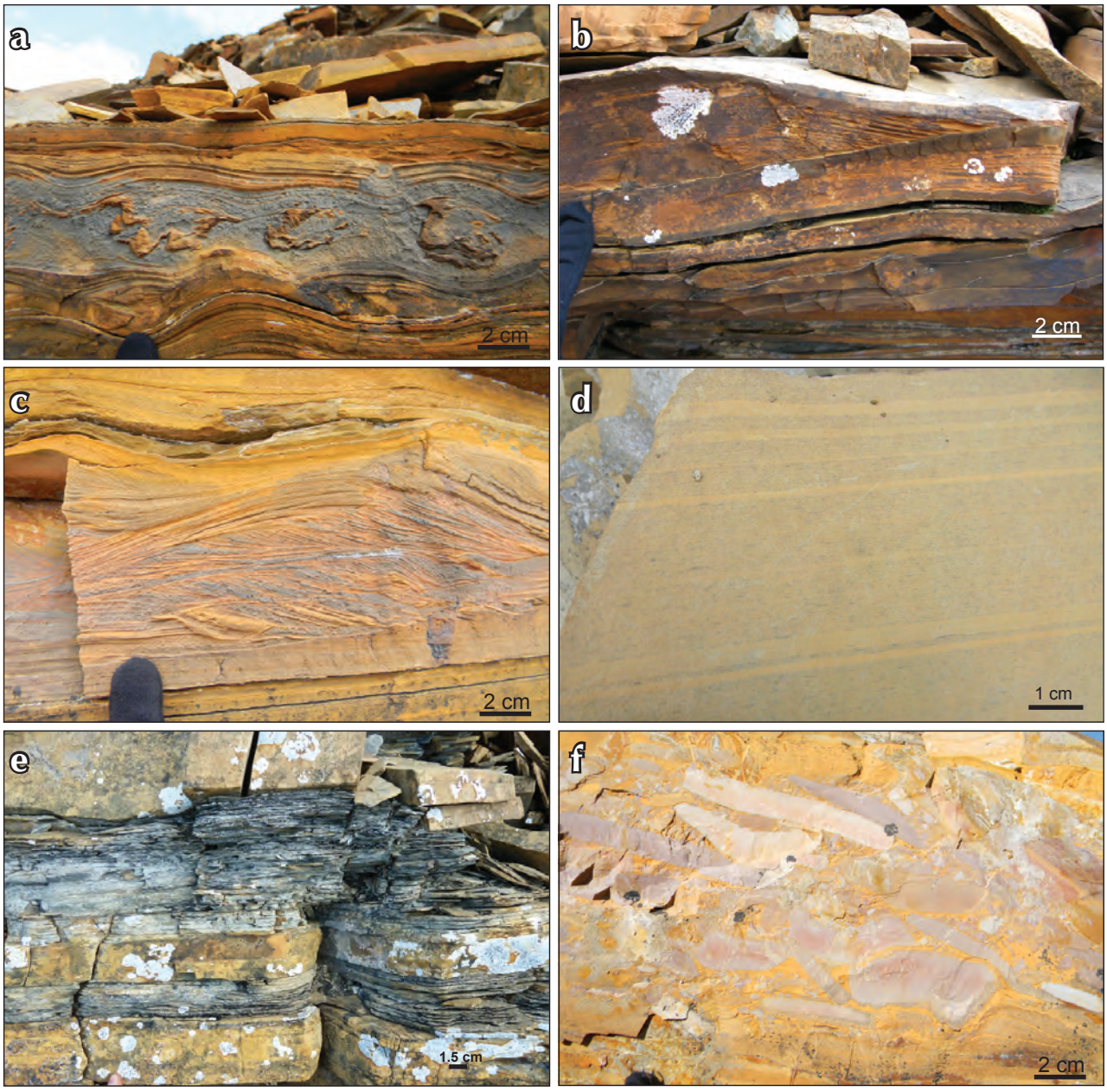

Figure 8. *Lithofacies of Pinguicula Group unit B in the Wernecke inlier.* ***(a)*** *Load casts from the lower 130 m of the section represent rapid deposition of high density sediment on low density sediment forming pillows.* ***(b)*** *Hummocky/swaley cross-stratification deposited above storm wave base in the lower 100 m of the section.* ***(c)*** *Ripple cross-lamination in orange-weathering silty calcareous dolostone. This is possibly a tempestite sequence with combined flow currents.* ***(d)*** *Parallel lamination in orange-weathering dolostone.* ***(e)*** *Argillaceous interbeds in silty calcareous dolostone.* ***(f)*** *Intraclast rudstone of limestone clasts in a dolostone matrix.*

small-scale intraclast rudstones are laterally discontinuous and suggest deposition onto a dolomud substrate.

In addition to limonite, pyrite is disseminated throughout beds in units 12, 15, 18, and 24 in the measured section (Fig. 9a). An in-filled cavity at ~147 m in unit 15 exhibits iron staining, pyrite, and void-filling, laminated argillaceous sediment, and possibly represents a hardground (Fig. 9b). Hardgrounds are lithified surfaces that develop on the sea floor because of low sedimentation rates or episodes of non-deposition (Collinson and Thompson, 1982; Flügel, 2004; Dalrymple *et al.*, 2010).

At approximately 185 m (unit 17) sparse extraformational matrix-supported clasts (orange-weathering limestone, green siltstone, and pink sandstone), several cm to >1 m in diameter, are randomly distributed in the dolostone (Fig. 9c). Some of the clasts are well rounded (*e.g.*, sandstone) whereas others are subangular (*e.g.*, siltstone and limestone).

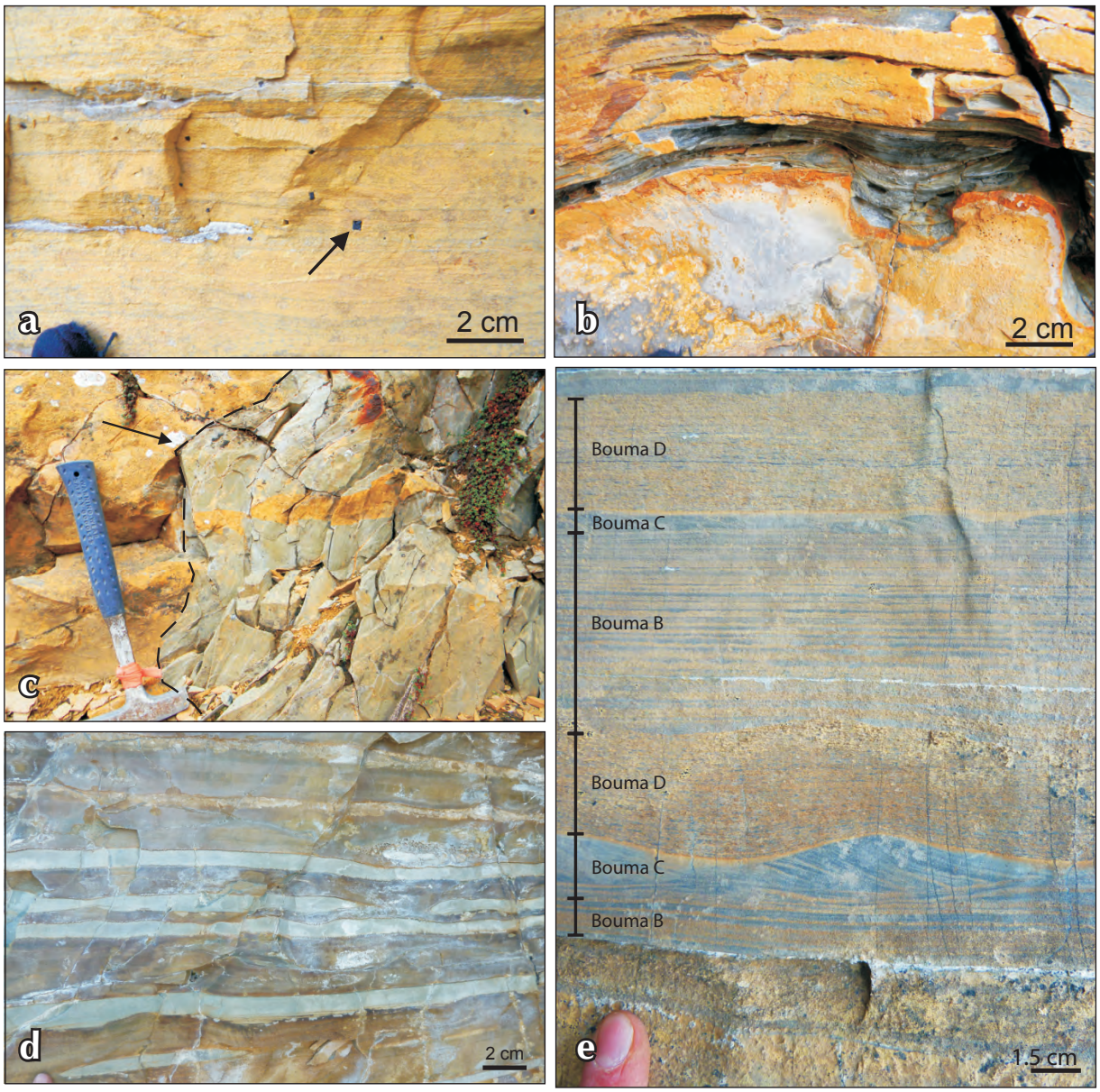

Figure 9. *Lithofacies of Pinguicula Group unit B in the Wernecke inlier.* ***(a)*** *Sparse sulphides in dolomudstone.* ***(b)*** *Hardground (lithified surface) that developed on the sea floor due to low sedimentation rates or episode of non-deposition.* ***(c)*** *Extraformational clast of green siltstone in orange-weathering dolomudstone possibly derived from the Wernecke Supergroup and transported into the basin.* ***(d)*** *Lime mudstone (grey) interbedded with dolomudstone (orange) is a common lithofacies in unit B.* ***(e)*** *Apparent partial Bouma sequences in unit 25 of measured section reflects transport and deposition of sediment on a carbonate slope or basin floor.*

Unit 18 (187 to 276 m) is silty calcareous dolostone with intraclast rudstone layers (30 cm thick) and pyrite crystals and limonite pseudomorphs. Massive microcrystalline dolostone laminae and beds are interbedded with wispy-laminated beds, as well as small-scale intraclast rudstone beds. At 257 m a graded bed with intraclasts at its base contains asymmetrical ripple foresets in which the grain size of foreset laminae alternates between silt and coarse sand grade.

Units 19 to 25 from 276 to 452 m (Fig. 9d) consist of distinctive interbedded grey-weathering limestone (cm-scale thickness) and orange-weathering dolostone (cm to dm-scale thicknesses). Both the lime mudstone and dolomudstone have more resistantly weathering wispy laminae with interlaminated particles and/or crystals of carbonate and quartz. The weathering colour grades from orange and yellow near the base of the formation to grey, with brown near the top of the section. In units 23-25, well-preserved ripples overlain by planar lamination (Fig. 9e) are present. Below the transition into unit C, three intraclast rudstone beds 20 cm - 1 m thick are present in unit 25. The transition from unit B to unit C is placed where planar-laminated, pervasively veined, predominantly grey-weathering dolomudstone first appears and yellow-weathering dolostone is less prevalent.

Regional Variation

Throughout the study area, unit B has a uniform assemblage of sedimentary structures, lithologies and stratigraphic patterns. Ripple cross-lamination, parallel lamination, hummocky and swaley cross-stratification, intraclast rudstone, and possible turbidites or tempestites are exposed in most outcrops of unit B. Differences in unit B stratigraphy throughout the study area are related to the scale of the structures and sedimentary components. For example, intraclast conglomerates are more abundant, thicker, and lower in the section at the PIKA mineral occurrence (UTM 573887E 7190732N) and other locations to its northeast. Pyrite is especially conspicuous at the measured section and locations to its south (UTM 580954E 7155399N).

UNIT C

Description

Unit C is a carbonate-dominated succession that is distinguished at the outcrop-scale from unit B by its blue-grey weathering colour. Unit C is also distinguished from unit B by its greater abundance of diagenetic features such as carbonate veins, zebra dolomite, masses of crosscutting coarse dolomite spar, locally abundant stylolites, and by a fetid odour when broken. Unit C conformably and gradationally overlies unit B, and is 590 m-thick in the measured section. It is thickest in the northern part of the study area (1800 m). Locally apparent thicknesses may be deceptive, especially where unit C has been thickened by structural repetition of strata by west-directed thrust faulting (Fig. 10; Thorkelson, 2000).

A detailed section was measured adjacent to the headwaters of 'Dolores Creek' (Figs. 11 and 12; 588305E 7190109N NTS 106C/14). The lower part of the section follows 'Dolores Creek' and a tributary of 'Dolores Creek' before tracing up a mountainside and ending at the top. Unit C is difficult to access in much of the study area due to its steep cliffs. Attempts were made to measure unit C strata in other locations, but were abandoned on account

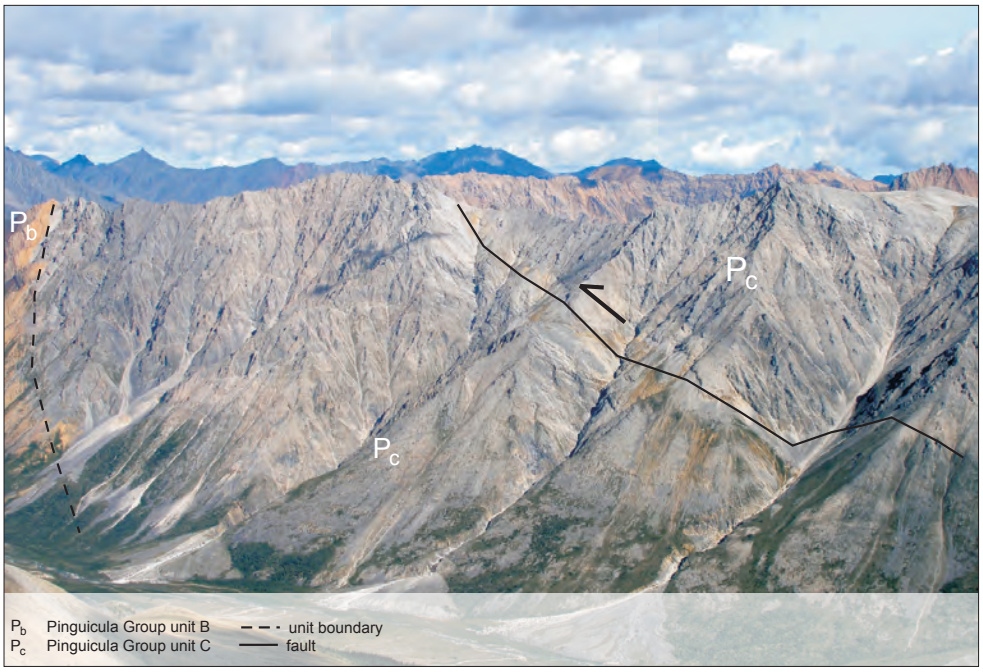

Figure 10. *Pinguicula units B and C with structural repetition of Unit C strata from west-directed thrust faulting. View to the northeast. NTS map area 106C/14 UTM 578147E 7193042N.*

of the impassible nature of the exposures. The measured section offers an accessible route to a gradational, although partly covered, lower contact with unit B. The upper contact with the overlying Dolores Creek Formation of the Hematite Creek Group (Turner, 2011) is possibly faulted. The contact throughout the study area varies from faulted to angular to concordant. An alternate location north of Pinguicula Creek provided an undisturbed section of unit C and the unit C-Dolores Creek Formation contact (575186E 7177355N NTS 106/C/14). At this location both the strike and dip of unit C and the Dolores Creek Formation differ by 30°, whereas east of the measured section the structural orientation of the two units do not differ; these observations suggest that unit C may have been locally tilted prior to deposition of the basal Mackenzie Mountains supergroup or that the units reacted differently during deformation.

At the measured section (Fig. 11), the base of unit C overlies a thin (6 m) covered interval. The transition from unit B to unit C is marked by the disappearance of interbedded cm-scale limestone and cm to dm-scale dolostone, turbidites, and yellow to brown-weathering; instead, strata are characterized by grey weathering, planar lamination, abundant carbonate veins, and zebra texture. The contact is placed where planar-laminated, pervasively veined, predominantly grey-weathering dolomudstone first appears. The lower part of the section from 0 to 48 m (units 1, 2, and 4) are yellow-orange to grey-weathering, blue-grey and white calcareous dolostone with planar, parallel-laminated to cm and dm-scale bedding. Both massive, microcrystalline mm to cm-scale beds, wispy planar laminations with millimetre carbonate crystals, and black intraclasts are present in the rock. Zebra dolomite texture (Vandeginste *et al.*, 2005) and dolostone breccia masses associated with copious volumes of coarsely crystalline sparry dolomite are common (Fig. 13a,b). Submillimetre to centimetre black and white banding is common, and may have formed by the same processes as the zebra texture that is apparent higher up in the section. After a short covered interval (7 m), buff to pale grey-weathering, medium to dark grey, planar, parallel-laminated to bedded calcareous dolostone with pervasive veining is present (56 to 190 m). Massive, microcrystalline beds are dominant, but wispy-laminated intraclastic beds are also present. The grey calcareous dolostone has a wispy white texture in unit 7 (Fig. 13c). There are two dm-scale intraclast rudstone

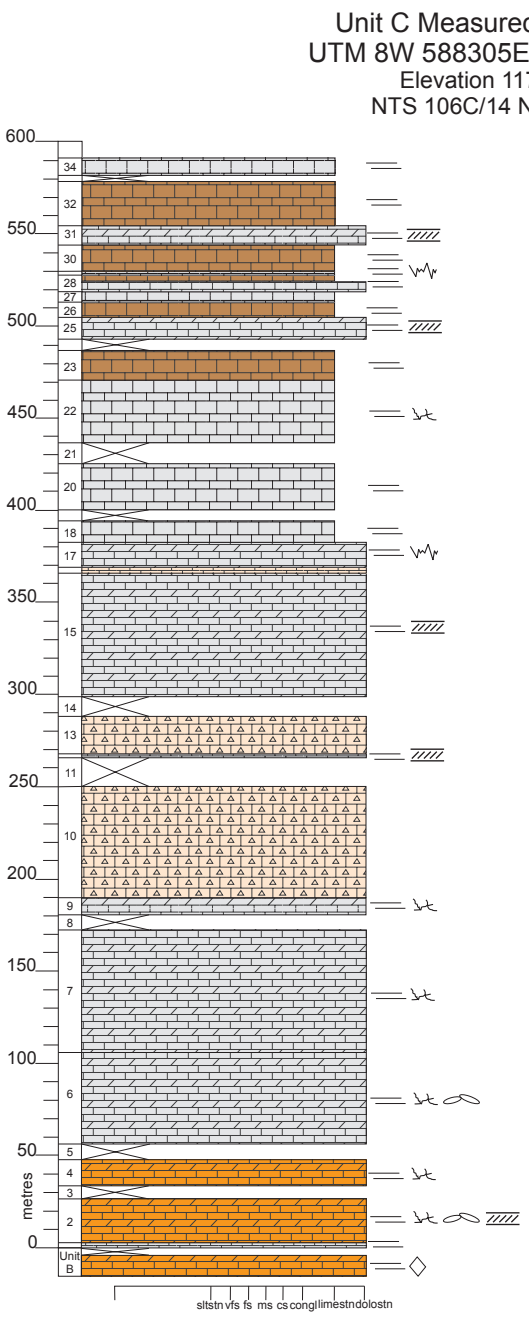

Figure 11. *Measured section of unit C. Column width indicates grain size for siliciclastics and rock type for carbonates. Coloured fills indicate approximate weathering colour and specific rock type.*

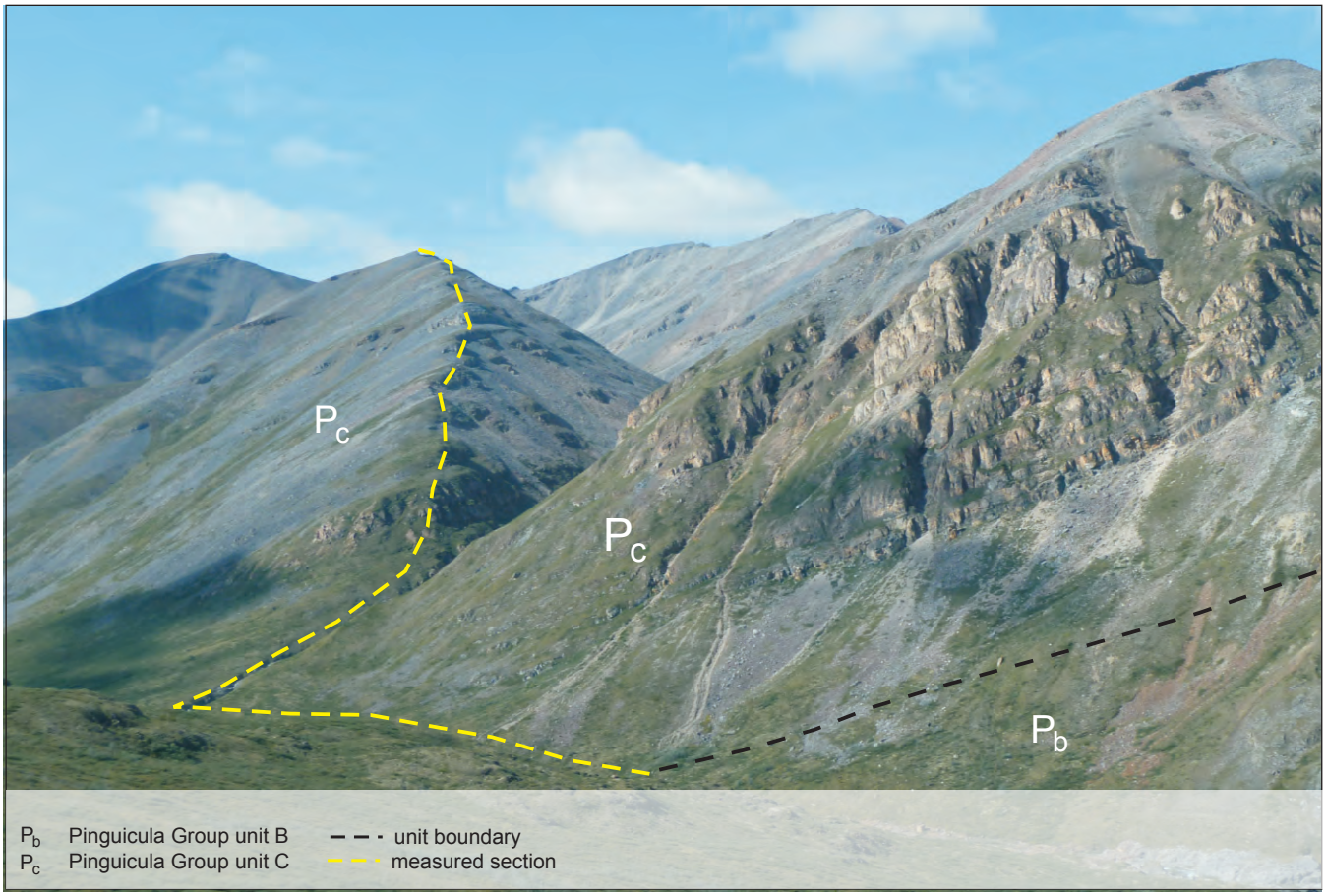

Figure 12. *Pinguicula units B and C. View to the southwest. Measured section runs along two creek beds before following the ridgeline up mountain. NTS map sheet 106C/14 UTM 8W 588305E 7190109N.*

layers in the lower 75 m of the section (units 2 and 6), with tabular clasts up to 7 cm long. The layers are similar to those described in unit B. A dense network of calcite veins cut across the lower 190 m of the section. Two distinctly pink-weathering units (units 10 and 13 from 190 to 287 m) of coarsely crystalline dolostone spar with cm-scale crystals occur midway through the section (Fig. 13d). In one location coarsely crystalline dolostone crosscuts the zebra dolostone, suggesting that units affected by zebra dolomitization were subsequently affected by a separate generation of coarsely crystalline dolomite veins and zones. The combined 80 m of exposed outcrop of coarsely crystalline dolostone (with a covered section and zebra dolomite bed in between) is overlain by ~80 m of yellow-grey-weathering, white and grey calcareous dolostone with planar, parallel-laminated cm to dm-scale beds containing zebra texture (units 15 and 17). These units are above and below a sparry dolostone layer (unit 16) approximately 3 m thick. In the overlying 100 m, units 18, 20, and 22, are yellow-grey-weathering, dark grey cm to dm-scale planar-bedded limestone with crosscutting veins (Fig. 13e). The uppermost 110 m of the section (units 23 to 34 with some covered intervals) consist of brown-weathering, thinly bedded limestone units interbedded with calcareous dolostone with zebra texture (Fig. 13f). The section ends at the top of the mountain in grey-weathering limestone. Where the upper contact is structurally undisturbed, it is an unconformity characterized by an angular to concordant boundary with the Dolores Creek Formation. Mineralization in unit C occurs as malachite and azurite staining, with rare galena and pyrite in crosscutting veins, zebra dolomite, and brecciated dolostone.

Regional Variation

Unit C thins toward the southern part of the study area, where it expresses the same features as in the north but in varying degrees. Zebra texture is less abundant in the south, but pervasively veined limestone beds are common. In some southern locations, unit C is interbedded with fissile black siltstone beds.

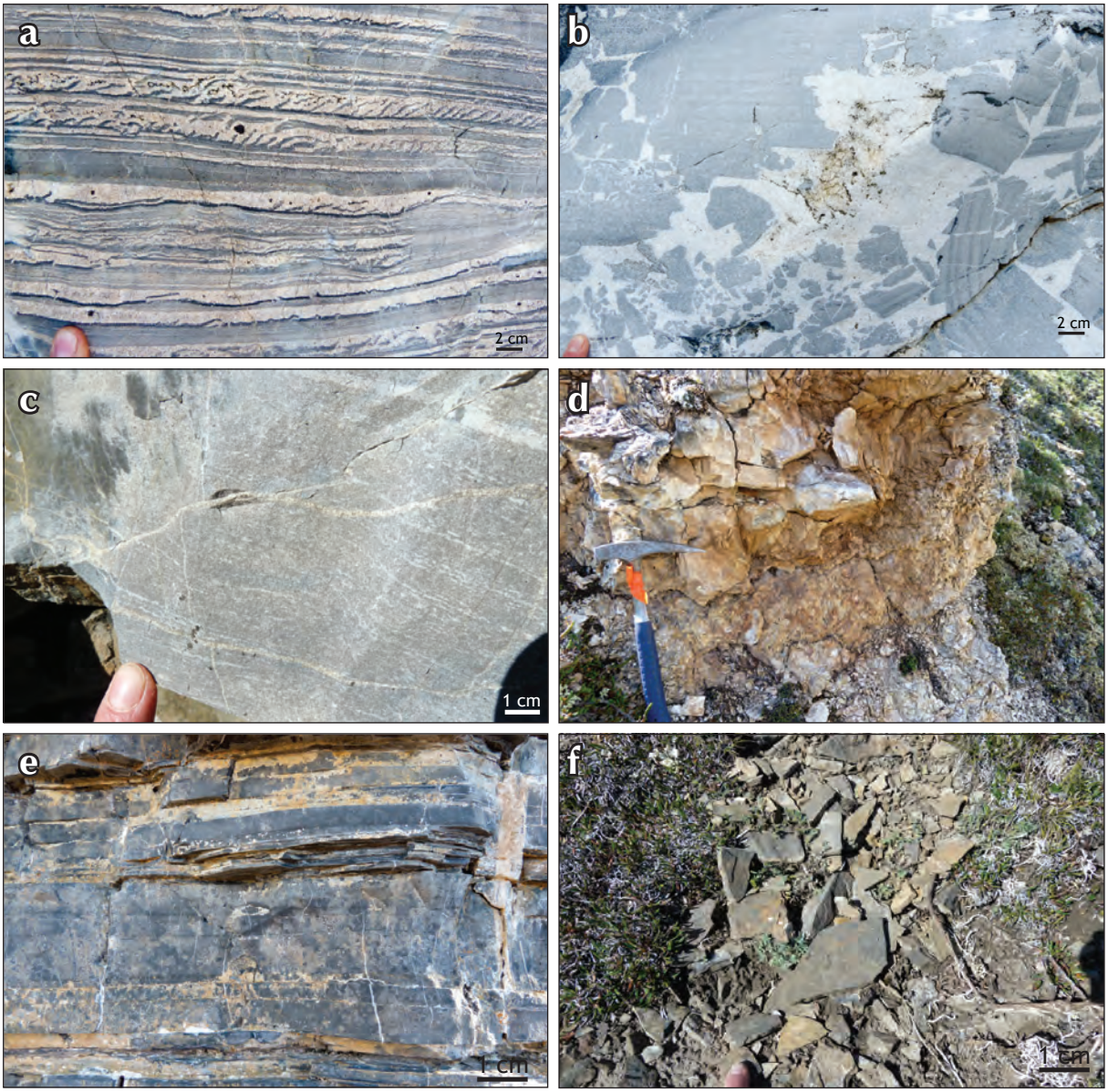

Figure 13. *Lithofacies of Pinguicula Group unit C in the Wernecke inlier.* ***(a)*** *Zebra texture in dolostone.* ***(b)*** *Brecciated and dolomitized limestone beds.* ***(c)*** *Wispy texture in dolostone in unit 7 of measured section.* ***(d)*** *Pink-weathering coarsely crystalline dolomite spar.* ***(e)*** *Dark grey limestone bedded limestone with pervasive veining.* ***(f)*** *Recessive brown-weathering, thinly bedded limestone that forms interbeds with thickly bedded grey-weathering, dark grey limestone near top of section.*

INTERPRETATION

Unit A is a fining-upward succession that appears to have been deposited in a subsiding basin. Based on thickness distribution, the deepest part of the basin was in the southern part of the study area. The basal pebble conglomerate and sandstone may represent beach deposits that accumulated during flooding of the underlying regolith of the Wernecke Supergroup. As the basin deepened, a monotonous succession of siltstone was deposited. The absence of sedimentary structures other than lamination, or significant grain size variation in the main siltstone-dominated part of the succession, suggests that this formation was deposited below storm wave-base and was largely unaffected by episodic flux in sediment supply.

Unit B was deposited mainly on a carbonate slope. As unit B grades from silty calcareous dolostone interbedded with siltstone at the base, the interpreted paleoenvironment

becomes deeper, and the rocks are dominated by carbonate. Load casts truncated by overlying beds and the prominence of hummocky/swaley cross-stratification (HCS/SCS) reflect storm activity and deposition below fair-weather wave-base but above storm wave-base (Dalrymple *et al.*, 2010). For the water column to develop sufficient fetch to form structures such as HCS/SCS, the basin would probably need to be several hundred kilometres across. As HCS/SCS become less prominent up-section, intraclast rudstone layers and lenses become conspicuous, reflecting redeposition of thin beds of early-lithified slope lime mudstone down-slope by debris flows triggered by gravitational failure. Prominent, large extraformational clasts are interpreted to be derived from exposures of Wernecke Supergroup strata; given the slope-environment of deposition, the clasts were probably eroded rapidly from uplifted subaqueous fault blocks, and, if so, would indicate syndepositional tectonic activity. Sparse, black argillaceous interbeds represent a terrigenous sediment component that was either delivered episodically, or that accumulated during times when carbonate sediment production temporarily ceased. Moving up-section, turbidites are present. The graded bed with intraclasts at its base and asymmetrical ripple foresets suggests deposition of the bed as a tempestite rather than from a turbidity current because of the interlamination of foreset grain size; turbidites are generally characterized by gradual upward fining rather than fining by intergradation. Moving up-section, through the monotonous, interbedded limestone and dolostone beds, thin Bouma like sequences reflect deposition on a carbonate slope during continued basin deepening.

Unit C transitions from a carbonate slope facies at its base to a deeper-water facies. Intraclast rudstone at the base of unit C may suggest that the lower part of the formation was deposited on a carbonate slope (Dalrymple *et al.*, 2010). Unit C lacks sedimentary structures such as hummocky cross-stratification that would support deposition of the succession above storm wave-base and higher up on the slope. The planar-laminated carbonate rock that dominates unit C appears to have been deposited on a basin floor that lacked a significant slope as evidence of tectonic or gravitational instability is lacking, except at the base of the formation. The lime mudstone laminae in unit C probably formed as carbonate that was directly precipitated from solution in the water column (Grotzinger, 1989). Black siltstone beds reflect either intervals of increased fine terrigenous sediment supply or temporary cessation of carbonate deposition.

The development of zebra texture throughout much of unit C has led to the textural obliteration of some sedimentary structures. Consequently, identifying the depositional facies in the layers that have been affected by zebra texture is problematic. The timing of the hydrothermal activity that affected unit C is unknown; similar sparry dolomite is not common in unit B or in carbonate-dominated strata of the overlying Hematite Creek Group. Future work should include examination of basal siltstone of the Dolores Creek Formation in search of coarse lags that may contain clasts of unit C, to determine whether the hydrothermal event predated deposition of the Mackenzie Mountains supergroup.

The amount of time represented by the unconformity at the top of the Pinguicula Group is unknown owing to the as-yet uncertain depositional ages of both the Pinguicula Group and the basal Mackenzie Mountains supergroup. Previous interpretations of the unconformity as a karst surface infilled with coarsely crystalline spar attributed to emergent conditions (Thorkelson, 2000) are suspect as the pockets of coarse spar are herein interpreted to have been developed at depth as a result of hydrothermal activity.

DETRITAL ZIRCON GEOCHRONOLOGY

Detrital zircon geochronology on Pinguicula Group unit A sandstone (Wernecke and Hart River inliers) and lower Fifteenmile Group siltstone (Coal Creek inlier) can be used to determine sediment provenance and to provide maximum depositional age constraints. The maximum depositional age of the Pinguicula Group age has hitherto been constrained by its unconformable relationship with underlying Hart River sills (1380 Ma) and the minimum age of detrital muscovite in the overlying Hematite Creek Group (<1033 Ma; Thorkelson, 2000; Medig *et al.*, 2010).

METHODS

Three samples from Pinguicula Group unit A sandstone in the Wernecke inlier, one sample from unit A sandstone in the Hart River inlier, and one sample from the lower Fifteenmile unit PR5 in the Coal Creek inlier were collected for detrital zircon U-Pb geochronology. Sample details are summarized in Table 1.

Samples were processed at Simon Fraser University using standard crushing and milling techniques, with mineral separation using a Wilfley table and heavy liquids. All samples, with the exception of KM09-10-3-1C, were

Table 1. *Detrital zircon samples and locations.*

Sample	Rock Type	UTM Coordinate NAD 27	Field Relation	Inlier
KM09-1-4-1C	sandstone	8W 572876E 7191172N	Pinguicula Unit A above bleached Wernecke Supergroup regolith	Wernecke
KM09-10-3-1C	sandstone	8W 573352E 7167986N	Pinguicula Unit A – base not exposed	Wernecke
KM09-12-2-2C	sandstone	8W 574603E 7159828N	Pinguicula Unit A – base not exposed	Wernecke
KM10-8-1-1C	sandstone	8W 418221E 7165910N	Pinguicula Unit A above Hart River sills	Hart River
KM09-18-1-1C	siltstone	7W 552687E 7186821N	Lower Fifteenmile PR5 above calcrete regolith of Wernecke Supergroup	Coal Creek

run through an LB-1 Frantz magnetic separator at a low current (0.25 A; 15° front slope, 10° side slope) to remove ferromagnetic and highly paramagnetic minerals. A low current was used to avoid biasing the sample by preferentially separating out the more paramagnetic zircon grains, which are typically removed at much higher currents (1.2–1.8 A). Grains were then randomly chosen from the processed sample to avoid biasing.

The grains were mounted on an epoxy puck, polished, and coated with a thin gold coating at the J.C. Roddick Ion Microprobe Laboratory at the Geological Survey of Canada in Ottawa. The mounted grains were then imaged on the scanning electron microscope (SEM) at the GSC using both backscatter (BSE) and cathodoluminesence (CL) imaging techniques.

The zircon grains were analysed on the Sensitive High Resolution Microprobe (SHRIMP II) at the Geological Survey of Canada in Ottawa following analytical procedures summarized by Stern (1997). Zircon standards appropriate for the expected Proterozoic age range of the unknowns were interspersed on the epoxy puck with sample grains. Both a primary and secondary zircon standard was used; z6266 Sri Lankan zircon dated at 559 Ma and z1242 dated at 2679 Ma, respectively. Errors associated with standards and calibration methods followed Stern and Amelin (2003).

A small proportion of the grains exhibit relatively high common Pb content, and/or high measured UO/U ratios. These features are commonly an indicator of altered or imperfect (cracked or with inclusions) zircon grains, and so the data were screened for low common Pb counts and UO/U ratios within the range of the calibration standard. SEM images of each grain were examined after analyses to determine if the ion beam spot intersected inclusions, cracks, mixing of compositional zones, or metamict zones within the grain that may account for high common lead and high UO/U ratios. Some of the ion beam spots did intersect such features, but most grains did not appear to have any characteristics that might compromise the results. Intersection with grain anomalies may be attributed to stage drift during automated acquisition. In total, 23 analyses were excluded from further data interpretation based on high common Pb contents and/or measured UO/U ratios.

PRELIMINARY RESULTS

A total of 342 grains were analysed from the five samples. The three samples of the Pinguicula Group from the Wernecke inlier show similar patterns, with most ages between *ca.* 1430 and 3300 Ma, with significant peaks between 1600 and 1950 Ma and 2300 to 2800 Ma (Fig. 14). Based on stratigraphic consideration, the Pinguicula Group was deposited at some time between 1380 and 1033 Ma (Medig *et al.*, 2010): this is supported by the age of the youngest zircons in the samples. Results for sample KM09-10-3-1C from the Wernecke inlier included a single zircon grain with a $^{207}Pb/^{206}Pb$ age of 1144±25 Ma[2]. This age was replicated with a second, although more discordant analyses on the same grain at 1131±27 Ma. Although the occurrence of this grain suggests that the depositional age of the Pinguicula Group could be younger than 1144±25 Ma, such an interpretation should not be made on the basis of a single, non-repeated result because it is not statistically viable. This result should be replicated with data from additional samples before accepting this as a maximum age. Until further work substantiates this result, the maximum age for the Pinguicula Group should be considered to be 1380 Ma based on the unconformable relationship with the Hart River sills (Medig *et al.*, 2010).

[2] *1σ errors reported on ages.*

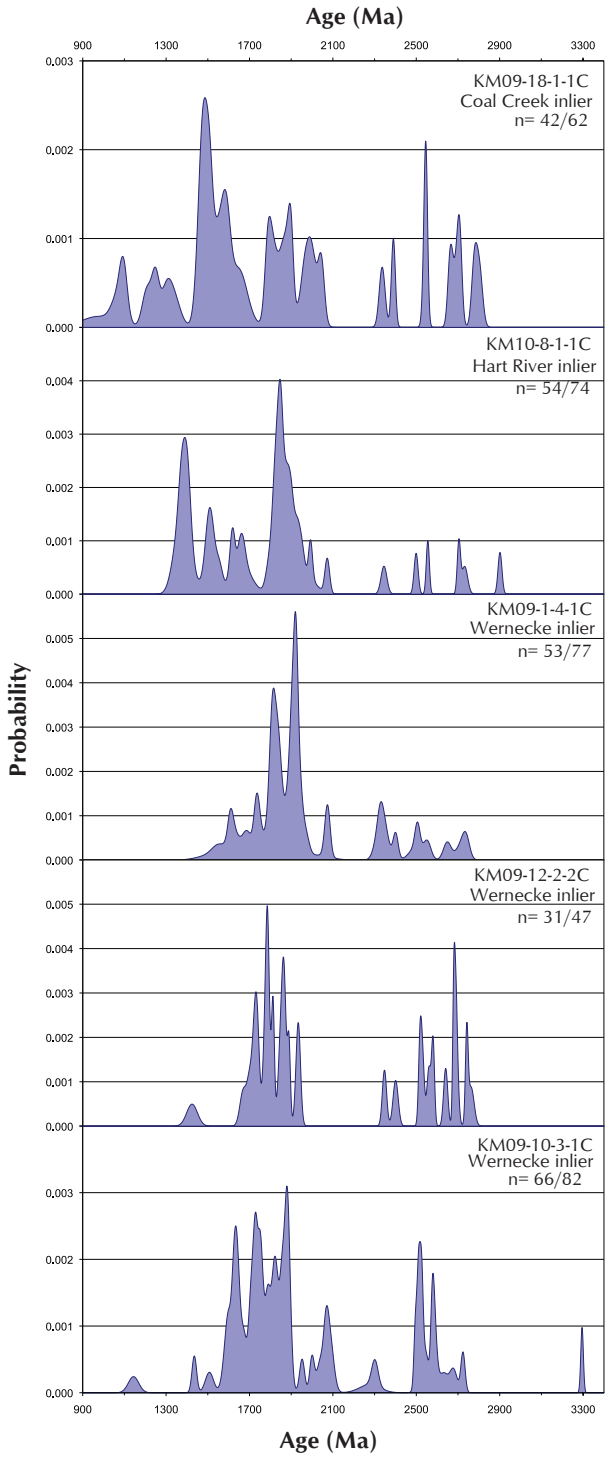

Figure 14. *Detrital zircon sample probability density distribution diagrams of $^{207}Pb/^{206}Pb$ ages. Grains with high common lead, high UO/U ratios, and/or analyses over 5% discordance were not included in the results. The quotient "n" indicates the number of 95-105% concordant grains over the total number of grains analysed. The graphs were produced using AgeDisplay (Sircombe, 2004).*

The sample from the Hart River displays significant 1750-2000 Ma and 1350-1450 Ma detrital zircon populations. There is also a series of minor peaks from the Neoarchean. The youngest zircon grains from the sample in the Hart River inlier (KM10-8-1-1C) have $^{207}Pb/^{206}Pb$ ages of 1342 ± 27 Ma and 1232 ± 172 Ma.

In the sample from the Coal Creek inlier, there is one prominent peak between 1450 and 1500 Ma. There are a series of smaller peaks between 1050 and 1350 Ma, 1500 and 2050 Ma, and 2300 and 2850 Ma. The youngest grain in the Coal Creek inlier sample, KM09-18-1-1C, has a $^{207}Pb/^{206}Pb$ age of 972 ± 78 Ma. Two other grains have $^{207}Pb/^{206}Pb$ ages of *ca.* 1100 Ma.

PROVENANCE

The samples analysed contain significant populations of Neoarchean and Paleoproterozoic detrital zircon grains. These grains may have been derived from the Laurentian craton or recycled from the underlying Wernecke Supergroup (Furlanetto, 2009). All samples have detrital zircon ages that overlap in time with the North American Magmatic Gap (NAMG; 1610-1490 Ma; Ross and Villeneuve, 2003). The underlying Wernecke Supergroup lacks grains from this time interval and is consequently not a plausible source. Ages in this range from North America have been recorded from the Western Channel diabase (*ca.* 1590 Ma), but the ages were derived from baddeleyite, which suggests that these mafic rocks would not be a plausible source for detrital zircon in the Pinguicula and lower Fifteenmile group samples (Ernst and Bleeker, 2010; Hamilton and Buchan, 2010). In addition, the age range from the Western Channel diabase does not encompass the full range of ages in the NAMG in Pinguicula and lower Fifteenmile group samples. Based on these two points, alternative sources for 1610-1490 Ma ages are needed to account for these grains. Other sources that have been proposed rely on paleocontinental reconstructions that suggest that Australia was adjacent to northwestern Laurentia in the Proterozoic and could be a source of 1610-1490 Ma zircon (Bell and Jefferson, 1987; Dalziel, 1991; Hoffman, 1991; Moores, 1991). Specific sources on the Australian continent include the Williams and Naraku batholiths in the Mt. Isa inlier (1520 to 1490 Ma), Hiltaba Granite Suite on the Grawler craton (1600 to 1560 Ma), and the Musgravian gneiss protoliths in the Musgrave Province (1600 to 1540 Ma; Betts and Giles, 2006; Wade *et al.*, 2008).

Another population of grains with ages between 1360 and 1400 Ma from the Hart River inlier sample are probably derived from the underlying Hart River sills. Three zircon samples were collected from the Hart River sills in the southern Ogilvie Mountains and all yielded zircon. Ages from these samples are 1380+4.0/-3.8 Ma, 1385.8±1.9 Ma, and 1383.0+5.9/-5/2 Ma[3] (Abbott, 1997). A sample collected from the Hart River sills in the Wernecke Mountains yielded an age of 1382 Ma (Thorkelson, 2000).

The youngest grain in the samples analysed, with an age of *ca.* 1150 Ma, may have been sourced from the Grenville orogen as has been proposed for younger Neoproterozoic successions that have significant detrital zircon populations from this time interval (Rainbird *et al.*, 1997). Metamorphic and igneous rocks with Grenville-like ages are present in the subsurface of Yukon and nearby Northwest Territories (Milidragovic *et al.*, 2011) and may have contributed zircon to the sample populations; however, this option would require local exhumation of the middle crust, and appropriate sources have not yet been identified.

In summary, the detrital zircon analytical results show that Neoarchean and Paleoproterozoic populations were possibly derived locally from the underlying Wernecke Supergroup, Wernecke breccia, and Hart River sills or from adjacent Laurentia. Mesoproterozoic populations may also have been derived from the Laurentia or from far away as the Grenville orogen. Other populations have no obvious sources in North America and as such could have been derived from an exotic continent such as Australia.

CORRELATION

Pinguicula Group unit A in the Wernecke inlier is correlated with unit A in the Hart River inlier (Abbott, 1997). This correlation is not disputed because both overlie the Hart River sills and both contain analogous stratigraphy[4] (Abbott, 1997; Medig *et al.*, 2010). The previous correlation between unit A and unit PR1 in the Coal Creek inlier may not be correct, because recent work in the area indicates that units PR1 and PR5 are laterally equivalent (Medig *et al.*, 2010; Macdonald *et al.*, 2011). Macdonald *et al.* (2011) suggested that much of this stratigraphy was incorrectly mapped and is in fact part of the Mackenzie Mountains supergroup. If so, then these units are probably younger than the Pinguicula Group. Further work is needed to resolve these correlation problems.

The Pinguicula Group has been correlated with the Dismal Lakes Group in the Coppermine Homocline (Cook and MacLean, 1995). The depositional age of the Dismal Lakes Group is constrained by the overlying Coppermine River basalts and is therefore older than 1270 Ma (LeCheminant and Heaman, 1989; Cook and MacLean, 1995; Frank *et al.*, 2003). Based on the dataset this correlation is possible, but analysis of a single 1144 Ma zircon from Pinguicula Group unit A in the Wernecke inlier raises uncertainties. Further work to recover additional grains of this age is required in order to test the correlation between the Dismal Lakes Group and Pinguicula Group.

CONCLUSIONS AND FUTURE WORK

The Pinguicula Group (composite thickness ~1350 m) was deposited in comparatively deep water in a subsiding basin. Initial deposits of unit A were deposited during flooding of the post-Wernecke Supergroup unconformity and were followed rapidly by deposition of a monotonous succession of fine terrigenous clastic rocks; textural evidence for shallow-water conditions is everywhere absent. Deposition of the carbonate-dominated unit B began as an ephemeral shallowing event, which brought the sea floor within range of storm waves. Regional conditions changed to limit the supply of terrigenous material and promote the precipitation of carbonate mud. Gradual deepening ensued and was accompanied by development of widespread slope environments characterized by gravitational instability and resedimentation of carbonate material downslope as early-lithified tabular clasts and turbidites; it is unclear whether one regional slope is implicated or numerous, presumably fault-related slopes were present. Rare evidence for development of fault scarps from which large clasts of the Wernecke Supergroup were shed is, however, locally present. Unit C records generally quiescent conditions on a basin floor below storm wave-base and below the photic zone.

Zircon grains with Neoarchean to Paleoproterozoic ages may have been locally derived from the underlying Wernecke Supergroup and/or from Laurentia. A distinct population of zircon grains between 1610-1490 Ma (NAMG) does not have any known sources in Laurentia. They do, however, have several possible sources in

[3] *2σ error reported on Hart River sill ages.*

[4] *Detailed stratigraphic sections measured in the Hart River inlier Pinguicula Group units A, B, and C and have analogous stratigraphy. This data will be published in a future paper.*

Australia. Other younger Mesoproterozoic zircon grains with 1360-1400 ages were probably derived from the underlying Hart River sills. The youngest sample population, approximately 1100 Ma, may have been derived from the Grenville orogen.

Previous attempts to correlate the Pinguicula Group with other Proterozoic units such as the lower Fifteenmile Group to the west or the Dismal Lakes Group to the east have been based on similarities in lithology and the stratigraphic position of the succession between the <1610 Ma Wernecke Supergroup (Furlanetto *et al.*, 2009) and the overlying <1033 Ma Mackenzie Mountains supergroup (Thorkelson, 2000). The ~500 million year age gap between these two supergroups allowed for significant latitude in the positioning of the Pinguicula Group and a range of possible correlations. Field observations indicate it unconformably overlies, and is therefore younger than, the Hart River sills, which are dated at 1380 Ma. One detrital zircon age from Pinguicula unit A in the Wernecke inlier suggests that it may be younger than 1144 Ma; however, further work is required to replicate this result and make definitive statements. If additional detrital zircon grains of this age are found in unit A and a statistically viable population established, then correlations with the Dismal Lakes Group, which was deposited before 1270 Ma, would be dismissed. However, unless additional grains with ages <1270 Ma are found, the correlation with the Dismal Lakes Group will remain plausible.

Much remains unknown about the Pinguicula Group and future work is warranted in a number of areas. Investigation of the geochemistry of the basin may provide additional information on Mesoproterozoic ocean chemistry and may assist in regional correlations. A detailed petrographic and trace element study of unit A hematitic, maroon siltstone and dark grey siltstone would help to determine whether the formation was deposited under open-marine conditions or in a restricted basin, and the extent of shallow-water ferruginous conditions and deep-water anoxia. This information could contribute to the growing knowledge of Proterozoic geochemical evolution of Earth's surface.

A paleocurrent study from unit B current ripples and turbidites would provide provenance direction for the sediment and if the assumption was made that the direction had not changed drastically since the deposition of unit A, it could be used for provenance determinations in unit A in addition to the detrital zircon grain ages and an investigation into clasts from unit A conglomerate. Paleocurrents could also be used to determine the configuration of the tectonically active stage of basin development and locations of possible paleofaults.

Further investigation of the different phases of hydrothermal fluids in unit C may provide further information on age, mineralization, and temperature at the time of formation. Base metal potential and the possibility of hydrocarbon migration in the dolostone should be assessed through a paragenetic study of the hydrothermal dolomite and breccia bodies in unit C, using cathodoluminesence, trace elements, and fluid inclusions to determine fluid temperature and composition.

Finally, continuing study of the overlying Dolores Creek Formation would help to resolve some of the unknowns related to the Pinguicula Group. A detrital zircon study of this formation may help to constrain the age of the underlying Pinguicula Group as well as offer a comparison of sediment provenance.

ACKNOWLEDGEMENTS

Funding for the project was provided by the Yukon Geological Survey, the Geological Survey of Canada, Northern Scientific Training Program (NSTP), and NSERC grants to Derek Thorkelson and Elizabeth Turner. Katie Hahn, Geoff Baldwin, and Tim Peters provided much appreciated enthusiasm and assistance in the field. Tom Pestaj provided help in the SHRIMP laboratory. Darrel Long is thanked for his critical review and assistance with interpretations.

REFERENCES

Abbott, G., 1997. Geology of the Upper Hart River Area Eastern Ogilvie Mountains, Yukon Territory (116A/10, 116A/11). Exploration and Geological Services Division, Yukon Region, Indian and Northern Affairs Canada, Bulletin 9, 92 p.

Bell, R. and Jefferson, C., 1987. An Hypothesis for an Australian-Canadian Connection in the Late Proterozoic and the Birth of the Pacific Ocean. Pacific Rim Congress 87, p. 1-15.

Betts, P. and Giles, D., 2006. The 1800-1100 Ma tectonic evolution of Australia. Precambrian Research, vol. 144, no. 1-2, p. 92-125.

Brideau, M.-A., Thorkelson, D.J., Godin, L., and Laughton, J.R., 2002. Paleoproterozoic deformation of the Racklan Orogeny, Slats Creek (106D/16) and Fairchild Lake (106C/13) map areas, Wernecke Mountains, Yukon. *In:* Yukon Exploration and Geology 2001, D.S. Emond, L.H. Weston and L.L. Lewis (eds.), Exploration and Geological Services Division, Yukon Region, Indian and Northern Affairs Canada, p. 65-72.

Collinson, J.D. and Thompson, D.B., 1982. Sedimentary structures. Allen & Unwin, London, Boston, 194 p.

Cook, D.G. and MacLean, B.C., 1995. The intracratonic Paleoproterozoic Forward orogeny, and implications for regional correlations, Northwest Territories, Canada. Canadian Journal of Earth Sciences, vol. 32, no. 11, p. 1991-2008.

Dalrymple, R.W., James, N.P. and Geological Association of Canada, 2010. Facies models 4. GEOtext. Geological Association of Canada, St. John's, Nfld., 586 p.

Dalziel, I., 1991. Pacific margins of Laurentia and East Antarctica-Australia as a conjugate rift pair: evidence and implications for an Eocambrian supercontinent. Geology, vol. 9, no.6, p. 598.

Eisbacher, G.H., 1978. Two major Proterozoic unconformities, northern Cordillera. Geological Survey of Canada Current Research, Paper 78-1A, p. 53-58.

Eisbacher, G.H., 1981. Sedimentary tectonics and glacial record in the Windermere Supergroup, Mackenzie Mountains, northwestern Canada. Geological Survey of Canada, Paper 80-27, 40 p.

Ernst, R. and Bleeker, W., 2010. Large igneous provinces (LIPs), giant dyke swarms, and mantle plumes: significance for breakup events within Canada and adjacent regions from 2.5 Ga to the Present. Canadian Journal of Earth Sciences, vol. 47, no.5, p. 695-739.

Flügel, E., 2004. Microfacies of carbonate rocks: analysis, interpretation and application. Springer, Berlin ; New York, 976 p.

Frank, T., Kah, L. and Lyons, T., 2003. Changes in organic matter production and accumulation as a mechanism for isotopic evolution in the Mesoproterozoic ocean. Geological Magazine, vol. 140, no. 4, p 397-420.

Furlanetto, F., Thorkelson, D.J., Davis, W.J., Gibson, H.D., Rainbird, R.H., and Marshall, D.D., 2009. Preliminary results of detrital zircon geochronology, Wernecke Supergroup, Yukon. *In:* Yukon Exploration and Geology 2008, L.H. Weston, L.R. Blackburn and L.L. Lewis (eds.), Yukon Geological Survey, p. 125-135.

Grotzinger, J., 1989. Facies and evolution of Precambrian carbonate depositional systems: emergence of the modern platform archetype. Controls on carbonate platform and basin development, vol. 44, p. 79–106.

Gordey, S.P. and Makepeace, A.J., 2003. Yukon Digital Geology, version 2.0. Geological Survey of Canada, Open File 1749; Yukon Geological Survey, Open File 2003-9 (D).

Hamilton, M.A. and Buchan, K.L., 2010. U-Pb geochronology of the Western Channel Diabase, northwestern Laurentia: Implications for a large 1.59 Ga magmatic province, Laurentia's APWP and paleocontinental reconstructions of Laurentia, Baltica and Gawler craton of southern Australia. Precambrian Research, vol. 183, no.3, p. 463-473.

Hoffman, P.F., 1991. Did the Breakout of Laurentia Turn Gondwanaland Inside-Out? Science, vol. 252, no. 5011, p. 1409-1412.

LeCheminant, A. and Heaman, L.M., 1989. Mackenzie igneous events, Canada: Middle Proterozoic hotspot magmatism associated with ocean opening. Earth and Planetary Science Letters, vol. 96, p. 38-48.

Long, D.G.F., Rainbird, R.H., Turner, E.C., and MacNaughton, R.B., 2008. Early Neoproterozoic strata (sequence B) of mainland northern Canada and Victoria and Banks Islands: a contribution to the Geological Atlas of the Northern Canadian Mainland Sedimentary Basin. Geological Survey of Canada, Open File 5700.

Macdonald, F.A., Smith, E.F., Strauss, J.V., Cox, G.M, Halverson, G.P., and Roots, C.F., 2011. Neoproterozoic and early Paleozoic correlations in the western Ogilvie Mountains, Yukon. *In:* Yukon Exploration and Geology 2010, K.E. MacFarlane, L.H. Weston and C. Relf (eds.), Yukon Geological Survey, p. 161-182.

Medig, K.P.R., Thorkelson, D.J., and Dunlop, R.L., 2010. The Proterozoic Pinguicula Group: Stratigraphy, contact relationships and possible correlations. *In:* Yukon Exploration and Geology 2009, K.E. MacFarlane, L.H. Weston and L.R. Blackburn (eds.), Yukon Geological Survey, p. 265-278.

Milidragovic, D., Thorkelson, D.J., Davis, W.J., Marshall, D.D., and Gibson, H.D., 2011. Evidence for late Mesoproterozoic tectonism in northern Yukon and the identification of a Grenville-age tectonothermal belt in western Laurentia. Terra Nova, vol. 23, p. 307-313.

Moores, E., 1991. Southwest US-East Antarctic (SWEAT) connection: a hypothesis. Geology, vol. 19, p. 425-428.

Rainbird, R.H., McNicoll, V.J., Theriault, R.J., Heaman, L.M., Abbott, J.G, Long, D.G.F., and Thorkelson, D.J., 1997. Pan-continental river system draining Grenville orogen recorded by U-Pb and Sm-Nd geochronology of Neoproterozoic quartzarenites and mudrocks, northwestern Canada. The Journal of Geology, vol. 105, no.1, p. 1-17.

Ross, G. and Villeneuve, M., 2003. Provenance of the Mesoproterozoic (1.45 Ga) Belt basin (western North America): Another piece in the pre-Rodinia paleogeographic puzzle. Geological Society of America Bulletin, vol. 115, no.10, p. 1191.

Sircombe, K.N., 2004. AgeDisplay: an EXCEL workbook to evaluate and display univariate geochronological data using binned frequency histograms and probability density distributions. Computers & Geosciences, vol. 30, issue 1, p. 21-31.

Stern, R. and Amelin, Y., 2003. Assessment of errors in SIMS zircon U-Pb geochronology using a natural zircon standard and NIST SRM 610 glass. Chemical Geology, vol. 197, no.1-4, p. 111-142.

Stern, R.A., 1997. The GSC Sensitive High Resolution Ion Microprobe (SHRIMP): analytical techniques of zircon U-Th-Pb age determinations and performance evaluation. Geological Survey of Canada, Current Research 1997-F (Radiogenic Age and Isotopic Studies: Report 10), p. 1-31.

Thompson, R.I., Roots, C.F., and Mustard, P.S., 1992. Geology of Dawson map area (116B, C) (northeast of Tintina Trench). Geological Survey of Canada, Open File 2849, 13 sheets, scale 1:50 000.

Thorkelson, D.J., 2000. Geology and mineral occurrences of the Slats Creek, Fairchild Lake and "Dolores Creek" areas, Wernecke Mountains (106D/16, 106C/13, 106C/14), Yukon Territory. Exploration and Geological Services Division, Yukon Region, Indian and Northern Affairs Canada, Bulletin 10, 73 p.

Thorkelson, D.J., Abbott, J.G., Mortensen, J.K., Creaser, R.A., Villeneuve, M.E., McNicoll, V.J., and Layer, P.W., 2005. Early and Middle Proterozoic evolution of Yukon, Canada. Canadian Journal of Earth Sciences, vol. 42, no.6, p. 1045-1071.

Thorkelson, D.J., Laughton, J.R., Hunt, J.A., and Baker, T., 2003. Geology and mineral occurrences of the Quartet Lakes map area (NTS 106E/1), Wernecke and Mackenzie mountains, Yukon. *In:* Yukon Exploration and Geology 2002, D.S. Emond and L.L. Lewis (eds.). Exploration and Geological Services Division, Yukon Region, Indian and Northern Affairs Canada, p. 223-239.

Turner, E.C., 2011. Stratigraphy of the Mackenzie Mountains supergroup in the Wernecke Mountains, Yukon. *In:* Yukon Exploration and Geology 2010, K.E. MacFarlane, L.H. Weston and C. Relf (eds.), Yukon Geological Survey, p. 207-231.

Vandeginste, V., Swennen, R., Gleeson, S.A., Ellam, R.M., Osadetz, K., and Roure, F., 2005. Zebra dolomitization as a result of focused fluid flow in the Rocky Mountains Fold and Thrust Belt, Canada. Sedimentology, vol. 52, no.5, p. 1067-1095.

Wade, B., Kelsey, D., Hand, M., and Barovich, K., 2008. The Musgrave Province: Stitching north, west and south Australia. Precambrian Research, vol.166, no.1-4, p. 370-386.

Yukon MINFILE 2009 – A database of mineral occurrences. Yukon Geological Survey, <http://www. geology.gov.yk.ca/databases_gis.html>.

Upper age constraint and paragenesis of the Tiger zone, Rau property, central Yukon

E.J. Thiessen[1], S.A. Gleeson, S.A. Dufrane
Department of Earth and Atmospheric Sciences, University of Alberta

R.C. Carne
ATAC Resources Ltd.

M. Dumala
Archer, Cathro & Associates (1981), Ltd.

Thiessen, E.J., Gleeson, S.A., Dufrane, S.A., Carne, R.C., and Dumala, M., 2012. Upper age constraint and paragenesis of the Tiger zone, Rau property, central Yukon. *In:* Yukon Exploration and Geology 2011, K.E. MacFarlane and P.J. Sack (eds.), Yukon Geological Survey, p. 151-164.

ABSTRACT

The Tiger zone, central Yukon is host to carbonate replacement gold-rich oxide and sulphide mineralization. A paragenetic study has revealed an early mineralization event characterized by hydrothermal dolomites, arsenopyrite and two phases of pyrite, and a late mineralization event that hosts silicate minerals, pyrite, bismuthinite, pyrrhotite and minor base metals and importantly late-stage monazite growth. Two stages of gold mineralization are present and manifest as 1) early arsenopyrite-bearing gold, and 2) a late-stage gold event which is associated with bismuthinite, pyrrhotite, minor base metals and anomalous antimony and arsenic concentrations and are assumed to be related to an adjacent Tertiary intrusive body. A U-Pb age of 58.37 ± 0.93 Ma (2σ) has been obtained from monazites that post-date both gold-bearing phases. The Tiger zone is interpreted to have formed by complex multistage fluid-flow which in part is directly associated with the emplacement and cooling of the 62.9 ± 0.5 Ma Rackla Pluton. Importantly, while the late stage gold-bearing event is the first significant Paleocene intrusion-related gold system identified in Yukon, the age of the earlier gold-bearing event remains unconstrained.

[1] *ericjamesthiessen@gmail.com*

INTRODUCTION

The Tiger zone, Rau property, is located approximately 100 km NE of Mayo (Fig. 1), central Yukon. The deposit is characterized by carbonate-replacement gold-bearing sulphide and oxide mineralization. Sulphide associated gold mineralization reaches 4.04 g/t over 96.01 m in the most well mineralized drill intervals reported (ATAC Resources Ltd., 2009). Only two other carbonate-hosted gold deposits are documented in Yukon, the Osiris showing 100 km east of the Tiger zone and the past-producing Ketza River oxide gold deposit in southeast Yukon (Fig. 1). Several authors have suggested that Ketza River may be an example of a gold-rich, base metal poor manto-type deposit (Fonseca, 1998; Stroshein, 1996), that formed at high temperatures (>300˚C) from hydrothermal fluids derived from intrusive rocks (Kojima *et al.,* 2009; Franchini *et al.,* 2007; Mach and Thompson, 1998). The Osiris deposit, however, is considered analogous to the giant Carlin-type carbonate-hosted disseminated gold deposits (R. Carne, pers. comm., 2011), with the world-class deposits occurring in Nevada, USA. Carlin-type deposits typically feature micron to sub-micron sized gold particles that are associated with disseminated sulphide minerals that occur as stratabound carbonate replacement bodies as well as entirely fault controlled mineralized bodies (Cline *et al.,* 2005; Arehart, 1996). A common model for Carlin mineralization involves derivation of fluids and gold from an igneous source that interacts with meteoric water to dissolve the carbonate host rock and subsequently mineralize the created pore space (*e.g.*, Muntean *et al.,* 2011).

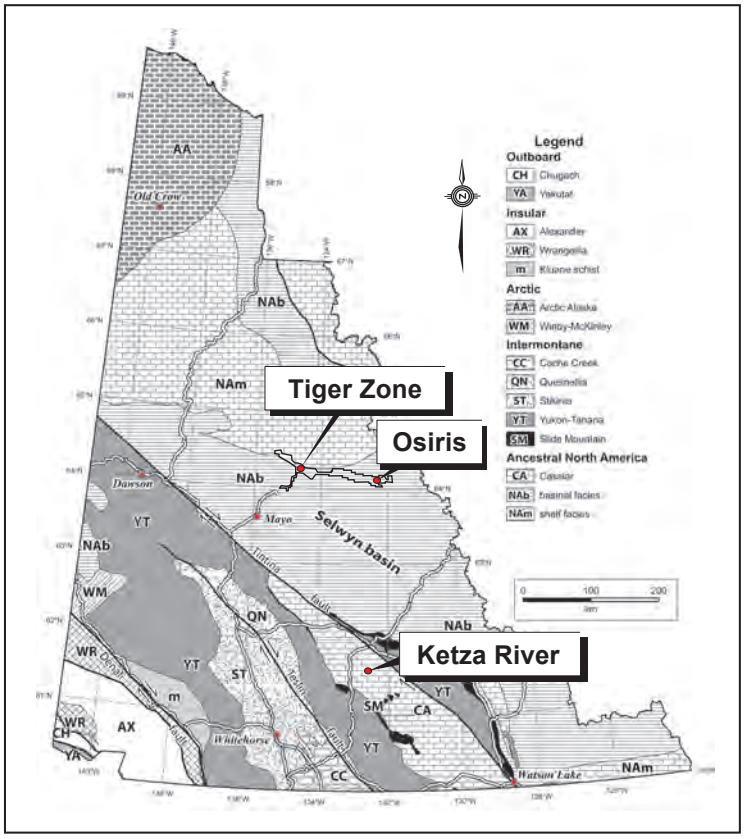

Figure 1. *Terrane map of Yukon illustrating location of the Tiger zone, Osiris and Ketza River occurrence (image courtesy of Yukon Geological Survey).*

Cretaceous age intrusion-related gold systems are common in Yukon and Alaska (Hart, 2007). These gold-bearing systems are often, but not always, characterized by sheeted quartz vein systems that are associated with 1) metaluminous, subalkalic felsic to intermediate intrusions; 2) carbonic hydrothermal fluids; 3) a metal assemblage of Bi, W, As, Mo, Te ± Sb ± Au – base metals; 4) a reduced ore assemblage of arsenopyrite, pyrrhotite and pyrite and a lack of magnetite; 5) aerially restricted and weak hydrothermal alteration; 6) a tectonic setting well inboard of convergent plate boundaries; and 7) within magmatic W and Sn provinces (Lang and Baker, 2001). The best example of reduced intrusion related gold in Yukon is the *ca.* 92 Ma Eagle Gold deposit, located at Dublin Gulch, ~50 km southwest of the Tiger zone (Hart, 2007; Stephens *et al.*, 2004).

The work presented here represents part of a MSc project that will characterize the origin, style, and timing of sulphide-gold mineralization in the Tiger zone in order to establish a deposit model. This paper presents preliminary results regarding the paragenetic history of the Tiger zone, the nature of gold mineralization and some age U-Pb age constraints for Tiger zone mineralization. The mineral paragenesis described herein involved analysis of ~650 core samples from 42 drillholes in addition to petrographic analysis of 95 thin sections from 15 select drillholes.

REGIONAL GEOLOGY

The earliest geological mapping of the Rau property and surrounding areas involved 1:250 000 scale reconnaissance work by the Geological Survey of Canada (Green, 1972; Blusson, 1978). The Tiger zone occurs in a regional Jura-Cretaceous fold and thrust belt comprising rocks of the Selwyn basin and the Mackenzie Platform (Fig. 2) (Abbott *et al.,* 1986). The Selwyn basin is a passive margin succession that accumulated on

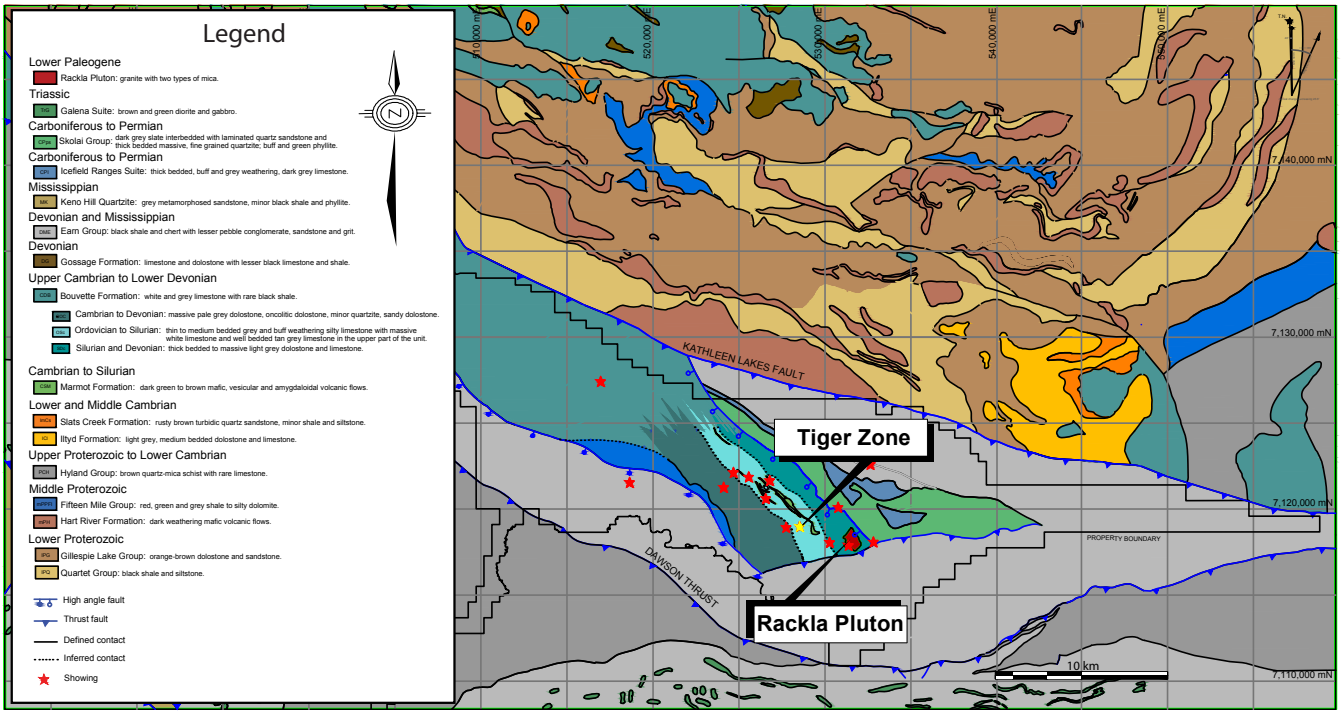

Figure 2. *Regional geology map of the Rau property including the Tiger zone, Rackla Pluton and regional mineral showings (modified from Dumala, 2011, Figure 7-3).*

the western border of ancient North America during the Neoproterozoic to Jurassic. Shallow water platform carbonates of the Mackenzie Platform interfinger with, and bound the time equivalent Selwyn basin rocks to the northeast. Rocks of the Selwyn basin are mostly characterized by deep-water black shales and cherts whereas the Mackenzie Platform is dominated by shelf carbonates (Abbott *et al.*, 1986).

Deformation of these basinal and platformal rocks occurred during the Mesozoic when extensive northeasterly directed compression imbricated and folded the strata (Murphy, 1997). Thrust faults associated with Mesozoic compression are generally oriented north-northeast and northwest (Fig. 2). The Dawson thrust, which broadly separates basinal sedimentary rocks to the southwest (hanging wall) from carbonate platformal rocks to the northeast (footwall; Murphy, 1997), bounds the Rau property on its southern border and occurs ~7 km from the Tiger zone (Fig. 2).

Two suites of intrusive rocks occur within 50 km of the Rau property including the 92±2 Ma Tombstone intrusions and the 64.0-66.8 Ma McQuesten intrusions (Murphy, 1997). Tombstone intrusive rocks range in composition from metaluminous granodiorite to syenite and are well known for their mineral and gold occurrences throughout Yukon (Hart, 2007; Baker and Lang, 2001; Lang and Baker, 2001; Murphy, 1997). McQuesten Suite intrusions comprise peraluminous biotite-muscovite granites and quartz monzonite compositions and have very few associated mineral occurrences (Murphy, 1997). A small granitic stock, the Rackla Pluton intrudes stratigraphy ~3 km east-southeast of the Tiger zone (Fig. 2). A U-Pb zircon age of 62.9±0.5 Ma (2σ) was determined for a large intrusive sill of the Rackle Pluton (V. Bennett, pers. comm., 2010). Additionally, small aplitic and pegmatitic dikes ~1km east of the Tiger zone yielded $^{40}Ar/^{39}Ar$ muscovite ages of 62.3±0.7 Ma, 62.4±1.8 Ma and 59.1±2 Ma (Kingston *et al.*, 2009).

In addition to the Tiger zone, regional exploration on the Rau property has resulted in the discovery of several polymetallic quartz veins±gold, scheelite-bearing tremolite skarn, pyrrhotite±scheelite±chalcopyrite-bearing actinolite-diopside-garnet skarn and wolframite±tantalite occurrences. Three scheelite-tremolite-actinolite skarn showings occur between the Tiger zone and the Rackla Pluton within the Bouvette Formation (Fig. 2). The most strongly altered skarn occurrences are associated with southwest striking quartz-muscovite-pegmatitic dikes. Geochemical anomalies for these skarns include elevated tungsten, gold and rare copper (Dumala, 2011).

DEPOSIT GEOLOGY

The Tiger zone is hosted by the Bouvette Formation, a carbonate sequence that is broadly assigned to Cambrian to Devonian carbonates of the Mackenzie Platform (Morrow, 1999). These rocks are locally bounded to the south by the Dawson thrust and to the north by the Kathleen Lakes fault (Fig. 2).

The Tiger zone stratigraphy consists of bedded limestones intercalated with locally extensive volcanic flows and volcaniclastic units all of which dip gently to the northeast (Fig. 3). Mineralization is primarily hosted in a carbonate package, the Discovery Horizon, which is bounded to the top (NE) and bottom (SW) by volcanic units (Fig. 3). The intercalated volcanic-carbonate package is truncated to the southwest by a northwest trending high-angle fault (Fig. 3).

Sulphide mineralization also occurs in the Upper Horizon which occurs adjacent to a volcanic unit stratigraphically above the main Discovery Horizon (Fig. 3). East of the Tiger zone, in a carbonate package the stratigraphic equivalent of the Discovery Horizon, is a pyrite-rich gold-poor horizon called the Lower Horizon. The prominent high-angle fault structure that bounds the Tiger zone to the southwest is characterized by a thick sequence of white marble in the immediate footwall and a distinctive volcaniclastic unit informally termed the 'Leopard unit' in the hanging wall (Fig. 3). The Leopard unit is distinctive from other volcanic rocks due to its high calcite content (>50%). Between this unit and the Discovery Horizon, an ~50 cm-thick magnetite bearing white marble typically occurs in sharp contact with the Discovery Horizon and may represent skarn mineralization.

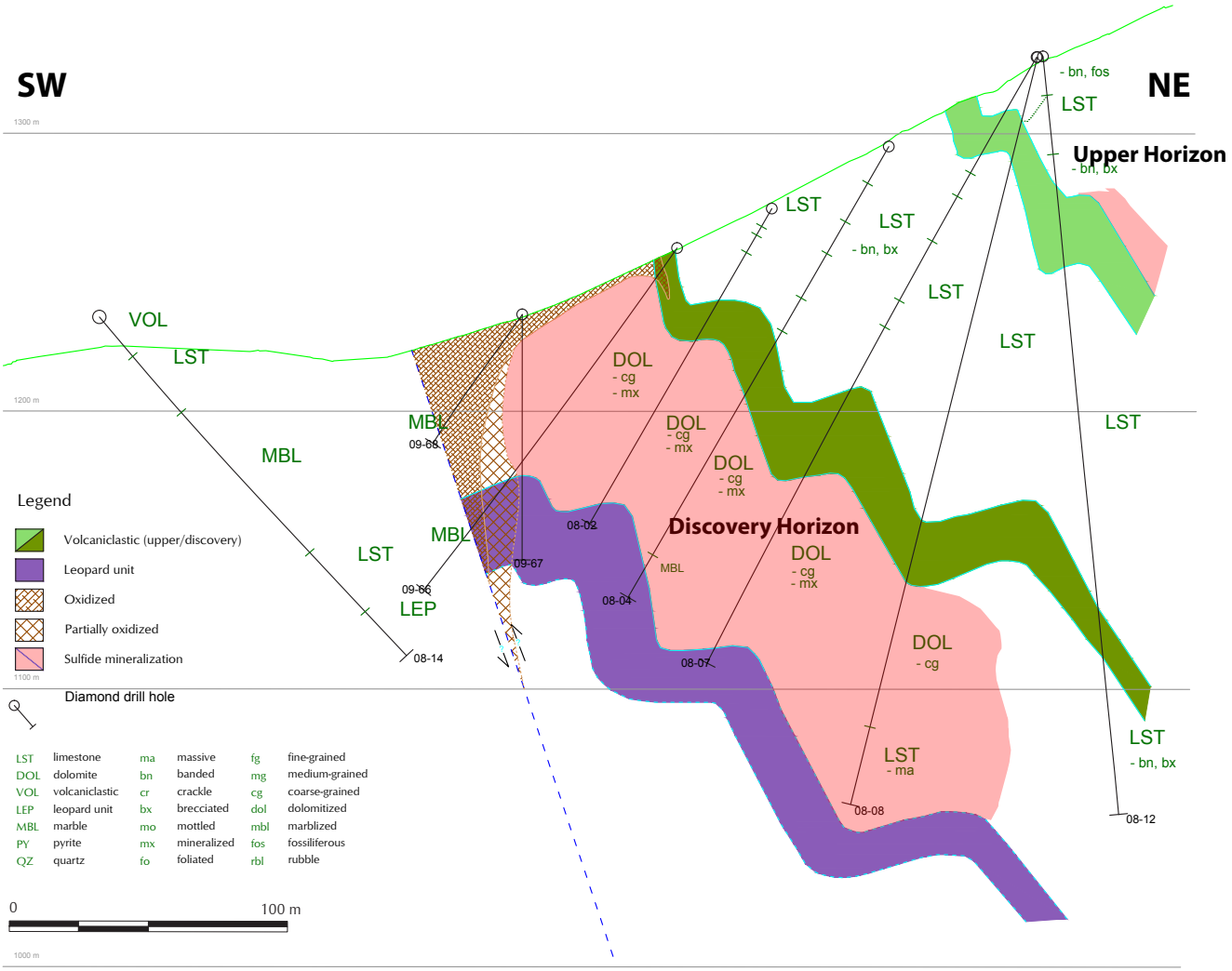

Figure 3. *Generalized cross section of the Tiger zone exemplified by the section line 10+000NW (modified from Dumala, 2011, Figure 11-1). The shaded red zones illustrate the Discovery Horizon and the Upper Horizon sulphide mineralization.*

ANALYTICAL TECHNIQUES

Hand-sample petrographic descriptions and thin section microscopy were supplemented with electron probe micro analyser (EPMA) techniques, including backscattered electron (BSE) imaging and wavelength dispersive spectrometry (WDS), as well as cathodoluminescence (CL) in order to better constrain Tiger zone paragenesis. A Cameca SX100 EPMA was used to analyse trace elements in sulphides, compositional zoning in sulphides and carbonates and for mineral identification by both electron dispersive spectrometry (EDS) and (WDS). Backscattered electron imaging was utilized to image compositional zoning in minerals not apparent by microscopy. A CL microscope was used to identify compositional zoning in carbonates as well as crosscutting carbonate phases not identifiable by microscopy due to epitaxial precipitation. All EPMA analyses were carried out in the Electron Microprobe Laboratory in the Earth and Atmospheric Sciences Department at the University of Alberta.

Laser ablation multicollector inductively coupled plasma mass spectrometry (LA-MC-ICPMS) was also utilized to determine a U-Pb age of monazite identified in the Tiger zone. Age dating was completed at the Radiogenic Isotope Facility in the Department of Earth and Atmospheric Sciences, University of Alberta using a NuPlasma MC-ICPMS and the UP213 laser ablation system by the methods described by Simonetti *et al.,* (2006).

RESULTS – PARAGENETIC SEQUENCE

The paragenesis of the host-rocks and Tiger zone mineralization are summarized in Figure 4 and described below. Four distinct stages of mineralization are documented in the Tiger zone. Stage 1 is host to gold-bearing arsenopyrite + saddle dolomite. Stage 2 comprises pyrite + zoned dolomite. Stage 3 consists of early pyrite + quartz + calcite + talc and late bismuthinite + gold + native bismuth + pyrrhotite associated with anomalous Sb and As suggesting an intrusion-related signature. Lastly, stage 4 hosts quartz + dolomite + sphalerite + minor chalcopyrite + monazite + amphibole + scheelite + muscovite + calcite + pyrite and trace uraninite.

HOST ROCK

Carbonate host rocks of the Bouvette Formation range from lime-mudstones (Fig. 5a) and dolo-mudstones to crinoidal packstones and coral rudstones that commonly have coarse dolomite recrystallization and dolomite replacement textures. These host carbonates are generally devoid of sedimentary structures due to dolomitization

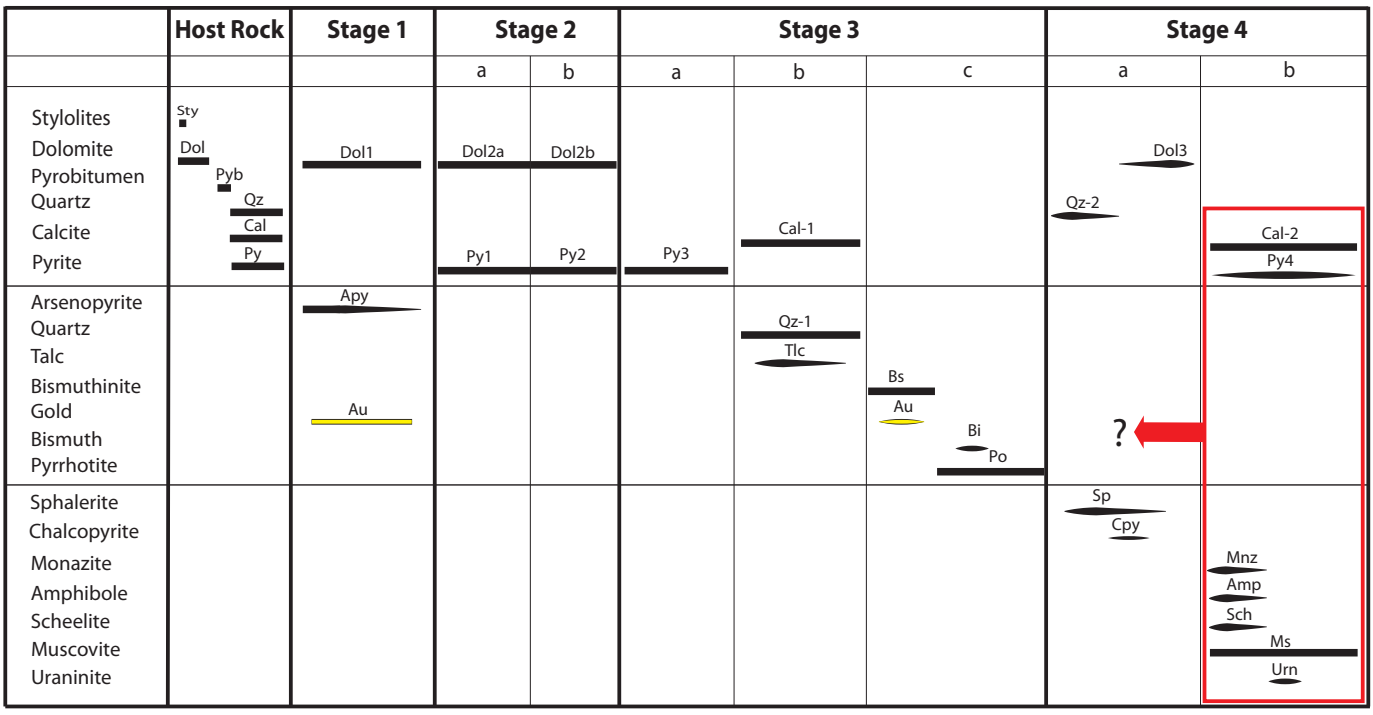

Figure 4. *Paragenesis of the Tiger zone highlighting the two distinct gold-bearing phases. The red box and arrow outlining Stage 4b represents the uncertainty of Stage 4a and 4b as being distinct stages.*

and/or bioturbation. The host carbonates are dark grey in colour and organic material comprises 10-50% of the rock (Fig. 5b). Extensive single-seam stylolite formation sub-parallel with bedding also occurs in these rocks (Fig. 5c).

These carbonates exhibit breccia textures (Fig. 5a,c) throughout the Rau property including brecciation developed within the deposit. The most common breccia type is a mosaic breccia where angular to subangular clasts of carbonate are slightly rotated and separated from one another by up to a few centimetres (Fig. 5c). The breccia fractures exhibit polyphase mineralization beginning with a 'dog tooth' dolomite spar that crystallize on carbonate clasts (Fig. 5a,c). This dolomite spar may form euhedral crystals up to 1 cm long and is commonly rimmed by a thin veneer of sub-millimetre sized tabular pyrobitumen (Fig. 5a,d). The remaining void space is filled by an assemblage of anhedral quartz and calcite with minor anhedral fine-grained pyrite (Fig. 5a).

TIGER ZONE MINERALIZATION

Stage 1: Dolomite 1 + Arsenopyrite + Gold

Stage 1 of the paragenetic sequence involves destructive and pervasive replacement of host-rock carbonate within the Discovery Horizon by dolomite 1 (Dol 1) + arsenopyrite (Apy) + gold (Au). Dolomite 1 (Fig. 5e) occurs as 2-4 mm equant to elongate-feathered and irregular crystals that commonly exhibit saddle morphology (curved crystal faces and sweeping extinction, Fig. 5f). These crystals commonly have angular crystal boundaries shared with other Dol 1 crystals that often exhibit triple-point grain boundaries (Fig. 5f). In hand samples Dol 1 may be a distinctive pale pink colour (Fig. 5e) or white. Both pink and white dolomite have a mottled texture and luminesce dark-red and black under cathodic light (Fig. 6a). This mottled texture is also visible under BSE imaging (Fig. 6b) as light (iron-rich) and dark (magnesium-rich) shades of grey for both pink and white dolomite. The similar chemistries, CL-active species, identical BSE response, and the indistinguishable nature of the pink and white dolomite phases under the microscope indicate a broadly co-eval origin.

Euhedral Apy is disseminated throughout Dol 1 (Fig. 5e). Importantly, Apy grains have angular crystal boundaries and no reaction rim with Dol 1 (Fig. 6c) and, thus, both these phases are considered to be coeval in the paragenetic sequence. Thin, <0.01 mm sub-parallel

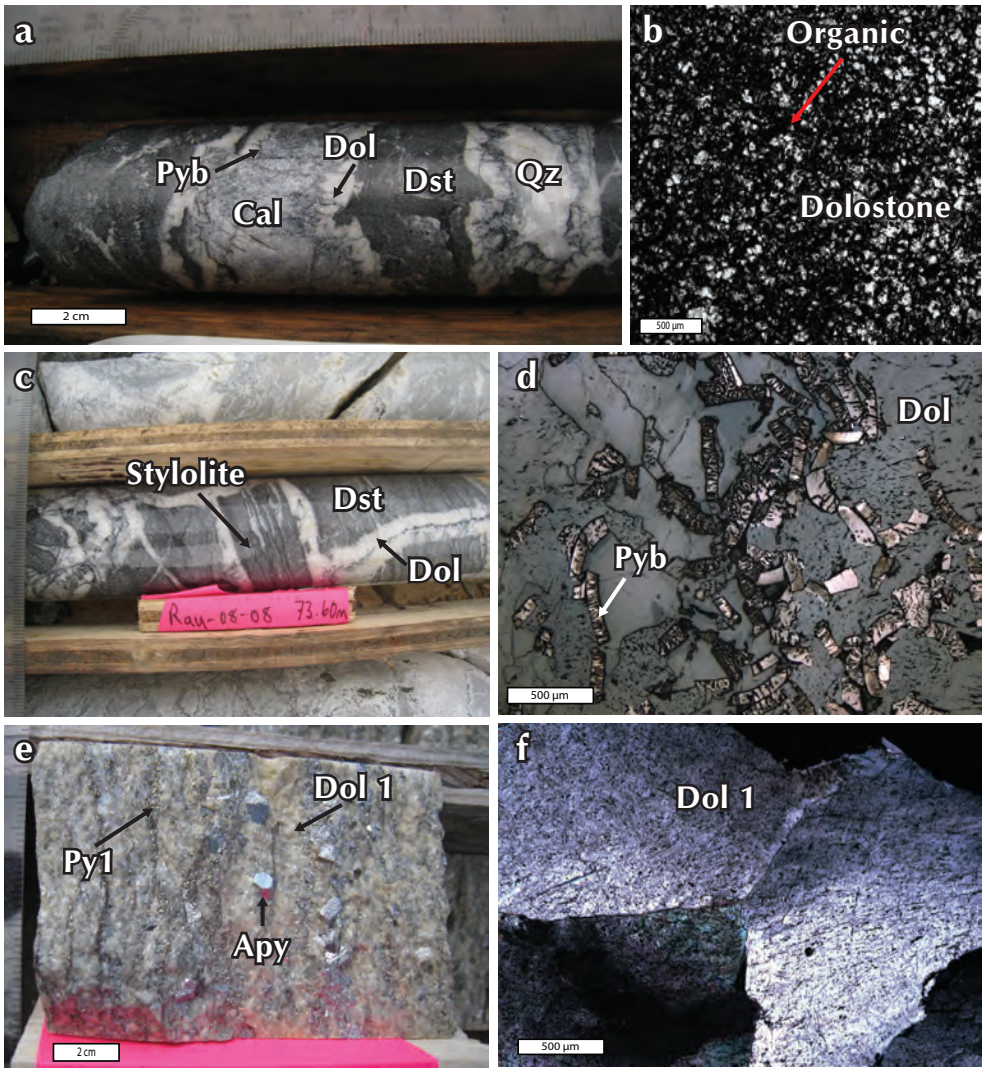

Figure 5. *Paragenesis supporting pictures and images of host-rock and Stage 1 including* ***(a)*** *brecciated host-rock limestone,* ***(b)*** *photomicrograph of organic material within limestone,* ***(c)*** *brecciated limestone clasts exhibiting stylolite development,* ***(d)*** *reflected light picture of pyrobitumen that rims dolomite spar,* ***(e)*** *pale pink Dol 1 with disseminated Apy and foliated Py 1 within the Discovery Horizon sulphide mineralization, and* ***(f)*** *Dol 1 saddle morphology in cross polarized light.*

fractures are restricted to Apy grains but are not observed to extend into the adjacent and inferred coeval Dol 1. Backscattered electron imaging of Apy crystals reveal faint euhedral zoning (Fig. 6c) where the lighter zones are characterized by higher levels of arsenic as quantified by EDS measurements. Eight Apy grain separates have been analysed by solution inductively coupled plasma mass spectrometry. Preliminary results indicate an average gold concentration of 12 ppm in the grains and a maximum value of 19 ppm, suggesting gold mineralization is directly associated with Apy formation.

Stage 2: (a) Pyrite 1+Dolomite 2a, (b) Dolomite 2b+ Pyrite 2

Stage 2a mineralization is characterized by an assemblage of fine-grained pyrite (Py 1) and dolomite (Dol 2a) that have grown in parallel tabular arrays and define a prominent foliation (Fig. 6d). Py 1 occurs as 0.1-0.5 mm equant subhedral-cubic crystals that have grown both interstitially within Dol 1 (Fig. 6e) and overprint Dol 1 and stage 1 Apy (Fig. 6f). Grain boundaries of Py 1 that are in contact with Dol 1 and Apy are sharp (Fig. 6e), have no reaction rimming or dissolution textures (Fig. 6f) and are inferred to be in textural equilibrium with Dol 1 and Apy. These pyrite crystals have a weak preferred orientation and commonly have grain boundary area reduction or triple-point textures (Fig. 7a). Backscattered electron imaging of Py 1 grains reveals that they are broadly homogeneous (Fig. 7b), although weak zoning is rarely observed. Wavelength dispersive spectrometry analysis of the brighter BSE zones of Py 1 grains demonstrates that arsenic-rich portions of crystals have concentrations averaging 2000 ppm As and less commonly containing 1 wt % As.

Dolomite 2a forms 1 mm to 1 cm equant blocky, light grey crystals (Fig. 6d) with angular (Fig. 6b) to irregular crystal boundaries. The abundance of angular crystal faces, absence of both saddle morphology textures and sweeping extinction (under polarized light) and fewer fluid inclusions, distinguishes Dol 2a from Dol 1. Weak undulose extinction and birdseye textures are much more common in Dol 2a. Although no internal deformation or crystal elongation is observed, Dol 2a occurs in elongate mineral clusters sub-parallel to Py 1 (Figs. 6b,d). Angular zonation visible by BSE imaging is characterized by alternating dark and light banding (Fig. 6b). Subsequent EDS analysis of this banding determines that the darker

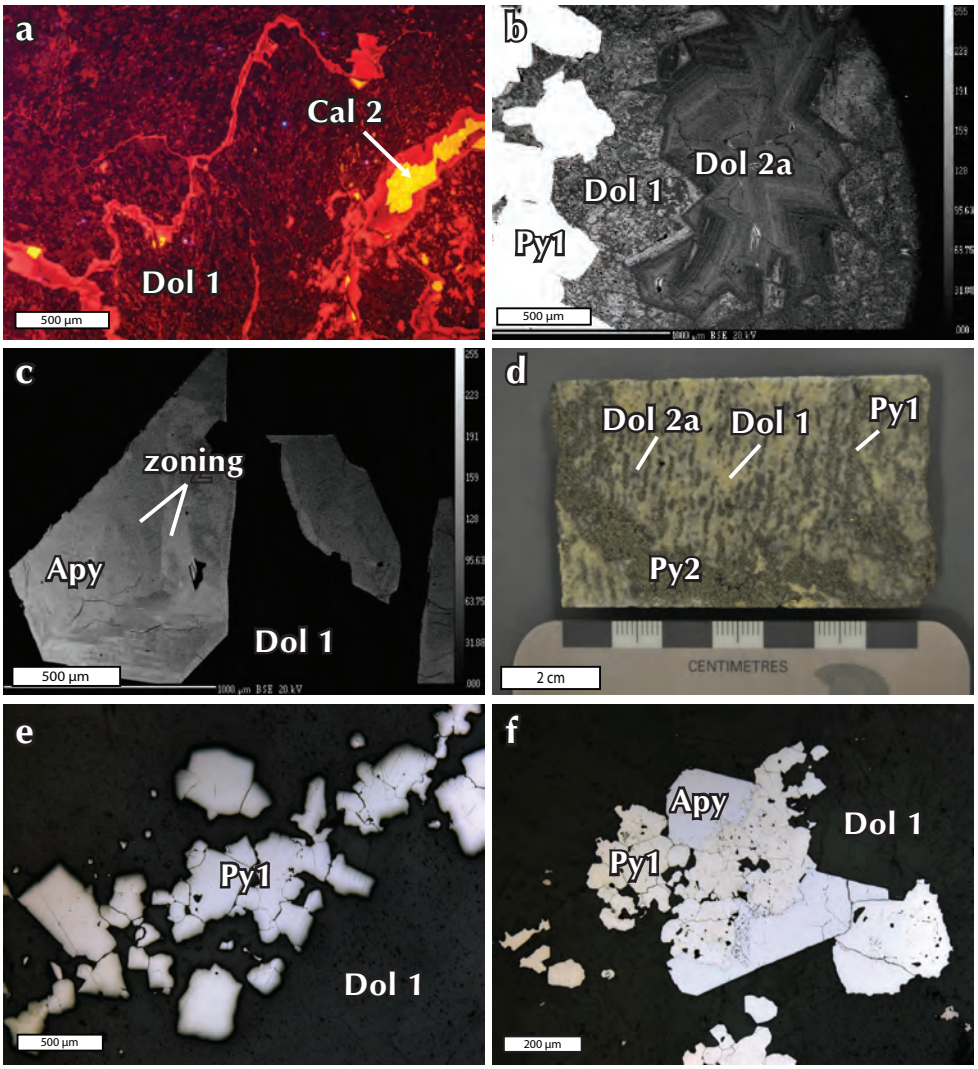

Figure 6. *Paragenesis supporting pictures of Stage 1-2 including* ***(a)*** *cathodic light picture of mottled Dol 1 and interstitial Cal 2,* ***(b)*** *BSE image of Py 1, Dol 1 and Dol 2 displaying mottled Dol 1 and zoned Dol 2a,* ***(c)*** *BSE image of weak zoning in Apy grain,* ***(d)*** *rock sample displaying Py 2 obliquely cross cutting foliated Dol 2a and Py 1 as well as Dol 1,* ***(e)*** *reflected light picture of Py 1 interstitial to Dol 1, and* ***(f)*** *reflected light picture of Py1 crosscutting Apy and Dol 1 in textural equilibrium.*

zones are magnesium-rich and the lighter zones are more iron-rich. Dolomite 2a has a dark-red to black luminescence similar to Dol 1 but is texturally and, we suggest, temporally distinct.

Stage 2b mineralization is characterized by an assemblage of fine-grained pyrite (Py 2) and dolomite (Dol 2b) that post-dates or crosscuts foliation. Py 2 occurs as 0.1-0.5 mm equant subhedral crystals that form irregular crystal masses oblique to Py 1 (Fig. 6d). Py 2 pervasively overprints Stage 1 and Stage 2a mineral assemblages with no preferred orientation (Fig. 6d). Py 2 does not show well-defined zoning in BSE imaging, however, brighter zones also have higher As contents.

Dolomite 2b forms 1 mm to 1 cm equant, blocky, and light grey crystals with angular grain boundaries. This dolomite appears almost identical to Dol 2a, however, Dol 2b does not have a preferred alignment parallel to foliation (Fig. 7c). Backscattered electron imaging of Dol 2a and 2b reveals more uniform growth zoning (Fig. 6b) whereas Dol 1 is characterized by a distinctive mottled appearance with saddle morphology (Figs. 5f, and 6a,b). Electron dispersive spectrometry analysis indicates that darker zones in Dol 2b represent higher Mg concentrations and lighter zones correspond to higher relative Fe contents. Cathodoluminescence colours for zoned Dol 2b range from dark-red to black (Fig. 7d) and are identical to the CL colours and textures of Dol 2a.

Stage 3: (a) Pyrite 3, (b) Quartz 1 + Talc + Calcite 1, (c)Bismuthinite + Gold + Bismuth + Pyrrhotite

Stage 3a mineralization is characterized by coarse-grained, brassy, euhedral to subhedral pyrite (Py 3) that overprints Stage 1 and Stage 2 mineralization. Py 3 is commonly associated with, but pre-dates quartz (Qz 1) (see below), forming crystals in excess of 1 cm in size (Fig. 7e). Backscattered electron imaging shows weak, subangular zoning within the Py 3 phase (Fig. 7f). Brighter BSE zones are determined by WDS to have higher As values, ~1000 ppm.

Stage 3b mineralization consists of variable amounts of Qz 1, talc (Tlc) and calcite (Cal 1) replacing and occurring in brittle fractures crosscutting Py 3 (Fig. 7e) and overprinting Stage 1 and Stage 2 mineral assemblages (Fig. 8a). Quartz 1 is the major constituent of Stage 3b and generally occurs as anhedral accumulations (Fig. 8b) replacing Stages 1 and 2 minerals or more rarely as euhedral crystals. Talc occurs as small 0.1-0.5 mm radiating acicular needles forming fans within Qz 1 (Fig. 8b). The Tlc and Qz 1 share sharp, angular grain boundaries (Fig. 8b) and thus are suggested to be coeval. Calcite 1 is characterized by cm-scale blocky and subhedral crystals

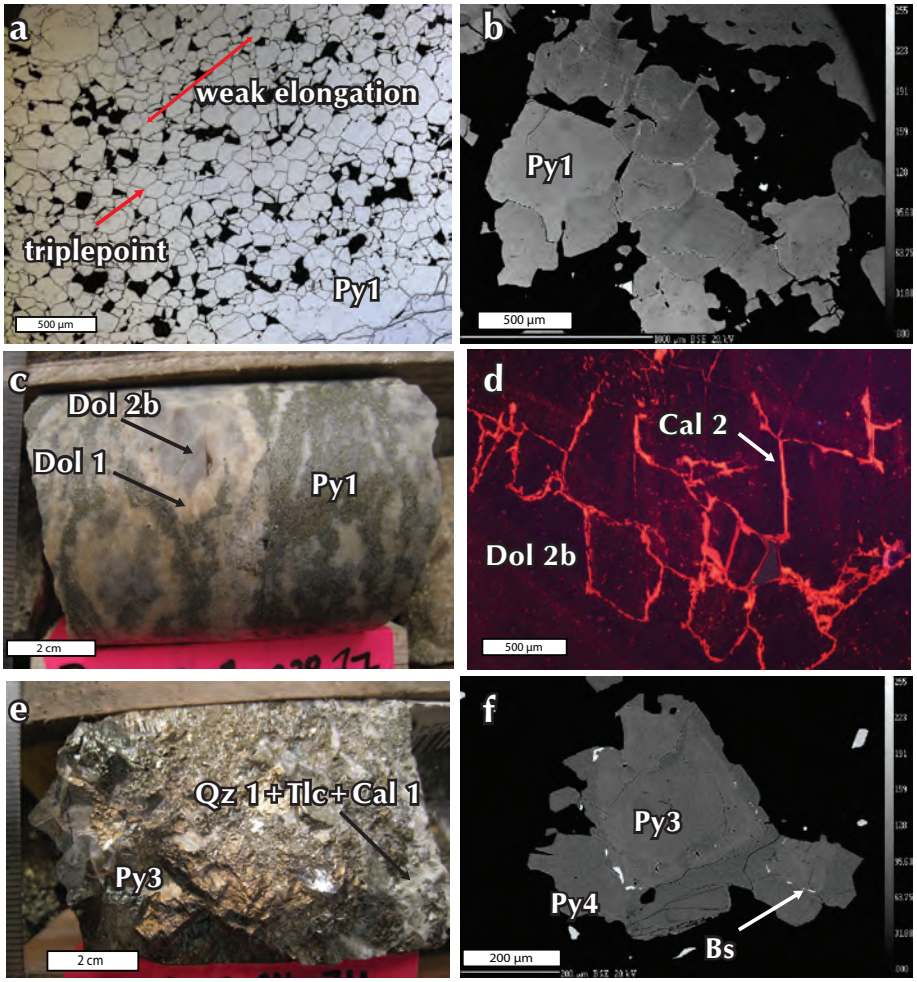

Figure 7. *Paragenesis supporting pictures of Stage 2-3 including* ***(a)*** *reflected light picture of Py 1 displaying elongate grains and triple point textures,* ***(b)*** *BSE image homogenous Py 1,* ***(c)*** *cathodic light picture of zoned Dol 2b and interstitial Cal 2,* ***(d)*** *Dol 2b crosscutting Dol 1 with no preferred orientation,* ***(e)*** *coarse Py 3 and interstitial Qz 1, Tlc and Cal 1, and* ***(f)*** *BSE image of zoned Py 3 rimmed by Bs and subsequent Py 4.*

occurring as a minor phase within quartz (Fig. 8b) or as cm-scale veins crosscutting Py 3.

Stage 3c mineralization consists of bismuthinite (Bs), native gold (Au), native bismuth (Bi) and pyrrhotite (Po) within fractures of Stage 3b Qz 1 and Stage 3a Py 3. Bismuthinite occurs as anhedral crystals within fractures of Stage 1 and Stage 2 sulphides, Py 3 and Qz 1 (Fig. 8c), and has been observed in a few drillholes to occur in large cm-scale accumulations. Backscattered electron imaging has revealed rare bismuthinite rimming Py 3 crystals which in turn are rimmed by a later anhedral pyrite (Fig. 7f). Native gold occurs as anhedral fracture fills within Stage 1 and 2 sulphide fractures and within Py 3 fractures. When native gold is present, it is adjacent to Bs within these fracture fills and suggests coeval growth (Fig. 8d). Analysis of Bs by WDS indicated the grains have elevated Sb (~5000 ppm) and anomalous As (~500 ppm) concentrations. Where observed, native bismuth occurs 'speckled' within Bs as small sub 0.1 mm anhedral crystals and also as fracture coatings of other sulphide phases. Similarly, Po commonly occurs in close proximity to Bs as anhedral masses with no apparent crosscutting relationship. However, native bismuth and Po are observed to crosscut Bs in fractures suggesting a coeval to slightly epigenetic relationship of Po to Bs-Au mineralization.

Stage 4: (a) Quartz 2 + Sphalerite + Chalcopyrite + Dolomite 3, (b) Monazite + Amphibole + Scheelite + Muscovite + Calcite 2 + Pyrite 4 + Uraninite

Stage 4a mineralization is characterized by fracture filling and replacement by quartz (Qz 2), sphalerite (Sp), chalcopyrite (Cpy) and dolomite (Dol 3). This mineral assemblage is commonly observed re-occupying bismuthinite-bismuth veinlets within Py 3 (Fig. 8e). Quartz 2 occurs as small 0.1 mm euhedral crystals along fractures in Py 3 (Figs. 8e,f) which may have Bs rimming the fractures suggesting Qz 2 post-dates Bs growth. These euhedral quartz crystals occur associated with anhedral Sp that also occupy these Py 3 fractures but are also occasionally crosscut by Sp veinlets (Fig. 8f). When Bs and Sp occupy a fracture the Bs is usually rimming the Py 3 crystals whereas the Sp is commonly central to the fracture (Fig. 8e). Rare anhedral crystals of Cpy occur within fractures of Sp (Fig. 9a) suggesting Cpy is coeval to slightly epigenetic to the Sp. In rare, large cm-scale Cal 1 veins, Sp has been observed to occur as mm-scale euhedral zoned crystals that overprint Cal 1. Associated with this phase is a euhedral to anhedral dolomite (Dol 3) that commonly occurs with euhedral Sp and is observed to crosscut and offset fractures filled with Sp.

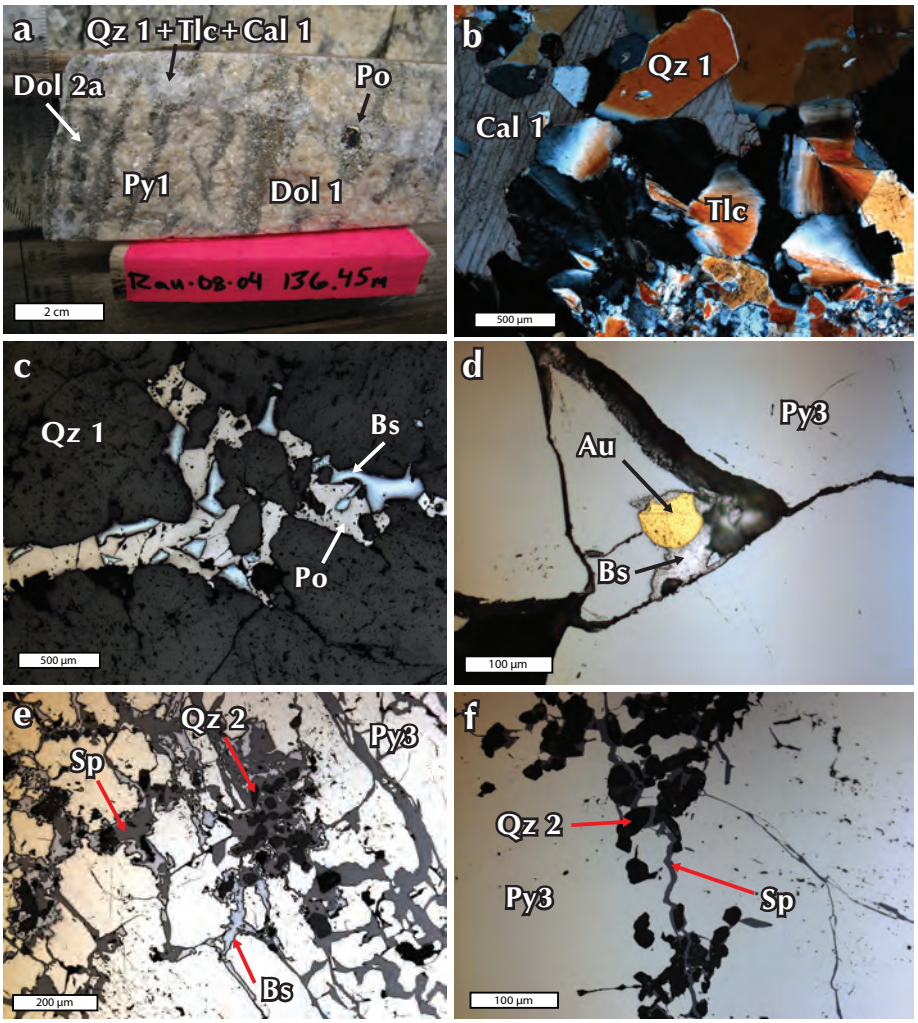

Figure 8. *Paragenesis supporting pictures of Stage 3-4 including* ***(a)*** *Stage 3b minerals crosscutting Stage 1-2,* ***(b)*** *cross polarized light picture of Qz 1, Cal 1 and Tlc in textural equilibrium with each other,* ***(c)*** *reflected light picture of Bs and Po in crosscutting fractures within Qz 1,* ***(d)*** *Au and Bs occurring in fractures of Py 3 in reflected light,* ***(e)*** *reflected light picture of Stage 4a minerals reoccupying Bs veinlets in Py 3, and* ***(f)*** *Sp crosscutting Qz 2 of Stage 4a within Py 3 in reflected light.*

Stage 4b mineralization consists of monazite (Mnz), amphibole (Amp), scheelite (Sch), muscovite (Ms), calcite (Cal 2), uraninite (Urn) and pyrite (Py 4). The main constituent of this phase is Cal 2 and Ms. Cal 2 occurs as subhedral crystals that range from 0.01 mm to 1 cm scale and are intergrown with muscovite (Fig. 9b). Muscovite commonly forms both parallel acicular crystals 0.5 mm long (Fig. 9b) and irregular radiating aggregates. Muscovite and Cal 2 commonly form along rheologic boundaries such as between Dol 1 or 2 and sulphides (Fig. 9c). Pyrite (Py 4) is a minor constituent of this phase and occurs interstitial to the Ms and Cal 2 as small 0.01 mm anhedral crystals (Fig. 9d). Pyrite 4 is also observed rimming earlier Bs (Fig. 7f). Stage 4b mineral phases destructively overprint Stage 1-3 mineral assemblages. Cal 2 has bright red and orange luminescence under cathodic light (Fig. 9b) that are very distinct from Stage 1 (Fig. 9b) and 2 dolomites. Cal 2 also occurs along grain boundaries Dol 1, 2a and 2b determined by CL (Figs. 6a and 7d).

Monazite, Amp and Sch are all present within the Ms-Cal assemblage but are not observed in contact with one another, thus, the relative crosscutting relationships are unclear. Monazite, which is observed to form only within Ms-Cal 2 aggregates, occurs as large 0.5-2 mm euhedral crystals (Fig. 9e). Small fractures in Mnz grains are occupied by Ms or Cal 2 crystals and locally small uraninite grains (Fig. 9e) suggesting monazite pre-dates these minerals. Amphibole is associated with the Ms-Cal 2 assemblage in dense mineral clusters (Fig. 9f). No obvious temporal relationship is observed between Amp grains. Scheelite is an extremely minor component of Stage 4b. It occurs as large 1 cm size subhedral crystals that have fractures infilled with Ms and Cal 2. Stage 4b minerals were not found in association with Stage 4a minerals, and thus the two stages may be coeval.

RESULTS – AGE CONSTRAINTS ON THE TIGER ZONE

The U-Pb age data presented here are the first to constrain a phase of alteration associated with the development of the Tiger zone. The age data represent a minimum (*i.e.*, the youngest possible age the late-stage gold mineralization could be) age of a phase of late-stage gold mineralization.

Earlier attempts to date Tiger zone Apy, Py 1, Py 2, Py 3, Po and Bs by the $^{187}Re/^{187}Os$ method failed due to the low concentrations of ^{187}Re present in those minerals.

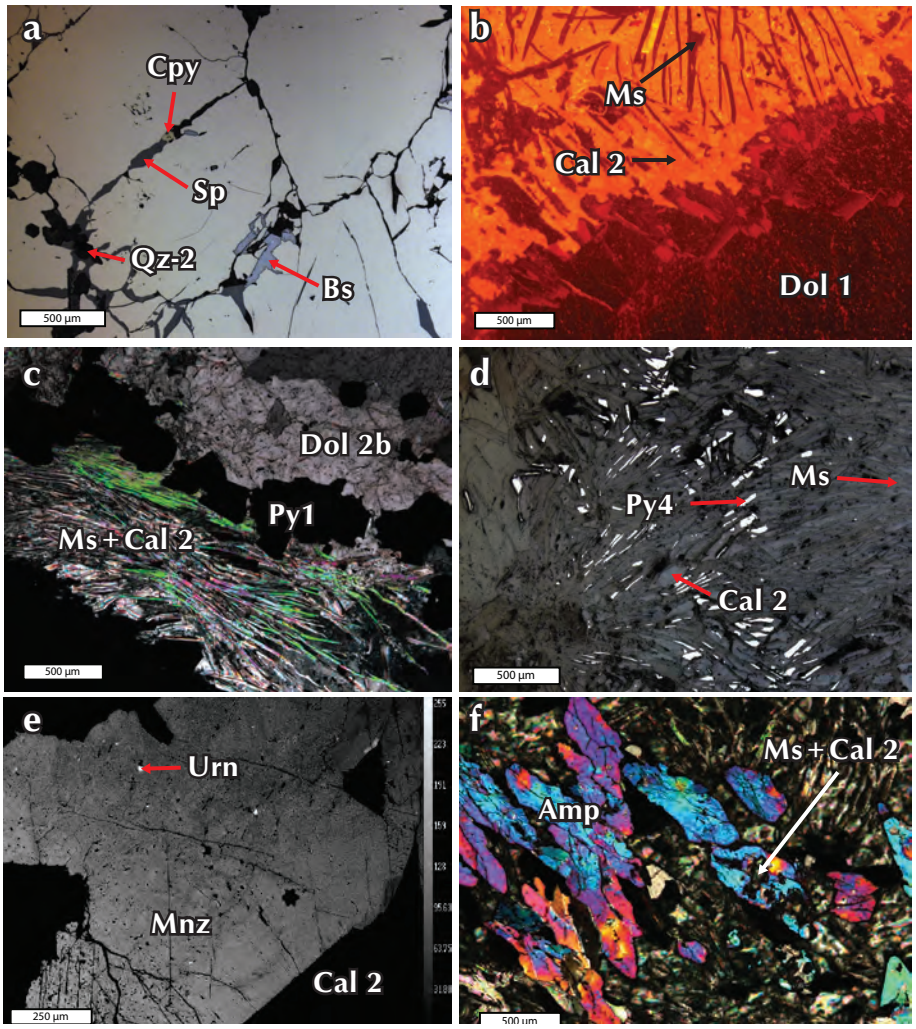

Figure 9. *Paragenesis supporting pictures of Stage 4 including* ***(a)*** *rare Cpy in veinlets of Sp and Qz 2 crosscutting Py 3 in reflected light,* ***(b)*** *cathodic light picture of Ms and Cal 2 overprinting early Dol 1,* ***(c)*** *cross polarized light picture of Ms and Cal 2 precipitating along rheologic boundaries,* ***(d)*** *reflected light picture of Ms, Cal 2 and Py 4 intergrown with each other,* ***(e)*** *BSE image of Mnz where bright spots are uraninite and fractures are filled with Ms, and* ***(f)*** *accumulations of amphibole overprint by Ms and Cal 2 in cross polarized light.*

Four large monazites from Stage 4b were analysed *in situ* by LA-MC-ICPMS (Appendix A). A monazite age of 58.37 ± 0.93 Ma (2σ) was obtained from 38 spots from the four monazites (Figs. 10a,b). High U contents within these monazite grains (up to ~8000 ppm) allowed the resulting precise analytical measurements.

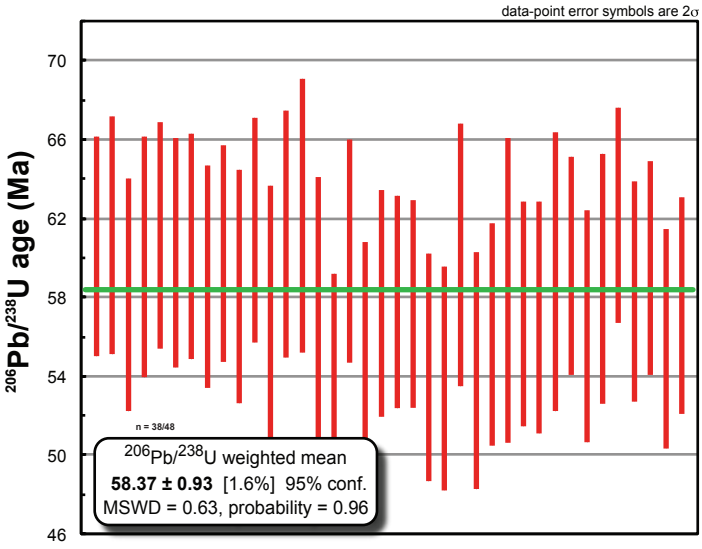

Figure 10. *Plot of weighted mean $^{206}Pb/^{238}U$ ages of 38 spots from 4 monazite grains. Of the 48 total analyses collected, only 38 analyses had reasonable count rates and only these are used to calculate the final weighted mean $^{206}Pb/^{238}U$ ages.*

DISCUSSION

A detailed paragenesis of the Tiger zone reveals two distinct mineralogical assemblages, an early carbonate-sulphide-gold assemblage and a later silicate-sulphide-gold phase.

The first assemblage comprises carbonates, sulphides and gold of Stage 1 and Stage 2. These carbonates pervasively overprint the Discovery Horizon limestone and display abundant coarse-grained, equant, saddle-shaped crystals with triple-point textures and lack significant evidence of veining. Well developed saddle morphology suggests hydrothermal dolomite precipitated in abundant open space. Gold values measured in Stage 1 arsenopyrite grains have concentrations up to 19 ppm Au. This early gold phase does not correlate with high Bi, W, Mo, Te, and Sb concentrations that are typically indicative of an intrusion-related ore-fluid, suggesting that two distinct gold forming events comprise the Tiger zone deposit. Currently, it is unclear whether this early gold is lattice bound to the arsenopyrite or whether the analysed gold was simply free gold from Stage 3c. Further LA-ICPMS analysis will better constrain whether gold is structurally bound in arsenopyrite. The occurrence of Bi, Au, Sb and As (Stage 3c) with minor base metals (Stage 4a) is similar to the element association characteristic of intrusion-related gold deposits. Therefore, late gold in Stage 3c associated with this intrusive signature likely represents a magmatic-hydrothermal event.

Skarn mineralization is commonly associated with intrusion-related systems that intrude into carbonate rocks. Skarn showings that have been identified between the Tiger zone and the Rackla Pluton are predominantly scheelite + amphibole ± gold, an assemblage that resembles Stage 3 and Stage 4 mineral assemblages of the Tiger zone. The uranium-thorium bearing monazite in Stage 4b has also been noted in skarn mineralization (Gross, 1996) and further supports the intrusion-related affinity of Stage 3 and Stage 4 assemblages. Additionally, the magnetite-bearing skarn that occurs basal to the Discovery Horizon crosscuts Stage 1 and Stage 2 mineralization locally and may be related to Stage 3 and Stage 4 mineralization.

The monazite age of 58.37 ± 0.93 Ma (2σ) falls within error of a single $^{40}Ar/^{39}Ar$ muscovite age (59.1 ± 2 Ma 2σ) from nearby granitic aplite and pegmatite dikes but is distinctly younger than two other $^{40}Ar/^{39}Ar$ muscovite ages of 62.3 ± 0.7 Ma and 62.4 ± 1.8 Ma (Kingston *et al.*, 2009). The Rackla Pluton age of 62.9 ± 0.5 Ma (2σ) (V. Bennett pers. comm., 2010) correlates well with the older $^{40}Ar/^{39}Ar$ muscovite ages however, it is at least 3 My older than the mineralization age of the Tiger zone monazite. The age similarities of the pegmatitic dikes and the Rackla Pluton as well as the mineralogical similarities to nearby skarn horizons strongly suggests that the last phase of Tiger zone mineralization is related to the Rackla Pluton.

CONCLUSIONS

Four distinct stages of mineralization are documented in the Tiger zone: 1) gold-bearing arsenopyrite + saddle dolomite of Stage 1; 2) pyrite + zoned dolomite of Stage 2; 3) early pyrite + quartz + calcite + talc and late bismuthinite + gold + native bismuth + pyrrhotite associated with anomalous Sb and As in Stage 3; and 4) quartz + dolomite + sphalerite + minor chalcopyrite + monazite + amphibole + scheelite + muscovite + calcite + pyrite and trace uraninite of Stage 4.

Tiger zone mineralization is, thus, associated with two distinct gold mineralizing events: early gold in Stage 1 of an unknown age and origin; and Stage 3c gold that has an intrusion-related gold signature which suggests Stage 3 mineralization is related to the 62.9±0.5 Ma Rackla Pluton.

ACKNOWLEDGMENTS

Rob Carne of ATAC Resources Ltd. is thanked for the financial and logistical support provided throughout the duration of this project. Matt Dumala and Julia Lane of Archer, Cathro & Associated (1981), Ltd., have contributed tremendous support during sample collection and through insightful geological discussions. Thanks are given to Venessa Bennett for discussions and critical reviews of this manuscript. This ongoing project has also benefited greatly from the financial support of the Yukon Geological Survey and Sarah Gleeson's NSERC Discovery grant.

REFERENCES

Abbott, J.G., Gordey, S. P., and Tempelman-Kluit, D.J., 1986. Setting of stratiform, sediment-hosted lead-zinc deposits in the Yukon and northeastern British Columbia. *In:* Mineral deposits of the northern Cordillera, J.A Morin (ed.), Canadian Institute of Mining and Metallurgy, Special vol. 37, p. 1-18.

Arehart, G.B., 1996. Characteristics and origin of sediment-hosted disseminated gold deposits: a review. Ore Geology Reviews, vol. 11, p. 383-403.

ATAC Resources Ltd., 2009. ATAC Resources Ltd. intersects 5.11 g/t gold over 70.80 metres on its Rau Gold Property. November 3rd, 2009. Retrieved from http://www.atacresources.com/s/NewsReleases.asp. Web. November 2011.

Baker, T. and Lang, J.R., 2001. Fluid inclusion characteristics of intrusion-related gold mineralization, Tombstone-Tungsten magmatic belt, Yukon Territory, Canada. Mineralium Deposita, vol. 36, p. 563-582.

Blusson, S.L., 1978. Regional geological setting of lead-zinc deposits in Selwyn Basin, Yukon. Current Research, Part A, Geological Survey of Canada, Paper 78-1a, p. 77-80.

Cline, J. S., Hofstra, A., Muntean, J.L., Tosdal, R.M., and Hickey, K.A., 2005. Carlin-Type Gold Deposits in Nevada: Critical Geologic Characteristics and Viable Models. Economic Geology 100th Anniversary Volume, p. 451-484.

Dumala, M., 2011. Assessment Report Describing Geophysics, Soil Geochemistry and Diamond Drilling at the Rau Property; prepared for ATAC Resources Ltd. October 20, 2011.

Fonseca, A.L., 1998. Origin of Carbonate Hosted Gold Rich Replacement Deposits and Related Mineralization Styles in the Ketza River Deposit, Yukon Territory. Unpublished MSc thesis, University of British Columbia, British Columbia, Canada.

Franchini, M.B., Barrio, R.E., Pons, M.J., Schalamuk, I.B., Rios, F.J., and Meinert, L., 2007. Fe Skarn, Iron Oxide Cu-Au, and Manto Cu-(Ag) Deposits in the Andes Cordillera of South-west Mendoza Province (34^0-36^0S), Argentina. Exploration and Mining Geology, vol. 16, p. 233-265.

Green, L.C., 1972. Geology of Nash Creek, Larsen and Dawson Map Areas, Yukon Territory. Geological Survey of Canada, Memoir 364, p. 157.

Gross, G.A., 1996. Skarn iron. *In:* Geology of Canadian Mineral Deposit Types, O.R. Eckstrand, W.D. Sinclair, and R.I. Thorpe (eds.), Geological Survey of Canada, no. 8, p. 489-495 (also Geological Society of America, The Geology of North America, v. P-1).

Hart, C.J.R., 2007. Reduced intrusion-related gold systems. *In:* Mineral deposits of Canada: A Synthesis of Major Deposit Types, District Metallogeny, the Evolution of Geological Provinces, and Exploration Methods, Goodfellow, W.D., (ed.), Geological Association of Canada, Mineral Deposits Division, Special Publication No. 5, p. 95-112.

Kingston, S., Mortensen, J., Dumala, M., and Gabites, J., 2009. Ar-Ar Geochronology and Pb Isotopic Constraints on the Origin of the Rau Gold- Rich Carbonate Replacement Deposit, Central Yukon. *In*: Yukon Exploration and Geology 2009, K.E. MacFarlane, L.H. Weston and L.R. Blackburn (eds.), Yukon Geological Survey, p. 213-222.

Kojima, S., Trista-Aguilera, D., and Hayashi, K.I., 2009. Genetic Aspects of the Manto-type Copper Deposits Based on Geochemical Studies of North Chilean Deposits. Resource Geology, vol. 59, issue 1, p. 87-98.

Lang, J.R. and Baker, T., 2001. Intrusion-related gold systems: the present level of understanding. Mineralium Deposita, vol. 36, p. 477-489.

Mach, C.J. and Thompson, T.B., 1998. Geology and Geochemistry of the Kokomo Mining District, Colorado. Economic Geology, vol. 93, p. 617-638.

Morrow, D.W., 1999. Lower Paleozoic stratigraphy of northern Yukon Territory and northwestern District of Mackenzie. Geological Survey of Canada, Bulletin 538, p. 202.

Muntean, J.L., Cline, J.S., Simon, A.C., and Longo, A.A., 2011. Magmatic-hydrothermal origins of Nevada's Carlin-type gold deposits. Nature, vol. 4, p. 122-127.

Murphy, D. C., 1997. Geology of the McQuesten River Region, northern McQuesten and Mayo map areas, Yukon Territory (115P/14, 15, 16; 105M/13, 14). Exploration and Geological Services Division, Yukon, Indian and Northern Affairs Canada, Bulletin 6, 122 p.

Simonetti, A., Heaman, L.M., Chacko, T., and Banerjee, N.R., 2006. In situ petrographic thin section U-Pb dating of zircon, monazite, and titanite using laser ablation-MC-ICP-MS. Journal of Mass Spectrometry, vol. 253, p. 87-97.

Stephens, J.R., Mair, J.L., Oliver, N.H.S., Hart, C.J.R., and Baker, T., 2004. Structural and mechanical controls on intrusion-related deposits of the Tombstone Gold Belt, Yukon, Canada, with comparisons to other vein-hosted ore-deposit types. Journal of Structural Geology, vol. 26, p. 1025-1041.

Stroshein, R., 1996. Geology and Gold Deposits at Ketza River, Yukon Territory A progress report. *In:* Yukon Exploration and Geology 1995, Exploration and Geological Services Division, Yukon, Indian and Northern Affairs Canada, p. 43-48.

Appendix A. *Selected U-Pb analyses of four monazite grains from the Tiger zone.*

sample name	$^{238}U/^{206}Pb$	2 s	$^{207}Pb/^{206}Pb$	2 σ	$^{206}Pb^*/^{238}U$ age (Ma)	2 σ error (Ma)
MNZ-1F	105.956	9.799	0.046	0.001	61	6
MNZ-1G	104.962	10.374	0.048	0.001	61	6
MNZ-1H	110.449	11.271	0.045	0.001	58	6
MNZ-1I	106.878	10.895	0.046	0.001	60	6
MNZ-1J	104.952	9.907	0.046	0.001	61	6
MNZ-1Q	106.492	10.334	0.046	0.001	60	6
MNZ-1R	105.951	10.025	0.045	0.001	61	6
MNZ-1S	108.693	10.487	0.045	0.001	59	6
MNZ-1T	106.553	9.784	0.045	0.002	60	6
MNZ-1U	109.619	11.133	0.043	0.002	59	6
MNZ-1V	104.520	9.726	0.042	0.001	61	6
MNZ-1W	112.520	13.176	0.040	0.002	57	7
MNZ-2A	104.875	10.772	0.045	0.001	61	6
MNZ-2B	103.280	11.578	0.044	0.002	62	7
MNZ-2C	111.870	13.121	0.043	0.001	57	7
MNZ-2D	119.441	12.196	0.044	0.002	54	5
MNZ-2E	106.321	10.037	0.044	0.001	60	6
MNZ-2F	115.292	10.711	0.044	0.001	56	5
MNZ-2G	111.260	11.138	0.041	0.002	58	6
MNZ-2H	111.116	10.430	0.041	0.003	58	5
MNZ-2I	111.324	10.202	0.043	0.001	58	5
MNZ-2J	117.935	12.526	0.042	0.002	54	6
MNZ-3B	119.169	12.662	0.045	0.001	54	6
MNZ-3C	106.677	11.872	0.045	0.001	60	7
MNZ-3D	118.269	13.198	0.045	0.001	54	6
MNZ-3E	114.405	11.601	0.044	0.003	56	6
MNZ-3F	109.998	14.661	0.046	0.001	58	8
MNZ-3H	112.281	11.260	0.044	0.002	57	6
MNZ-4A	112.621	11.705	0.046	0.001	57	6
MNZ-4B	108.265	12.962	0.045	0.001	59	7
MNZ-4C	107.682	10.095	0.046	0.001	60	6
MNZ-4D	113.553	11.859	0.046	0.001	57	6
MNZ-4E	108.946	11.784	0.046	0.001	59	6
MNZ-4F	103.220	9.117	0.048	0.001	62	5
MNZ-4G	110.075	10.616	0.046	0.001	58	6
MNZ-4H	107.921	9.877	0.046	0.001	59	5
MNZ-4I	114.861	11.485	0.046	0.001	56	6
MNZ-4J	111.489	10.685	0.046	0.001	58	5

not common Pb corrected